$P. 212$

Composite Load Spectra for Select Space Propulsion Structural Components

Final Report

J.F. Newell, H.W. Ho, and R.E. Kurth
Rockwell International
Canoga Park, California

November 1991

NASA

National Aeronautics and
Space Administration

CONTENTS

i

TABLES

1.0 INTRODUCTION

1.1 General

Requirements for better performance have pushed engine designs to lighter weight systems, higher pressures, and more severe temperature environments. Temperatures, external and internal fluids flow noise, and mechanical vibration levels have increased markedly and have been shown to limit hardware designs. Advanced engine concepts and designs are enough different so that the loads cannot be simply scaled from other engines.

The use of engine cycles, such as staged combustion on the space shuttle main engine (SSME), result in engine operating pressures in the 3000 to 7000 psi regime. High performance turbomachinery operates in the 30,000 to 100,000 RPM regime. These operational requirements result in complex high energy loading throughout the engine. The difficulty in installation, the burden in cost and the potential for destroying an engine have severely limited required instrumentation and measurements to adequately define loads of key components, such as turbine blades. Also, accurate analytical methodologies for defining internal flow-related loads are just emerging for problems typically found in rocket engines. The difficulty of obtaining measured data and verified analysis methodologies has led to the probabilistic load definition approach of this contract.

Current loads analyses methodologies are driven by their usage in deterministic analysis methods. This includes strength and fatigue analysis as well as mechanical vibration. The deterministic solution typically uses an upper bound approach where maximum loads and minimum properties are used. For critical hardware, a separate sensitivity study is often made to determine nominal operation and which of the loads and their variations govern the hardware design. Quantification of the actual variations and their frequency of occurrence is a crucial weakness.

The Composite Load Spectra (CLS) contract and the associated Probabilistic Structural Analysis Method (PSAM) contract from Lewis Research Center are developing an integrated probabilistic approach to the structural problem. The probabilistic loads approach has the ability to quantify knowledge more technically relative to the loads. The use of mean values and distributions of engine loads, rather than maximum or enveloped loads, can add greatly to the understanding of normal engine operation while furnishing good or better knowledge of maximum conditions.

Present techniques often result in manufacturing of components that, in many cases, greatly exceed design requirements; however, there is no way of assessing this margin for extending the useful life margin. Thus, to formulate more effective designs, it is necessary that loads on components of rocket engines be derived so that they can be applied by probabilistic analysis methods such as PSAM. More effective designs will result in more accurate methods reflecting the true risk. An assessment would be much easier to perform if a probabilistic analysis and associated risk assessment were available.

This project will provide methods to combine technologies of analytical (deterministic) loads and probabilistic modeling. Since these methods will be developed from a generic approach, they will be applicable to current or advanced liquid rocket engine designs.

1.2 Project Objective

The objective of this program is to develop generic load models. Multiple levels of progressive sophistication will simulate the CLS induced in space propulsion system components and will be representative of SSME, such as transfer ducts, turbine blades and liquid oxygen (LOX) posts. These models will be developed using two independent approaches. The first approach consists of describing CLS simulation, using state-of-the-art probabilistic methods to describe the individual loading conditions and combinations of these loading conditions to synthesize the CLS.

The second approach consists of developing coupled models for CLS simulation which combine (deterministic) models for composite load dynamic, acoustic, high-pressure and high rotational speed, etc., load simulation using statistically varying coefficients. These coefficients will then be determined using advanced probabilistic simulation methods with and without strategically selected experimental data. The first approach effort has been completed and work on the second approach started.

The unified theory required to combine various individual load simulation models (hot-gas dynamic, vibrations, instantaneous-position, centrifugal field, etc.) into CLS simulation models will be developed under this program. Results obtained from tests models will be compared with available numerical results with the loads induced by individual load simulation models. Results will also be obtained with available structural analysis results from independent analyses and tests. These theories, developed under both approaches, will be further validated with respect to level of sophistication and relative to predictive reliability and attendant level of confidence.

A computer code incorporating the various individual and CLS models will be developed to construct the specific load model desired. The approach is to develop and deliver the computer code at intervals in the contract. The first version was an initial code for turbine blade loading. Subsequent code versions have added sophistication to the component probabilistic load definition and the decision making processes, as well as installing a new set of loads for an additional component. This allows for ongoing evaluation and usage of the system by Rocketdyne and NASA.

2.0 SUMMARY

The development of the CLS is a 4-year base program and a 2-year option program. Rocketdyne is the prime contractor and is responsible for the overall project. Battelle Columbus Laboratories (BCL) is the major subcontractor for developing the probabilistic methods and related tasks. The effort is divided into three tasks: probabilistic method and load model development, load-expert system development; and code validation and verification. The CLS base program is essentially complete. Since January 1989, the option program is carrying out. There is no clear-cut separation between the base program and the option program. The option program is really a natural extension of development work from the base program. This final report presents the accomplishments of the CLS efforts during the last 4 years. It summarizes experiences gained during the base program efforts, details the status of the CLS code, and presents some perspectives of the program and its future direction.

The SSME is being used as a baseline model for defining the loads and requirements. The SSME configuration of the four components studied are shown in Figures 2.1 and 2.2. Figure 2.1 is a cross section of the SSME powerhead showing typical LOX posts in the three combustors (two preburners and a main injector), transfer ducts between the turbines, and the main injector and turbine blades. Figure 2.2 shows the HPOTP discharge duct in an overall SSME powerhead view. This duct was chosen as the fourth component because of its history of fluid vibration-related problems.

During the base program, a probabilistic multilevel engine model was developed. The SSME is being used as a baseline model; however, the engine model implemented on the CLS program is generic. The multilevel engine model is composed of the engine system influence model and various component load models as shown in Figure 2.3. The engine system influence model is the foundation of the multilevel engine model which allows various component load models to be built on it. The engine system model evaluates system performance variables and engine subsystem operation loads. Both load types are

SSME POWERHEAD COMPONENT ARRANGEMENT

OXIDIZER PREBURNER

HPOTP DISCHARGE DUCT

TRANSFER DUCT

HIGH PRESSURE OXIDIZER TURBOPUMP

LOX POSTS

MAIN COMBUSTION CHAMBER

FUEL PREBURNER

HIGH PRESSURE HYDROGEN TURBOPUMP

TURBINE BLADES

SC87C-4-2848
1888m/8

Rockwell International
Rocketdyne Division
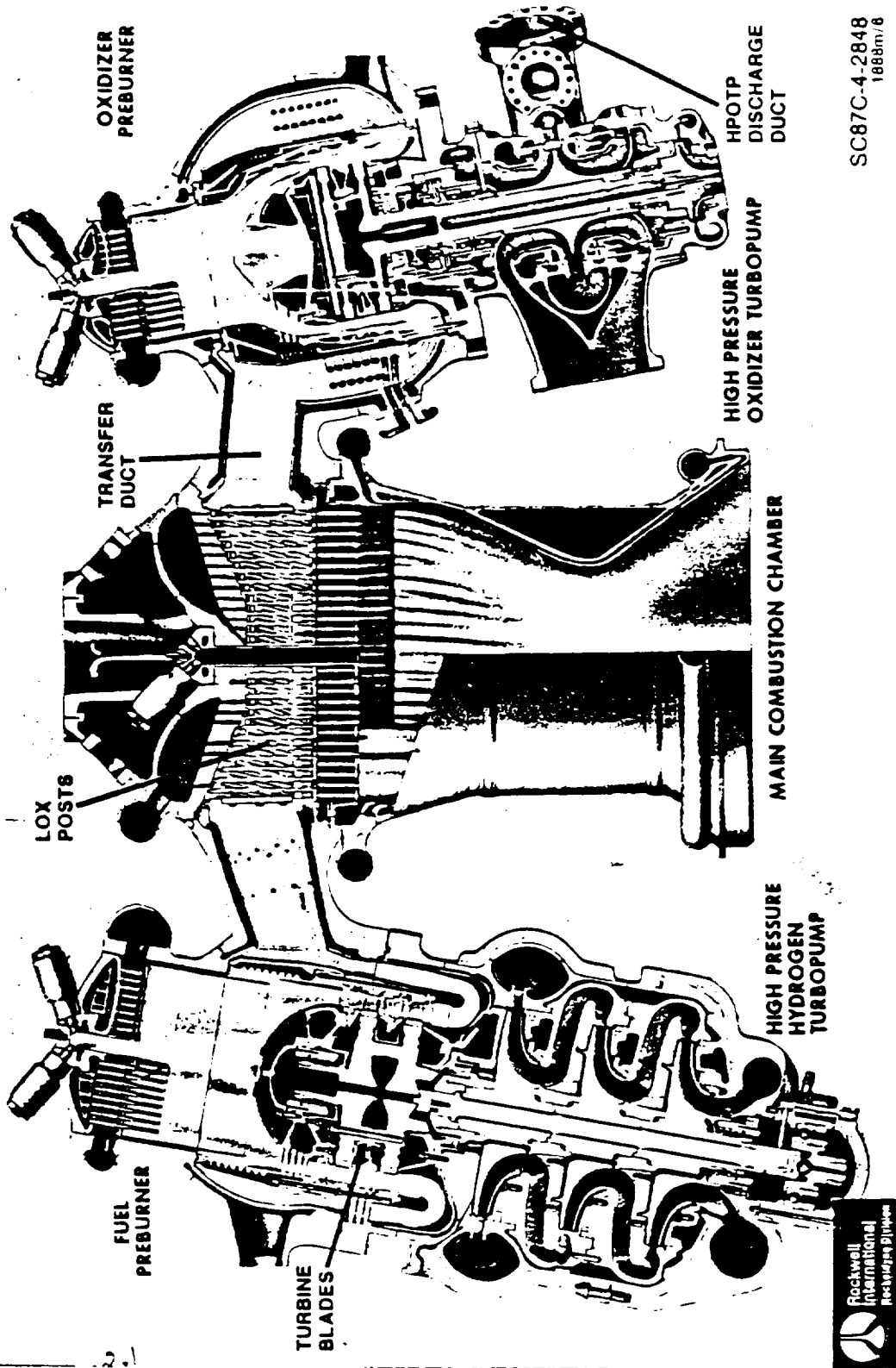
Figure 2.1. SSME Powerhead With LOX Posts,
Transfer Ducts and Turbine Blades Identified
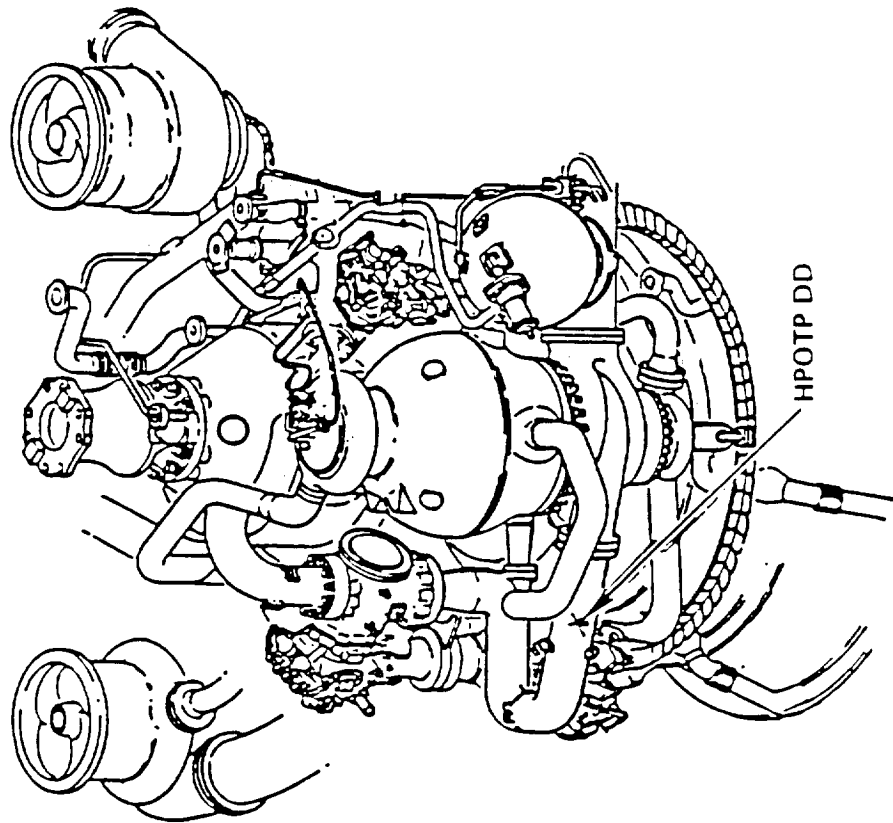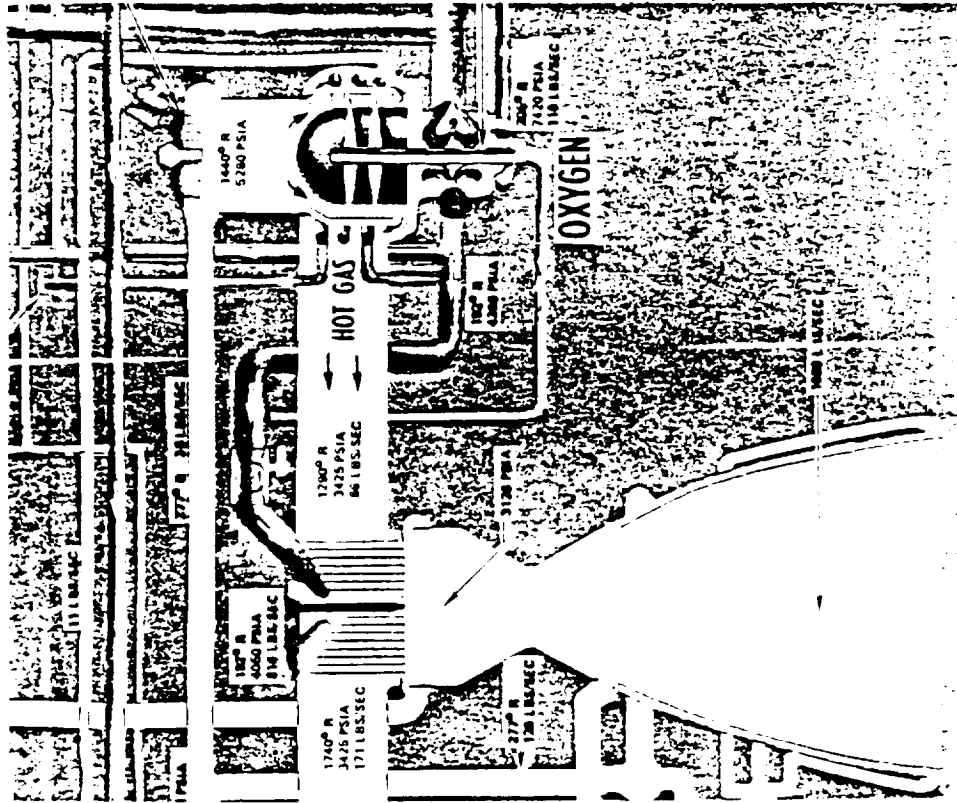
Figure 2.2. SSME HPOTP Discharge Duct
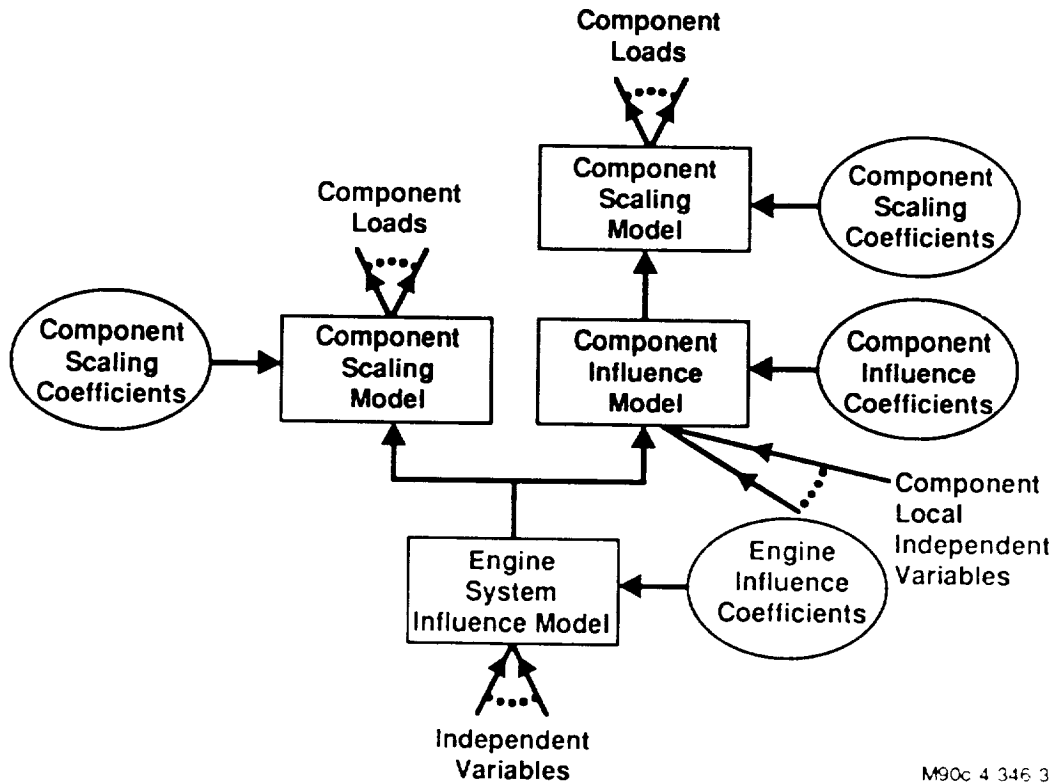
Figure 2.3. Multi-Level Engine Model

classified as system dependent loads from now on as a convenient convention. The evaluation is based on the engine operating power level, engine hardware, and operating parameters. Engine hardware and operating parameters are classified as system-independent loads from now on. The load definitions will be defined in the next section.

Component load models evaluate loads local to a component (classified as component loads) using system loads as the component boundary loads (subsystem interface operating loads).

The base program engine system influence model, which is implemented into the probabilistic load model, has 23 independent loads and 62 dependent loads. The load selection was developed mainly for the purpose of engine performance

evaluation. Independent loads do not include most engine hardware parameters. When this model was employed to calculate dependent loads, the load distribution results (mainly the load variation) did not compare well with the 10-second average load database data. Investigation indicates that the engine-to-engine variation was not included in the engine system model. This variation is contributed mainly from engine hardware variations as a result of different manufacturing processes used by different manufacturers and different environmental conditions during the manufacturing process. This pointed out a need for an expanded engine system influence model. As a result of this investigation, an expanded list of independent loads and dependent loads were identified. The lists include 64 independent loads and 99 dependent loads. A request was made to the engine performance group for a new influence coefficient set for the expanded list of loads. The new influence coefficient set has been generated and is planned to be implemented during the option program of this contract.

The probabilistic methods were surveyed and three methods were selected to be implemented in the CLS code. The three probabilistic methods selected are (1) the Gaussian moment method, (2) the random sampling condensation algorithm (RASCAL) method, and (3) the Monte Carlo method.

The Gaussian moment method assumes all random variables are normally distributed. The variation of a combined load is evaluated, based on Gaussian algebra. This method is best used for a quick evaluation or sensitivity study.

The RASCAL method is a variance of the discrete probability distribution (DPD) method. It is versatile in that it can handle almost all types of distribution, even those without closed forms. It is efficient if very high accuracy is not required.

The Monte Carlo method is the most powerful method because it can be applied to any situation. The conventional wisdom is that the Monte Carlo method is computational-expansive and inefficient; however, with available high speed computers, this is probably not a factor. If high accuracy is required, the Monte Carlo method is probably the best way to solve the problem.

The three methods were implemented to the engine system influence model. RASCAL was chosen to be the principal method as most component load models were implemented with the method. Validation of RASCAL has been performed. High accuracy comparable to the Monte Carlo method can be obtained if a large enough bin size is used. But then the efficiency advantage of RASCAL is lost.

Generic probabilistic models were developed and implemented for load calculations using the probabilistic methods discussed above. Each engine mission, either a real flight or a test, has three mission phases: the engine start transient phase, the steady state phase, and the engine cut off transient phase. Power level and engine operating inlet conditions change during a mission. The load calculation module provides the steady-state and quasi-steady state calculation procedures with duty-cycle-data option. The quasi-steady state procedure is for engine transient phase calculations. In addition, a few generic probabilistic load models were also developed for specific conditions. These include the fixed transient spike model, the poison arrival transient spike model, and the rare event model. These generic probabilistic load models are valuable tools for simulating loads with specific conditions. They were implemented in place. However, more study and development is required to build sufficient knowledge base and database to facilitate general usage. As it stands now, only experts with full knowledge of the loads to be simulated can use these models to synthesize desired loads with the specific conditions.

Four SSME components, turbine blades, transfer ducts, LOX post, and the high pressure oxidizer turbopump (HPOTP) discharge duct were selected for application of the CLS program. The loads for these four components provide a fairly complete picture of loads for the SSME. Loads developed for the four components are listed in Table 2.1. They include static pressure loads and dynamic pressure loads for all four components, centrifugal force for the turbine blade, temperatures or thermal loads for all four components, and structural vibration loads for the ducts and LOX posts (ref. 2.1).

Table 2.1. Composite Load Spectra
Scope of the Load Knowledge Base

Individual Load	Turbine Load	Transfer Duct	LOX Post	HPOTPDD
Static pressure	X	X	X	X
Dynamic pressure				
Turbulence				
Sinusoidal (repeated pulse)	X	–	–	–
Random	–	X	X	X
Centrifugal	X	–	–	–
Temperature	X	X	X	X
Structural vibration				
Transient	–	X	X	X
Steady-state	–	X	X	X

89c-4-339-26

The probabilistic load development has proceeded in parallel with the load definition work. The goal is to address generic engines that may include different mission profiles or incorporate design changes. This will require that a robust and general probabilistic approach be adopted for inclusion in the expert system. Generic component load models were developed to synthesize probabilistic loads of components. In the CLS load expert system, the generic static pressure scaling model, the generic probabilistic thermal load model, and the generic fluctuation pressure (dynamic pressure load for ducts and LOX posts) load model were implemented. With appropriate database, the generic load models will provide the correct loads for each component. The sinusoidal dynamic pressure load for turbine blades is unique and a dedicated turbine-blade dynamic-pressure model was implemented for it. There is a vibration model in place. More development and improvement of the vibration model is required for any real applications.

Probabilistic load models were integrated into a load-expert system. The primary function of the load-expert system is to provide a development environment for integrating the load knowledge domain with the probabilistic models. Advantages of an expert system environment for the CLS program are that it facilitates incremental development of the probabilistic load models especially for building generic models, provides a better knowledge representation, avoids data and knowledge redundancy, and provides a friendly user interface for interactive computing.

The intensive computation requirement for load modeling and the nonproprietary requirement dictated that the expert system program be developed in-house and in FORTRAN language so that it could be easily integrated with the FORTRAN routines developed for probabilistic methods and load models. The philosophy is to learn from the experiences gained by artificial intelligence (AI) pioneers and to make the system simple and efficient. As Feigenhaum (ref. 2.2) put it, "knowledge is power." The goal is to put all the knowledge together in a suitable representation which can be utilized efficiently by the load calculation module. Based on this philosophy, the CLS program employs a decision tree inferencing scheme chosen for its simplicity and efficiency coupled with a database system for data management. The engineering data is handled by the database system. The data processing and load modeling were hardwired into decision tree rule modules. The process control and queries are handled by the expert system. With this simple structure, the expert system achieves its goal of providing a convenient way of retrieving load information to users, performing simple calculations using different load models, and preparing input file for a full-blown load calculation.

3.0 SSME OVERVIEW

The orbiter vehicle main propulsion system includes three SSMEs. An SSME is a reusable, high-performance, liquid-propellant rocket engine with variable thrust. All three SSMEs are ignited on the ground at launch, operating in parallel with solid rocket boosters during the initial ascent phase, and continuing to operate for approximately 550 seconds during total firing duration. Each engine operates at a mixture ratio (liquid oxygen/liquid hydrogen) of 6:1 and a chamber pressure of approximately 3,000 psia to produce a sea level thrust of 375,000 pounds and a vacuum thrust of 470,000 pounds. The engines are throttleable over a thrust range of 65 to 109% of the rated power level. This provides a higher thrust level during lift-off and the initial ascent phase, and allows orbiter acceleration to be limited to 3 g during the final ascent phase. The engines are gimbaled to provide pitch, yaw, and roll control during orbiter boost phase.

A typical flight profile is shown in Figure 3.1. This basic profile is characteristic of a majority of the pressure, flow, and pump characteristic parameters.
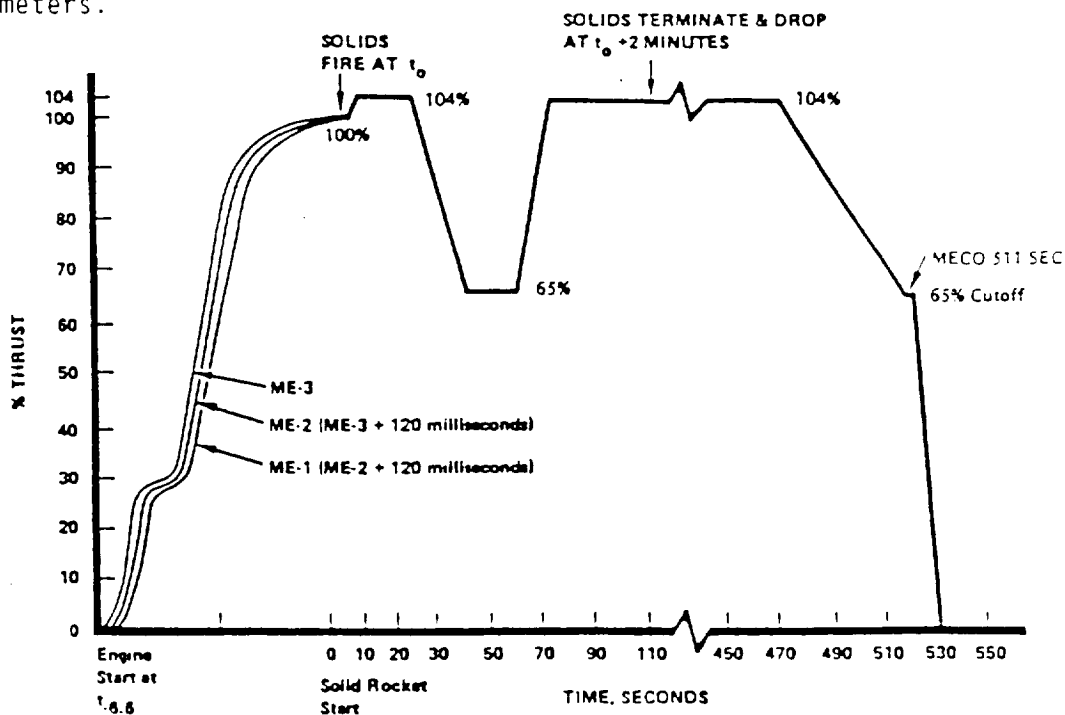
Figure 3.1. Typical SSME Thrust Profile

A brief description of the engine operation and propellant flow schematic is
provided in order to furnish an overall perspective of the engine and its
loads. Figure 3.2 is a simplified flow schematic where main engine components
and flows are shown.

A description of the start sequence follows.
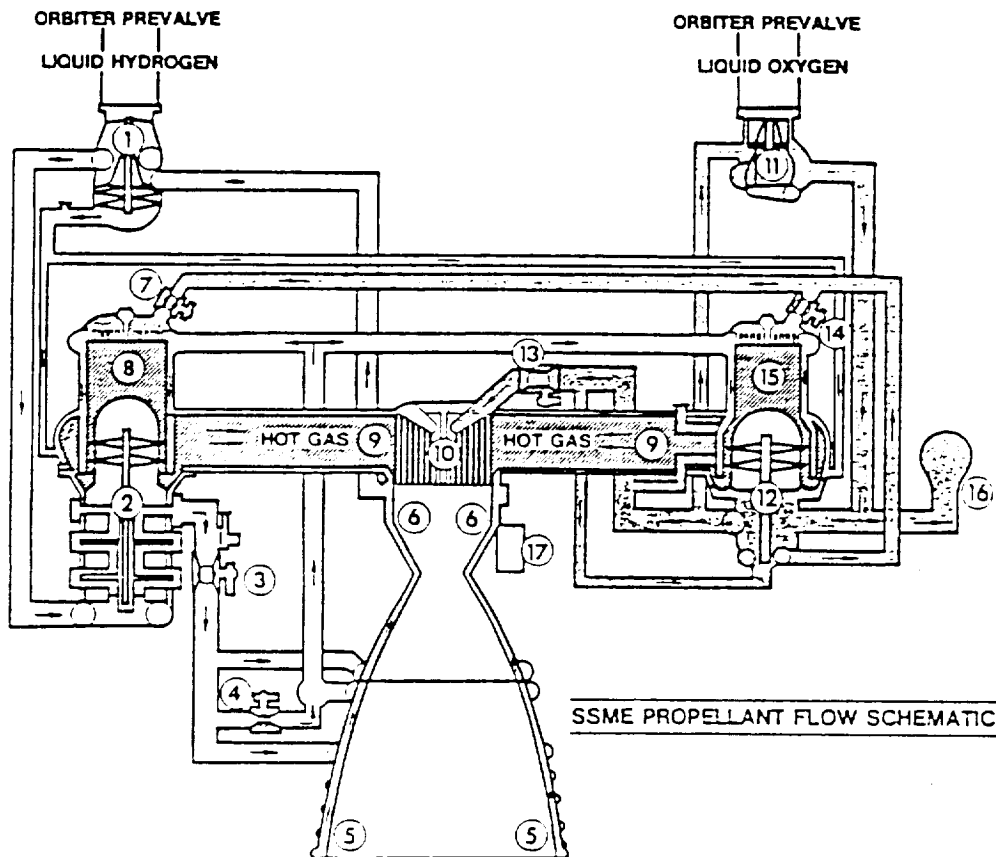
Figure 3.2. SSME Propellant Flow Schematic

Components

1.	Low Pressure Fuel Turbopump	10.	Main Injector (LOX Posts)
2.	High Pressure Fuel Turbopump	11.	Low Pressure Oxidizer T/P
3.	Main Fuel Valve	12.	High Pressure Oxidizer T/P
4.	Chamber Coolant Control Valve	13.	Main Oxidizer Valve
5.	Nozzle	14.	Oxid. Preburner Control Valve
6.	Main Combustion Chamber	15.	Oxidizer Preburner
7.	Fuel Preburner Oxidizer Valve	16.	Pogo Suppressor
8.	Fuel Preburner (LOX Posts)	17.	Controller
9.	Hot Gas Manifold (& Transfer Tubes		

The flow of liquid hydrogen (or fuel) and liquid oxygen (or oxidizer) from the space shuttle external tank is restrained from entering the engine by pre-valves (or isolation valves) located in the orbiter above the low pressure turbopumps (1 and 11). Approximately 1 hour prior to firing, the prevalves are opened to allow propellants to flow through the low pressure turbopumps (1 and 11), and through the high pressure turbopumps (2 and 12), and then to the main propellant valves (3 and 13). On the liquid oxygen side, the system also fills two preburner valves (7 and 14). The cryogenic propellants are held in ducts for sufficient time to chill the engine and attain liquid conditions in the respective propellant systems. The chill process is aided by bleedlines to remove gaseous propellants as they are formed.

In the start sequence, hydrogen and oxygen sides operate almost simultaneously. The hydrogen (or fuel) side is explained first.

Upon receipt of the ignition command from the orbiter, the main fuel valve (3) is opened. This permits hydrogen to flow into the coolant loop, through nozzle tubes (5), and through channels in the main combustion chamber (6). Part of this coolant loop flow is diverted by the coolant control valve (4) to the preburners (8 and 15) for combustion and cooling of the preburner walls. Some of the hydrogen used in the coolant loop is warmed in the process to virtually ambient conditions and is tapped off at the main combustion chamber (6) for routing back to the low pressure turbopump (1) to drive the turbine for that pump. This flow passes through the turbine and is returned to the walls of the hot gas manifold (9) and the main injector (10) to provide cooling.

On the oxygen (or oxidizer) side, the ignition command opens the main oxidizer valve (13). The liquid oxygen flows through the two turbopumps (11 and 12) to the main injector (10) and also (through valves at 7 and 14) to the two pre-burners (8 and 15). Oxygen, tapped off downstream of the high pressure oxidizer turbopump (12), is routed to the low pressure turbopump (11) and to serve as the turbine-drive fluid for that pump. This flow continues through the low pressure oxidizer turbopump (11), thus re-entering the circuit.

Spark igniters located in the dome of both preburners (8 and 15) and the main chamber (10) initiate combustion.

After the engine is signaled to start, the initial combustion occurs in the preburners. There are two preburners: one provides power to the high-pressure fuel turbomachinery (8), and the other provides power to high pressure oxidizer turbomachinery (15). Proper sequencing of these two preburners allows the engine to start repeatedly regardless of engine inlet conditions. Each of the two preburners operates at a low mixture ratio of less than one part oxygen to hydrogen to produce hot gas (or hydrogen-rich steam) to provide low-temperature gases for turbomachinery operation. Each temperature can be varied by moving a single valve. The two preburners thus provide a convenient method for controlling engine thrust and mixture ratio. The preburners operate over a broad range of pressure and temperature to achieve a full range of engine operating conditions.

As the fuel-rich gases leave the preburners, they immediately enter high-pressure turbomachinery. The gases are expanded in a turbine and the expansion reduces the temperature. After the gases leave the turbomachinery, they enter the hot-gas manifold. This manifold transports and distributes the gases to the main injector. The hot-gas manifold serves multiple functions. It supports the two preburners and two high-pressure turbopumps, and also forms a portion of the thrust chamber structure. The compactness of the hot-gas manifold allows the powerhead diameter to be minimized, and its orientation permits access for the removal and inspection of turbomachinery and preburners.

After the gases are routed through the hot-gas manifold, they enter the thrust chamber. The thrust chamber consists of three major parts: the main injector (10), the main combustion chamber (6), and the nozzle (5).

Fuel-rich gases from the hot gas manifold enter the thrust chamber through the injector and are distributed in the injector. Liquid oxygen from the high pressure oxidizer turbopump (2) enters at the top of the injector, is uniformly distributed within the oxidizer dome. The oxygen then enters the

center tube of each of the injector coaxial elements. The fuel-rich hot gas enters the large annular tube of the coaxial element. The coaxial elements are designed and optimized so that the hot gas, plus the oxygen, is uniformly distributed throughout the combustion chamber. This is achieved by proper matching of gas and oxygen velocities and uniform spacing of elements across the injector face. A portion of the injector elements is extended into the combustion chamber to form acoustic baffles. These elements, quite similar to those used on the injector face, inject hydrogen and oxygen at the same mixture ratio as the elements on the injector face and maintain uniform distribution and high performance.

Propellants injected into the main chamber are combusted rapidly at a mixture ratio of six parts of oxygen to one part hydrogen. The gases are accelerated to sonic velocity and supersonically expanded in the aft portion of the main combustion chamber and the nozzle.

There is a standard set of engine measurements that are taken on each SSME engine ground test that is used for calculating engine performance, measuring critical levels of vibration, temperature, etc. for engine redlines and measuring general engine operation. A subset of the information applicable to the CLS contract (Figure 3.3) includes measured data related to LOX posts, turbine blades and transfer ducts. Most of the measurements are low frequency digital data. The accelerometer data are all high frequency analog measurements.

Figure 3.4 shows the standard flow of engine test data processing on the SSME. For low frequency data, the information is processed through a data reduction code and either plotted as the variable versus time or further processed to obtain steady-state performance calculations that include both measured and calculated flows, temperatures, pressures, torques, speeds, power level, etc. The analog data passes through a high frequency data processing facility and produces a series of standard plots. These data are all reviewed prior to the next test firing of the engine and are also collected in various databases for later use and review. Data tapes are saved from all engine tests and information is recoverable at any time.

Figure 3.3.   SSME Standard Instrumentation Available on Powerhead

The right side of Figure 3.4 depicts the interrelationship of the engine per-
formance model and the engine data analysis. The engine data reduction model
and the performance model are essentially the same code. For data analysis,
engine measurements are used as input variables. For the performance model,
design conditions are used for the input variables. Based on empirical
measurements on more than 1000 engine tests, coefficients for these models
have been adjusted. The influence conditions or coefficients and nominals are
a set of equations with coefficients that are varied as a function of power
level to accurately represent the results of the performance model at specific
power levels between 65 and 109% power level. Influence coefficients and
nominals are a cost effective method of determining engine parameters for a
limited set of independent and dependent variables.
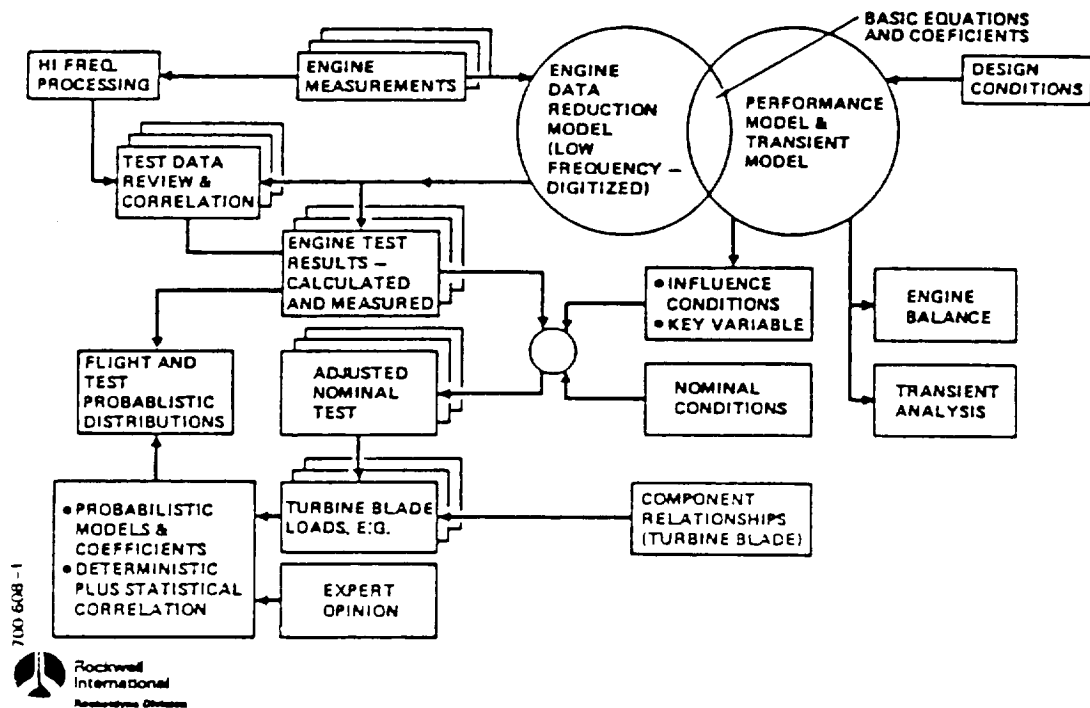
Figure 3.4. Data Analysis

The engine measurements form the best ready database for developing probabilistic loads. Since they are all time-phased, it is a convenient method for obtaining some of the combined load effects. In the development of the individual loads, key variables (e.g., power level, torques, and flow rates) are available to aid in developing correlations in order that generic loads can later be scaled using these parameters.

Table 3.1 summarizes and classifies an overall perspective of where information is obtained for detail analysis of components. The first two items relate to the direct engine measurements and analysis discussed above.

The engine balance and engine transient model have similar simulation codes for modeling engine components. The engine balance model furnishes higher accuracy steady-state quantities, whereas the transient model depicts a full range of engine test conditions. Both models project standard engine or typical engine operating conditions. Engine test results are not directly

Data/Analysis	Availability	Examples
1) Engine test measurements • Low frequency (digital) • Hi frequency (FM tape)	• Every engine test • Various types of processed data and records	• Turbine discharge temp, P_c, • Turbopump or injector accelerometers

2) Engine test calculated variables
• Low freq (digital)
• Steady state only
  1 sec, 3 sec,
  10 sec avg
• Major component level
	• Every engine test	• Pump torque, flow rates

3) Engine transient simulation model • Low frequency digital analysis • Major component level	• Specific simulations for understanding start and cutoff • Not test specific, but correlated to test results	• Engine valving and sequencing of overall engine start and cutoff • Major component variables
4) Engine balance model • Steady state analysis • Specific operating conditions • Nominals, max, mins	• Specific engine operation conditions	• RPL, FPL, 111% and other power levels • Various engine configurations • Major component variables
5) Shock and Vibration environments • Design and test environments	• Specific zones on engine • Expected max conditions • Different thrust level and engine configurations • Historical database for engine	• Zone A, main combustion chamber zone • Zone E, fuel preburner

6) Special measurements	• Limited database
	• Critical hardware
	• Few measurement
	• Difficult to obtain
		• Instrumented turbopumps
		• Structural and vibration tests
		• Instrumented injector
		  . SWHGM cold flow
		  . Engine 0110 tests

7) Individual component analysis
• Steady state basis
  . Engine balance conditions
  . Vibration environment
• Transient analysis
  . Engine transient
  . Shock environment
• Expert opinion
	• Some information for all components
	  . Level of detail dependent on - criticality of component, accuracy of model and knowledge of loads
	  . Steady state primarily
	  . Limited duty cycle analysis
	• Limited engine and lab test measurements
		• LOX post
		• Turbine blades
		• Transfer ducts

used as input, but are used as correlation data to compare with engine testing. In general, the engine balance data, and to a lesser extent engine transient simulation model results, are used for component analysis.

Structural vibration loads are based on shock and vibration environment definitions rather than on individual engine measurements.

Detailed structural analyses are usually based on limited or maximum conditions that occur within the load duty cycle of the component rather than a detailed time-dependent analysis of a mission history profile. Most of the available loads are not readily available in the proper format.

The following figures and discussion are furnished to give a perspective of the form of the available engine data and some of its characteristics. Figure 3.5 is the data processed by Rocketdyne for the fuel preburner chamber pressure (FPB Pc) during a typical test. This trace mirrors the thrust profile trace in Figure 3.6. Since pressure and temperature changes at engine propellant inlets affect engine performance, the thrust profile trace also notates when venting of run tanks occurs in tests.

High frequency sample data processing examples include AMS, PSD, ISOPLOTS, Tracking Filter and STATOS. Figure 3.7 shows the power level profile of a test. This test was chosen since it varies the power level in 1% decrements from 109% to 90%. Each step has a steady-state response of 3 sec. This incremental change is easily noted in the high pressure fuel pump speed profile in Figure 3.8. Figure 3.9 is a typical AMS plot that furnishes a composite level squared time history of the variables noted. These traces show transient effects during start and cutoff, as well as the variation caused by changes in steady-state power level. Figure 3.10 is a power level spectral density (PSD) plot of a selected time interval of the test (14 to 24 seconds from start). The variable is the fuel preburner longitudinal acceleration. This plot shows the HPFTP sinusoidal harmonics at 12N, 18N, 24N and 30N that stand out above the average RMS level of the signal. Also, the HPOTP sinusoidal harmonic at 16N is annotated. The same HPFTP sinusoidal frequencies are easily seen on the ISOPLOT in Figure 3.11. Since they are pump-speed dependent, the ISOPLOT also shows how these harmonics drop off as the power level is decreased from 109%.

Figure 3.5. Time from Engine Start, Seconds

**TEST 902 252
THRUST PROFILE**

Figure 3.6. Thrust Profile
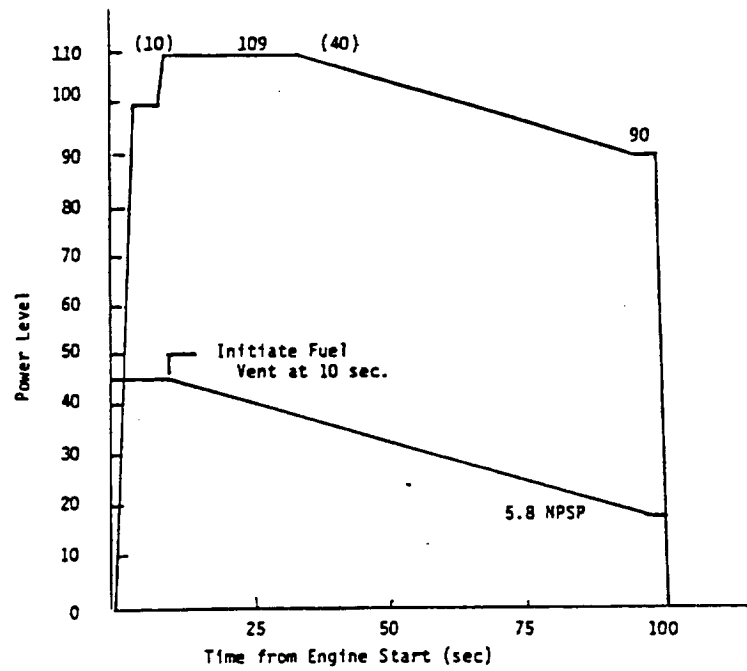
Figure 3.7. Pump Signature Test

PUMP SPEED
(RPM VS. TIME)

ROCKETDYNE
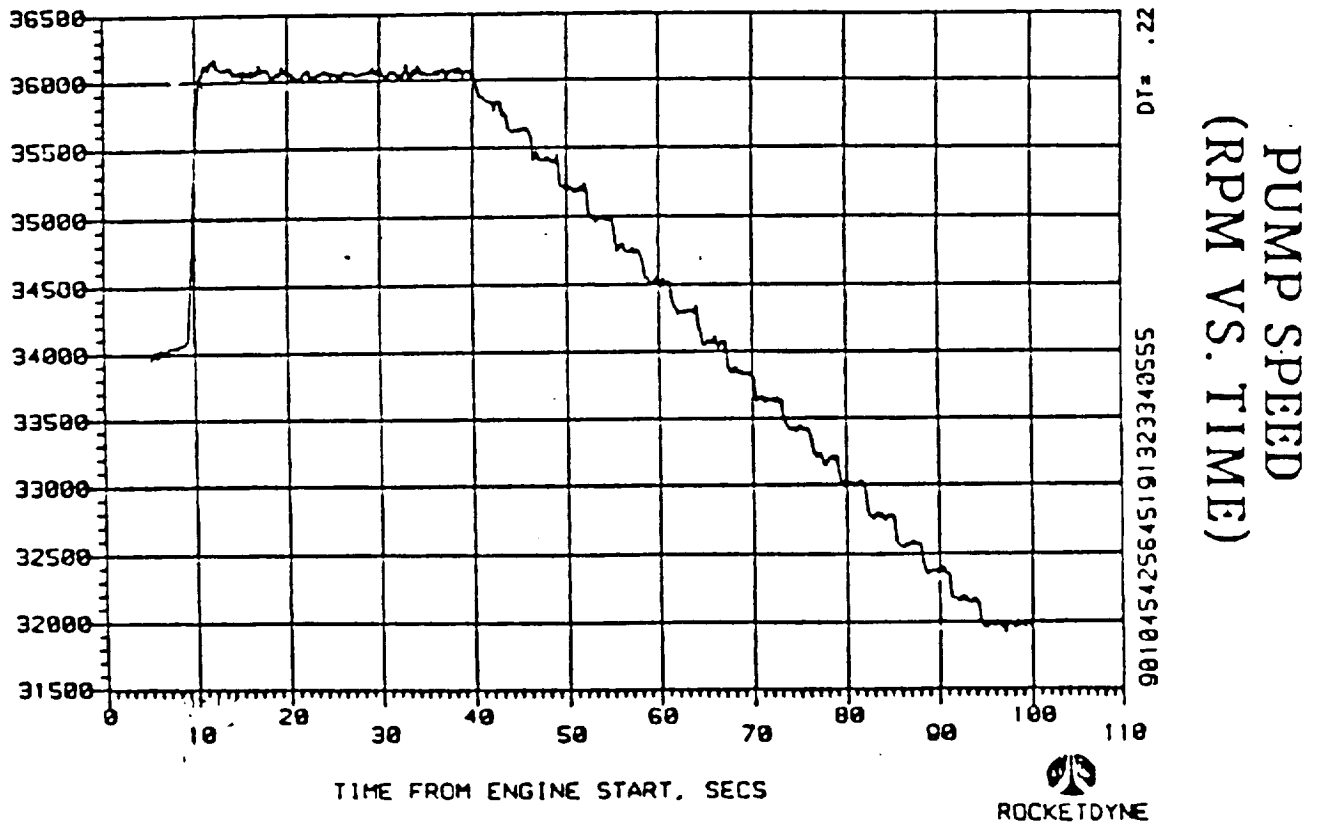
Figure 3.8. High Pressure Fuel Pump Speed

3-11

Figure 3.9.   AMS Fuel Preburner Pc
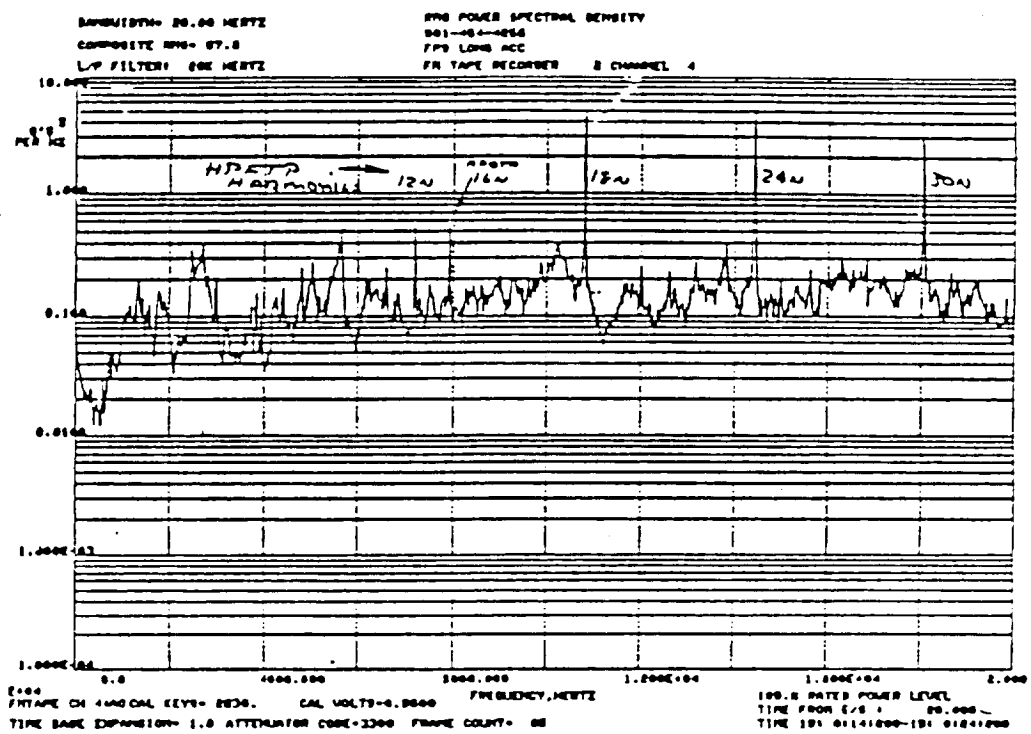
FUEL PREBURNER LONGITUDINAL ACCELEROMETER PDS

Figure 3.10. PSD Fuel Preburner Longitudinal Accel.
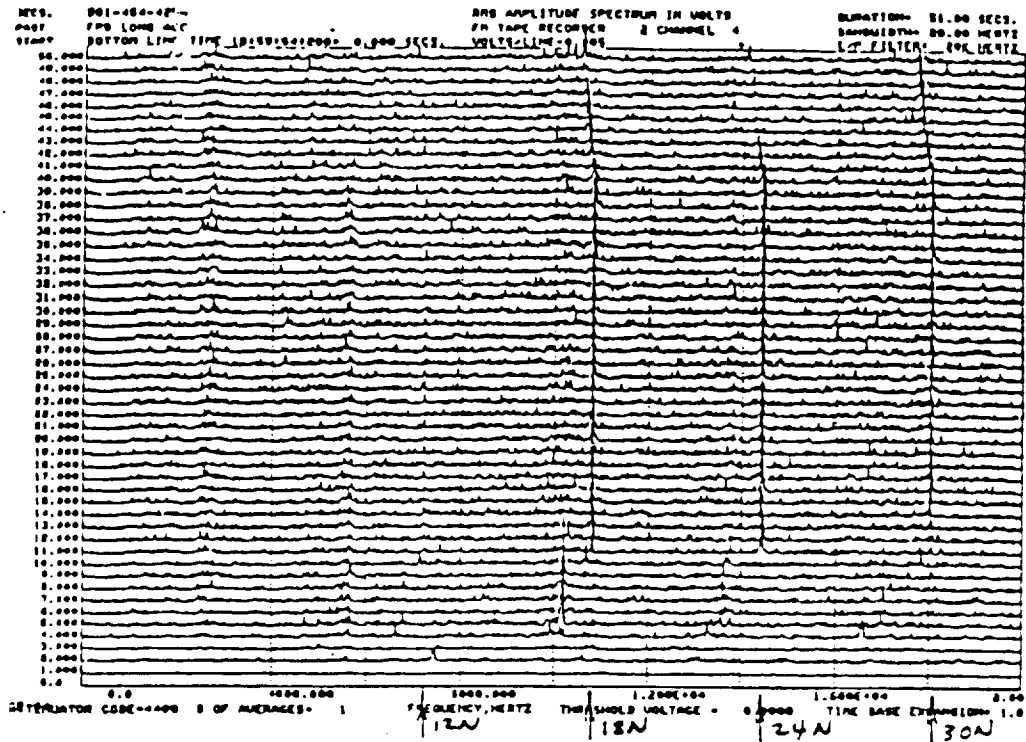
Figure 3.11. Isoplot Fuel Preburner Longitudinal Accel.

The PSD shown demonstrates that high frequency inputs from both pumps are carried through the powerhead and drive the fuel preburner accels. Similar responses are found in the main injector accelerometers.

The STATOS record (Figure 3.12) is included to show that the accelerometer response is such a wide spectrum that the special (standard) processing shown in the previous figures is required to gain intelligent information from the data.
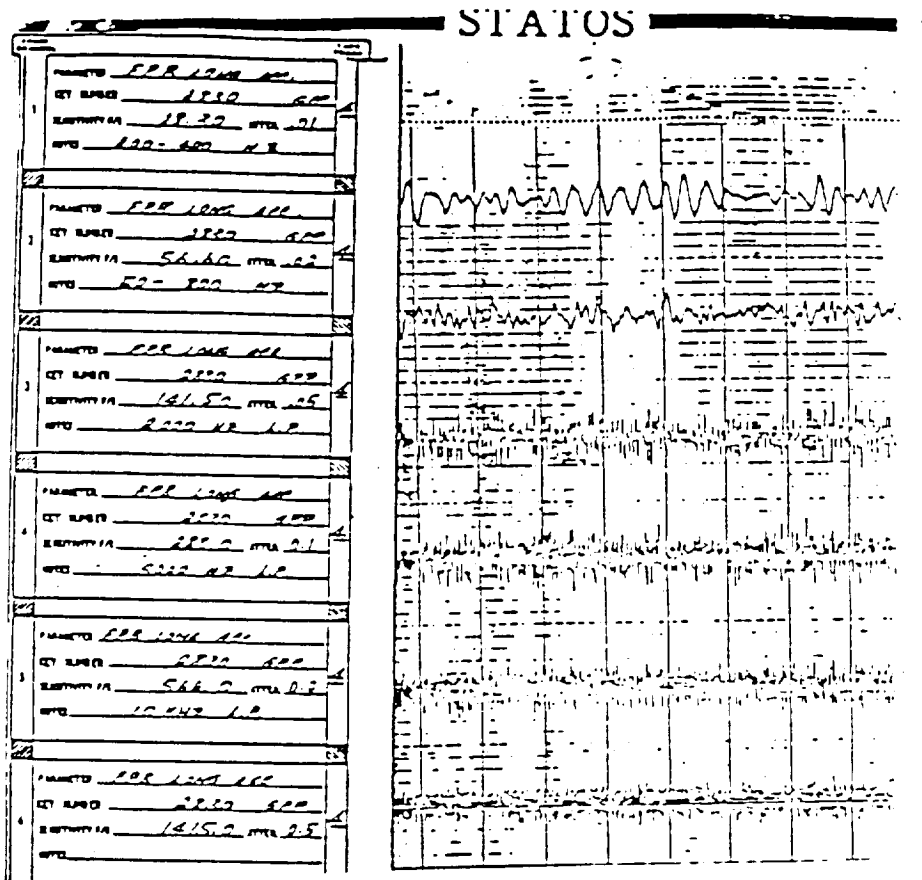
Figure 3.12. Statos Record

4.0 ENGINE LOADS AND CLS ENGINE LOAD MODELS

4.1 Background

Individual loads applicable to the four components in this project are summarized in Table 2.1. Those loads cover a major portion of the loading throughout a rocket engine and are an excellent representative set to develop into an engine loads expert system. Where applicable, individual loads are modeled for the entire duty cycle.

The loads are essentially self-generated or self-induced loads except for steady-state g-forces and gimbaling requirements during flight. This allows the engines to be readily separated from the vehicle loads analysis as a subsystem with specific requirements.

The vehicle design can be divided into conceptual, preliminary, detail, and design verification phases. This is followed by flight support and possible uprating and problem resolutions. During the conceptual and preliminary design phases of a vehicle, major decisions are reached that spawn requirements for engine design. Vehicle requirements often are related to load alleviation or preventative measures and performance requirements to optimize vehicle design with engine design. Examples include: (1) controlled thrust rise rate, (2) in-flight load alleviation, (3) cutoff impulse requirements, (4) engine inlet operating pressures and temperatures, and engine gimbal angle and rate requirements. A description of the approach to deriving the loads design criteria for the space shuttle and its payload is given in Reference 4.1. The vehicle system requirements reduce to a set of engine loads and system requirements (ref. 4.2) that define limits and engine duty cycles that end up defining a part of the engine individual and composite loads. (Note: most examples in the discussion presented herein are related to the SSME, but they are also appropriate for generic rocket engines.)

The basic engine duty cycle is controlled by engine thrust buildup limits (Figure 4.1) engine thrust decay limits (Figure 4.2) and overall flight requirements such as maximum operational power, throttling during maximum dynamic loads, and throttling near the end of flight to maintain a maximum g-load limit (Figure 4.3). These and other engine requirements are used to develop engine configurations and design.

4.2 SSME Deterministic Engine Model

Deterministic models of varying complexity are used in all analysis efforts to evaluate engine performance, engine operating conditions, and component operating loads. The steady-state engine simulation model, i.e., the engine performance model relates engine operating parameters and inlet conditions to engine system performance parameters and engine subsystem operation conditions. The engine performance model is a fairly complex system. Trend charts for engine parameters and pump curves as functions of power level are used in the model to anchor experimental and test data. Engine hardware parameters are calibrated for each engine so that the model evaluation of measured loads agrees with measurements. This, in turn, produces accurate performance evaluation and other unmeasured subsystem operating loads.

To facilitate the engine performance evaluation and prediction, a production influence coefficient model has been developed by the Engine Performance Analysis group at Rocketdyne. The model uses some 20 independent operating parameters and inlet conditions to calculate system-dependent variables used to assess engine performance. Engine operating parameters and inlet conditions are classified as engine-direct variables. The 23 engine-direct variables, listed in Table 4.1, include propellant inlet temperatures and pressures, line resistance changes due to gimbaling, and tank repressurization flow settings. Engine system performance parameters and engine subsystem operating conditions are classified as the system-dependent loads listed in Table 4.2. Based on the evaluation of the engine performance model, the influence coefficients were obtained. To account for an as-built engine condition, tag values are used for engine subsystem operating conditions as the
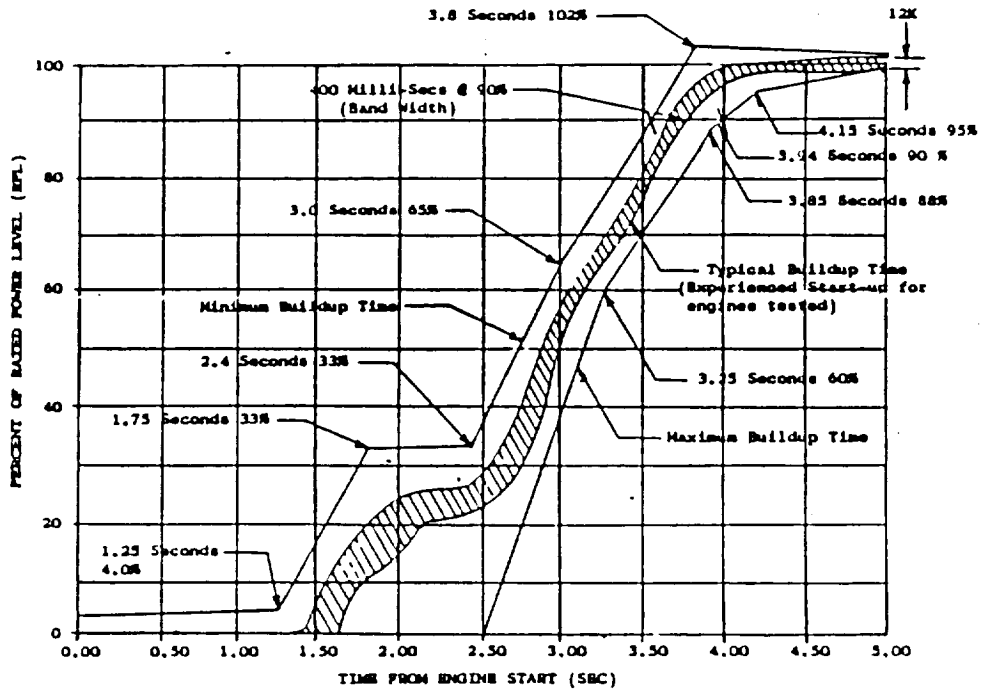
Figure 4.1. SSME Thrust Buildup Limits
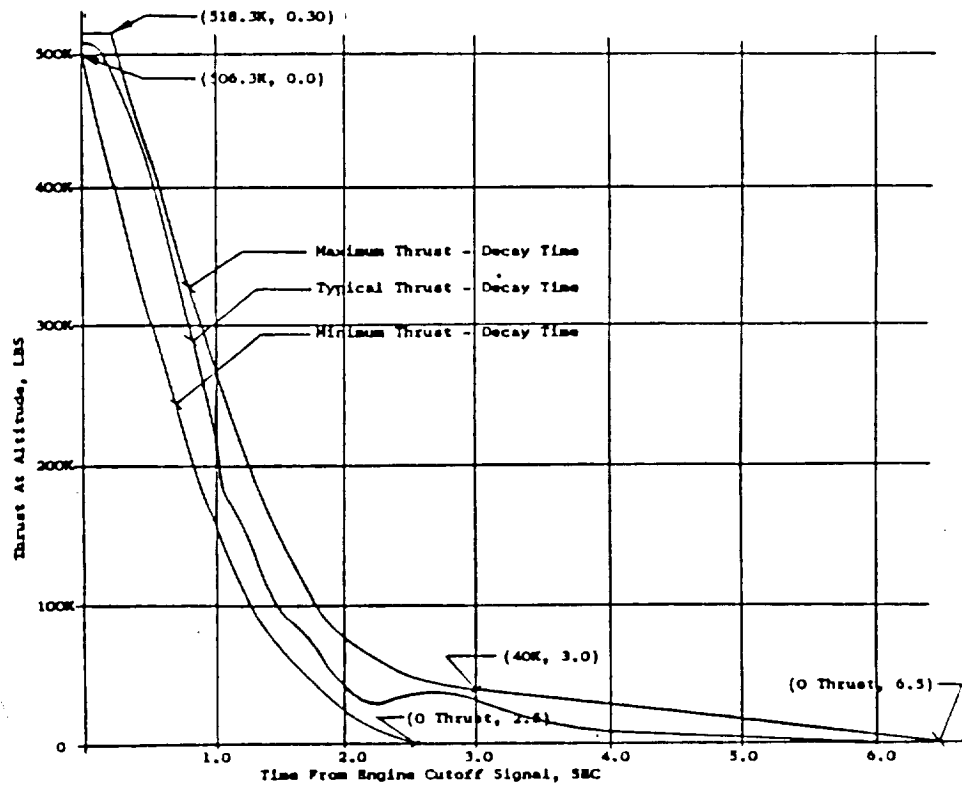
Figure 4.2. SSME Engine Shutdown Thrust Decay from FPL (Altitude)
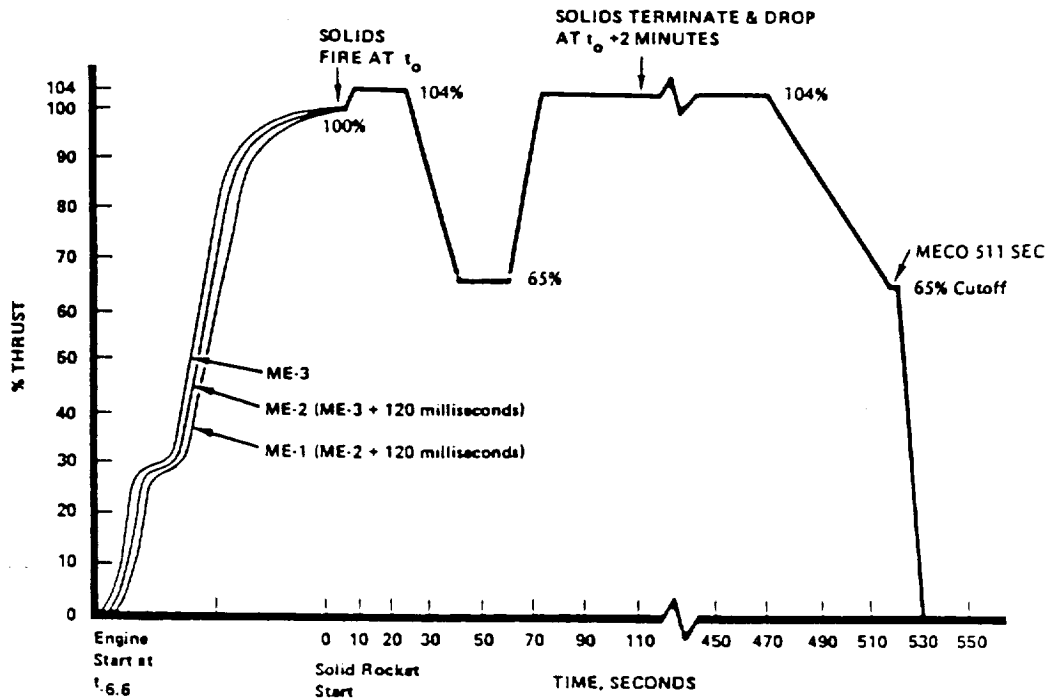
Figure 4.3. SSME Typical Flight Profile

nominal values of the engine. Tag values are obtained by adjusting 41 random variables relating to engine hardware parameters in the engine performance model such that measured variables match measurements from the acceptance tests of the engine. The deterministic adjustment removes the engine-to-engine variation and allows the engine influence coefficient model to accurately predict the engine performance.

It is known that engine-to-engine variations, due to manufacturing and other environmental conditions, are significant. A list of 46 random variables listed in Table 4.3 was developed to account for variations in hardware. The variations were based on consultations with component experts to define how much each item was expected to vary from a manufacturing, performance, or test-to-test basis. The performance unit then combined these variations with design requirements and knowledge of past engine performance to develop a set of variances for the random variables. The combined effect of these variables

4-4

Table 4.1. SSME Table of Influence Coefficients

Independent Parameter	Nominal Value
1 Commanded mixture ratio	6.0000
2 Fuel inlet total pressure (psia)	30.0000
3 Oxidizer inlet total pressure (psia)	100.0000
4 Fuel inlet temperature (R)	37.0000
5 Oxidizer inlet temperature (R)	164.0000
6 HPFTP turbine efficiency multiplier	1.0090
7 HPFTP turbine flow multiplier	1.0125
8 HPOTP turbine efficiency multiplier	1.0152
9 HPOTP turbine flow multiplier	0.9741
10 T/C characteristic velocity multiplier (C*)	1.0004
11 Main fuel valve resistance	0.0138
12 Main oxidizer valve resistance	0.0107
13 Coolant control valve resistance	$-1.942890E-16$
	$1.000000E+00$
	$0.000000E+00$
	$0.000000E+00$
14 FPB fuel injector resistance	0.1550
15 OPB fuel injector resistance	0.6850
16 LPFTP turbine inlet orifice resistance	0.7160
17 LPFTP turbine nozzle area (in^2)	0.9500
18 Oxidizer pressurant flowrate (lb/sec)	$3.666887E+01$
	$-9.966946E+01$
	$9.016788E+01$
	$-2.711157E+01$
19 Fuel pressurant flowrate (lb/sec)	$1.676685E-01$
	$1.764161E+00$
	$-3.111869E-01$
	$0.000000E+00$
20 LPOTP Pump cavitation correction	1.0000
21 LPOTP Pump cavitation correction	1.0000
22 LPOTP Pump cavitation correction	1.0000
23 LPOTP Pump cavitation correction	1.0000

Remarks: A one percent increase in the independent parameter
will cause the percentage change in the dependent
parameter as given by the curve-fit coefficients
listed below.

Table 4.2. SSME Influence Coefficient Dependent Parameters for CLS

1. HPOTP TURBINE SPEED (RPM)
2. HPFTP TURBINE SPEED (RPM)
3. HPOTP PUMP DISCHARGE PRESS.(PSIA)
4. HPFTP PUMP DISCHARGE PRESS.(PSIA)
5. OPB CHAMBER PRESSURE (PSIA)
6. FPB CHAMBER PRESSURE (PSIA)
7. ENGINE OXIDIZER FLOWRATE (LB/SEC)
8. ENGINE FUEL FLOWRATE (LB/SEC)
9. ENGINE THRUST (LB)
10. OXIDIZER PRESS. FLOWRATE (LB/SEC)
11. FUEL PRESSURANT FLOWRATE (LB/SEC)
12. OPB OXIDIZER VALVE POSITION
13. FPB OXIDIZER VALVE POSITION
14. MCC OXIDIZER INJECTOR PRESS (PSIA)
15. MCC OXIDIZER INJECTOR TEMP (R)
16. HOT GAS INJECTOR PRESSURE (PSIA)
17. MCC INJECTOR END PRESSURE (PSIA)
18. HPOTP PUMP INLET PRESSURE (PSIA)
19. HPFTP PUMP INLET PRESSURE (PSIA)
20. PB PUMP DISCHARGE PRESSURE (PSIA)
21. HPOTP PUMP INLET TEMPERATURE (R)
22. HPOTP PUMP DISCHARGE TEMP. (R)
23. HPFTP PUMP DISCHARGE TEMP. (R)
24. MFV DISCHARGE TEMPERATURE (R)
25. PB PUMP DISCHARGE TEMP. (R)
26. HPFTP PUMP INLET TEMPERATURE(R)
27. LPOTP TURBINE SPEED (RPM)
28. LPFTP TURBINE SPEED (RPM)
29. HPOT DISCHARGE TEMP (R)
30. HPFT DISCHARGE TEMP (R)
31. OPB OXIDIZER VALVE RESISTANCE
32. FPB OXIDIZER VALVE RESISTANCE
33. OXIDIZER PRESSURANT PRESSURE (PSIA)
34. FUEL PRESSURANT TEMPERATURE(R)

35. OXIDIZER PRESSURANT TEMPERATURE (R)
36. FUEL PRESSURANT TEMPERATURE (R)
37. LPOTP PUMP SUCTION SPECIFIC SPEED
38. LPFTP PUMP SUCTION SPECIFIC SPEED
39. HPOTP PUMP SUCTION SPECIFIC SPEED
40. HPFTP PUMP SUCTION SPECIFIC SPEED
41. MCC COOLANT DISCHARGE PRESSURE (PSIA)
42. MCC COOLANT DISCHARGE TEMPERATURE (R)
43. LPOTP TURBINE TORQUE (FT-LB)
44. LPFTP TURBINE TORQUE (FT-LB)
45. HPOTP TURBINE TORQUE (FT-LB)
46. HPFTP TURBINE TORQUE (FT-LB)
47. LPOTP TURBINE FLOWRATE, LBM/S
48. LPFTP TURBINE FLOWRATE, LBM/S
49. HPOTP TURBINE FLOWRATE, LBM/S
50. HPFTP TURBINE FLOWRATE, LBM/S
51. LPOTP TURBINE INLET PRESSURE, PSIA
52. LPFTP TURBINE INLET PRESSURE, PSIA
53. HPOTP TURBINE INLET PRESSURE, PSIA
54. HPFTP TURBINE INLET PRESSURE, PSIA
55. LPOTP TURBINE INLET TEMPERATURE, (R)
56. LPFTP TURBINE INLET TEMPERATURE, (R)
57. HPOTP TURBINE INLET TEMPERATURE, (R)
58. HPFTP TURBINE INLET TEMPERATURE, (R)
59. LPOTP TURBINE DISCHARGE PRESS., PSIA
60. LPFTP TURBINE DISCHARGE PRESS., PSIA
61. HPOTP TURBINE DISCHARGE PRESS., PSIA
62. HPFTP TURBINE DISCHARGE PRESS., PSIA

are used in the definition of max/min conditions used for the engine balance limits. These max/min conditions, together with the design limits of the engine inlet conditions, are used for design purpose as boundaries to check that the engine operation will satisfactorily continue into another test or flight.

The engine dynamic (transient) simulation model is also formulated using generic engine process descriptions, constitutive equations, and detailed tabulation of propellant physical properties. The description of the basic processes of the system simulation involves all applicable static and dynamic formulations considered important in accurately representing the overall behavior of the engine during start, mainstage control, and cutoff. The validity and veracity of these process descriptions, in terms of their ability to describe the overall system behavior, have been proven by correlation of simulation results with engine test results from previously developed rocket engines.

Table 4.3.   SSME Model Random Variables

VARIABLE NAME	2σ VARIATION %	POWER HEAD	LPFTP	LPOTP	HPFTP	HPOTP	NOZZLE	HEAT EXCHANGER
1. Main Chamber Throat Area	0.2	X	X	X	X	X	X	X
2. Efficiency C_F (thrust coefficient)	0.2	X	X	X	X	X	X	X
3. Efficiency C* (characteristic velocity)	0.25	X	X	X	X	X	X	X
4. Chamber Coolant Resistance	8.0	X	X		X		X	
5. Main Oxidizer Injector Resistance	5.0	X		X	X	X		X
6. Main Hot Gas Injector Resistance	5.0	X			X	X	X	X
7. FPB Fuel Injector Resistance	2.0	X			X	X	X	X
8. OPB Fuel Injector Resistance	2.0	X			X	X	X	X
9. Fuel Hot Gas Manifold Resistance	10.0	X	X		X	X	X	X
10. LOX Hot Gas Manifold Resistance	10.0	X	X		X	X	X	X
11. Main LOX Dome Resistance	4.0	X		X	X	X		X
12. OP2 Discharge Duct Resistance (HPOT discharge press.)	4.0	X		X	X	X		X
13. LPFT Nozzle Area	2.0	X	X		X	X	X	
14. LPOP Efficiency	1.0			X		X		
15. LPOT Efficiency	4.0			X		X		
16. LPOT Nozzle Area	2.0			X		X		
17. HPFP Efficiency	1.6	X	X	X	X	X	X	X
18. HPFT Efficiency	2.0	X	X	X	X	X	X	X
19. HPFT Nozzle Area	2.0	X	X	X	X	X	X	X
20. HPOP Efficiency	0.8	X	X	X	X	X	X	X
21. HPOT Efficiency	2.0	X	X	X	X	X	X	X
22. HPOP Head Coefficient	0.8					X		
23. HPFP Head Coefficient	1.6				X			
24. HPOT Nozzle Area	2.0	X			X	X	X	
25. Preburner Pump Efficiency	0.8					X		
26. Preburner Pump Head Coefficient	0.8					X		
27. Chamber Coolant Valve Resistance	17.6		X		X		X	
28. Main LOX Valve Resistance	12.7			X		X		
29. Main Fuel Valve Resistance	12.7		X		X			
30. Primary Faceplate Resistance	15.0	X	X		X		X	
31. Secondary Faceplate Resistance	15.0	X	X		X		X	
32. MCC Baffles Resistance	6.6	X	X		X		X	
33. Heat Exchanger Bypass Resistance	2.63*							X
34. Heat Exchanger Tube Thickness A	8.5*							X
35. Thrust	1.3	X	X	X	X	X	X	X
36. Engine Mixture Ratio	1.0	X	X	X	X	X	X	X
37. GOX Tank Press.	100.0*							X
38. GH2 Tank Press.	100.0*	X					X	
39. HPOP COV	5.0	X	X	X	X	X	X	X
40. LPOP Head Coefficient	2.0			X				
41. LPFP Head Coefficient	2.0		X					
42. Nozzle Coolant Res.	8.0	X	X		X	X	X	X
43. LPFT In Duct Res.	4.0		X		X			
44. LPOT Area	2.0			X		X		
45. Nozzle ΔT	5.0	X	X		X		X	X
46. MCC Coolant ΔT	8.0	X	X		X		X	X

*Note: not relevant to CLS work

The transient phase of the load definition is based on a combination of vehicle requirements, engine simulation models and engine test results. Typical vehicle requirements were discussed earlier: start and cutoff transient envelopes specified to minimize vehicle loads. Additional requirements, like rates of power level changes during throttling and associated up-thrusts, are additional requirements that size-control some of the nominal loads on components during transient operation. Thrust control drives pump speeds, torques, and system pressures and temperatures. Generally, the dynamic simulation models are used for transient conditions below 65% power level. Various transient models are employed for surveying system characteristics, tradeoff and optimization of the control system, and evaluating system design changes simulating nonlinear operating conditions.

The dynamic simulation models and steady-state performance models describe the same processes; however, the performance models stress accuracy of steady-state operation parameters, but the dynamic simulation models have to consider the overall system behavior throughout the duty cycle. Figure 4.1 shows how the SSME thrust buildup is contractually controlled. The shape of the thrust buildup, as well as the shape of the transient duty cycle loads, are governed by the event sequences defined for startup and shutdown transients.

The SSME start transient event sequence is shown in Figure 4.4. These events are control system parameters, e.g., either valve opening conditions or analysis events known to occur in the transient operation, such as injector dome priming, fuel side oscillation. They can be related to surges, large thermal transients, chugging, pops, and sideloads.

The dynamic simulation model is essentially a nominal operation description of engine startup and shutdown operations.

The engine performance model and the dynamic simulation model furnish the system's operating load conditions: pressures, temperatures, vibration levels for inlet and outlet conditions of transfer ducts, preburners, injectors, and turbopumps (Figure 4.5). These interface loads are used with deterministic models to evaluate loads on individual components like turbine blades,
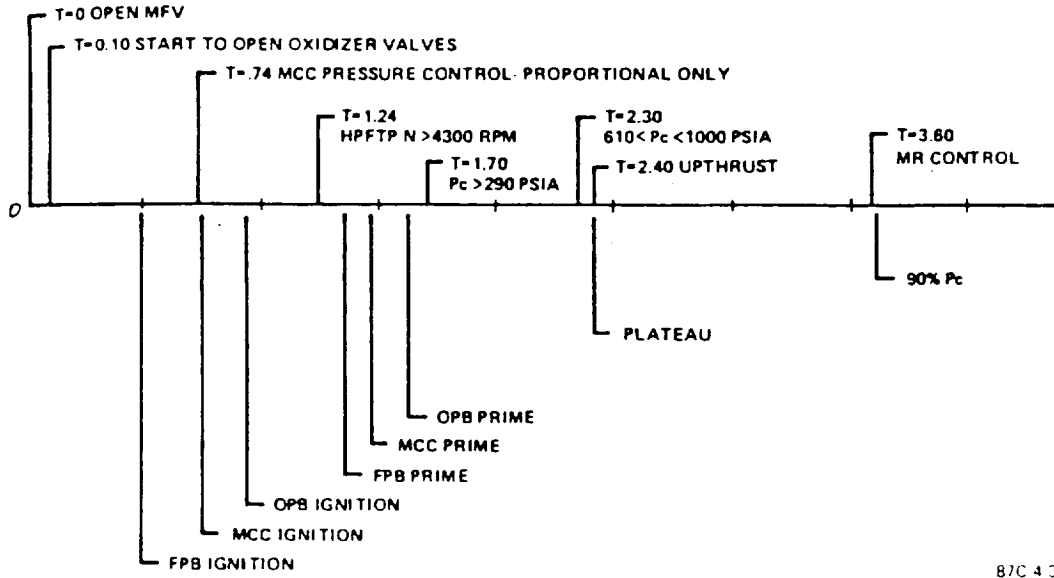
Figure 4.4. SSME Start Timeline
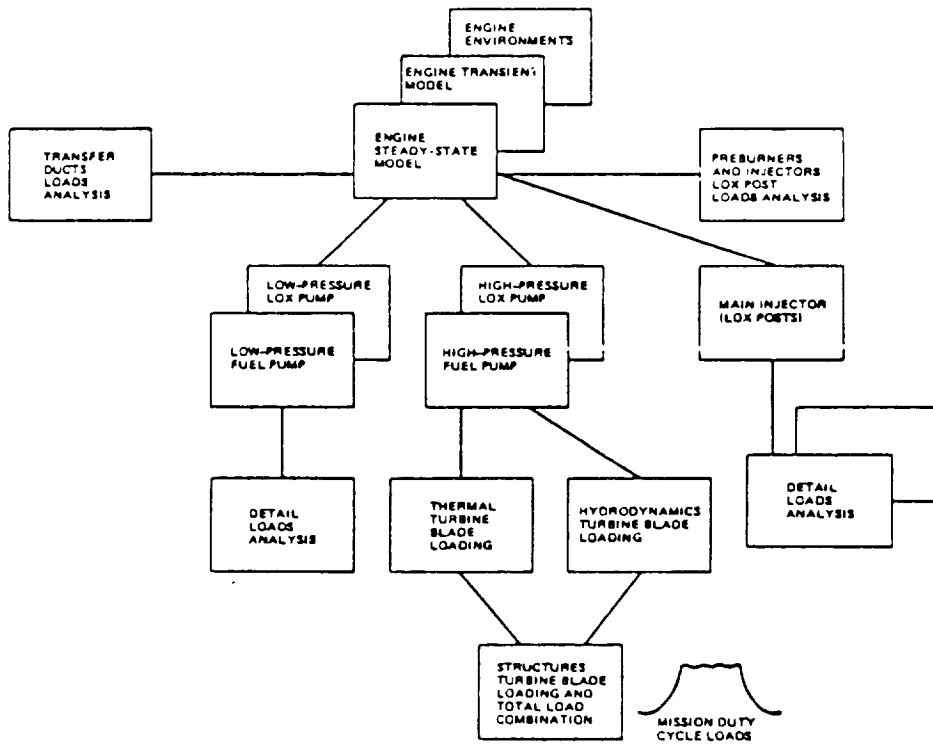
Figure 4.5. Interrelation of SSME Analysis Models

4-9

transfer ducts, LOX posts, etc. For instance, the steady-state loads are used by the hydrodynamics specialists to determine loads across each turbine stage or blade. The heat transfer specialists use information from the same model results to determine blade temperatures. The dynamics experts use the model results to determine turbine blade dynamics. The structural and analysis experts use model information and input loads from other experts to develop the total load and structural analysis.

4.3 Probabilistic Load Models

The engine performance model, dynamic simulation model, and other deterministic models are too complex to be used as basic tools to synthesize engine loads. The CLS approach to probabilistic load development is to synthesize loads with information extracted from engine data and detail analysis results of the deterministic engine load models. The CLS probabilistic load models treat the engine operation as a stochastic process. The engine hardware parameters, operating inlet condition variables, and all engine loads are assumed to be random variables. Scaling models are utilized whenever possible.

The influence model developed for engine performance evaluation is ideal for CLS. It is a numerical abstract of the engine model. It can evaluate engine loads for different power levels. With the random variable assumption, probabilistic methods can be applied to the influence model to obtain load distributions. This probabilistic influence model thus becomes the CLS system-level engine model. It provides all of the system's operating loads subsequently used by component load models to generate component loads.

The probabilistic influence model utilizes influence coefficients to correlate changes in engine operating parameters and inlet condition variables (classified as system-independent loads) to changes in system operating conditions and performance variables classified as system-dependent loads. The influence equation is:

$$\frac{\text{del } Y_i}{Y_{io}} = \sum_j (IC)_{ij} \frac{\text{del } X_j}{X_{jo}} \tag{4.1}$$

where, X_{jo} is the nominal value of the jth engine independent load

$\text{del } X_j$ is the change in the jth independent load

Y_{io} is the nominal value of the ith dependent load

$\text{del } Y_i$ is the change in the ith dependent load

$(IC)_{ij}$ is the influence coefficient correlating the jth independent load to the ith dependent load

With few exceptions, the nominal values for the independent loads are not varied with the command power level. The nominal values for dependent loads and influence coefficients are functions of power level. Their variations are fitted into a polynomial function of the commanded power level as below:

$$Y_{jo} = a_0 + a_1{}^*T + a_2{}^*T{}^*T + a_3{}^*T{}^*T{}^*T$$
$$(IC)_{ij} = c_0 + c_1{}^*T + c_2{}^*T{}^*T + c_3{}^*T{}^*T{}^*T$$

where, a_i's and c_i's are constant coefficients,

T is the commanded power level in fraction of the rated power.

The probabilistic influence model implemented on the load-expert system has 23 system-independent loads as listed in Table 4.1 and 62 system-dependent loads as listed in Table 4.2. The distribution information of independent loads is obtained based on a 10-sec average database of the SSME flight and test data. These load parameters are stored in the load-expert system knowledge base in database format. They can be conveniently retrieved and updated.

The deterministic influence model is valid for the power range from 65% to 110% power levels. In CLS, the power range of the probabilistic influence model is extended down to zero. The complete duty cycle of the engine operation is therefore modeled by the same influence model. During the transient phase of the duty cycle, a quasi-steady state is assumed, i.e., the loads behave as steady-state loads within each time step. Discussion on the duty cycle load calculation and transient model is deferred to next section.

Verification of the probabilistic influence model was performed by comparing load calculations with the SSME 10-sec average database. The general finding is that variations of the system loads, as calculated with the probabilistic influence model, do not cover the corresponding variations of the SSME 10-sec average database. Initially, the load calculations were thought to be related to instrumentation measurement errors as the HPFTP discharge temperature calculation was under investigation. However, the same thing happened when the pump speed calculation was evaluated. The pump speed measurement has about the best measurement accuracy. This pointed out the inadequacy of the probabilistic model.

The SSME 10-sec average database includes data from flights and tests. The database includes data from numerous engines. Variations in the database consist of engine-to-engine variations and test-to-test variations. Engine-to-engine variations account for the changes in engine hardware, whereas test-to-test variations account for variations from different tests of an engine. In the deterministic modeling, tag values are used to account for engine-to-engine variations due to the use of different engines as well as changing components. Tag values are calculated by the engine performance model. The tag value method does not quite fit into the probabilistic influence model because tag values have to come from outside of the model.

It is known that engine-to-engine variations are related to engine hardware. Different manufacturing processes, different manufacturers, and different assembling procedures, etc. all contribute to hardware variations. A set of random variables related to engine hardware, as listed in Table 4.3, has been determined to have significant effect on components of interest in this project. As shown in Table 4.3, the letter X in each column indicates sig-nificant effects of the hardware random variable to the hardware identified at the top of the column. These random variables fit naturally into the proba-bilistic influence model as system-independent hardware parameter variables. Therefore, an expanded list of engine system-independent loads and dependent loads were developed for the next version of the CLS engine load model. The new list of system-independent loads with their means and coefficients of

variation is shown in Table 4.4. System-dependent loads are shown in Table 4.5. A new influence coefficient set is required for the expanded list of engine system loads. The probabilistic influence model with the expanded set of influence coefficients will be implemented on the CLS load-expert system during the option phase of the project. To reiterate, this is an excellent solution to meet contract requirements for modeling a generic engine, not necessarily of the SSME type.

With the probabilistic influence model as the overall engine system model synthesizing system interface loads or system-dependent loads, various component load models can be built on the next level (ref. Figure 2.3). The component load models use system-dependent loads as input loads and generate component loads local to the components. In modeling component loads, generic scaling technique and influence method are employed. The goal is to build generic models which can be utilized across different components and for different engines. This goal has been satisfied. The CLS now has a generic static pressure scaling model, a generic probabilistic thermal load model, and a generic fluctuation pressure load. These models will be described in the CLS load implementation section.

5747a/bes

Table 4.4. Engine Influence Model Independent Loads

ID	INDEPENDENT LOAD	NOMINAL VALUE	C.O.V.
1	Commanded mixture ratio	6.0	0.002
2	Fuel inlet pressure (psia)	30.0	0.259
3	Oxidizer inlet pressure (psia)	100.0	0.327
4	Fuel inlet temperature (R)	37.0	0.016
5	Oxidizer inlet temperature (R)	164.0	0.011
6	Fuel pressurant flowrate (lbm/sec)	0.7	0.0065
7	Oxidizer pressurant flowrate (lbm/sec)	1.5968	0.015
8	HPFP cavitation (%)	1.0	0.001
9	LPFP cavitation (%)	1.0	0.001
10	LPOP cavitation (%)	1.0	0.001
11	Nozzle, mixer delta P (%)	1.1455	
12	MCC throat diameter (in)	10.293	0.001
13	Nozzle exit diameter (in)	90.324	0.001
14	LPFT nozzle area (in^2)	0.95	0.1
15	LPOT nozzle area (in^2)	1.386	0.1
16	LPFP efficiency (%)	1.11	0.0017
17	HPFP efficiency (%)	1.00	0.008
18	LPFT efficiency (%)	1.025	0.0027
19	HPFT efficiency (%)	1.0355	0.01
20	LPOP efficiency (%)	1.14	0.005
21	HPOP efficiency (%)	1.02	0.004
22	PBP efficiency (%)	1.022	0.0016
23	LPOT efficiency (%)	1.022	0.02
24	HPOT efficiency (%)	1.0152	0.01
25	HPOP cavitation (%)	1.0	0.001
26	LPFP head coefficient (%)	0.99	0.007
27	HPFP head coefficient (%)	1.0237	0.008
28	LPOP head coefficient (%)	1.0	0.013
29	PBP head coefficient (%)	1.155	0.004
30	MCC OX dome resistance	0.0384	0.02
31	HGM OX side resistance	0.0032	0.05
32	HGM fuel side resistance	0.0275	0.05
33	MCC Hot Gas injector resistance	0.0031	0.025
34	HGM coolant OX side resistance	0.1040	
35	LPOP disch duct resistance	0.0021	
36	Primary faceplate resistance	15.0	0.075
37	Secondary faceplate resistance	11.17	0.075
38	LPFT seal resistance	7283.0	
39	HPOT coolant circuit resistance	2066.0	
40	HPFP disch duct resistance	0.0123	
41	Main fuel valve resistance	0.0138	0.064
42	Main oxidizer valve resistance	0.0107	0.064
43	MCC OX injector resistance	0.0602	0.025
44	MCC cooling jacket delta pressure	1.031	

Table 4.4.   Engine Influence Model Independent Loads (Continued)

ID	INDEPENDENT LOAD	NOMINAL VALUE	C.O.V.
45	OPB fuel injector resistance	0.685	0.01
46	FPB fuel injector resistance	0.155	0.01
47	LPFT disch duct resistance	0.104	
48	LPFT inlet duct & F-7 resistance	0.5689	0.01
49	PBP inlet duct resistance	0.134	
50	Coolant control valve resistance	0.05568	0.088
51	Baffle flow coefficient	0.95	
52	PB fuel supply duct resistance	0.0071	
53	Nozzle delta P (%)	0.6889	
54	HPOTP turb-end bearing coolant res	65000.0	
55	MCC combustion efficiency (MCC C*)	1.0004	0.001
56	Nozzle heat load (%)	0.884	
57	MCC chamber heat load (%)	0.7932	
58	HPFT flow coefficient	1.0125	0.01
59	HPOT flow coefficient	0.9741	0.01
60	Preburner combustion efficiency (%)	0.98	
61	Mixer delta P (%)	1.0	
62	LOX flow constant (c2)	2.8952	
63	MCC pc measurement error (%)	1.0	
64	Engine fuel flowmeter error (%)	1.0	

Table 4.5. Engine Influence Model Dependent Loads

ID	INDEPENDENT LOAD	NOMINAL VALUE	C.O.V.
1	Engine altitude thrust (lbf)	471067.522	0.005
2	HPOTP speed (rpm)	27239.145	0.004
3	HPFTP speed (rpm)	34517.69	0.008
4	HPOP disch pressure (psia)	1595.403	0.0089
5	PB pump disch pressure (psia)	7185.46	0.0098
6	HPFP disch pressure (psia)	6161.829	0.009
7	OPB chamber pressure (psia)	5039.427	0.0129
8	FPB chamber pressure (psia)	4876.04	0.0137
9	Engine oxidizer flowrate (lbm/sec)	894.34	0.0062
10	Engine fuel flowrate (lbm/sec)	149.06	0.0069
11	Oxidizer pressurant flowrate(lbm/sec)	1.5968	0.015
12	Fuel pressure flowrate (lbm/sec)	0.6996	0.0065
13	OPB oxidizer valve position (%)	0.6495	0.0147
14	FPB oxidizer valve position (%)	0.7652	0.0135
15	MCC oxidizer injector pressure(psia)	3540.82	0.0086
16	MCC Hot Gas injector pressure (psia)	3237.36	0.0064
17	MCC injector end pressure (psia)	3006.0	0.0058
18	HPOP inlet pressure (psia)	380.07	0.0228
19	HPFP inlet pressure (psia)	226.084	0.0263
20	HPOP disch temperature (R)	190.195	0.002
21	HPFP disch temperature (R)	94.904	0.0114
22	MFV disch temperature (R)	95.491	0.0114
23	PB pump disch temperature (R)	203.377	0.0025
24	HPOP inlet temperature (R)	169.425	0.006
25	HPFP inlet temperature (R)	42.472	0.0019
26	LPOTP speed (rpm)	5042.8	0.008
27	LPFTP speed (rpm)	15850.64	0.0087
28	HPOT disch temperature (R)	1352.533	0.0274
29	HPFT T/D disch temperature (R)	1625.723	0.0193
30	OPB oxidizer valve resistance	130.79	0.098
31	FPB oxidizer valve resistance	13.18	0.15
32	Oxidizer pressurant pressure (psia)	3439.598	0.0092
33	Fuel pressurant pressure (psia)	3348.296	0.0079
34	Oxidizer pressurant temperature (R)	838.0	0.0245
35	LPFT disch temperature (R)	472.95	0.0125
36	LPOP suction specific speed (NSS)	8054.341	0.02
37	LPFP suction specific speed (NSS)	19738.26	0.02
38	HPOP suction specific speed (NSS)	11295.08	0.0185
39	HPFP suction specific speed (NSS)	6017.04	0.024
40	MCC coolant disch pressure (psia)	4840.48	0.0108
41	LPOT torque (ft-lbf)	1565.124	0.0159
42	LPFT torque (ft-lbf)	996.605	0.0182
43	HPOT torque (ft-lbf)	4436.78	0.0108
44	HPFT torque (ft-lbf)	9452.388	0.0142

Table 4.5. Engine Influence Model Dependent Loads (Continued)

ID	INDEPENDENT LOAD	NOMINAL VALUE	C.O.V.
45	LPOT flowrate (lbm/s)	176.17	0.01
46	LPFT flowrate (lbm/s)	26.46	0.0175
47	HPOT flowrate (lbm/s)	58.95	0.01
48	HPFT lfowrate (lbm/s)	158.92	0.0107
49	LPOT inlet pressure (psia)	3947.348	0.0895
50	LPFT inlet pressure (psia)	4508.63	0.0105
51	HPOT inlet pressure (psia)	5019.85	0.00875
52	HPFT inlet pressure (psia)	4857.17	0.0095
53	LPOT inlet temperature (R)	190.195	0.002
54	LPFT inlet temperature (R)	489.121	0.0122
55	HPOT inlet temperature (R)	1501.062	0.0266
56	HPFT inlet temperature (R)	1812.757	0.0186
57	LPOT disch pressure (psia)	414.28	0.0208
58	LPFT disch pressure (psia)	3403.035	0.0076
59	HPOT disch pressure (psia)	3318.146	0.0066
60	HPFT disch pressure (psia)	3439.885	0.0067
61	LPOT power (bhp)	1502.269	0.024
62	LPFT power (bhp)	3013.01	0.027
63	HPOT power (bhp)	23012.439	0.0155
64	HPFT power (bhp)	62192.2	0.0175
65	HGM inlet pressure, fuel (psia)	3356.87	0.0075
66	HGM inlet pressure, OX (psia)	3302.345	0.0075
67	Oxidizer T/D dynamic pressure (psia)	16.6	0.01
68	Oxidizer T/D flow velocity (ft/s)	454.81	0.01
69	Fuel T/D dynamic pressure (psia)	25.72	0.01
70	Fuel T/D flow velocity (ft/s)	578.4	0.01
71	HPOT mixture ratio (O/F)	0.7323	0.034
72	HPFT mixture ratio (O/F)	0.9267	0.0227
73	OPB power (bhp)	168661.0	0.02
74	FPB power (bhp)	544895.0	0.02
75	MCC power (bhp)	1.2473E+07	0.005
76	OPB OX in manifold pressure (psia)	5927.91	0.013
77	OPB fuel in manifold pressure (psia)	5360.543	0.0085
78	FPB OX in manifold pressure (psia)	6088.94	0.0137
79	FPB fuel in manifold pressure (psia)	5400.416	0.0088
80	PBP disch, PB OX supply temp (R)	203.377	0.0025
81	Mixer disch, PB fuel supply temp (R)	275.777	0.0045
82	Fuel HGM velocity (ft/s)	1322.532	0.01
83	Fuel HGM dynamic pressure (psia)	132.983	0.01
84	LOX HGM velocity (ft/s)	214.13	0.01
85	LOX HGM dynamic pressure (psia)	3.737	0.01
86	OPB fuel dynamic pressure (psia)	0.1978	0.01
87	OPB fuel flow velocity (ft/s)	367.214	0.01
88	FPB fuel dynamic pressure (psia)	44.647	0.01

Table 4.5. Engine Influence Model Dependent Loads (Continued)

ID	INDEPENDENT LOAD	NOMINAL VALUE	C.O.V.
89	FPB fuel flow velocity (ft/s)	411.96	0.01
90	HPOP disch dynamic pressure (psia)	230.658	0.01
91	HPOP disch velocity (ft/s)	174.213	0.0052
92	HPOP head rise (ft)	7545.048	0.0095
93	HPFP disch dynamic pressure (psia)	123.277	0.01
94	HPFP disch velocity (ft/s)	469.11	0.0055
95	HPFP head rise (ft)	174050.04	0.0085
96	PBP disch dynamic pressure (psia)	32.48	0.01
97	PBP disch velocity (ft/s)	65.14	0.0052
98	HGM coolant inlet pressure (psia)	3346.037	0.0074
99	Engine nozzle exit velocity (ft/s)	14562.83	0.01

5.0 PROBABILISTIC METHODOLOGY

5.1 Introduction

This section reports on the progress and development of the probabilistic load model for generic space propulsion engines. This effort is part of the program being conducted by Rocketdyne and Battelle Columbus Division for NASA Lewis Research Center to develop an expert system to predict composite loads in a generic space propulsion engine. The ultimate goal of the program is to address generic engines that may include different mission profiles or incorporate design changes. The program requires that a robust and general probabilistic approach be adopted for inclusion in the expert system model. During the first year of the program, a survey was conducted to select these models and the initial programming, debugging, and shake-down analyses were performed. The second year of the program was oriented towards building the probabilistic methodology. A database was developed that could be used by both the probabilistic methodology and the expert system. The database included different functional forms for the load description, model verification and validation, and the generalization of the computer program system. The third year of the program focused primarily on the refinement of current methodology, improvement of the transient load model, incorporation of the periodic load model, verification of the probabilistic methodology, and documentation.

The probabilistic model includes three probabilistic methods: (1) a Gaussian moment propagation method which assumes that all load variables and engine parameters are normally distributed, (2) a discrete probability method (RASCAL), and (3) Monte Carlo. The Gaussian moment propagation method, referred to as the Quick Look Model (QLM) provides a fast, efficient method for determining the composite load distribution, providing that basic variable distributions are not severely skewed. RASCAL is a discrete method capable of handling standard distributional forms (e.g., normal, lognormal, Weibull, etc.), and nonstandard forms such as bi-modal. RASCAL also provides a range

of levels for accuracy. RASCAL also performs important sampling used to examine regions of concern for the composite load although such values would be unexpected during nominal engine operation. Finally, Monte Carlo analysis is available so that classical confidence limits can be obtained to assess the accuracy of the composite load prediction.

All phases of the mission history profile are addressable by the probabilistic load model. Currently, each mission profile is divided into phases defined as transient, quasi-steady, or steady-state phases. The transient phase is characterized by rapid changes in the amplitude of individual loads and engine parameters. Rapid changes allow the program to ignore small oscillations about the much larger nominal load fluctuations. Uncertainty in the load is caused by variability in the peak load value and its time of occurrence. The quasi-steady phase is that portion of the mission where the nominal value of the load is slowly changing and can thus be approximated by staircase type quasi-steady state steps. The steady-state region is where the nominal values of all of the individual and composite loads are approximately constant. Unlike the transient phase, both the quasi-steady and steady-state phase do have fluctuations superimposed upon the nominal behavior. Additionally, each of these phases can have spike values superimposed which represent the occurrence of rare events.

5.2 Probabilistic Methods Quick Look Model

In some analysis, only an approximation to the variability of the load is needed. In such a case, the relatively long running time of RASCAL or Monte Carlo simulation models is not justified. To provide a program which quickly calculates such an approximation, the QLM was developed.

The basic assumption made in the QLM model is that all of the individual loads and engine parameters used to predict individual and composite loads are normally distributed. In this case, the influence function tables can be used

directly to calculate the mean and variance of the output. If there are dependencies among variables, then some modification to the current program is needed. However, if the correlation coefficient is provided or calculated, then exact solutions are still available. The basic formulas used to perform these calculations are given by the algebra of normal distributions presented below. In these formulas, μ represents the mean or expected value of the random variable, and σ is the standard deviation, i.e., the square root of the variance.

These formulas are used in conjunction the influence equations to provide mean and variance estimates of load variables. Since influence functions currently in the probabilistic load model do not involve any divisions, all of the formulations are exact (assuming independence), if the probability density functions are all Gaussian.

Statistics Of The Sum: Z = X + Y

$$E[Z] = \mu_x + \mu_y$$

$$VAR[Z] = \sigma_x^2 + \sigma_y^2 + 2\rho\sigma_x\sigma_x \qquad (3)$$

Statistics Of The Difference: Z = X - Y

$$E[Z] = \mu_x - \mu_y$$

$$VAR[Z] = \sigma_x^2 + \sigma_y^2 - 2\rho\sigma_x\sigma_y \qquad (4)$$

Statistics Of The Product: Z = X * Y

$$E[Z] = \mu_x * \mu_y + \rho\sigma_x\sigma_y$$

$$VAR[Z] = \mu_y^2\sigma_x^2 + \mu_y^2\sigma_x^2 + \sigma_x^2\sigma_y^2 2\rho\mu_x\mu_y\sigma_x\sigma_y + \rho^2\sigma_x^2\sigma_y^2 \qquad (5)$$

Statistics Of The Quotient: Z = Y / X

$$E[Z] \simeq \frac{\mu_y}{\mu_x} \left[1 + \frac{\sigma_x}{\mu_x} \left(\frac{\sigma_x}{\mu_x} - \rho \frac{\sigma_y}{\mu_y} \right) \left(1 + 3 \frac{\sigma_x^2}{\mu_x^2} + \ldots \right) \right]$$

$$VAR[Z] \simeq \frac{\mu_y^2}{\mu_x^2} \left[\frac{\sigma_x^2}{\mu_x^2} + \frac{\sigma_y^2}{\mu_y^2} - 2\rho \frac{\sigma_x \sigma_y}{\mu_x \mu_y} + 8 \frac{\sigma_x^4}{\mu_x^4} \right] \tag{6}$$

Two options exist in the computer code for using the QLM model. If the user requests that the QLM model be used and all of the input distributions are not normal, then the corresponding mean and variance are calculated by the appropriate moment transformation. On the other hand, if the user does not request the QLM model, yet all input distributions are gaussian, then the QLM model is substituted. The QLM substitution is made since there is no reason to run a simulation to approximate an answer which can be obtained exactly with the QLM model.

Discrete Probability Distribution Method

Discrete probability distributions (DPDs) are tools in risk analysis to simplify the computations necessary to determine failure probabilities. DPDs may be used to investigate probabilistic functions: (1) functions whose exact form is uncertain, and (2) calculation of quantities where there is significant uncertainty numerical quantities that should be replaced by probability distributions. Mathematical operations between these quantities should be replaced by analogous operations between probability distributions.

Suppose the initial values of loads are discretized into M values. Each value of each variable is then assigned a probability of occurrence. If these

discrete values are paired with their probabilities, the following vectors of ordered pairs result for two loads, X and Y:

$$X = (X_1, p_1), (X_2, p_2), \ldots, (X_m, p_m))$$

$$Y = (Y_1, q_1), (Y_1, q_2), \ldots, (Y_m, q_m)).$$

The number of discrete points in each of these vectors has been chosen to be the same, although it is not necessary to do so. The addition of two discrete vectors is defined by

$$Z = Y + X$$

$$Z = (Y_i, p_i) + (X_j, q_j), \text{ and}$$

$$Z = (X_j + Y_i, p_i q_j) \text{ for all i and j.}$$

Therefore, the addition of two vectors containing m-ordered pairs results in each vector having m^2-ordered pairs. The multiplication of DPDs is similarly defined:

$$Z = X * Y$$

$$Z = [X_j * Y_i, p_i * q_j)] \text{ for all i and j}$$

For the combination of a large number of loads, the amount of computer storage increases very quickly. If there are k loads, each described by M discrete points, then the vector will contain M^k-ordered pairs. Since, even for relatively small values of M and K (on the order of 20), the computer storage capability will quickly be exceeded, it is necessary to examine some procedure for reducing this vector's size. This leads to the introduction of a condensation or aggregation procedure.

The condensation operation must preserve the total probability and mean within each vector while ensuring that the residual error afterwards is as small as possible. A new procedure for handling such problems was developed by Kurth (ref. 5.2) and has been denoted RASCAL. This algorithm is covered in detail in reference 5.2 but its basis is the DPD algorithm, even though, strictly speaking, it is not a DPD process. The RASCAL algorithm is the primary analysis method used throughout this program.

RASCAL can be summarized as follows. The input variables are discretized into DPDs denoted:

$$X_i = [X_{i,j}, P_{i,j})]$$

where

$i = 1, 2, \ldots, n$

$j = 1, 2, \ldots, ND$

n = number of variables

ND = number of discrete points

$X_{i,j}$ = conditional mean of variable i in discrete interval j

$P_{i,j}$ = probability of $X_{i,j}$

X_i = input variable i.

The input variables are related to a response, R, by some function, denoted f. Thus,

$$R = f (X_1, X_2, \ldots, X_n) .$$

At this point, it is decided how many points one wishes to use to characterize the conditional mean of each interval in R after condensation (this number is denoted by M). If

$$ND \cdot M > ND^n$$

then the standard DPD algorithm is used. This is done to minimize the calculational time since, in this case, duplicate values will be produced. If (ND•M) is less than ND^n, then n random integers between 1 and ND are generated:

$$k_1, k_2, \ldots k_n .$$

A response, R_1, is calculated by

$$R_1 = f (X_{1,k_1}, X_{2,k_2}, \cdots X_{n,kn})$$

and the associated probability is given by[†]

$$q_1 = \prod_{i=1}^{n} P_{i,k_i}$$

The process is repeated (ND•M) times to give an array of ordered pairs of the responses:

$$V = [R_1, q_1), (R_2, q_2), \ldots, (R_L, q_L)]$$

$$L = ND•M$$

Condense V to V_R, to produce the desired distribution:

$$V_R = [(R_1, P_1), (R_2, P_2), \ldots, (R_{ND}, P_{ND})]$$

[†]This calculation assumes that the input variables are independent.

The RASCAL method provides accuracy close to the Monte Carlo method in less computational time. In addition, if a given region of the input variable's range needs to be examined more accurately, RASCAL provides a means for doing so by input rather than by requiring coding changes. The RASCAL method does not provide any way to estimate the confidence level of the result available with the Monte Carlo analysis. However, the true result can be approached asymptomatically by increasing the number of data points used in individual DPDs. Later chapters in this report discuss validation of the RASCAL methodology.

Monte Carlo

The Monte Carlo technique is a method for solving problems by constructing a random process for each problem. This random process is so devised that parameters and quantities of interest may be calculated from random samples from a given distribution. In effect, it is simply a method for adding a probabilistic structure to a deterministic model.

As an example, consider a specific piece of equipment in a space propulsion engine. Suppose the composite load, denoted by $L_c(t)$, is related to the individual load $L_i(t)$, by a general function

$$L_c(t) = f(L_1(t), L_2(t), \ldots, L_n(t))$$

For instance, consider $L_c(t)$ for the turbine blades where the $L_i(t)$ are loads due to the effects of temperature, pressure, vibrational modes, and so forth. If each individual load has been characterized by a probability distribution function (PDF), then the following procedure is used during a Monte Carlo simulation:

1. The cumulative distribution function (CDF) of each individual load is generated by integrating the PDF.

2. Invert the CDF.

3. Generate a random number, r_1, between the values of 0 and 1.

4. Let $F(L_j(t_1))$ represent cumulative probability of realizing a load $L_j(t_1)$ at time step t_1. From the inverted CDF, the value of $L_j(t_1)$ is uniquely determined, where $F(L_j(t)) = r_1$.

5. Let N be the total number of individual loads. Let M be the total number of time steps, ti. Repeat Steps 3 and 4 for each $L_j(t_i)$: $1 \leq j \leq N$, for a given t_i. A value of $L_c(t_i)$, where

$$L_c(t_i) = f(L_1(t_i), L_2(t_i), \ldots, L_N(t_i))$$

is calculated. The entire process is repeated until the number of time steps exceeds M (or insufficient computer time terminates execution.

The result is an M-dimensional vector of composite loads: $(L_c(t)$, $L_c(2), \ldots, L_c(M))$. This vector is used to construct a histogram of the composite load. This histogram can now be analyzed statistically to obtain estimates of the mean, kurtosis, probability of the load being exceeded, and so on. By the law of large numbers, the vector described above approaches the continuous distribution in the limit as M tends to infinity. In order to achieve accurate results, however, the value of M must be so large that alternate sampling schemes must be utilized.

The Monte Carlo technique has been included in the probabilistic methods for the load model construction because of the accuracy which can be obtained from the model. Classical statistical estimates of the confidence level can be obtained. If the N responses calculated by the Monte Carlo simulation method are ordered from smallest to largest, then the $(100 * \alpha)$th percentile of the load can be bounded by

$$L_U = INT[N\alpha + \Phi(0.5(1+\beta))(N\alpha(1-\alpha))^{1/2}]+1$$

$$L_L = INT[N\alpha - \Phi(0.5(1+\beta))(N\alpha(1-\alpha))^{1/2}]+1$$

where α is in fractional form, Φ is the cumulative distribution function of the standard normal variable, INT[...] is the truncated integer part of a real number and β is the desired confidence level. For example, if β is equal to 95% then

$$L_U = INT[N\alpha + 0.83525(N\alpha(1-\alpha))^{1/2}]+1$$

$$L_L = INT[N\alpha - 0.83525(N\alpha(1-\alpha))_{1/2}]+1$$

The major disadvantage to the Monte Carlo method is the cost. Because it is a 'brute force' method, the number of simulations which must be performed to estimate low probability loads grows very quickly. While there are methods available for estimating with greater confidence low probability events for relatively low values of N (for example, importance or stratified sampling methods), the accuracy must necessarily decrease elsewhere. Thus, if the entire range of loads must be determined, then importance sampling methods are not very useful.

Summary and Recommendations

The three methods described above are those which have been used in the probabilistic load model development. There is a variety of other investigations which deal with the combination of random and randomly occurring loads. However, most of the other methods are very mathematical in nature and either require or use many assumptions about load types or distributions. In the development of a generic probabilistic load model, it is necessary to limit the number of assumptions so that the widest possible spectrum of load types

can be handled by the model. The following probabilistic methods were recommended for use in the probabilistic load model development:

1. Gaussian Algebra
2. RASCAL
3. Monte Carlo

The literature of available probabilistic methods for developing a probabilistic load model for generic space propulsion engines has been reviewed. An assessment of the ability of each method to perform the task required for such a complex environment has been made. There are four important considerations in the development of this model: (1) the ability of the model to handle nonstandard distributional forms, (2) the treatment of nonstationary processes, (3) the handling of physical dependencies in the model, and (4) the ability of the method to operate efficiently so that it will be included in an expert system computer code.

5.3 Probabilistic Models

Introduction

The construction of a probabilistic load model requires that the physical processes occurring during engine start-up, operation, and cut-off be modeled by techniques that can handle the unique characteristics of the associated processes. For example, during steady-state operation it seems reasonable to assume that the variability in the various individual engine loads will, in most cases, be independent.* This is a much less valid assumption during such

---

*This is not meant to imply that the magnitude of the pressures and temperatures, for example, suddenly become independent of each other, but rather that the statistical variability can be treated as independent in the probabilistic model. This assumption of independence will not be made in the coupled engine model to be developed later.

transient operations as engine start, when large changes in loads are coupled by the demand to reach a specified power level. To deal with such nonstationary behavior, the mission history profile is divided into mission history phases. The phases are so defined that either the process can be assumed to be stationary over the phase (quasi-steady) or it has specified models for dealing with nonstationary behavior, i.e., the transient model.

Mission history phases are defined by relating each time period to an event timeline. The event timeline defines the controller-demanded power level of the engine and the associated relative times from engine start when the power is changed. It is also possible to define near instantaneous load changes on the event timeline. This allows such processes as spike transients or rare event loads (i.e., debris loading), to be incorporated into overall probabilistics analysis.

Steady-State Operation

In all discussions of the different mission history phases, emphasis will be on their relationship to the statistical and probabilistic modeling since it is assumed that such relatively basic concepts are already familiar to most users of this program.

As the name implies, the steady-state mission phase is used when the demanded engine power level is at a constant value for a period of time. During this time there will be nominal engine loads which are the design loads. About these nominal levels there will be fluctuations due to the stochastic behavior of the processes. For a steady-state mission phase, the probabilistic model assumes that the ratio of the variance of the engine load or parameter to its nominal value is constant. This is reasonable from a physical standpoint since we do not design engines so that their nominal operation leads to an unstable growth in the variability of a load about its mean value. Therefore, once the PDF for the steady-state power level has been calculated, it is not

necessary to perform any time-dependent calculations because all probabilistic information is contained in this PDF. Subsequent calculations determining stresses induced by such loads would require a sample path obtained from this information; this is easily done using the PDF.

Quasi-Steady Approximation

During the quasi-steady state mission phase, the assumption is made that individual and composite loads can be modeled as steady-state loads over a sufficiently small time step. Assume that the current time is given as t_ϕ. Then between t_ϕ and $(t_\phi + \Delta t)$, the mean and variance is assumed to be constant. After $(t_\phi + \Delta t)$, the variance and the mean must be adjusted to account for new nominal conditions. In the absence of any other information, it is assumed that this ratio, which is the coefficient of variation, remains constant. After mean values and variances have been updated, the process is repeated from $t_\phi + \Delta t$ to $t_\phi + 2\Delta t$. The entire process keeps repeating until the end of the quasi-steady phase is reached.

Transient Load Model

The transient load model is provided to predict individual and composite load results during the physical transient portion of the engine mission history profile. Usually during these phases, significant departures from nominal behavior occur due to the nonequilibrium operation of the engine. During the engine ignition, for example, the temperature in the transfer ducts, turbines, and LOX posts will change rapidly in what are referred to in this document as spike-type events. A generic methodology has been developed to handle the spike-type events.

The transient model is identified as mission phase 4 or 5 in the computer code input. Mission phase 4 implies that the number of randomly occurring spikes

obey a Poisson arrival rate model. Mission phase 5 implies that the random spikes occur uniformly during the mission phase. The reason both models are available in a Poisson model is that if the mean arrival rate is N events during the mission phase, then during the simulation there will be instances in which many more than N events occur. In many cases, this is physically unrealistic. Therefore, a uniform model is also provided since the user can then be insured that there is an upper bound for the number of spike-type events which occur.

Due to the physics of the engine, the second problem encountered in developing a transient load model is that there are some events which must always occur while subsequent events are randomly occurring. For example, there is always a temperature spike which occurs due to the engine ignition, but, subsequently, there are one or two spikes which can occur. Therefore, a third type of model is available which always requires that fixed spikes occur.

While the number of spikes which occur may be random, there may still be a time dependency, i.e., given that the spike does occur, it is always within a specified time range. This capability is also included in the model.

The following paragraphs provide a more detailed explanation of the transient model operation. After this discussion, an example calculation is presented and discussed.

Transient Model: Determination of Number of Spike Events

For the purpose of the following discussions, it will be assumed that the current mission phase, denoted as IMP for load variable IR, has already been determined to be of type 4 (Poisson model) or type 5 (Uniform model). These parameters are input as MP(IR,IMP) and are discussed in the users manual input description in more detail. The operation of the model for the quasi-steady and steady-state type of mission phases is unaffected by these new changes.

The first step in the load model calculation is the determination of the number of spike values seen during the mission phase. To calculate this number, three options are available to the user: (1) a Poisson arrival rate model, (2) a uniform arrival rate model, and (3) a fixed time-of-arrival model. The Poisson arrival rate model is obtained by inputting MP (IR, IMP) equal to 4, while the uniform model is obtained with MP (IR, IMP) equal to 5. The definition of the subsequent inputs changes, depending upon the value of the MP(IR,IMP).

The parameter needed as input for the Poisson arrival model is the mean arrival rate, called RAMDA(IR,IMP) in the program. This is equal to the mean number of spike events per mission phase time period. Thus, if there are 3 spike events, the average for mission phase IMP, and the phase is 5 sec long, then RAMDA(IR,IMP) is equal to 0.6 (3 events/5 sec).

The Poisson model does not have an upper bound on the number of events which can occur. For example, the values given in the previous paragraph where the mean arrival rate is 3, there is approximately a 3.4% probability that there will be seven or more events occurring in the 5-sec interval. Since this can lead to physically unrealistic scenarios and mission profiles, an option for a two-sided distribution was believed to be necessary. For some load variables, there will never be more that N events during the mission phase, and zero will always be a lower bound*, a uniform distribution is included to provide both an upper and a lower bound to the calculations. When MP(IR,IMP) is equal to 5 the uniform distribution is chosen. For this case RAMDA(IR,IMP) is equal to N+1, i.e., the maximum number of events which can occur plus one.

Finally, there should be a method for handling spike events which always occur but have some variability about either the nominal spike amplitude or the time of occurrence. This is input as NFIX(IR,IMP) greater than zero.

---

*Although, it may not be the maximum lower bound.

These are the only parameters which are needed to determine the number of spike events which occur during the transient mission phase. The next step is to determine when the event occurs.

Transient Model: Determination of Timing of Spike Events

The timing of the spike events must rely on some basic information about the mission phase definition. The previous transient model assumed that the spike event began and ended with the beginning and ending of the mission phase definition. This implies that the spike width is equivalent to the mission phase length. The new model allows for multiple peaks within the transient mission phase. However, this implies that the information about the spike width is lost. There are several options for dealing with the replacement of this information, but the one chosen for this model development is to input the nominal spike width and leave it fixed throughout the current mission phase. If the spike width changes dramatically from peak to peak, then two approaches may be considered. The simplest approach is to divide the current mission transient phase into multiple mission phases in which the spike width can be considered constant. The second option is to make the spike width a random variable. This option requires information more detailed than the approximate nature of the model warrants. Therefore, the second option is not contained in the current version of ANLOAD. It can be added later if new data or information indicates that this is the better method.

The information on the spike width is input in the array denoted WIDTH(IR,IMP). The width of the spike is then constant for this mission phase time period, defined by the start time STIME(IR,IMP) and the end time ETIME(IR,IMP).

The start of the spike transient event is obtained in two different ways, depending on the type of model used for the transient load modeling. For the uniform model, the spike transient can occur with equal probability in the mission phase time interval defined by ETIME(IR,IMP)-STIME(IR,IMP). For the

Poisson model, the arrival of the spike transient is given by a Poisson distribution with the mean time of occurrence equal to (1/mean arrival rate). This model will more likely cause the spike values to occur earlier in the mission phase than later in the mission phase. This is intuitively correct since one expects less of a departure from the nominal engine conditions as the mission phase is leaving the transient regime and approaching a quasi-steady or steady-state operating condition.

The previous description relates to how the initial spike transient peak is placed in the mission phase time interval. Because there is some probability that more than one peak can occur, one must decide if the peaks can overlap or if there is some time delay before the next spike transient value can occur. This is done by inputting the number of spike widths that must pass before the next peak can occur, denoted IDLAY in the ANLOAD program. If IDLAY is zero, then peaks can overlap. This will cause a masking of peaks so that multiple peaks may actually appear as single peaks. This can lead to a reduction in the calculated variance.

The amplitude of peak values is calculated after the timing of the peak occurs. This is done to reduce the array storage requirements in the program. Since peak amplitudes are calculated at each time interval, there is no need to store their values. The calculations proceed by calculating the first four moments of the load amplitudes. These moments are then sent to the distribution fitting subroutine and the best fit distribution is used to summarize the results on the output file.

Transient Load Model Sample Calculation

A sample problem which uses all of the available options was run. This was not meant to be a physically realistic run, but rather was used to demonstrate the options.

All mission phases were constructed to be 5 sec in duration. The Poisson arrival rate in each case where this model is used was 0.6, i.e., a mean arrival rate of three events per 5-sec interval. The spike width for all cases was given as 0.25 sec and a delay time of two spike widths (0.5 sec) was used. Subsequently, five mission phases were defined. The first phase used the Poisson model with no fixed spikes. The second phase used the Poisson model with two fixed spikes. The third phase used the Poisson model, but the spikes were forced to occur in a Gaussian distribution of about 12.5 sec with a standard deviation of 0.25 (this is the NFIX less than zero option). The fourth phase was the final transient phase and used the uniform model with the maximum number of peaks equal to 3. The final phase was a quasi-steady state phase which went from 65% to 104% power levels. The fifth phase was included to check that there was a correct time phasing between the models. Figure 5.1 shows the results of mission phases.

As Figure 5.1 indicates, the transient model appears to be working well. The Poisson Model shows peaks occurrence in the expected manner. The second mission phase, between 5 and 10 sec, shows the variance getting smaller near 7.5 and 8 sec. This is expected because there are two fixed peaks at those times when mean time of occurrence is equal to these values. The uniform model, used between 15 and 20 sec, also behaves as one would expect, since the time of a peak occurrence is likely to occur equally anywhere in this phase.

The third phase is where the number of peaks behaves similarly to a Poisson arrival rate model, except that the timing is within a specified distribution, is expanded and shown in Figure 5.2. In this figure, one can more clearly see the load prediction follows the base curve with no variation until 11.75 sec. At this time, the load shows a sharp increase and associated variability. This ends at 14.0 sec. This is precisely the expected result. Since 11.75 sec is three standard deviations away from the mean time occurrence, it would not be likely to see any spike values occurring until after that time. The peak at 12.5 sec is exactly where it should be and the smaller peaks at 13.0 and 13.5 sec are also seen. Therefore it is concluded that the model is working as planned.

5-18

Test Case: HPOTP Torque
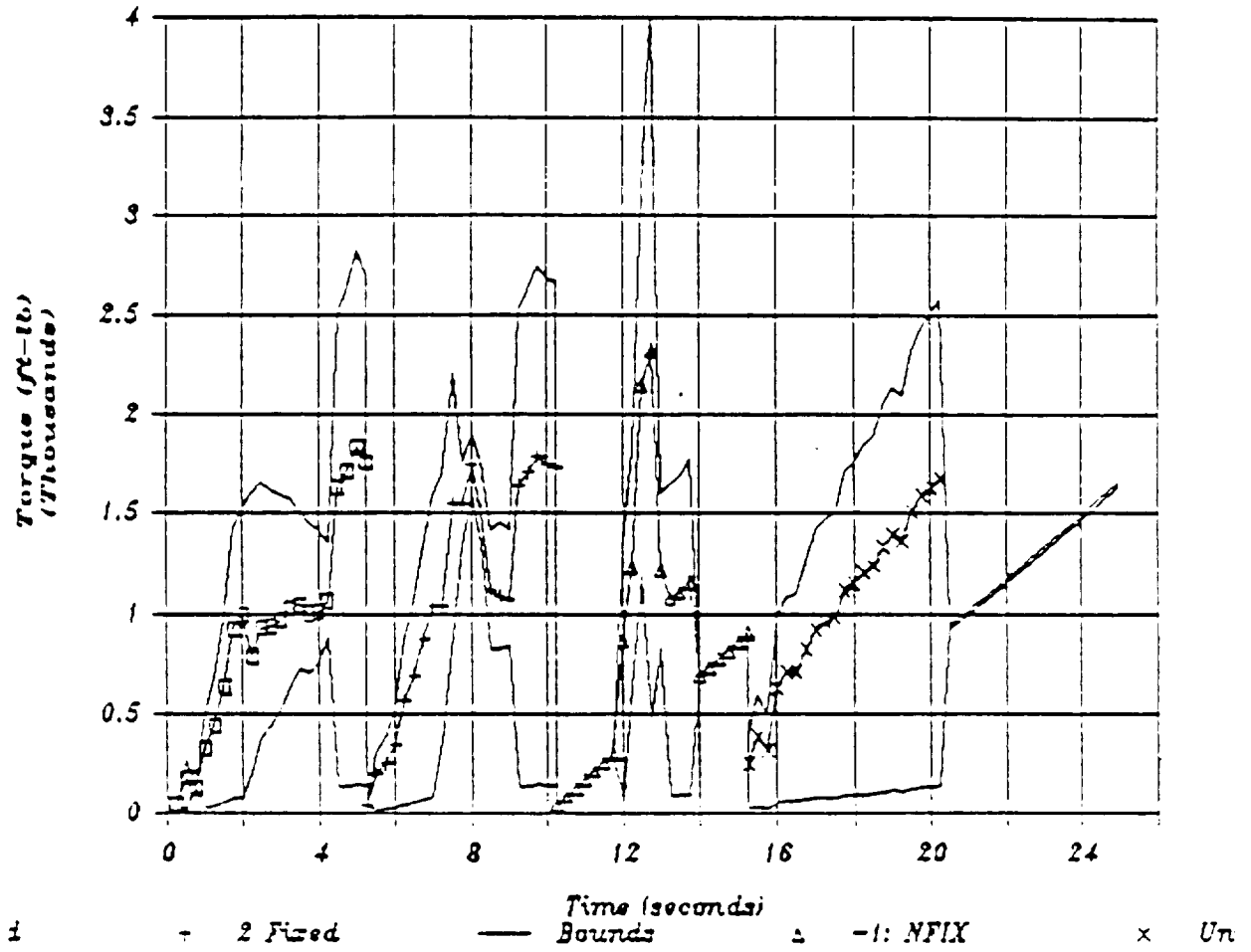
Figure 5.1. Sample Transient Calculation: Five Mission Phases

Test Case: HPOTP Torque
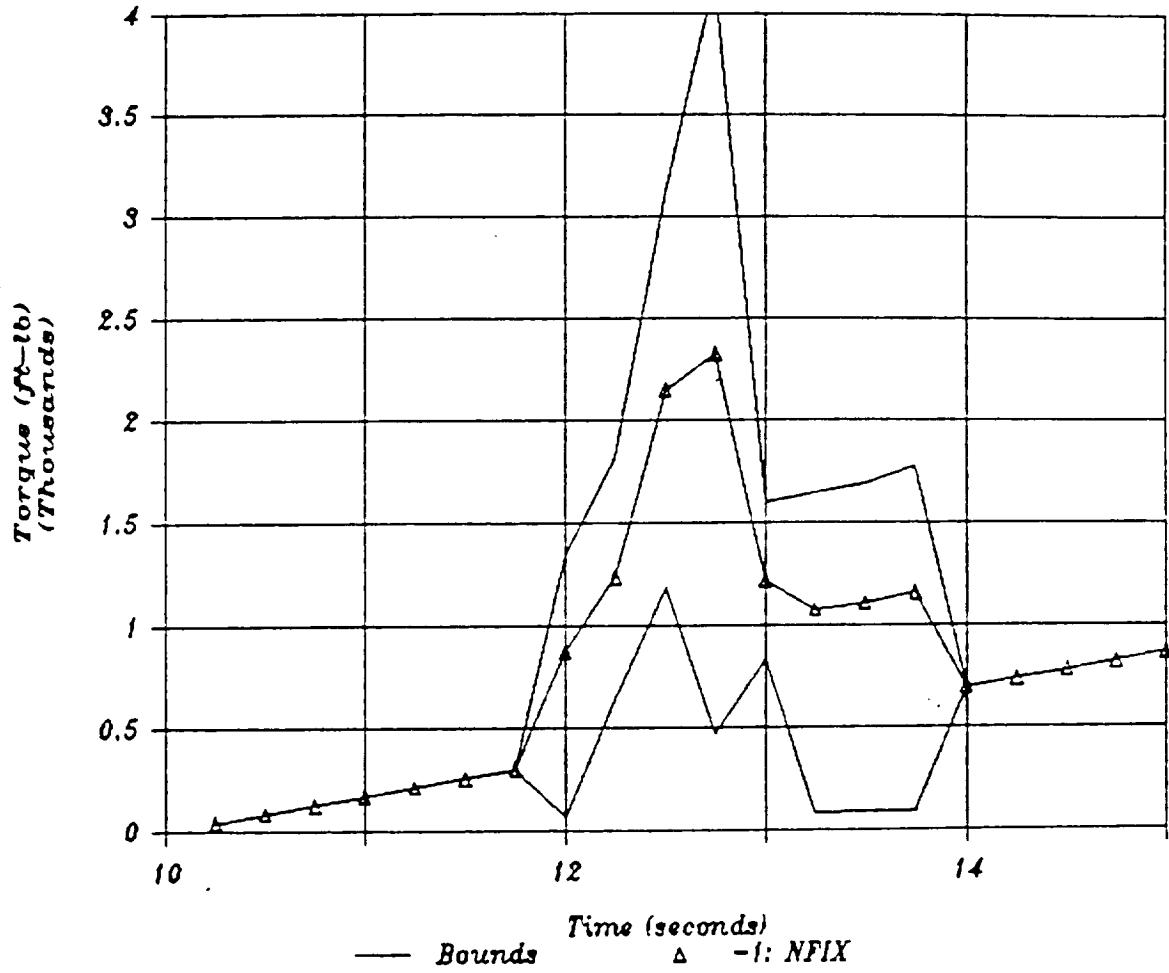
Figure 5.2. Poisson Transient Model With NFIX = -1

As a final test case, the entire probabilistic load model was run using the Poisson transient model with no fixed spikes from 0 to 2.5 sec, and a quasi-steady state calculation from 65% to 104% power from 2.5 sec to 10 sec. These results are shown in Figure 5.3. Again, the model behaves as expected.

5.4 Validation Studies

Introduction

The latest version of the probabilistic load model must have validation studies performed on the code to insure that the methodology is performing as intended. The verification of probabilistic methodologies can only take place under limited testing conditions. The limitations on verification conditions arise because there are very few distribution types which can have an analytical solution derived for a specified combination of distributions. Additionally, dependent variables, nonlinearities, etc., all provide conditions for which only bounding types of solutions are available.

There are two probabilistic methods which must be validated: RASCAL and Monte Carlo. The validation analyses, which has been performed, involve only normal distributions. It is believed that if the probabilistic model can produce accurate results in comparison to the theoretically calculated values for normal distributions, then it will also produce accurate results for nonnormal distribution types. This is clearly the case for lognormal distribution since it is a simple transformation of the normal algebra. For most other distribution types, it would be necessary to run Monte Carlo analyses to check the RASCAL results. This does not seem to be valid use of the available resources: if RASCAL compares well with Monte Carlo for normal distributions then it will also compare well with Monte Carlo when non-normal distributions are used. This is because, in limitations where the number of intervals used for RASCAL approaches infinity, RASCAL methodology becomes the Monte Carlo method. Therefore, only normal distributions are used in validation studies for probabilistic methods.

Test Case: HPOTP Torque
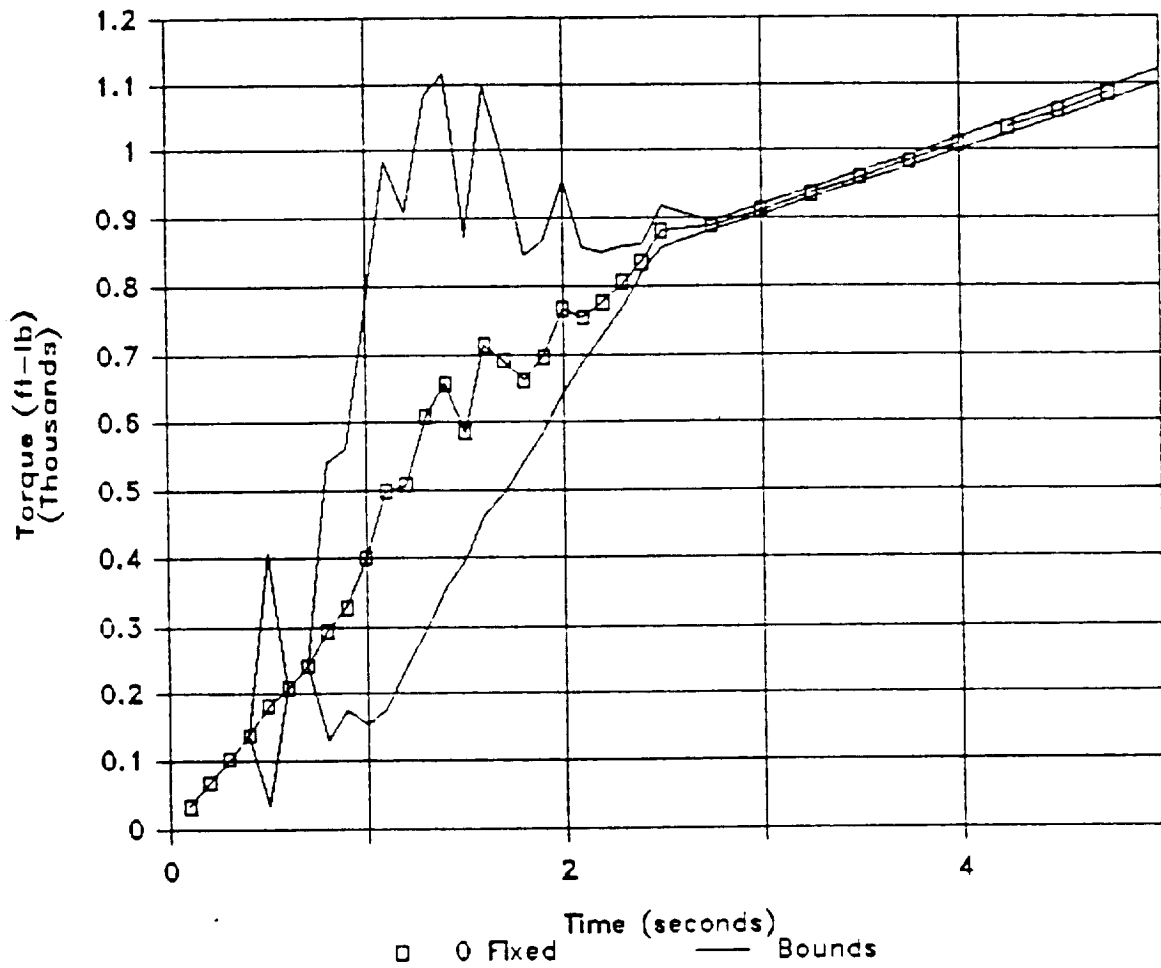
Figure 5.3.   ANLOAD Calculation For HPOTP Torque

There are three case studies which were employed. These are:

Case Study I.   Sum Of Three Normal Distributions: Y = A + B + C
Case Study II.   Product Of Three Normal Distributions: Y = ABC
Case Study III.   Sum And Product Normal Distributions: Y = A + BC

In all three studies, the mean and variance of random variables A, B, and C are those given in Table 5.1. Using the algebra of normal distributions, it is straightforward to calculate the mean and variance of combinations in these distributions. These results are also shown in Table 5.1. These are the theoretical values of the mean and variance which both the Monte Carlo and RASCAL methods should reproduce accurately. In addition, if the distribution for Y is also normal then it is possible to compare the CDF, which one obtains from the computer analyses, to the theoretical distribution. These comparisons are made in the following discussions.

TABLE 5.1. MEAN AND VARIANCE OF RANDOM VARIABLES FOR VERIFICATION STUDIES

Variable	Mean	Variance
A	10.0	1.0
B	10.0	4.0
C	10.0	9.0
Y=A+B+C	30.0	14.0
Y = ABC	1000	380.705
Y=A + BC	110.	36.5650

Case Study I. Sum Of Three Normal Distributions: Y = A + B + C

The sum of three normal distributions with parameters given in Table 5.1 results in a normal distribution in which the mean value is equal to the sum

of the three means and the variance is the sum of the variances. Therefore, it is possible to exactly calculate the resulting distribution. This is a normal distribution with a mean of 30.0 and a variance equal to 14.0. The results of RASCAL calculations are shown in Figure 5.4. In this figure, the squares represent RASCAL results when equal probability intervals are used. The plus signs represent the results when an equal space interval (between the first and 99th percentile values) option is used. As the figure readily demonstrates, RASCAL calculation is very close to the theoretically correct result.

Figure 5.5 demonstrates the key difference between RASCAL calculations and the Monte Carlo Method. In Figure 5.4 the Monte Carlo results were not shown because they are also as close to the theoretical line as the RASCAL results were over the entire CDF scale. However, in the expanded view shown in Figure 5.5, one can see that the Monte Carlo result does not perform as well in the upper tail region as the equal space RASCAL result. For these calculations, the Monte Carlo analysis used the same number of sample points as did the RASCAL analysis (1000). The error bars on the Monte Carlo result (ref. Figure 5.5) represent the 95% confidence intervals. Thus, in the Monte Carlo analysis, there are three points shown above the eighty percentile value that will not encompass the theoretically correct line 95% of the time. This is an important point to makein the calculation of confidence limits with the Monte Carlo method. The confidence limits calculated with Monte Carlo do not imply that 95% of the time the confidence limit will encompass the true result: rather they imply that if the Monte Carlo analysis is repeated, that 95% of the time the Monte Carlo result will lie within the error band. While RASCAL does not currently have an analogous calculation for confidence limits, the ability to sample more frequently in the tail region will insure that the prediction will be closer to the true result than a standard Monte Carlo analysis.

PROBABILISTIC LOAD MODEL VALIDATION
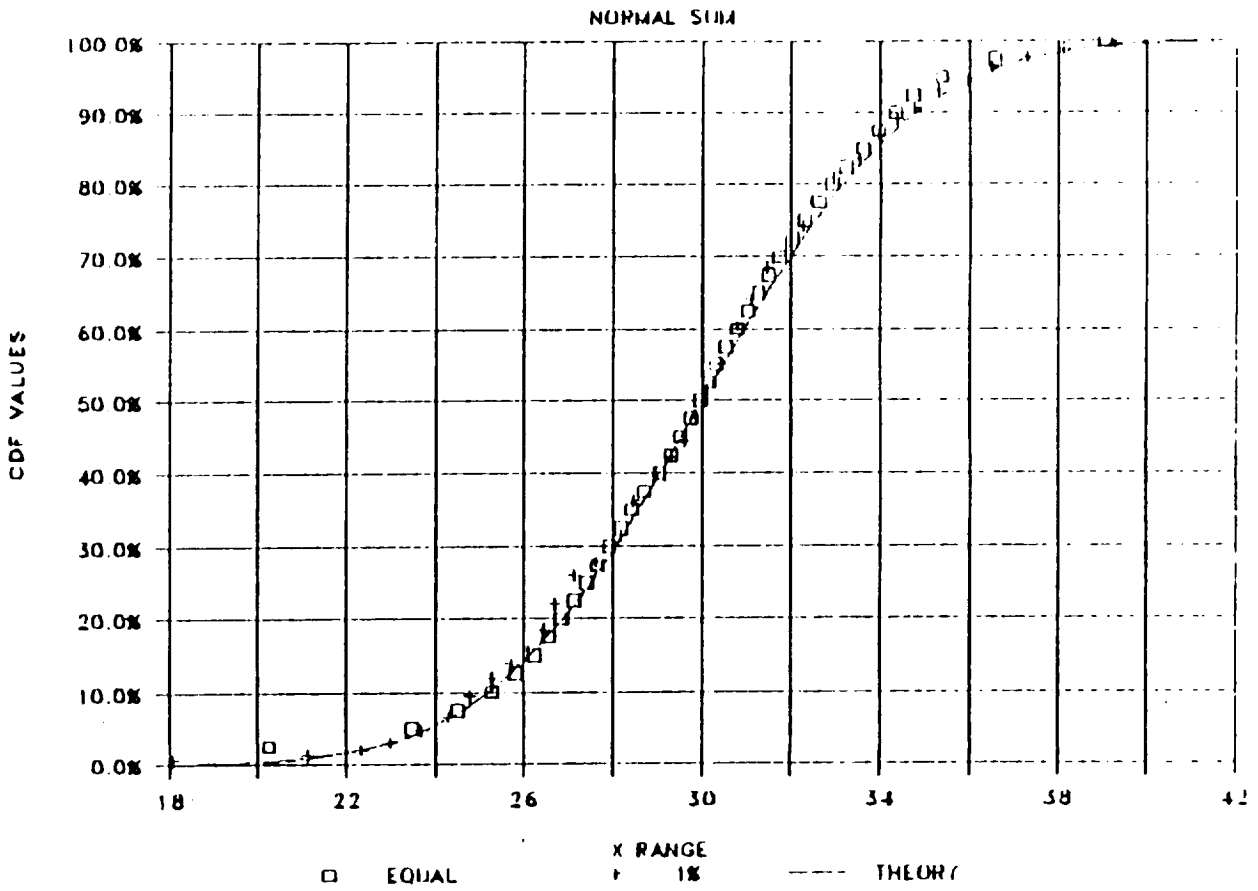
Figure 5.4. Case Study I: Sum of Three Normally Distributed Variables

PROBABLISTIC LOAD MODEL VALIDATION
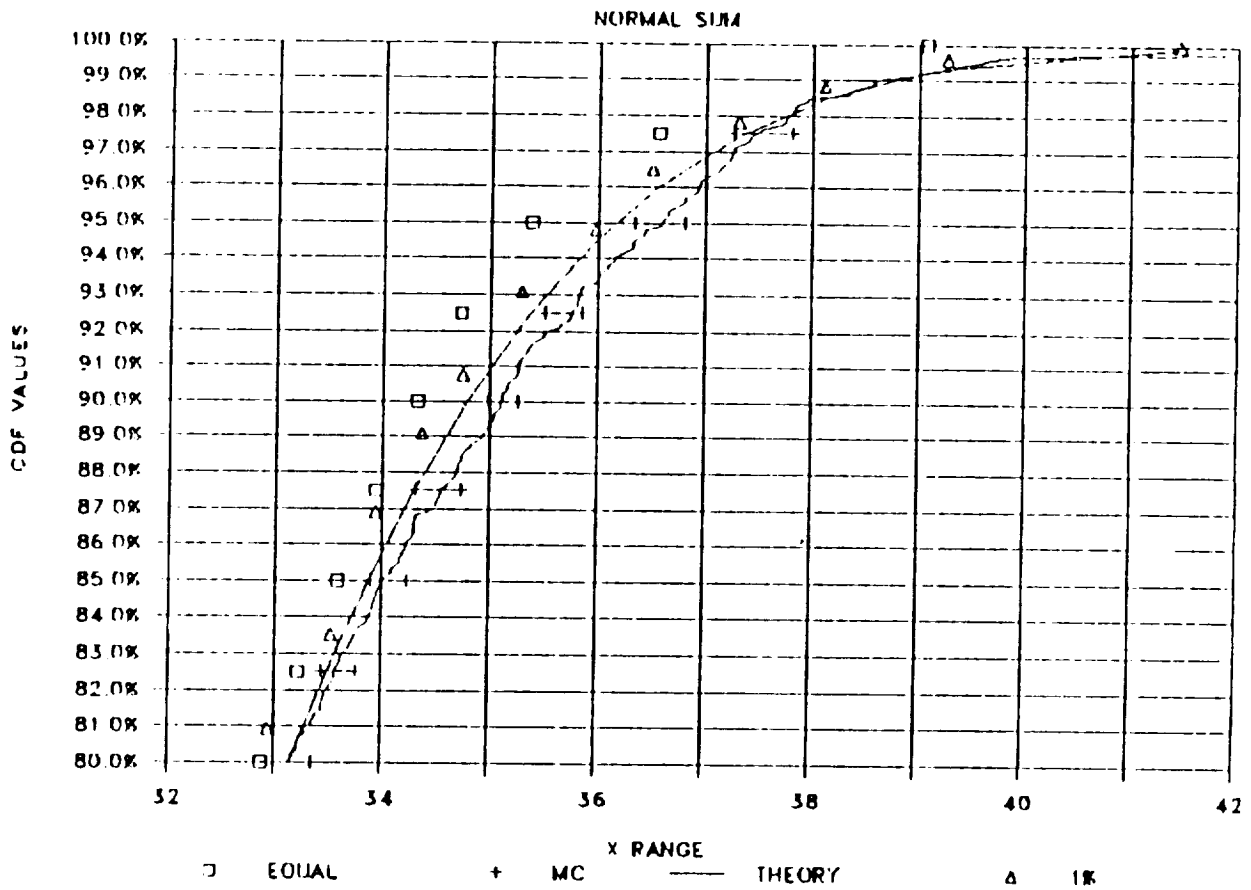
Figure 5.5. Case Study I: Upper Tail Values For Normal Sum

Case Study II. Product Of Three Normal Distributions: Y = ABC

In this study, RASCAL, Monte Carlo, and other theoretical results are compared for a product of three normally distributed random variables. In computing a product of three normal distributions the variance component increases as a function of both the mean squared value and the variance of inputs so that the spread in the dependent distribution is much larger than the case in which the sum is used. Figure 5.6 shows the results of the CDF calculation for RASCAL and normal distribution calculations. The expanded view of the upper tail region, which also includes the Monte Carlo result, is given in Figure 5.7. Again, the results are similar to Case I, however, the equal probability calculation appears to actually perform better than the equal space calculation. This is caused by the sampling procedure, i.e., this is an unlikely scenario that, on the average, we do not expect to see repeated. In either case, RASCAL methodology performs as well as, or better than, the Monte Carlo given the same number of sample points.

Case Study III. Sum And Product Normal Distributions: Y = A + BC

The final case study looks at an algebra of normal distributions in which both a product and a sum are included. Results similar to Case I and II are shown in Figures 5.8 and 5.9. The conclusions to be drawn from these figures are the same as those previously stated. That is, the Monte Carlo and RASCAL methods perform well when compared to the theoretically correct results with the RASCAL results being as good as, or better than, the Monte Carlo calculation for the equivalent number of sample points.

SUMMARY

The validation of probabilistic methodologies has been performed. The comparison of simulation methods, RASCAL and Monte Carlo, to theoretically available methods has demonstrated good statistical agreement among results. The methods provide the user with parameters that can control the accuracy,

PROBABLISTIC LOAD MODEL VALIDATION
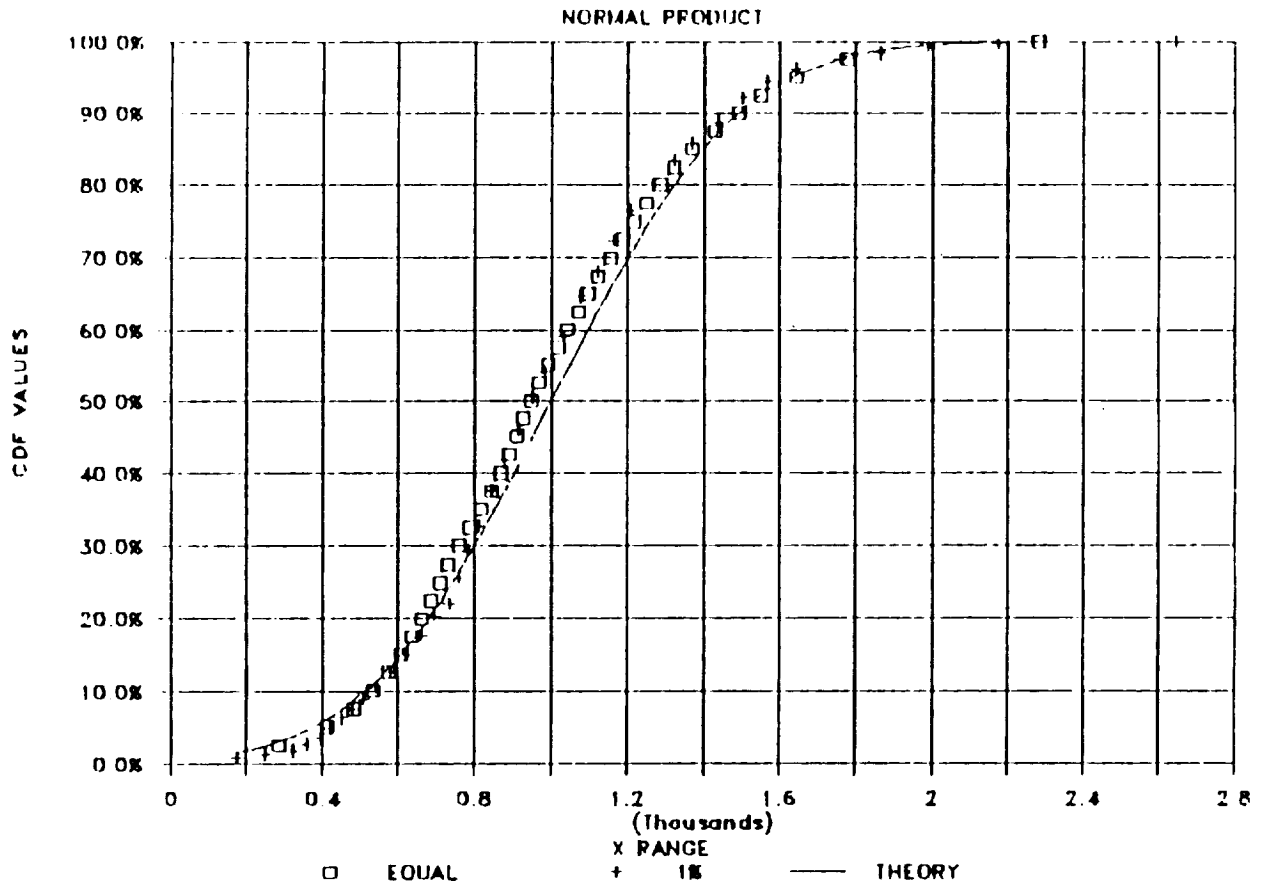
NORMAL PRODUCT

Figure 5.6. Case Study II: Product of Three Normally Distributed Variables

PROBABILISTIC LOAD MODEL VALIDATION
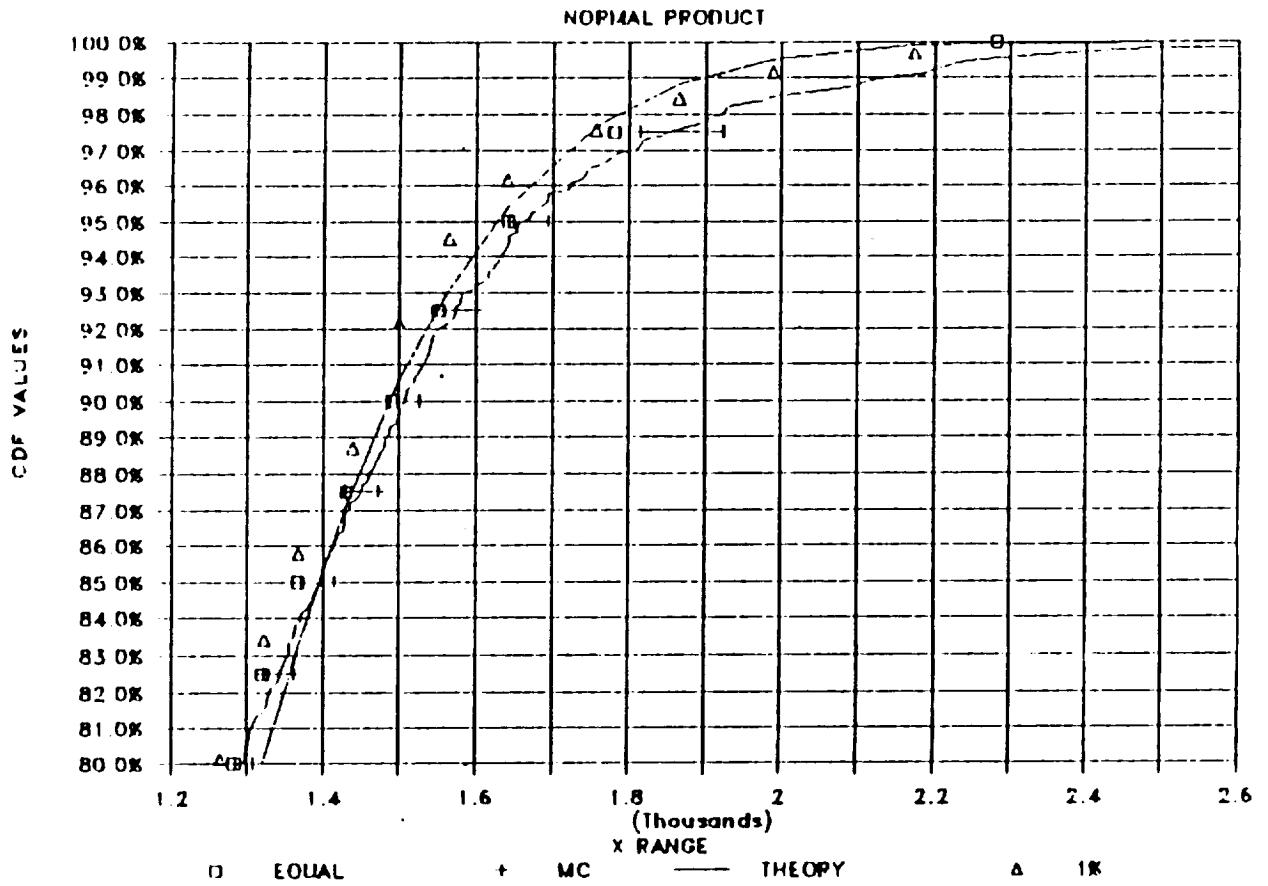
NOPMAL PRODUCT

Figure 5.7. Case Study I: Upper Tail Value For Normal Product
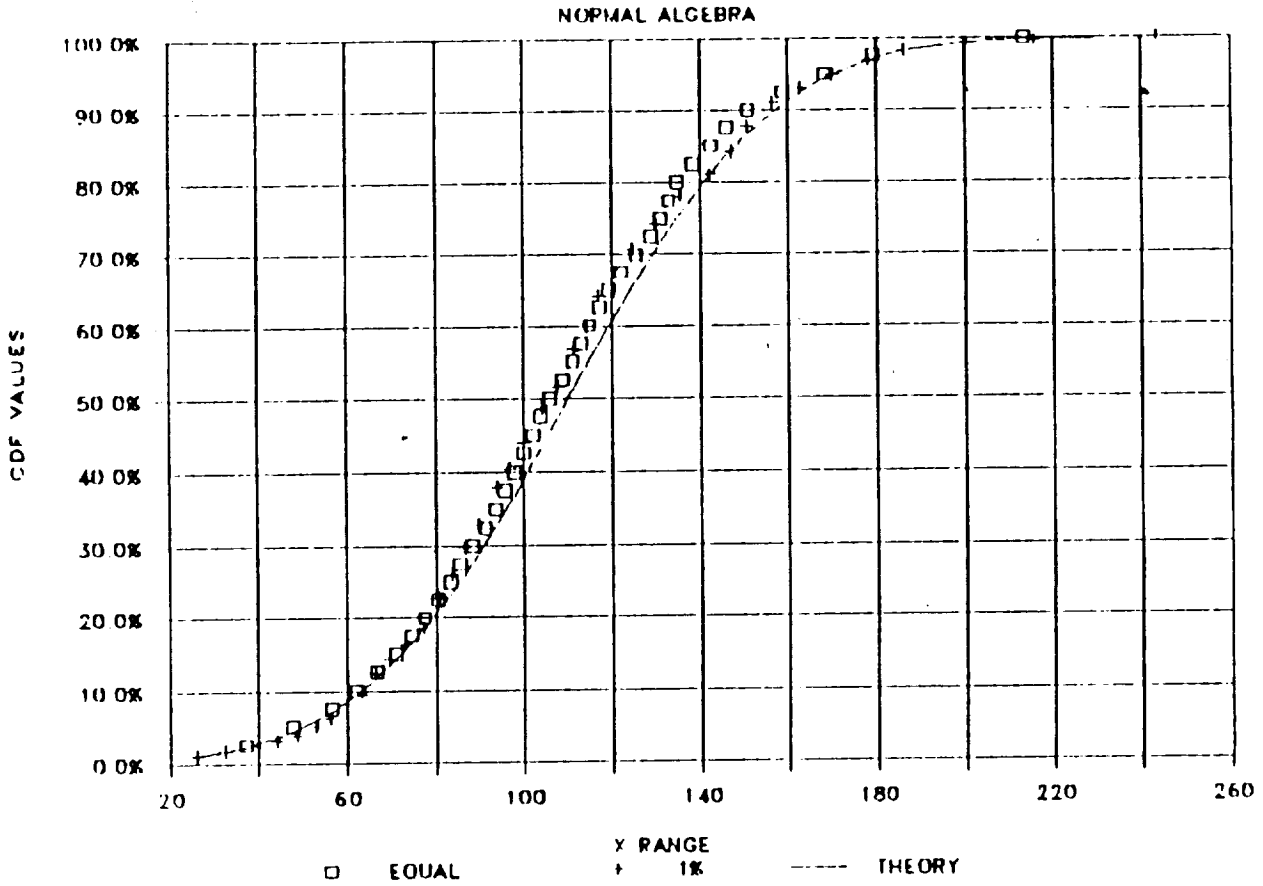
Figure 5.8.   Case Study III: Algebra of Three Normally Distributed Variables
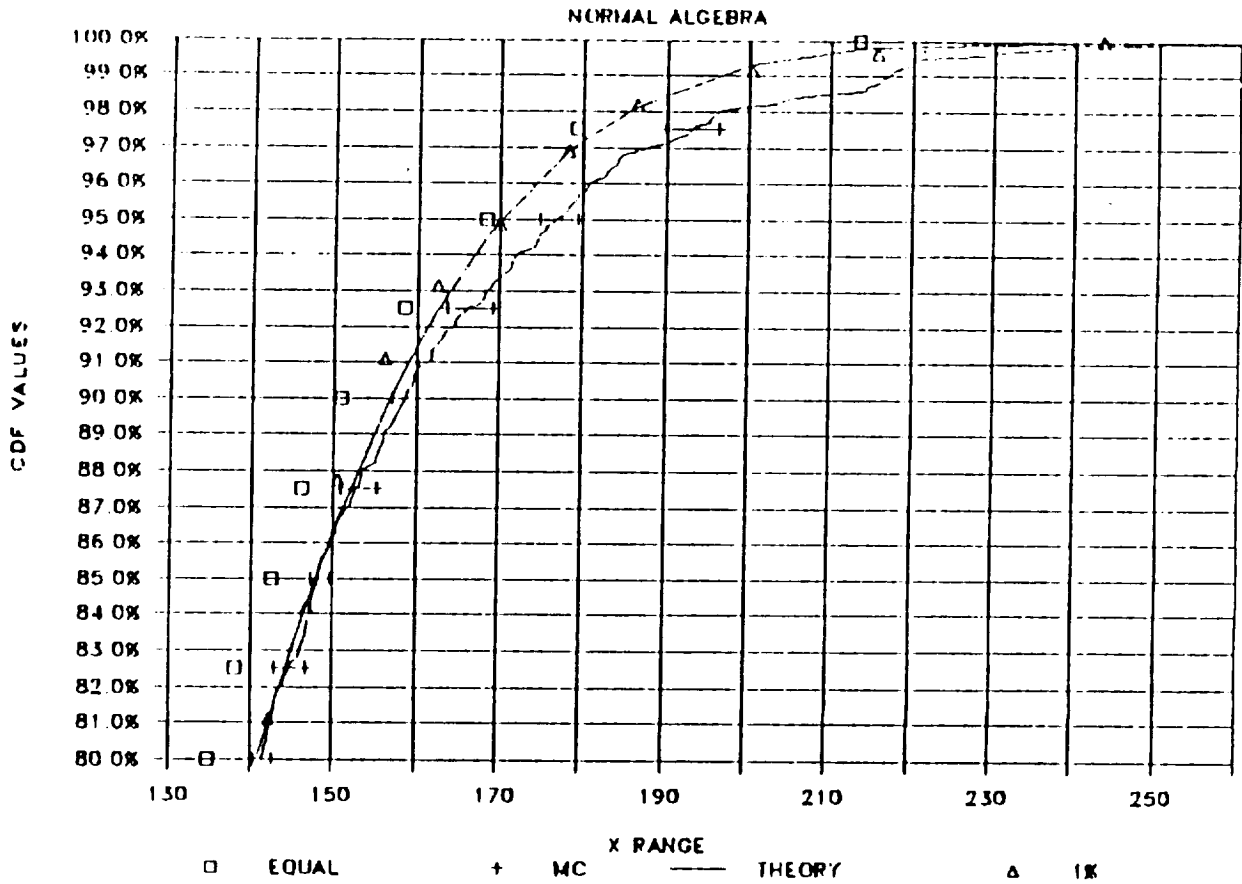
Figure 5.9 Case Study III: Upper Tail Value For Normal Algebra

as well as the confidence, of the predicted results. The next chapter investigates more fully the question of the accuracy of probabilistic methodologies.

5.5 VERIFICATION STUDIES

INTRODUCTION

Ultimately, the probabilistic load model must be able to predict, within the limits of statistical accuracy, the behavior of loads in a space propulsion engine. While the initial phase of this study has no requirements for the physical process to be accurately modeled, it would be foolhardy to proceed without considering such processes. Therefore, the probabilistic model is driven by the influence function coefficient model and can be used to compare to the data received from flight and test stand data. The results of such comparisons are called verification studies. These analyses are used to calibrate the current status of the model, as well as indicating where additional effort was needed during the second phase of this program.

There are a variety of data sets available from the SSME test program and the subsequent flight data. There is limited data contained in the current expert system database for other engine types. Therefore, at this time, the validation studies are limited to SSME type engines. As the database is expanded, additional verification work will be performed.

For the available data sets and influence function data sets, there were five engine variables which were identified as being statistically valid for verification studies. The engine variables are listed in Table 5.2 and include the H2 mass flow rate, LOX mass flow rate, OPB discharge temperature, HPOT discharge temperature, and LPOT turbine shaft speed. These five variables were chosen for two reasons: (1) there was a match between the available data and the dependent variable list from the influence functions, and (2) there was a statistically significant number of data points available

TABLE 5.2. ENGINE VARIABLES INCLUDED IN THE VALIDATION STUDIES

H2 MASS FLOW RATE

LOX MASS FLOW RATE

OPB DISCHARGE TEMPERATURE

HPOT DISCHARGE TEMPERATURE

LPOT TURBINE SHAFT SPEED

for analysis. There is a significant difference in the type of loading associated with each of these engine variables.

The data that was obtained for use in the verification studies is the 10-sec averaged data set from both the test stand and flight databases. The test or flight data identifiers, together with the engine and component identifiers, are contained in Tables 5.3 and 5.4, respectively. These data are compared to results obtained from the ANLOAD program in the following sections.

EXAMPLE SPACE SHUTTLE MAIN ENGINE ANALYSES

Introduction

The comparison of the ANLOAD and data requires that the influence function data set and the data set that is being examined be carefully scrutinized. As will be shown below, the slightest bias in the prediction from the influence coefficients can cause results of the probabilistic model to appear to be skewed. It is also important to note that the influence function model is based on an engine balance computer simulation model assuming in-flight conditions. This is in contrast to selected tests which are purposely set to limit state-type conditions that would be unacceptable sets of engine parameters for actual flight. Therefore, after examining this point in some detail below, the mean predictions will be shifted to match the data set so that the probabilistic results can be examined efficiently.

TABLE 5.3.   TEST DATA USED IN VERIFICATION STUDIES

Test No	VEHICLE	ENG POS	ENGINE NO	DUR	M/S PL	PWR HD	MCC	NOZZLE	CNTRLR	HPFTP	LFFTP	HPOTP	LPOTP
901-391	A-1	1	2011	500	104	2016	2016	2016	F-16	2214B1	9106	9010	9005
901-413	A-1	1	2018	130	104	2019	4002	4001	F-17	0209	4001B1	9211	2016
901-414	A-1	1	2018	500	104	2019	4002	4001	F-17	2314	4001B1	9211	2016
901-427	A-1	1	2010	510	104	0107	2011	2014	F-05	5101B1	2117	0310	2110
901-430	A-1	1	2017	510	104	2018	4001	2018	F-17	2415	9206	9010B1	2211
901-438	A-1	1	2019	510	104	2020	2019	2017	F-16	9210	2118	2019	2017
901-439	A-1	1	2019	250	104	2020	2019	2017	F-19	2020	2022	2022	2017
901-440	A-1	1	0207	250	104	2020	2019	2017	F-19	4002	2118	2022	2017
901-477	A-1	1	2105	250	104	4002	2116	4010	P-08	5102B1	9105B1	9505B2	2022
902-302	A-2	1	2016	215	104	2106	2018	2017	F-16	9011	9005B2	2016	2015
902-307	A-2	1	2017	500	104	2018	4001	2018	F-10	2016B1	9106	9010	2211
902-311	A-2	1	2011	500	104	2016	2020	4002	F-18	2017B1	9005B3	2018	9005
902-313	A-2	1	2019	190	104	2020	2019	2017	F-19	9210	2118	2019	2017
902-314	A-2	1	2019	500	104	2020	2019	2017	F-19	9210	2118	2019	2017
902-318	A-2	1	2109	190	104	2109	2018	4004	F-04	5105	9105	2020	2018
902-319	A-2	1	2109	510	104	2109	2018	4004	F-10	5101	9105	2020	2013
902-323	A-2	1	2020	510	104	2021	4004	2020	F-22	2018	2019	2021	0208
902-326	A-2	1	2021	510	104	2023	2105	2021	F-19	2019	9105B1	4001	2019
902-329	A-2	1	2010	510	104	0107	2011	2014	P-13	2410	2314	9110	2110
902-335	A-2	1	2022	250	104	2022	2022	4005	P-07	4001	2020	2015B1	2020
902-337	A-2	1	2022	510	104	2022	2022	4005	F-22	2020B1	2020	2022	4002
902-339	A-2	1	2023	250	104	4001	4003	4003	F-24	2021	4002	2019B1	2015
902-340	A-2	1	2023	250	104	4001	4003	4003	F-24	2515	2118	2019B1	2015
902-341	A-2	1	2023	510	104	4001	4003	4003	F-24	2515	2118	2019B1	2015
902-343	A-2	1	2014	250	104	2011	2015	2011	F-13	9310	2118	2016R1	4003
902-344	A-2	1	2014	250	104	2011	2015	2011	F-09	9311	2314	2117	2021
902-346	A-2	1	2014	250	104	2011	2015	2011	F-13	2313	2021B1	2117	2021
902-347	A-2	1	2014	250	104	2011	2015	2011	F-13	2118	4002B1	2115	2021
902-348	A-2	1	2014	250	104	2011	2015	2011	F-13	2118	2314	2016B2	2021
902-349	A-2	1	2014	250	104	2011	2015	2011	F-13	9310B1	2314	2018B1	90403
902-350	A-2	1	2014	250	104	2011	2015	2011	F-13	2216	2314	2018B1	4004
902-351	A-2	1	2014	250	104	2011	2015	2011	F-13	4202	2314	2022B1	2022
902-352	A-2	1	2014	250	104	2011	2015	2011	P-08	4003	2311	4102	2022
902-356	A-2	1	2015	250	104	2015	2014	2015	F-04	4101	2022	0310B2	2113
902-357	A-2	1	2015	510	104	2015	2014	2015	F-15	2413	2022	4003	2113
902-360	A-2	1	2014	250	104	2011	2015	2011	F-26	2120	2314	4003	2021
902-361	A-2	1	2014	250	104	2011	2015	2011	F-06	2218	2109R3	9211B1	4003
902-363	A-2	1	2024	250	104	2025	4005	2011	F-23	4201	2116	2020B2	4003
902-364	A-2	1	2024	250	104	2025	4005	2011	F-23	4202	2411	2020B2	4003
902-365	A-2	1	2024	510	104	2025	4005	2011	F-21	2218B1	4003	4003B1	4003
902-366	A-2	1	2024	250	104	2025	4005	2011	F-27	2413	2109B4	2504	4101

5-34

TABLE 5.4. FLIGHT DATA IN VERIFICATION STUDIES

FLT NO	VEHICLE	POS	ENG NO	DURATION	M/S PL	PWR HD	MCC	NOZZLE	CNTRLR	HPFTP	LPFTP	HPOTP	LPOTP
STS-06	OV-099	1	2017	505.757	104	2018	4001	201	F-10	9110	9106	9010	2211
STS-06	OV-099	2	2015	505.874	104	2015	2014	2015	F-11	2215	2211	2015	2113
STS-06	OV-099	3	2012	505.990	104	2014	2017	2016	F-12	2213E1	2016	2016	2012
STS-07	OV-099	1	2017	506.501	104	2018	4001	201	F-10	2315	9106	9010	2211
STS-07	OV-099	2	2015	506.634	104	2015	2014	2015	F-11	9211	2211	2015	2113
STS-07	OV-099	3	2012	506.750	104	2014	2017	2016	F-12	2213E1	2016	2016	2012
STS-09	OV-102	1	2011	515.518	164	2016	2020	4002	F-11	2017E1	2115	2018	9005
STS-09	OV-102	2	2018	515.652	104	2019	4002	4001	F-04	2213E1	4001E1	9211	2016
STS-09	OV-102	3	2019	515.780	104	2020	2019	2017	F-06	9210	2118	2019	2017
STS-13	OV-099	1	2109	517.140	104	2109	2018	4004	F-10	5101E1	2117	2020	2018
STS-13	OV-099	2	2020	517.246	104	2021	4004	2020	F-05	2018	2019	2021	0208
STS-13	OV-099	3	2012	517.396	104	2014	2017	2016	F-12	2116E2	2016	2016	2012
STS-14	OV-103	1	2109	521.525	104	2109	2018	4004	F-10	2020E1	2117	2020	2018
STS-14	OV-103	2	2018	521.666	104	2019	4002	4001	F-04	2017E2	4001E1	9211	2020
STS-14	OV-103	3	2021	521.784	104	2023	2105	2021	F-16	4001E1	9105E1	4001	2019
STS-19	OV-103	1	2109	519.525	104	2109	2018	4004	F-10	2020E1	2117	2020	2018
STS-19	OV-103	2	2018	519.666	104	2019	4002	4001	F-09	2017E2	4001E1	9211	2020
STS-19	OV-103	3	2012	519.784	104	2014	2017	2015	F-12	2118	9206	9110	2012
STS-20	OV-103	1	2109	517.024	104	2109	2018	4004	F-10	4202	2117	2020	2018
STS-20	OV-103	2	2018	517.146	104	2019	4002	4001	F-09	2017E2	4001E1	2019E1	2020
STS-20	OV-103	3	2012	517.266	104	2014	2017	2016	P-07	4003	9206	9110	2012
STS-24	OV-099	1	2023	521.347	104	4001	4003	4003	F-24	2515E1	4002E1	2019E1	2015
STS-24	OV-099	2	2020	521.465	104	2021	4004	2020	F-05	9311E1	2019	2021	0208
STS-24	OV-099	3	2021	521.567	104	2023	2105	2021	F-06	2216	2021E1	4001	2013
STS-25	OV-103	1	2109	522.127	104	2109	2018	4004	F-10	2121	2117	2115	2018
STS-25	OV-103	2	2018	522.245	104	2019	4002	4001	F-22	4201	4001E1	2016E3	2020
STS-25	OV-103	3	2012	522.366	104	2014	2017	2016	P-07	4003	9206	9110	2012
STS-26	OV-099	1	2023	349.600	104	4001	4003	4003	P-20	2515E1	4002E1	2019E2	2015
STS-26	OV-099	2	2020	587.730	104	2021	4004	2020	F-27	4202E1	2019	4003E2	0208
STS-26	OV-099	3	2021	587.849	104	2023	2105	2021	F-06	2216	2021E1	4001E1	2019
STS-27	OV-103	1	2109	513.924	104	2109	2018	4004	F-10	2121	2117	2115	2018
STS-27	OV-103	2	2018	514.046	104	2019	4002	4001	F-22	4201	4001E1	2016E3	2020
STS-27	OV-103	3	2012	514.167	104	2014	2017	2016	P-07	4003E1	9206	2018E2	2012

Comparison Of Probabilistic Predictions And Data

Figure 5.10 shows the predicted fuel mass flow rate and the empirical CDF constructed, using all of the data from both test stands and flights. The ANLOAD prediction was obtained using the RASCAL method. In each of these RASCAL analyses, 40 discrete intervals were used and 25 samples per interval were obtained. Also, the RASCAL method was used by requiring that the input PDFs were calculated between the 1 and 99 percentile values.

The independent, or input, variables used in these analyses are the first five independent variables from the influence function list: the commanded mixture ratio, fuel inlet total pressure, oxidizer inlet total pressure, fuel inlet temperature, and the oxidizer inlet temperature. These independent parameters were chosen because they introduce the most variability in predicted results and previous analyses have characterized their PDF forms. The inputs used are contained in Table 5.5.

TABLE 5.5. INDEPENDENT ENGINE VARIABLE PDF PARAMETERS

Independent Variable	Distribution	Parameter 1*	Parameter 2**
Commanded Mixture Ratio	Uniform	5.97443	6.05108
Fuel Inlet Pressure	Normal	30.0	1.5
Oxidizer Inlet Pressure	Normal	64.3341	21.0374
Fuel Inlet Temperature	Lognormal	3.61308	0.0162595
Oxidizer Inlet Temperature	Lognormal	5.10174	7.19274E-03

---

*Parameter 1 is the lower bound for a uniform distribution, the mean for a normal distribution, and the modal for the lognormal.

**Parameter 2 is the upper bound for a uniform distribution, the standard deviation for a normal distribution, and the transformed standard deviation for the lognormal.

FUEL MASS FLOWRATE COMPARISON
104% POWER TEN SECOND DATA BASE
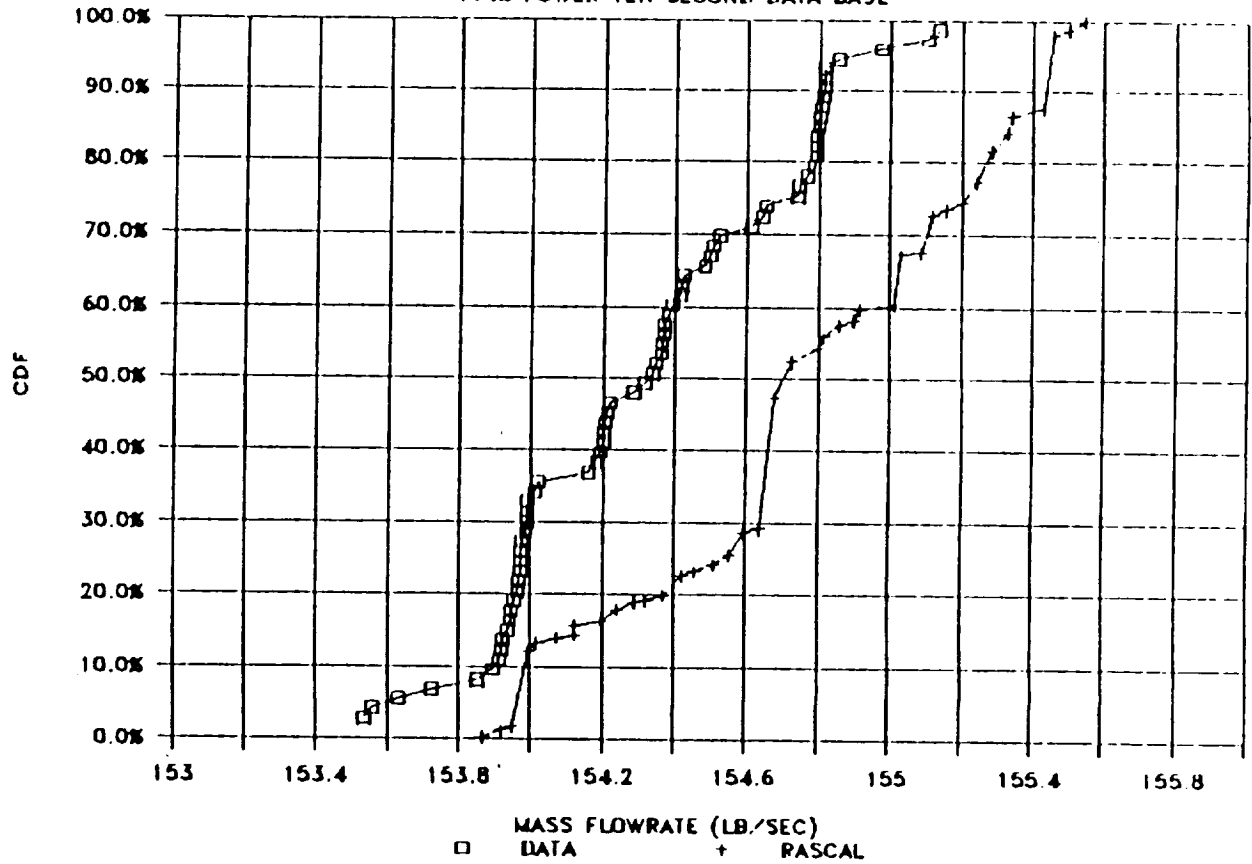
Figure 5.10.   Comparison of ANLOAD Prediction and Data For Fuel Mass Flow

As Figure 5.10 indicates, the general shape of both CDFs are the same but the ANLOAD prediction is shifted to the right. Figure 5.11 shows a similar result for the LOX mass flowrate. Figures 5.12, 5.13, and 5.14 do not show the pronounced shift that the previous two figures indicated, but there is an obvious bias in the prediction for the OPB and HPOT discharge temperature. This bias does not appear as a skewness in the CDF but rather is a uniform shift of data.

There are two possible explanations for this shift.* One explanation is that the influence coefficients are not sufficiently accurate in their prediction of engine variables. The other is that the data sets have a built-in bias. This bias can arise because the ANLOAD predictions are based on combining inputs from which distributions are calculated from a data set which is different from the data used to compare dependent variable results. The first explanation is believed to be the more plausible. There is some error associated with the use of the influence functions: by definition they are approximations to the detailed analysis. If the predicted average values and the averages calculated from the data are compared (ref. Table 5.6), it is quickly seen that these values are all within 1.0% of each other. This implies that the influence functions are predicting absolute values of five engine variables correctly, within the 1.0% error. To some extent, the shift seen in Figures 5.10 through 5.14, especially in the 20 to 80 percentile ranges, is also caused by the use of RASCAL in which the lower and upper tail regions are calculated more accurately. (Remember that 40 discrete intervals would lead to estimates between the 2.5 and 97.5 percentile values while the input required analyses between the first and 99 percentile values). Figures 5.15 and 5.16 show this increased accuracy in the upper tail regions for two of the five engine variables.

---

*The possibility of an incorrect results from ANLOAD is discounted because of validation studies reported in the previous section.

LOX MASS FLOWRATE COMPARISON

104K POWER TEN SECOND DATA BASE
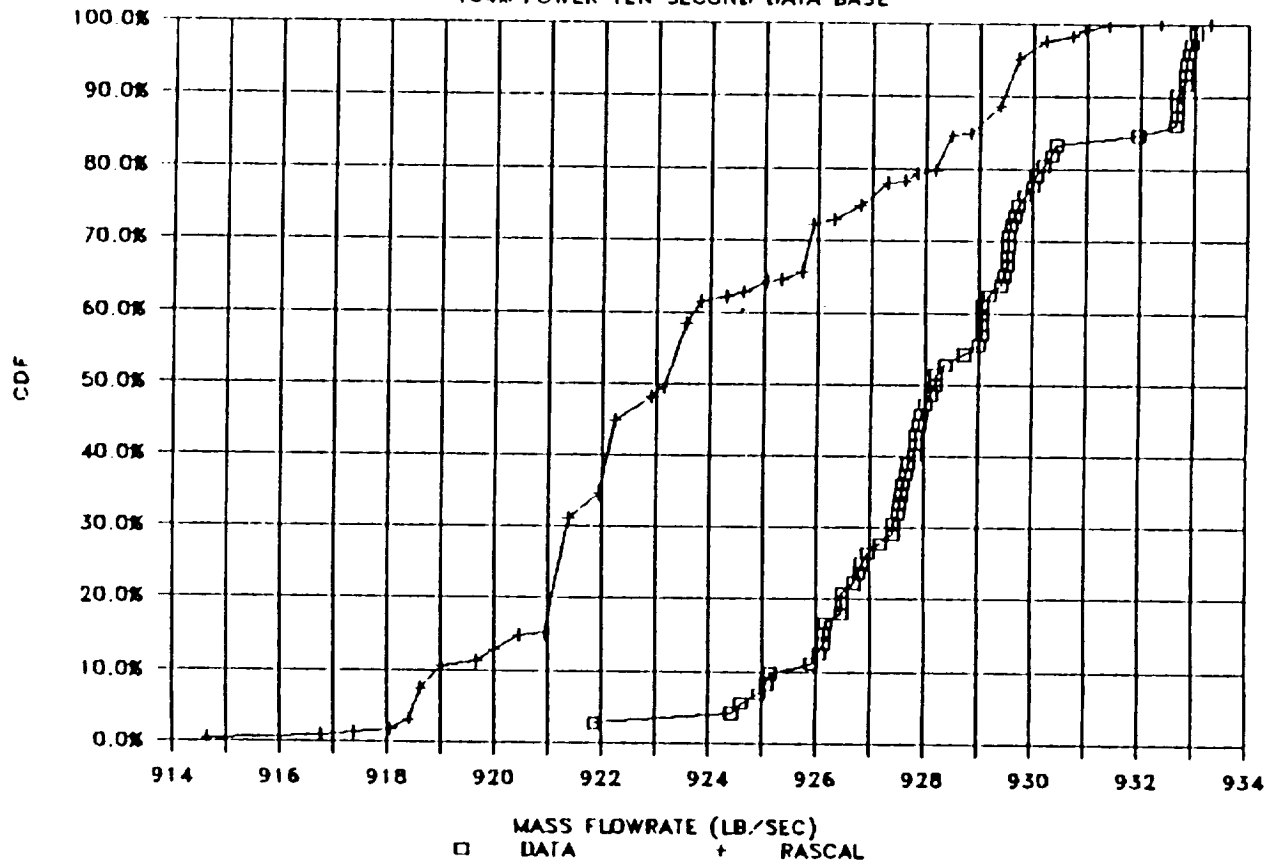
Figure 5.11.   Comparison of ANLOAD Prediction and Data for LOX Mass Flow

OPB DISCHARGE TEMPERATURE COMPARISON

104% POWER TEN SECOND DATA BASE
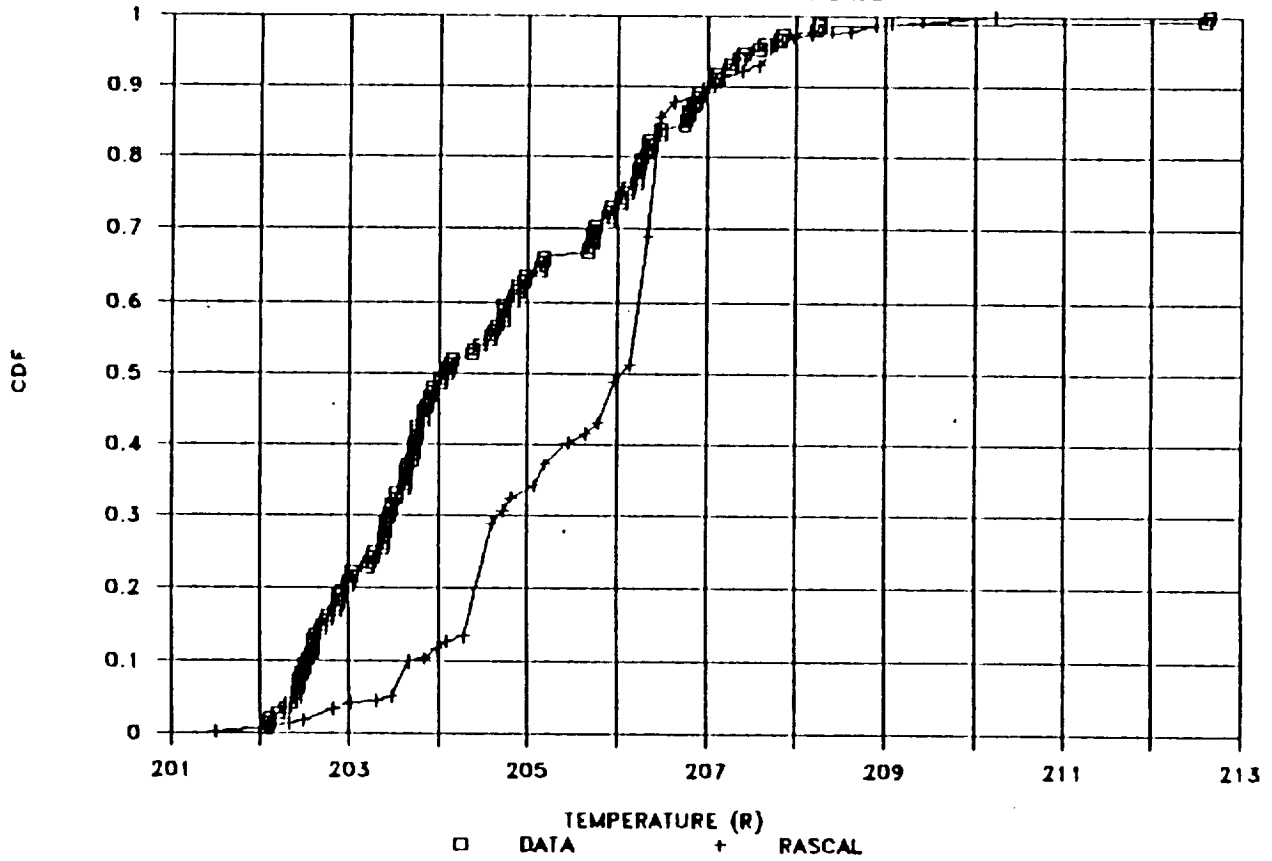
Figure 5.12.   Comparison of ANLOAD Prediction and OPB Discharge Temperature

HPOT DISCHARGE TEMPERATURE COMPARISON
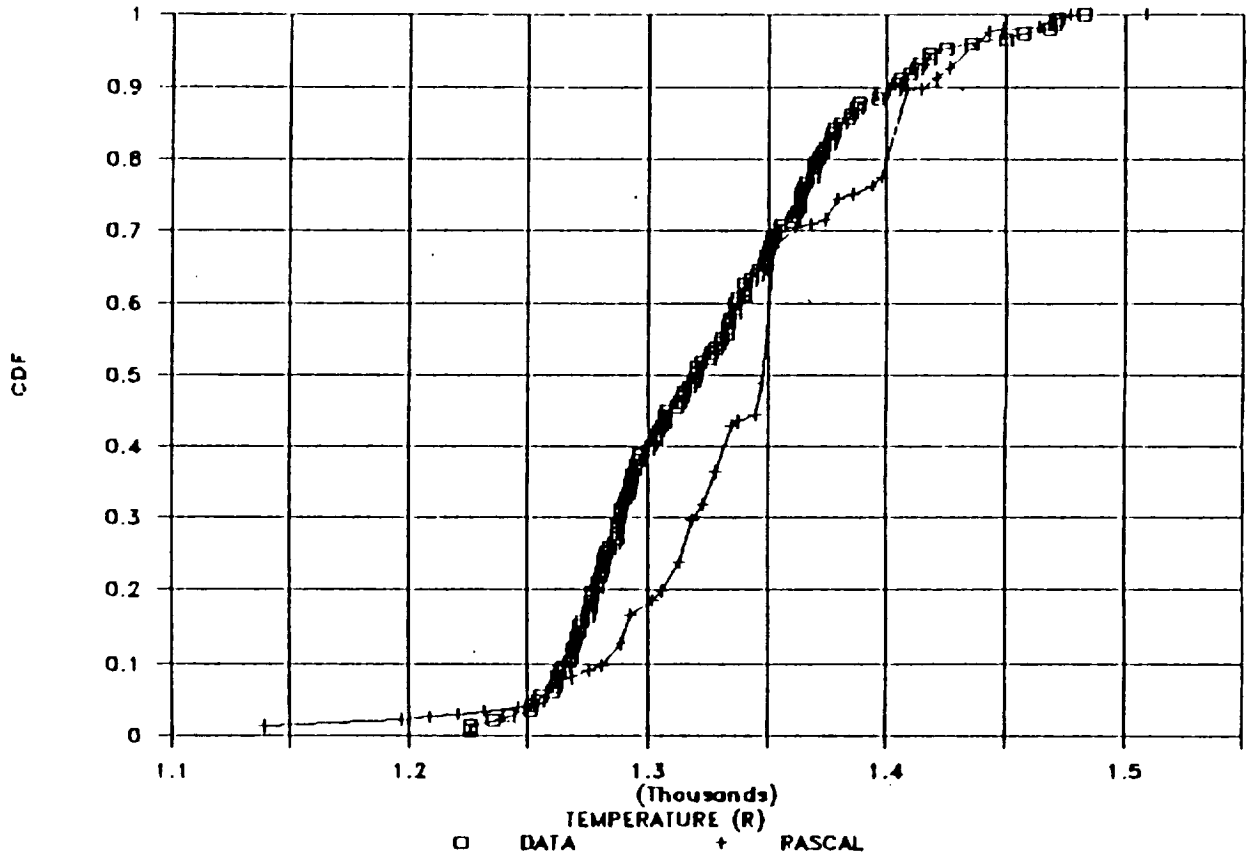
Figure 5.13. Comparison of ANLOAD And HPOT Discharge Temperature

LPOT TURBINE SHAFT SPEED COMPARISON

104% POWER TEN SECOND DATA BASE
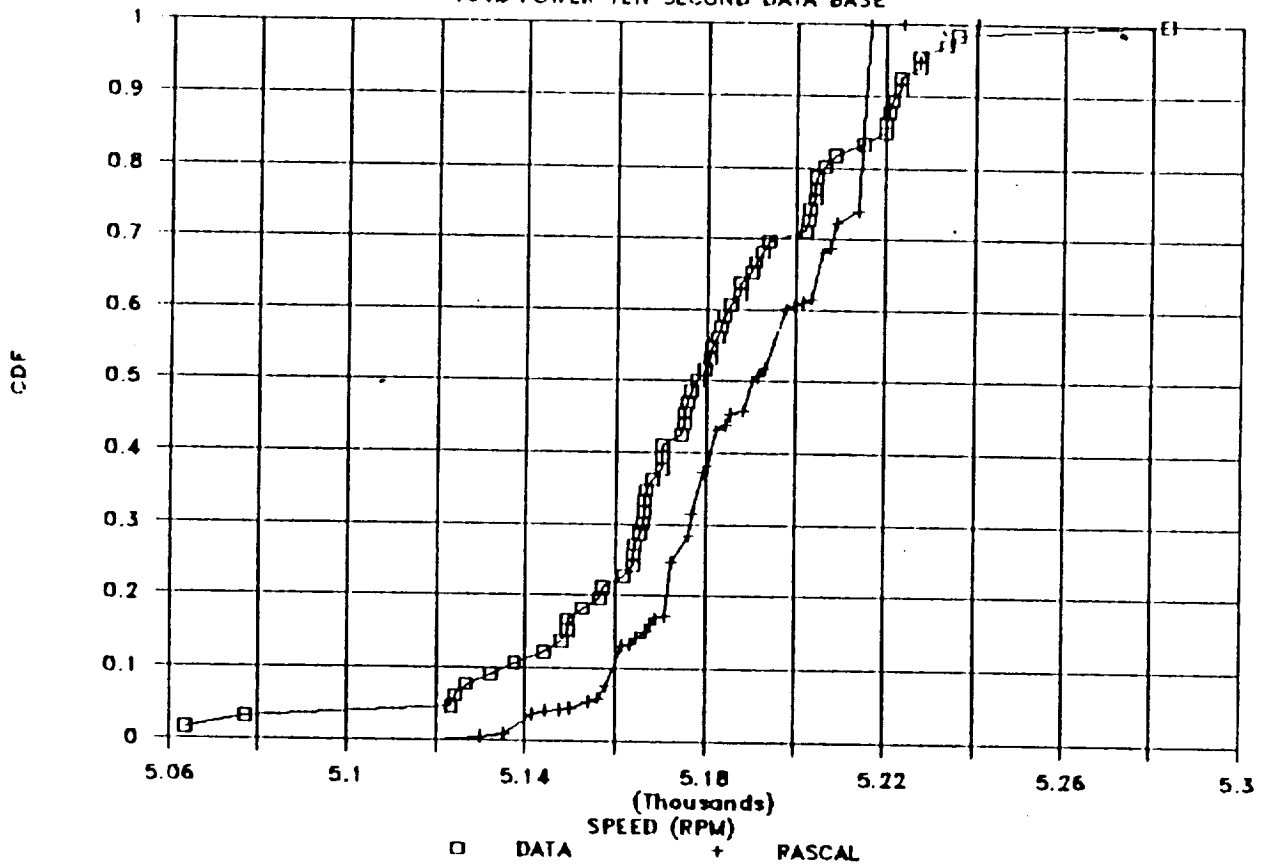
Figure 5.14.   Comparison of ANLOAD and LPOT Turbine Speed

TABLE 5.6.   CALCULATED AND PREDICATED AVERAGE VALUES FOR ENGINE ANALYSES

	ANALYSIS METHOD				
	MONTE CARLO	RASCAL EQUAL	RASCAL EQUAL	DATA: FLIGHT	DATA: TESTS
LOX Mass Flow Rate					
Mean Value	930.745	930.740	924.018	927.721	929.849
Standard Deviation	1.359	1.438	3.641	1.492	2.745
Coefficient of Variation	0.15%	0.15%	0.39%	0.16%	0.30%
Error in Mean (Flight)	-0.32%	-0.32%	0.40%	NA	-0.23%
H₂ Mass Flow Rate					
Mean Value	154.711	154.671	154.704	154.294	154.347
Standard Deviation	0.499	0.500	0.475	0.300	0.431
Coefficient of Variation	0.32%	0.32%	0.31%	0.19%	0.28%
Error in Mean (Flight)	-0.27%	-0.24%	-0.26%	NA	-0.03%
OPB Discharge Temperature					
Mean Value	205.925	205.967	206.001	203.676	205.215
Standard Deviation	1.642	1.567	1.540	1.436	1.284
Coefficient of Variation	0.80%	0.76%	0.75%	0.71%	0.63%
Error in Mean (Flight)	-1.09%	-1.11%	-1.13%	NA	-0.75%
LPOT Shaft Speed					
Mean Value	5181.90	5180.24	5180.66	5130.26	5184.05
Standard Deviation	15.255	15.785	16.125	2116.561	30.326
Coefficient of Variation	0.29%	0.30%	0.31%	41.26%	0.58%
Error in Mean (Flight)	-1.00%	-0.96%	-0.97%	NA	-1.04%
HPOT Discharge Temperature					
Mean Value	1349.79	1350.38	1298.18	1298.18	1272.44
Standard Deviation	20.551	21.353	75.929	22.907	16.053
Coefficient of Variation	1.52%	1.58%	5.85%	1.76%	1.26%
Error in Mean (Flight)	-3.82%	-3.87%	-3.79%	NA	2.07%

To correctly remove the bias from the data and make direct comparisons of CDF values, it is necessary to rerun the analyses using equal probability intervals. Equal probability intervals are needed in order to subtract the bias in the results without changing the distribution shape. Thus, if the difference in the mean value calculated from the data and the predicted mean value from

the ANLOAD calculation is subtracted from each of the dependent engine variable's DPD, then the predicted standard deviation will remain constant. This then allows the predicted CDF to be shifted left or right without affecting the shape of the distribution. If unequal probability intervals are used, then this simplified modification to the results is not possible and comparisons are difficult.

These analyses were performed, again using RASCAL, but with 25 discrete intervals used to describe each of the five input CDFs.

OPB DISCHARGE TEMPERATURE COMPARISON
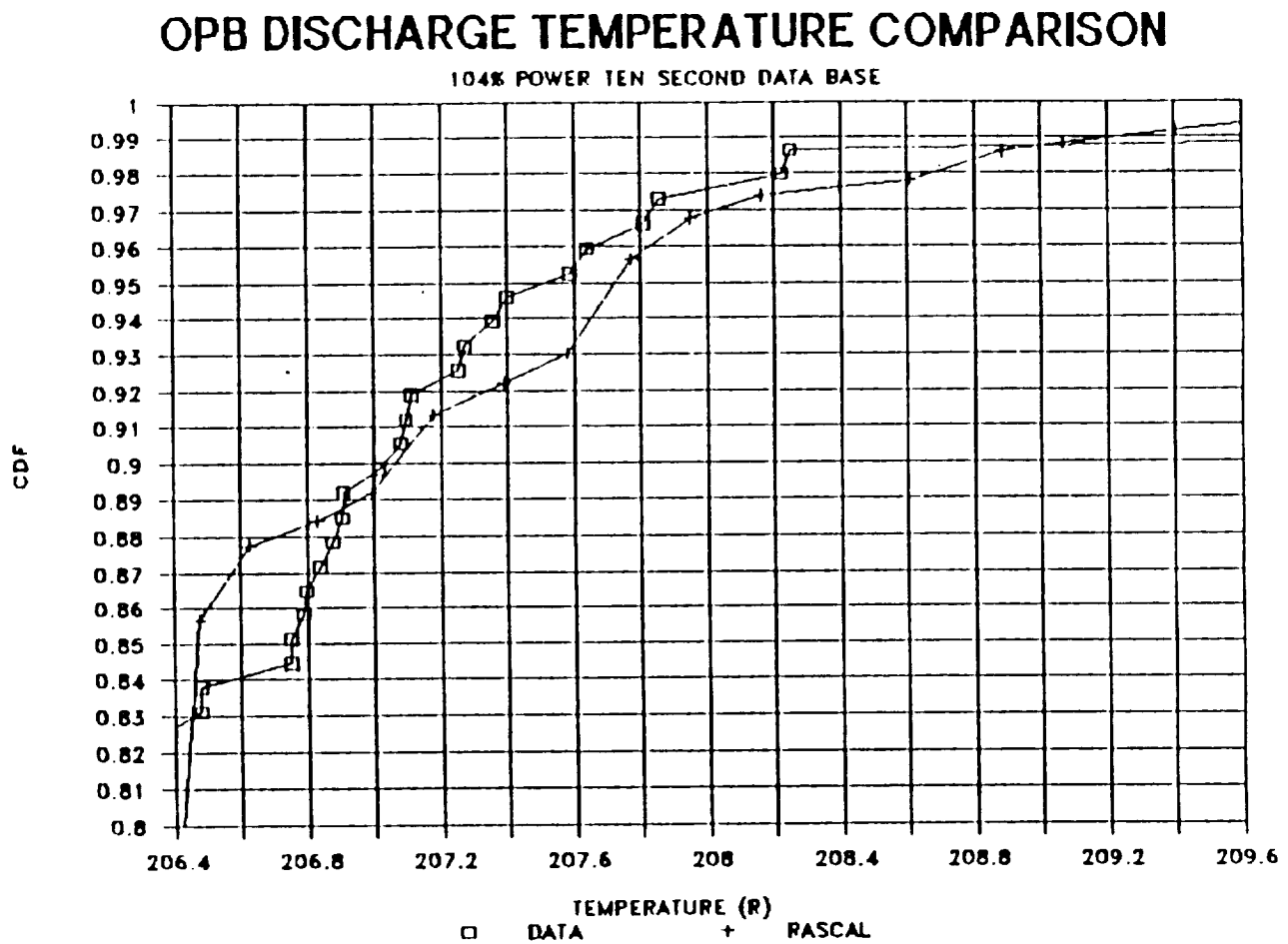
Figure 5.15. Upper Tail Comparison For OPB Discharge Temperature

HPOT DISCHARGE TEMPERATURE COMPARISON

104% POWER TEN SECOND DATA BASE
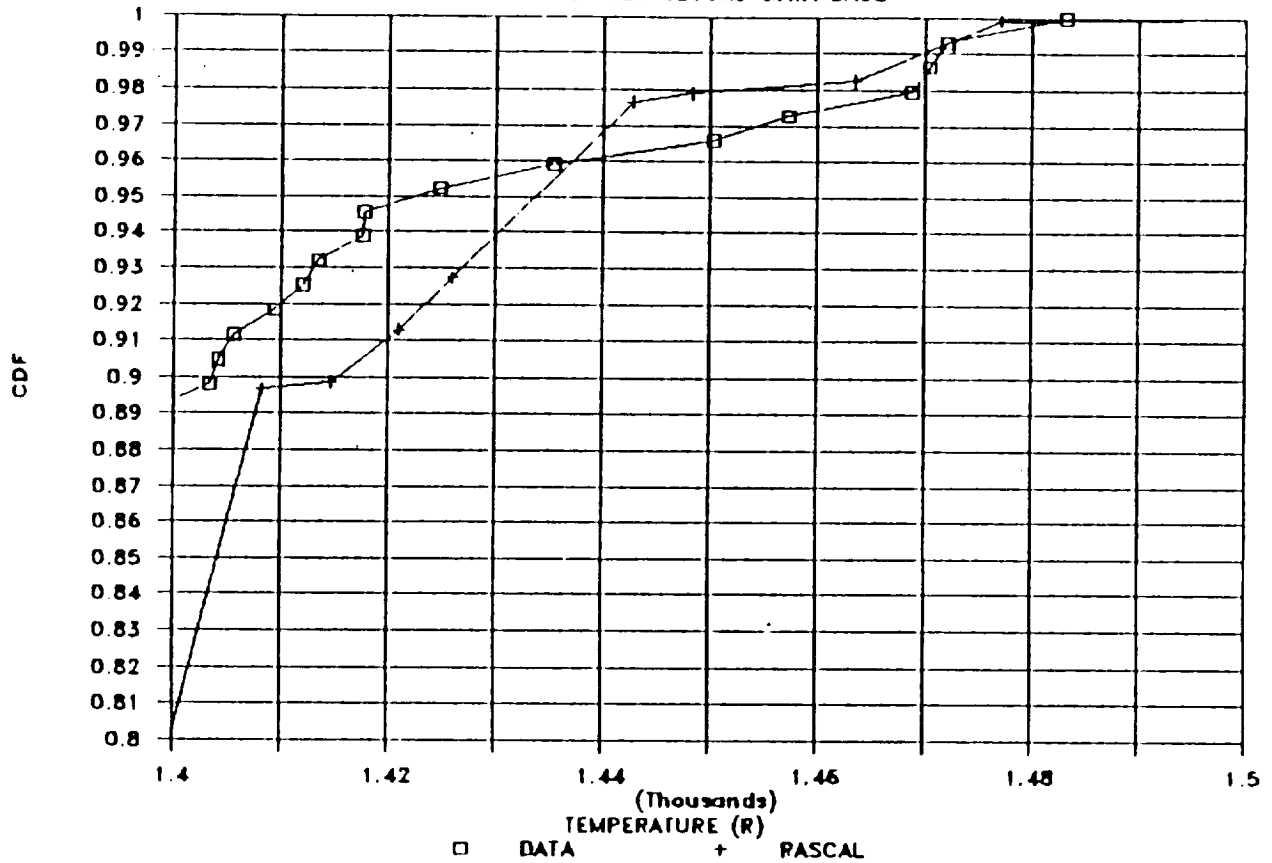
Figure 5.16 Upper Tail Comparison For HPOT Discharge Temperature

The independent parameter otherwise remained the same as the previous analyses. In addition, a Monte Carlo analysis was performed for each of the five dependent variables so that confidence limits on the predictions could be obtained. This was also done to demonstrate the fact that the RASCAL methodology, with equal probability intervals, is not causing any shift (systematic or otherwise) in the predicted CDF values.

The results of the calculations when all of the data are plotted as a single CDF value is similar to the previous analyses and are not reproduced here. The form of the CDF is similar for both the predicted and calculated data

values but there is still much more variability in the data than is being predicted by the ANLOAD results. To explain this inconsistency, the data was examined in many ways. What was determined is that the ANLOAD program agrees well with the flight data and exhibits less variability than the test data. This is shown graphically in Figures 5.17 through 5.26. For example, in Figure 5.19, the LOX mass flow rate from the flight has a standard deviation of approximately one-half of that from the test data. This is to be expected since flight conditions are much more tightly controlled than the possible range of conditions that the designers of an engine may want to retest to certify the engine performance. (This is not meant to imply that tests are not well controlled but that the range of conditions allowed during tests is larger than that allowed during flights). When the test data is removed from the plot (Figure 5.20), one can see how well the prediction actually matches the flight data. The LOX mass flow rate is one of the most accurate predictions, but all of the other predictions follow this same pattern. Each of the figures repeats this same pattern and indicate that the choices for input variables and influence function set reproduces the flight data in a statistically consistent fashion.

FUEL MASS FLOWRATE COMPARISON

104% POWER TEN SECOND DATA BASE
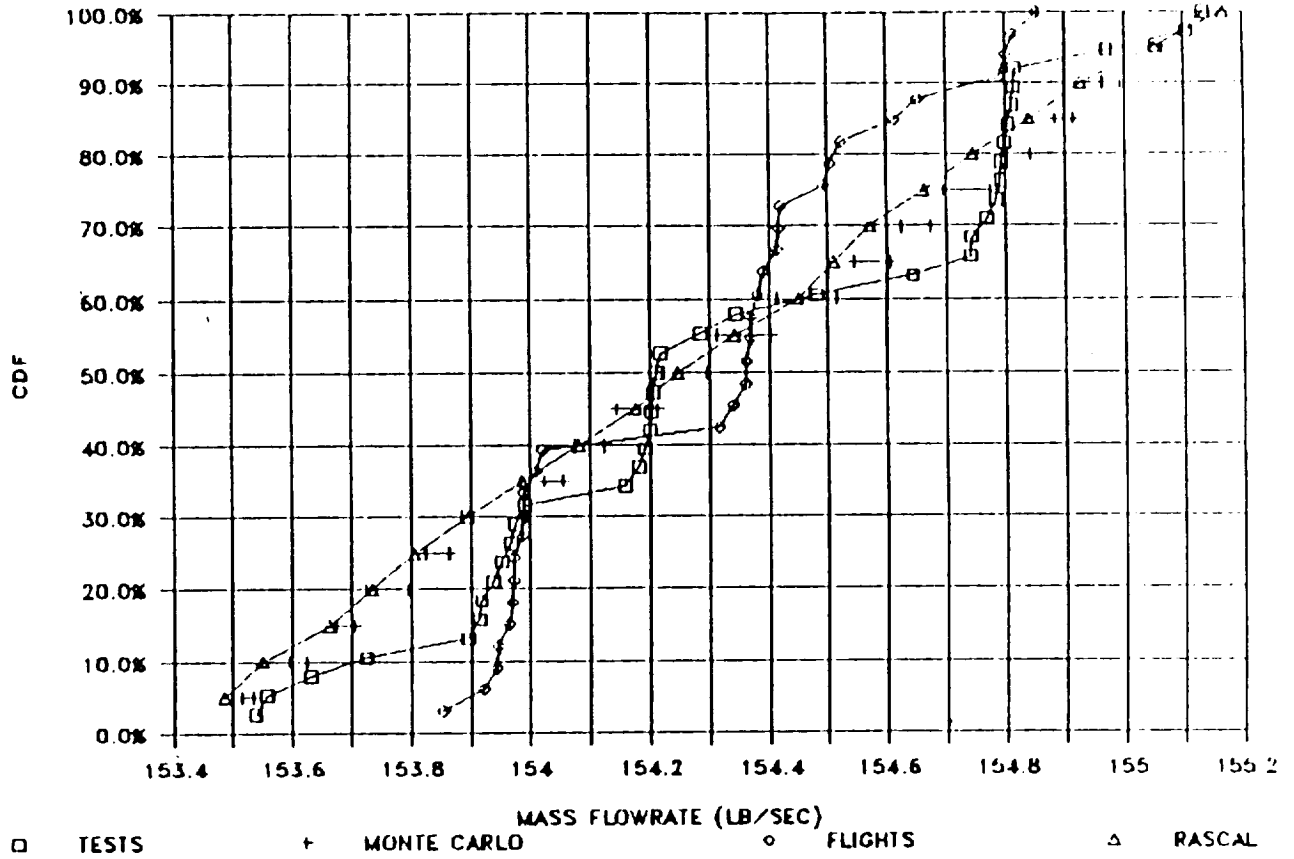
Figure 5.17   Test Data, Flight Data and ANLOAD Comparison for Fuel Flow

FUEL MASS FLOWRATE COMPARISON

104% POWER TEN SECOND DATA BASE
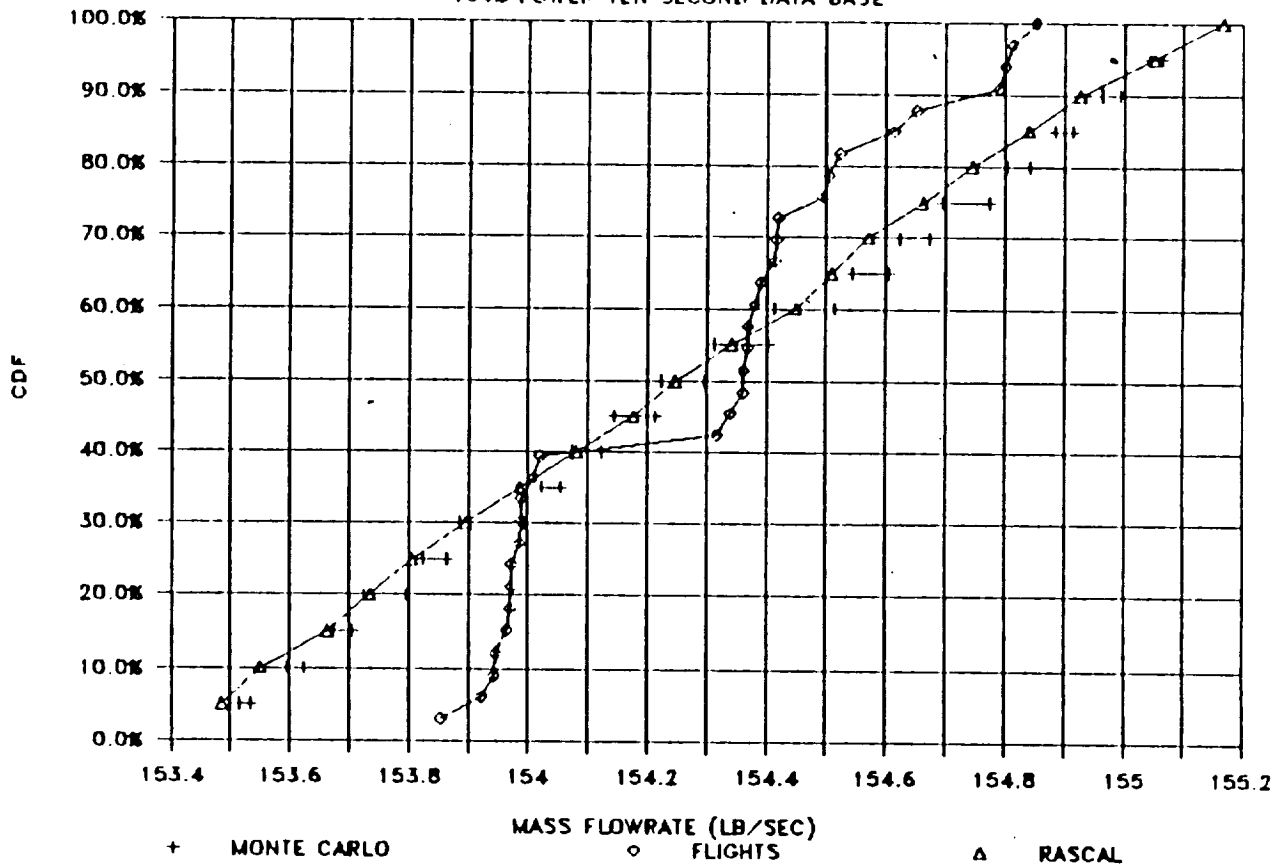
Figure 5.18   Flight Data and ANLOAD Comparison for Fuel Flow

5-48

C-2

LOX MASS FLOWRATE COMPARISON

104% POWER TEN SECOND DATA BASE
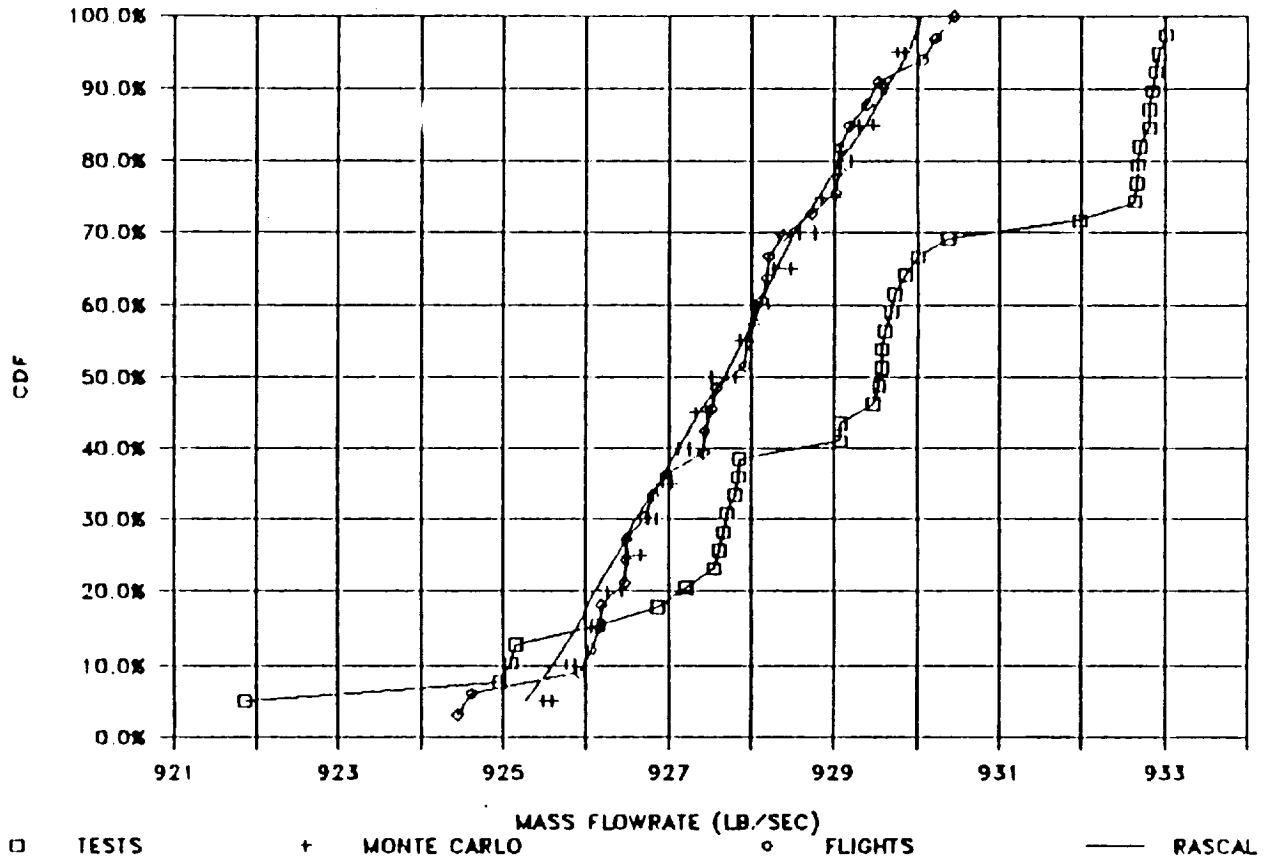
Figure 5.19 Test Data, Flight Data And ANLOAD Comparison For LOX Flow

LOX MASS FLOWRATE: FLIGHTS ONLY

104% POWER TEN SECOND DATA BASE
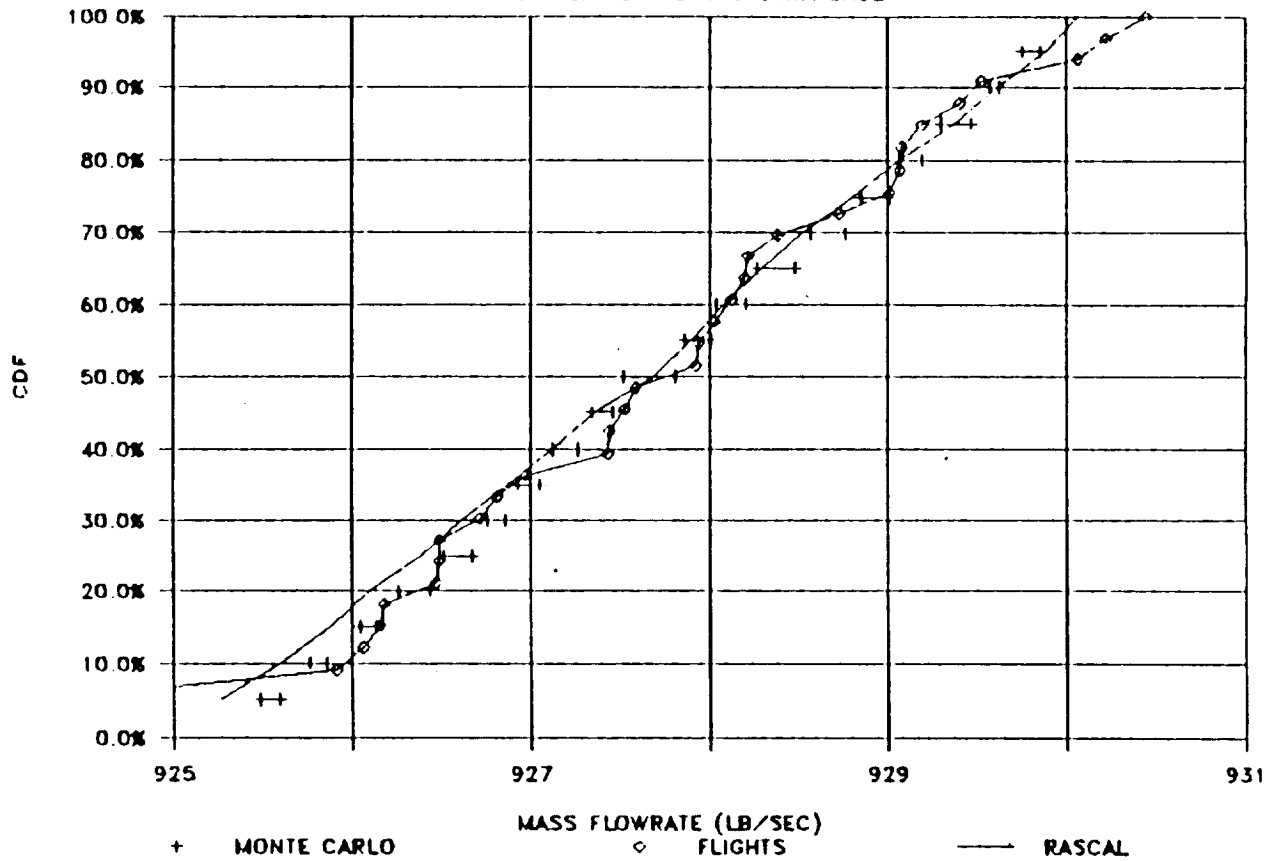
Figure 5.20   Flight Data And ANLOAD Comparison For LOX Flow

OPB DISCHARGE TEMPERATURE COMPARISON

104K POWER TEN SECOND DATA BASE

□ TESTS   + MONTE CARLO   ◇ FLIGHT   △ RASCAL
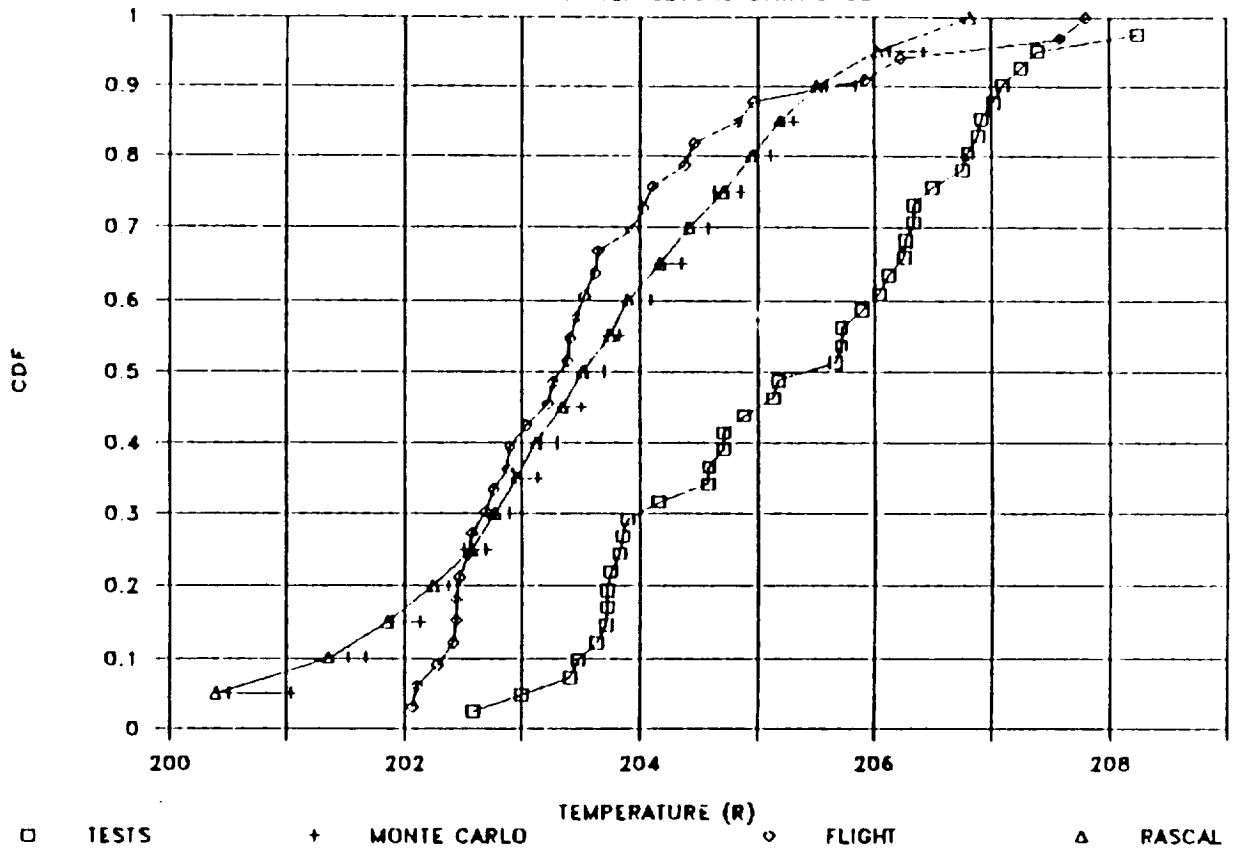
Figure 5.21   OPB Discharge Temperature Validation Using Flight/Test Data
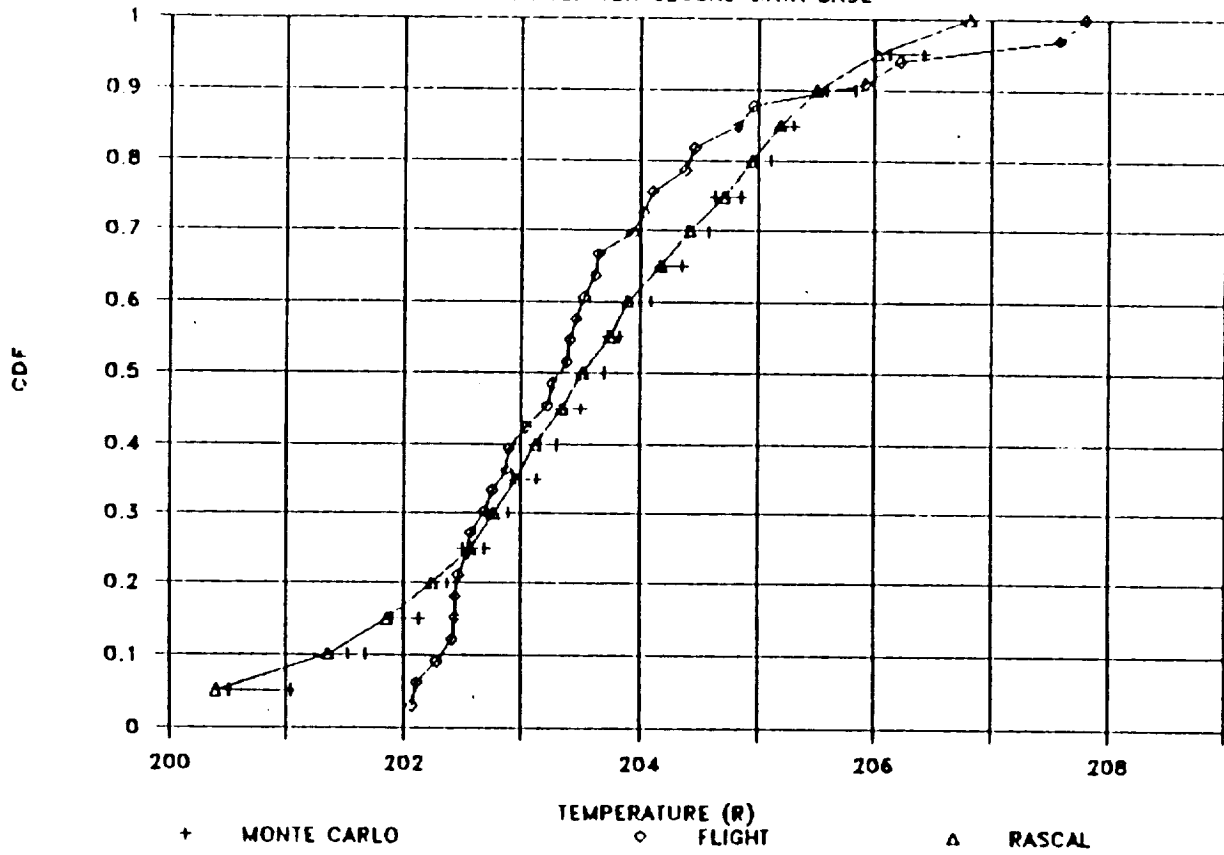
Figure 5.22 OPB Discharge Temperature Validation Using Flight Data

HPOT DISCHARGE TEMPERATURE COMPARISON

104% POWER TEN SECOND DATA BASE
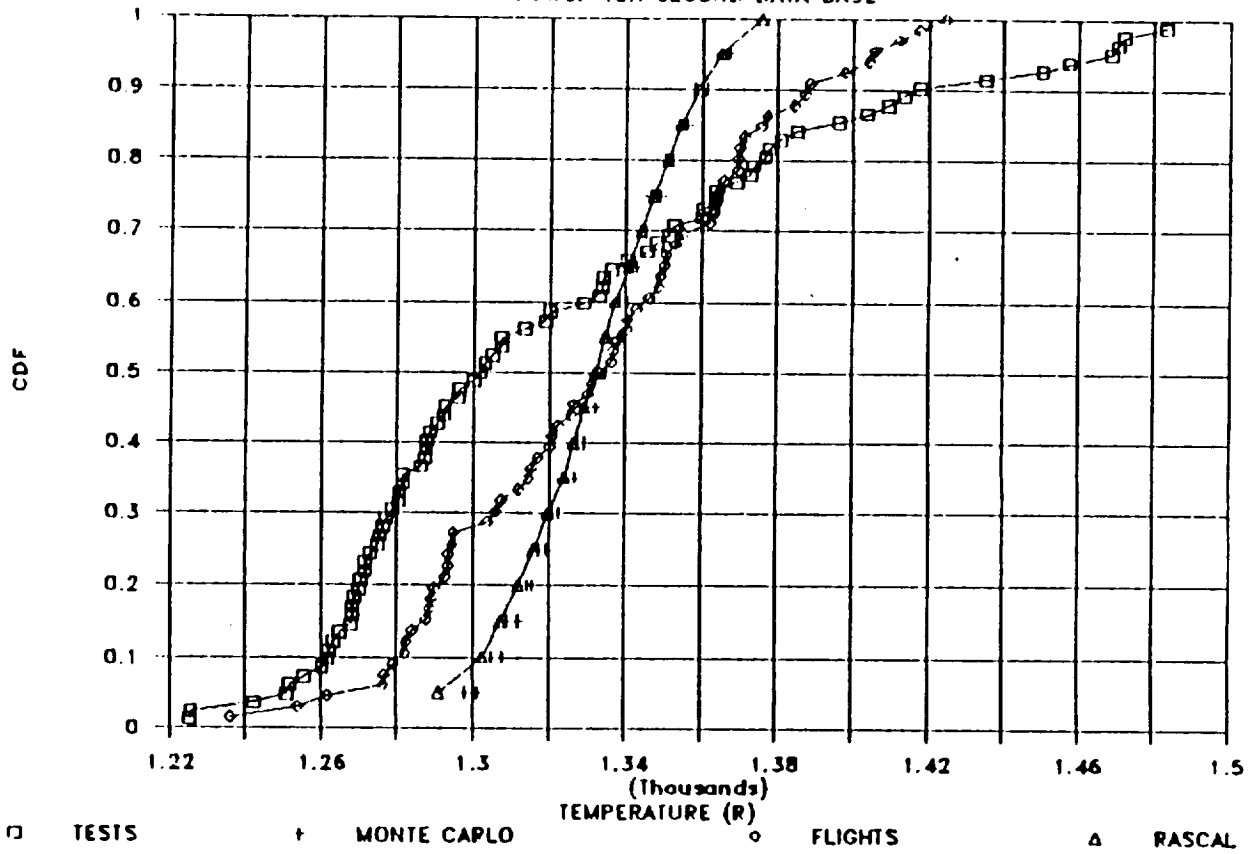
Figure 5.23 HPOT Discharge Temperature Validation Using Flight/Test Data
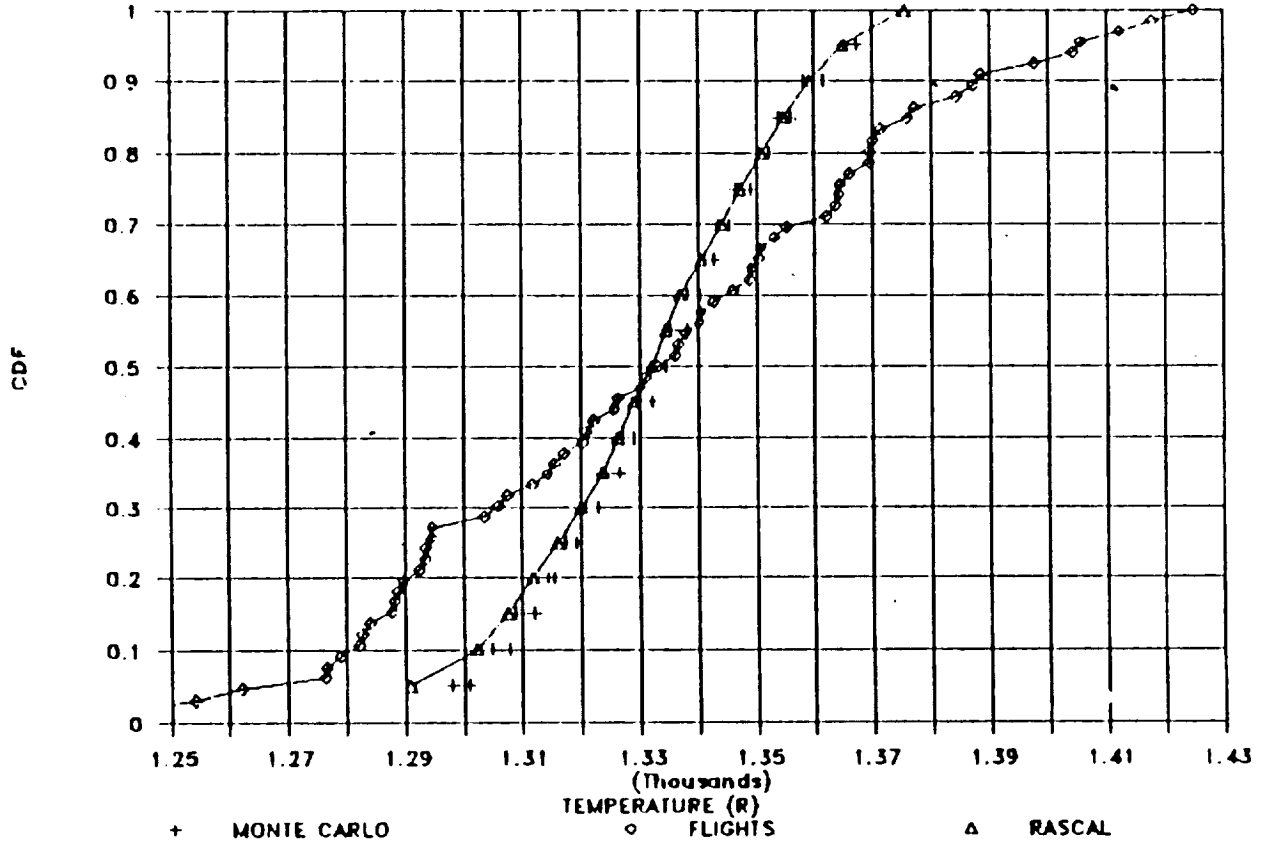
Figure 5.24 HPOT Discharge Temperature Validation Using Flight Data

Figure 5.25 LPOT Turbine Speed Validation Using Flight/Test Data

LPOT TURBINE SHAFT SPEED COMPARISON

104% POWER TEN SECOND DATA BASE
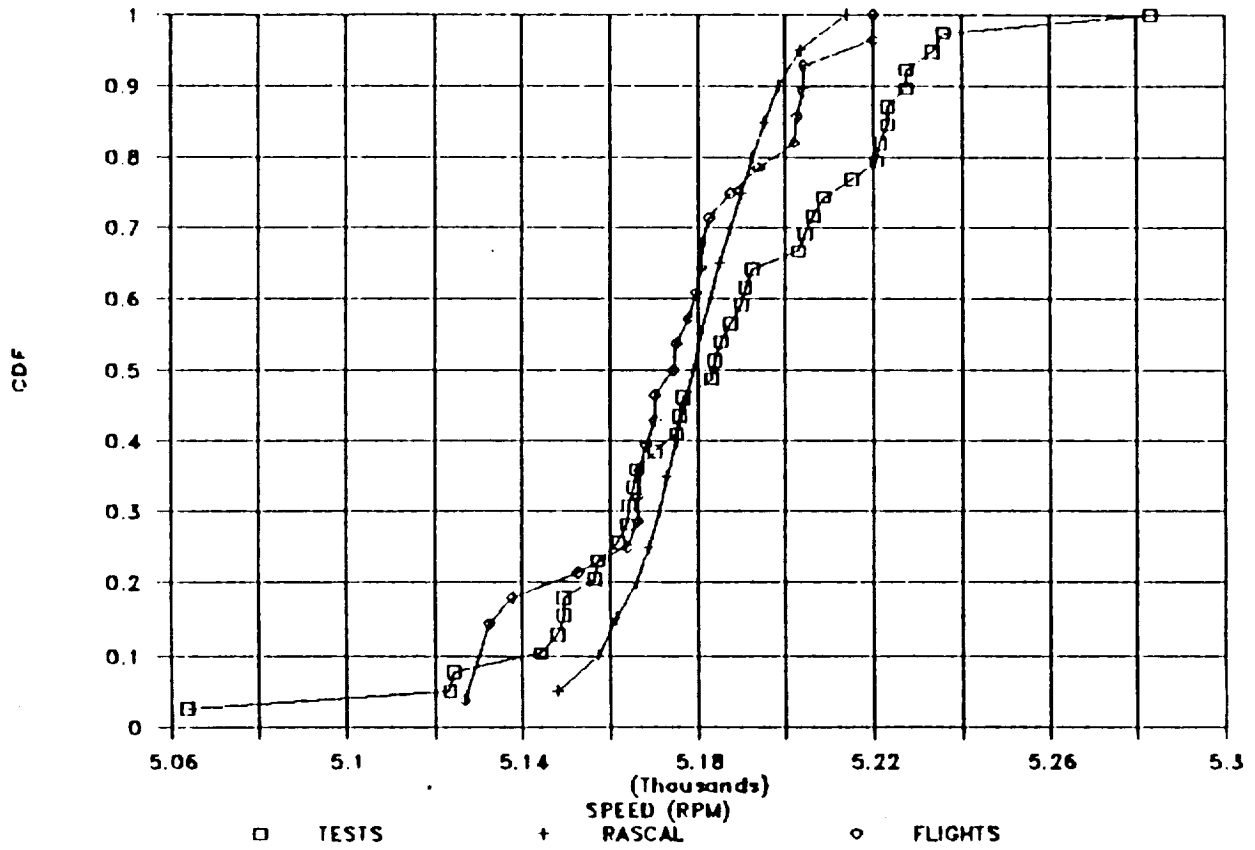
Figure 5.26 LPOT Turbine Speed Validation Using Flight Data

Summary

The set of influence functions used to perform these calculations were derived from a nominal engine balance computer code. Since the code was assuming that the engine would not undergo severe transient behavior during flight, it was expected that the variability built into the coefficients would be minimized. This was exactly what was found. The probabilistic model contained in ANLOAD predicted the variability in flight data well, but did not predict as large a spread in the data as was seen in test data. This was also expected since the input distributional forms were derived primarily from flight data, although there was some mixing of results in the distributional fitting procedure. It is believed that the spread in the entire data set can be predicted if the input distributional forms are changed to reflect the larger variability contained in test conditions.

However, one must keep in mind the ultimate purpose of the program development: to derive an expert system model that can be employed by a relatively inexperienced engine designer. If the large variability contained in the entire data set is included in base coefficients, then unnecessarily stringent tolerances will result because the predicted variability in the load would be much larger than that which would credibly be encountered in flight conditions. Therefore, the set of coefficients and input distribution descriptions for independent loads are believed to be the best representation of the currently used space propulsion engine parameters and loads.

6.0 LDEXPT, The Load-Expert System

6.1 Objective and Approach

The objective of the CLS is to develop generic load models with multiple levels of progressive sophistication to simulate the CLS induced in space propulsion system components, representative of SSMEs. A computer code, incorporating the various individual and CLS models, is being developed to construct the specific load models desired. The approach is to develop incremental versions of the code. Each subsequent version will add sophistication to the component probabilistic load definition and decision rules. The probabilistic loads thus generated will be useful in space propulsion system design and probabilistic structural analyses.

The space propulsion system is a complex machinery. Tremendous amounts of load information and numerous engine data are being generated over the years. Probabilistic load synthesis not only demands sophisticated probabilistic methodology, but it requires knowledge of state-of-the-art space propulsion system load analyses and calculations. It encompases the knowledge of over 30 years of experience of rocket engine design, analysis and manufacturing at Rocketdyne, NASA, and other institutions. The approach for the CLS program is to develop a knowledge-based or expert system which can interface with the load calculation routines to synthesize the load spectra of a generic propulsion engine.

A knowledge-based system has the facility of building a domain knowledge base which, in a broad sense, includes decision rules, numerical data, and evaluation procedures. It has the capability to perform logical deduction and inferences and, as such, can help users make decisions and solve problems. A knowledge-base environment also allows incremental development and modularization of the knowledge. The knowledge implemented (load models, load data, or load calculation procedures) is readily available to other modules.

The CLS program requires a knowledge-based system that has built-in sophisticated probabilistic modeling and statistical tools, and a large database of rocket engine information. This knowledge-based system will help engineers generate probabilistic loads for select space propulsion system components and will provide probabilistic information for structural analyses. The functions of this knowledge-based system are to manage the load information database, provide expert knowledge in load models and load synthesis, and generate user requested loads. In other words, the CLS program needs a coupled symbolic and numeric processing system. With these constraints, a knowledge-based system in FORTRAN was developed from scratch for the CLS program. The advantage of developing one's own knowledge-based system is that there is no licensing restriction. A knowledge system in FORTRAN facilitates the interface with FORTRAN probability evaluation and load calculation routines. In addition, FORTRAN programs are fairly portable and can be easily implemented into most any computer system. The disadvantage of building one's own system is that generally the user interface is primitive because of cost constraint.

6.2 Intelligence Database System Design

The CLS load-expert system is a hybrid knowledge-based system different from the conventional rule-based product system. The design of the CLS load-expert system follows the "knowledge is power" philosophy. That is the power of a knowledge-based system is its capability for having a vast amount of domain knowledge without the necessity of a complex inferencing scheme. A decision tree inference scheme is employed for simplicity. Each decision tree is implemented as a rule module. To facilitate the communication between rule modules, a simple working memory is implemented for passing information from one rule module to another. The load-expert system has a rule-based module and a knowledge-based module (ref. Figure 6.1). The rule-based module has many rule modules, each of which model a decision tree which performs certain tasks, such as the QLM. The QLM retrieves the load distribution data to do a Gaussian moment method calculation in order to obtain a system load distribution. A user interface module SESUIM takes care of user queries and answers. The knowledge-based module uses a database system to store and manage load

information and data, such as engine system load distribution data. The CLS knowledge-based module is similar to a simple frame-based system except that no inheritance mechanism is built into the system.

The knowledge representation in database format has proven to be the correct and viable choice. The database system manages the large volume of load information. It helps maintain data integrity and avoid data redundancy. It standardizes the data storage and retrieval procedures. It facilitates the communication between the expert system rule-based module and the knowledge base. The CLS approach is to couple the knowledge-based system to a genuine database system which can retrieve and update records, add and delete records, etc. not just a data file, to become an intelligence database system. This approach has demonstrated in this project to be excellent for engineering applications.

The large volume of domain knowledge in data format almost dictates the use of a database system. Writing rules to manipulate the data intelligently, to select and utilize the relevant data in computations increases the power and flexibility of a database system tremendously. Such an intelligent database system is the system being built for the CLS program. Our experience on the system is that the system does well what it intended to do and we are satisfied with the design of the system.

6.3 Knowledge Engineering

Knowledge engineering is the most important task for building a knowledgebased system. Generally, one or more experts are available who know how to solve the problems at hand. In this case, the knowledge engineering task is to extract the knowledge from the expert(s) to transform into rules or other forms that can be implemented on a knowledge-based system. Things are a little more difficult for a research project such as the CLS program. Here, new methodology needs to be developed. First, probabilistic methods need to be implemented. The methodology is available, but the application of the methodology to mechanical loads requires research effort. Next, probabilistic load

models for space propulsion system and components need to be developed. There is a vast amount of knowledge on space propulsion system design and load evaluations accumulated at Rocketdyne. Most of the analyses, however, are using deterministic models and algorithms. The probabilistic load modeling is at the forefront of the research. Knowledge engineering for this task includes learning how Rocketdyne experts model and evaluate the loads. Knowledge engineering also includes transformation of deterministic models into probabilistic models, utilization of the deterministic results, and development of new probabilistic models.

As an example of knowledge engineering, transformation from a deterministic model to a probabilistic model is the rocket engine influence model described in section 4. The deterministic influence model performs engine load evaluation and engine performance prediction. Transformation of the model into a probabilistic one is not as straightforward. One of the reasons is that the purpose of the probabilistic engine model is to provide engine system-dependent loads (system interface operation conditions) to be used as boundary conditions for probabilistic component load models. The deterministic model uses tag values to normalize engines for engine performance prediction, whereas the probabilistic engine model treats all engine operating variables and loads as random variables. Nevertheless, the CLS project has benefited greatly from the availability of rocket engine deterministic influence model and the depth of the Rocketdyne experience in rocket engine design, modeling and evaluation. Without the Rocketdyne team providing their expertise in respected areas, the CLS effort would be futile.

There are situations wherein there are no appropriate models available for generating a certain load. In this case, an appropriate probabilistic model needs to be invented. Such are the cases for the generic probabilistic component thermal load model and the duct fluctuation pressure load model. For example, in developing the thermal load influence model, our aerothermal dynamics expert initially did iterative perturbation analyses using a deterministic thermal analysis code. He then massaged the results and developed the thermal load influence model. The process was a lot more difficult than

described here. It relies on the expert's knowledge of component structure, geometry, and thermal environment. Selection of the system operation condition loads (system-dependent loads) which are the most influential to the component thermal load, requires in-depth knowledge of the system interaction of the component with its environment. For example, in developing the thermal load for the turbine blade temperature, coolant leakage through the worn-off seal has significant effect on the temperature profile at the turbine blade shank region.

Once a probabilistic load model was developed, it was integrated into the load-expert system. Databases for the loads and geometry information were designed and added to the knowledge base file. A rule module for the load model was coded and added to the rule-based module. Queries were written and inserted into the problem text file (query file used by the user interface driver). It is here that the advantage of an incremental development environment for the knowledge-based system is apparent. New knowledge is being added to the system. New rule modules can be built with the new knowledge as well as the information that was already in the knowledge base.

Knowledge engineering is the most crucial step in developing a knowledge-based system. The success of this program depends largely on it. The fact that there is a Rocketdyne team with 30 years of expertise in rocket engine design and development to draw from ensures Rocketdyne the highest probability of success.

6.4   The Load-Expert System: LDEXPT Version 2.1

The load-expert system, LDEXPT version 2.1, was implemented on the NASA Lewis Research Center's mainframe computer. It is in the VM/CMS operating system. At the writing of this report, the load-expert system is being updated to LDEXPT version 3.0. As mention earlier, an expanded loads and influence coefficient set will be implemented. The load-expert system is an interactive system. The structure of the system is shown in Figure 6.1. The load-expert

system has a rule-based module and a knowledge-based module. The rule-based module has the user interface system SESUIM taking care of user query and answer functions. The rule-based driver RBMS controls the overall process of running a user-selected rule module, performing a load calculation with the ANLOAD module, etc. The knowledge-based module has a database system, a duty-cycle-data processing module, and a file I/O module. The database system manages the knowledge base and takes care of database functions, such as database retrieval and update. The file I/O module performs file input and output to the operating system.

The Database

The database system of the load-expert system is a genuine database system. It is a flat-file database system which has most of the database operations. An index sequential access method (ISAM) algorithm is employed for the retrieval of the database records. A key file is constructed for each database table. The keys are sorted in ascending order. Records are then retrieved through the indices stored in the key file. The system can be upgraded to a relational database system if the relational algebra, such as joining (union and intersection) the database tables, is implemented. If such need arises, the relational algebra will be implemented.

Available database functions include: database table creation, record selection, record deletion, updating database tables, building key files, and saving database. The database commands of the load-expert system as follows:

COMMAND	FUNCTION
?DBCR	Create a database table
?DBCF	Create fields for a database
?DBBK	Build key file
?DBSL	Select database record(s)
?DBDL	Delete database record(s)
?DBDF	Display field and key names
?DBUP	Update and/or add database record(s)
?DBRD	Open a database file

COMMAND	FUNCTION
?DBSV	Save an updated database
?DBLT	List all records of a database table
?DBLK	List all key variables of a database
?INLD	Special command for input SSME loads
?INFL	Special command for input infl. coeffs
?HELP	List available database commands
?RETN	Return to KBMS
?QUIT	Exit LDEXPT

The Knowledge Base

The domain knowledge for the probabilistic engine load synthesis of a space propulsion system consists of two main areas: the probabilistic methodology and modeling, and the rocket engine structural load information and evaluation. The probabilistic methods and calculation are implemented on the load-expert system with traditional algorithmic and procedural codes. These coding routines are included in the load calculation module ANLOAD as discussed in section 5. The load information and the load model information are implemented in the knowledge base. The information of the knowledge base is utilized and processed by the rule modules. The synergism of the two domain knowledge bases and the coupling of the symbolic and numeric processing have to be brought about to a successful knowledge-based system for the CLS project.

The knowledge base of the load-expert system is managed by the database system. The knowledge base includes the following database tables:

TABLE GROUP NAME	NUMBER OF TABLES	INFORMATION DESCRIPTION
LIDP	1	System independent loads
LDEP	1	System dependent loads
INFC	16	Influence coeff's set
DFAT	1	Duty-cycle-data file IDs
LTBC	1	Turbine blade static pressure loads

TABLE GROUP NAME	NUMBER OF TABLES	INFORMATION DESCRIPTION
LCTH	1	Component loads
SCTH	1	Component load models
ICTH	1	Component load scaling coeffs
DUCT	1	Duct geometries
CLFP	1	Fluctuation pressure loads

The knowledge base has engine load information and their distribution parameters as delineated in Figure 6.2 and 6.3. The engine loads can be classified by four categories: (1) system-independent loads, (2) system-dependent loads, (3) component independent local loads, and (4) the component loads. The system-independent loads include engine inlet operating parameters and engine hardware parameters. Engine inlet operating parameters are the engine mixture ratio, the fuel inlet pressure and temperature, and the oxidizer inlet pressure and temperature. Engine hardware parameters relate to hardware performance, i.e., turbopump efficiency, turbine efficiency, and valve resistance, etc. The system-dependent loads are the engine performance-related variables and the system interface loads. Engine performance variables are the engine thrust, fuel and oxidizer flowrates, etc. Engine system interface loads are the system operating boundary condition loads, such as turbine inlet and discharge pressures and temperatures, and the HGM (Hot Gas Manifold) fuel inlet pressure. These loads define the operating conditions for system components. The component independent local loads and component loads are loads local to the components. The component local independent loads are related to geometry and other effects local to the component under consideration. An example is the coolant seal leakage geometry factor for the turbine blade. The component loads are important in structural analysis and failure probability evaluation of the particular component. Examples of the component loads are the turbine blade pressure and temperature, transfer duct static and dynamic pressures, etc. The knowledge base has the mean values, coefficients of variation and distribution type for all these loads. The information is stored in database format. Examples of the databases LIDP and LDEP are shown in Figures 6.4 and 6.5. In these databases, the load

Independent Loads

- Commanded power level
- Engine inlet operating parameters
  - Mixture ratio
  - Fuel inlet pressure & temperature
  - Oxidizer inlet pressure & temperature
- Engine hardware parameters
  - Pump efficiency
  - Turbine effeciency
  - Main oxidizer valve resistance
  - Turbine flow coefficient

System Level Dependent Loads

- Engine performance parameters
  - Engine fuel flowrate
  - Engine oxidizer flowrate
  - Engine thrust
- Engine operating parameters
  - Pump speed
  - Turbine inlet & discharge pressures
  - Turbine torque
  - HGM fuel inlet pressure

Component Level Composite Loads

- Component loads
  - HPFTP turbine blade pressure & temperature
  - Transfer duct static pressure
  - Transfer duct dynamic pressure
  - LOX post temperature
- Local independent loads
  - Coolant seal leakage
  - Hot gas seal leakage
- Composite loads for
  - Turbine blades
  - Transfer ducts
  - LOX posts
  - HPOTP discharge duct

90c-4-339-30

Figure 6.2. Load–Expert System Load Model Knowledge Base

Rockwell International
Rocketdyne Division

6-10

Engine System Model

- Load distributions
  Means
  Coefficients of variation
  Distribution types
  Nominal value coefficients
- Probabilistic influence model
  Influence coefficients
  1 σ gain values

Component Load Models

- Generic static pressure scaling model
- Generic probabilistic thermal load model
- Generic turbine blade pressure load model
  Tip, mean & hub cross section pressures
  Turbine blade pressure interpolation scheme
- HPFTP 2nd stage turbine blade pressure & temperature loads
  2519 nodes geometry model
  Reference nodal pressures & temperatures
- Turbine blade dynamic pressure load model
- Duct dynamic pressure load model
  Transfer ducts, LOX posts, HPOTP discharge duct
- Transient LOX post thermal load model
- Vibration model

Figure 6.3.   Load-Expert System Load Knowledge Base

Rockwell International
Rocketdyne Division

6-11

LIDP-ID	LD-NAME	MEAN	COV	P3	DIST	NE-COEF1	NE-COEF2	NE-COEF3	NE-COEF4
1	MR	0.60000E+01	0.20000E-02	0.00000E+00	UNIFORM	0.60000E+01	0.00000E+00	0.00000E+00	0.00000E+00
2	F-PI	0.30000E+02	0.25900E+00	0.00000E+00	EV-1	0.30000E+02	0.00000E+00	0.00000E+00	0.00000E+00
3	O-PI	0.10000E+03	0.32700E+00	0.00000E+00	NORMAL	0.10000E+03	0.00000E+00	0.00000E+00	0.00000E+00
4	F-TI	0.37000E+02	0.16000E-01	0.00000E+00	LOGNORM	0.37000E+02	0.00000E+00	0.00000E+00	0.00000E+00
5	O-TI	0.16400E+03	0.11000E-01	0.00000E+00	LOGNORM	0.16400E+03	0.00000E+00	0.00000E+00	0.00000E+00
6	HF-TB-EM	0.10090E+01	0.10000E-01	0.00000E+00	NORMAL	0.10090E+01	0.00000E+00	0.00000E+00	0.00000E+00
7	HF-TB-FM	0.10125E+01	0.10000E-01	0.00000E+00	NORMAL	0.10125E+01	0.00000E+00	0.00000E+00	0.00000E+00
8	HO-TB-EM	0.10152E+01	0.10000E-01	0.00000E+00	NORMAL	0.10152E+01	0.00000E+00	0.00000E+00	0.00000E+00
9	HO-TB-FM	0.97409E+00	0.10000E-01	0.00000E+00	NORMAL	0.97409E+00	0.00000E+00	0.00000E+00	0.00000E+00
10	TC-CVM	0.10004E+01	0.10000E-01	0.00000E+00	NORMAL	0.10004E+01	0.00000E+00	0.00000E+00	0.00000E+00
11	MFV-R	0.13800E-01	0.64000E-01	0.00000E+00	NORMAL	0.13800E-01	0.00000E+00	0.00000E+00	0.00000E+00
12	MOV-R	0.10700E-01	0.64000E-01	0.00000E+00	NORMAL	0.10700E-01	0.10000E+01	0.00000E+00	0.00000E+00
13	CCV-R	0.10000E+01	0.88000E-01	0.00000E+00	NORMAL	-0.19429E-15	0.00000E+00	0.00000E+00	0.00000E+00
14	FPB-F-IR	0.15500E+00	0.10000E-01	0.00000E+00	NORMAL	0.15500E+00	0.00000E+00	0.00000E+00	0.00000E+00
15	OPB-F-IR	0.68500E+00	0.10000E-01	0.00000E+00	NORMAL	0.68500E+00	0.00000E+00	0.00000E+00	0.00000E+00
16	LF-TB-OR	0.71600E+00	0.10000E-01	0.00000E+00	NORMAL	0.71600E+00	0.00000E+00	0.00000E+00	0.00000E+00
17	LF-TB-NA	0.95000E+00	0.10000E-01	0.00000E+00	NORMAL	0.95000E+00	0.00000E+00	0.00000E+00	0.00000E+00
18	O-PRS-FL	0.55695E-01	0.15000E-01	0.00000E+00	NORMAL	0.36669E-02	-0.99669E+02	0.90168E+02	-0.27112E+02
19	F-PRS-FL	0.16206E+01	0.65000E-02	0.00000E+00	NORMAL	0.16767E+00	0.17642E+01	-0.31119E+00	0.00000E+00
20	LO-PM-CC	0.10000E+01	0.10000E-02	0.00000E+00	NORMAL	0.10000E+01	0.00000E+00	0.00000E+00	0.00000E+00
21	HO-PM-CC	0.10000E+01	0.10000E-02	0.00000E+00	NORMAL	0.10000E+01	0.00000E+00	0.00000E+00	0.00000E+00
22	LF-PM-CC	0.10000E+01	0.10000E-02	0.00000E+00	NORMAL	0.10000E+01	0.00000E+00	0.00000E+00	0.00000E+00
23	HF-PM-CC	0.10000E+01	0.10000E-02	0.00000E+00	NORMAL	0.10000E+01	0.00000E+00	0.00000E+00	0.00000E+00

Figure 6.4. Independent Loads Database

LDEP-ID	LD-NAME	MEAN	COV	P3	DIST	NE-COEF1	NE-COEF2	NE-COEF3	NE-COEF4
1	HO-TB-SP	0.27098E+05	0.52000E-02	0.00000E+00	NORMAL	0.55834E+04	0.20905E+05	0.61012E+03	0.00000E+00
2	HF-TB-SP	0.34625E+05	0.55000E-02	0.00000E+00	NORMAL	0.15410E+05	0.16751E+05	0.24632E+04	0.00000E+00
3	HO-PH-PO	0.41075E+04	0.89000E-02	0.00000E+00	NORMAL	0.14544E+03	0.24759E+04	0.18903E+04	-0.40409E+03
4	HF-PH-PO	0.61998E+04	0.90000E-02	0.00000E+00	NORMAL	0.14515E+04	0.23857E+04	0.23626E+04	0.00000E+00
5	OPB-CH-P	0.50592E+04	0.12900E-01	0.00000E+00	NORMAL	0.25803E+03	0.44060E+04	0.48415E+03	0.42709E+03
6	FPB-CH-P	0.49555E+04	0.13700E-01	0.00000E+00	NORMAL	0.10327E+04	0.75249E+04	-0.35029E+04	0.19661E+04
7	ENG-O-FL	0.89435E+03	0.62000E-02	0.00000E+00	NORMAL	0.10448E+01	0.89777E+03	-0.44638E+01	0.00000E+00
8	ENG-F-FL	0.14906E+03	0.69000E-02	0.00000E+00	NORMAL	0.54315E+00	0.14848E+03	0.37899E+00	-0.34476E+00
9	ENG-THRU	0.47107E+06	0.50000E-02	0.00000E+00	NORMAL	0.10474E+04	0.46729E+06	0.38848E+04	-0.11461E+04
10	O-PRS-FL	0.16206E+01	0.15000E-01	0.00000E+00	NORMAL	0.16767E+00	0.17642E+01	-0.31119E+00	0.00000E+00
11	F-PRS-FL	0.70031E+00	0.65000E-02	0.00000E+00	NORMAL	0.34437E-01	0.63776E+00	0.28114E-01	0.00000E+00
12	OPB-O-VP	0.65025E+00	0.14700E-01	0.00000E+00	NORMAL	0.61621E+00	-0.40203E+00	0.43606E+00	0.00000E+00
13	FPB-O-VP	0.78974E+00	0.13500E-01	0.00000E+00	NORMAL	0.69291E+00	-0.15036E+00	0.24719E+00	0.00000E+00
14	MCC-O-IP	0.35372E+04	0.86000E-02	0.00000E+00	NORMAL	0.78808E+02	0.27181E+04	0.95671E+03	-0.21637E+03
15	MCC-O-IT	0.19024E+03	0.64000E-02	0.00000E+00	NORMAL	0.16512E+03	0.12433E+02	0.14775E+02	-0.20906E+01
16	HG-IP	0.32438E+04	0.64000E-02	0.00000E+00	NORMAL	0.13722E+03	0.36198E+04	-0.50439E+03	0.26555E+03
17	MCC-IEP	0.30060E+04	0.58000E-02	0.00000E+00	NORMAL	0.16085E+03	0.30060E+04	0.00000E+00	0.00000E+00
18	HO-PH-PI	0.37915E+03	0.22800E-01	0.00000E+00	NORMAL	0.11593E+03	0.33464E+03	-0.21946E+02	-0.47482E+02
19	HF-PH-PI	0.20900E+03	0.26300E-01	0.00000E+00	NORMAL	0.26705E+03	-0.15416E+03	0.96111E+02	0.00000E+00
20	PB-PH-PO	0.70920E+04	0.98000E-02	0.00000E+00	NORMAL	0.53504E+03	0.67636E+04	0.86343E+03	0.00000E+00

Hit any key to continue
>

LDEP-ID	LD-NAME	MEAN	COV	P3	DIST	NE-COEF1	NE-COEF2	NE-COEF3	NE-COEF4
21	HO-PH-TI	0.16943E+03	0.60000E-03	0.00000E+00	NORMAL	0.16478E+03	0.28248E+01	0.24169E+01	-0.59064E+00
22	HO-PH-TO	0.19024E+03	0.20000E-02	0.00000E+00	NORMAL	0.16512E+03	0.12433E+02	0.14775E+02	-0.20906E+01
23	HF-PH-TO	0.95571E+02	0.11400E-01	0.00000E+00	NORMAL	0.60135E+02	0.19283E+02	0.16152E+02	0.00000E+00
24	MFV-TO	0.96151E+02	0.11400E-01	0.00000E+00	NORMAL	0.59810E+02	0.20174E+02	0.16176E+02	0.00000E+00
25	PB-PH-TO	0.20306E+03	0.25000E-02	0.00000E+00	NORMAL	0.16959E+03	0.15697E+02	0.17775E+02	0.00000E+00
26	HF-PH-TI	0.42210E+02	0.19000E-02	0.00000E+00	NORMAL	0.43963E+02	-0.46672E+01	0.29147E+01	0.00000E+00
27	LO-TB-SP	0.50366E+04	0.80000E-02	0.00000E+00	NORMAL	0.17100E+04	0.36940E+04	-0.36734E+03	0.00000E+00
28	LF-TB-SP	0.14921E+05	0.90000E-02	0.00000E+00	NORMAL	0.13081E+05	-0.45270E+04	0.63678E+04	0.00000E+00
29	HO-TB-TO	0.12890E+04	0.27400E-01	0.00000E+00	NORMAL	0.54480E+03	0.62070E+03	0.12346E+03	0.00000E+00
30	HF-TB-TO	0.13143E+03	0.19300E-01	0.00000E+00	NORMAL	0.14807E+04	-0.16428E+03	0.38645E+03	0.00000E+00
31	OPB-O-VR	0.92308E+01	0.98200E-01	0.00000E+00	NORMAL	0.35530E+04	-0.59476E+04	0.27260E+04	0.00000E+00
32	FPB-O-VR	0.33703E+04	0.15550E+00	0.00000E+00	NORMAL	0.14670E+03	-0.23255E+03	0.95001E+02	0.00000E+00
33	O-PRS-P	0.33486E+04	0.92000E-02	0.00000E+00	NORMAL	0.19042E+03	0.20001E+04	0.15816E+04	-0.40989E+03
34	F-PRS-P	0.83918E+03	0.79000E-02	0.00000E+00	NORMAL	0.29694E+03	0.26309E+04	0.41269E+03	0.00000E+00
35	O-PRS-T	0.47628E+03	0.24500E-01	0.00000E+00	NORMAL	0.26014E+03	0.53012E+03	0.48920E+02	0.00000E+00
36	F-PRS-T	0.80451E+04	0.12500E-01	0.00000E+00	NORMAL	0.33444E+03	0.33432E+03	-0.19248E+03	0.00000E+00
37	LO-PH-SP	0.18573E+05	0.10000E-01	0.00000E+00	NORMAL	0.23949E+03	0.68697E+04	0.93589E+03	0.00000E+00
38	LF-PH-SP	0.11258E+05	0.10000E-01	0.00000E+00	NORMAL	0.80230E+04	0.18191E+04	0.87307E+04	0.00000E+00
39	HO-PH-SP	0.64475E+04	0.10500E-01	0.00000E+00	NORMAL	0.14279E+04	0.11165E+05	-0.39312E+04	0.25960E+04
40	HF-PH-SP	0.64475E+04	0.24000E-01	0.00000E+00	NORMAL	0.13590E+03	0.65834E+04	0.00000E+00	0.00000E+00

Hit any key to continue
>

Figure 6.5. LDEP: Dependent Load Database

LDEP-ID	LD-NAME	MEAN	COV	P3	DIST	NE-COEF1	NE-COEF2	NE-COEF3	NE-COEF4
41	MCC-C-PO	0.48950E+04	0.10800E-01	0.00000E+00	NORMAL	0.96970E+03	0.23960E+04	0.15293E+04	0.00000E+00
42	MCC-C-TO	0.49091E+03	0.12200E-01	0.00000E+00	NORMAL	0.34914E+03	0.33369E+03	-0.19193E+03	0.00000E+00
43	LO-TB-TQ	0.15626E+04	0.15900E-01	0.00000E+00	NORMAL	-0.13432E+03	0.12386E+04	0.45839E+03	0.00000E+00
44	LF-TB-TQ	0.97352E+03	0.18200E-01	0.00000E+00	NORMAL	0.35028E+03	0.29032E+03	0.33292E+03	0.00000E+00
45	HO-TB-TQ	0.44605E+04	0.10800E-01	0.00000E+00	NORMAL	-0.24908E+03	0.23122E+04	0.27374E+04	-0.34008E+03
46	HF-TB-TQ	0.95479E+04	0.14200E-01	0.00000E+00	NORMAL	-0.93543E+02	0.54258E+04	0.42156E+04	0.00000E+00
47	LO-TB-FL	0.17602E+03	0.99000E-02	0.00000E+00	NORMAL	0.34972E+02	0.17332E+03	-0.38821E+02	0.65423E+01
40	LF-TB-FL	0.26343E+02	0.17500E-01	0.00000E+00	NORMAL	0.10065E+02	0.31578E+01	0.12321E+02	0.00000E+00
49	HO-TB-FL	0.59921E+02	0.10100E-01	0.00000E+00	NORMAL	-0.16929E+01	0.49960E+02	0.11654E+02	0.00000E+00
50	HF-TB-FL	0.16065E+03	0.10700E-01	0.00000E+00	NORMAL	-0.12655E+02	0.14826E+03	0.16415E+02	0.86202E+01
51	LO-TB-PI	0.39407E+04	0.90000E-02	0.00000E+00	NORMAL	0.14676E+03	0.23734E+04	0.18122E+04	-0.39173E+03
52	LF-TB-PI	0.44928E+04	0.10500E-01	0.00000E+00	NORMAL	0.79100E+03	0.24002E+04	0.13015E+04	0.00000E+00
53	HO-TB-PI	0.50394E+04	0.88000E-02	0.00000E+00	NORMAL	-0.24624E+03	0.43569E+04	0.51853E+03	0.41025E+03
54	HF-TB-PI	0.49362E+04	0.95000E-02	0.00000E+00	NORMAL	-0.10228E+04	0.74803E+04	-0.34717E+04	0.19504E+04
55	LO-TB-TI	0.19024E+03	0.20000E-02	0.00000E+00	NORMAL	0.16515E+03	0.12327E+02	0.14901E+02	-0.21390E+01
56	LF-TB-TI	0.49091E+03	0.12100E-01	0.00000E+00	NORMAL	0.34906E+03	0.33392E+03	-0.19207E+03	0.00000E+00
57	HO-TB-TI	0.14290E+04	0.26600E-01	0.00000E+00	NORMAL	0.53754E+03	0.69823E+03	0.19324E+03	0.00000E+00
58	HF-TB-TI	0.18973E+04	0.18600E-01	0.00000E+00	NORMAL	0.16639E+04	-0.27369E+03	0.50710E+03	0.00000E+00
59	LO-TB-PO	0.41335E+03	0.20000E-01	0.00000E+00	NORMAL	0.10909E+03	0.35361E+03	-0.69451E+01	-0.42401E+02
60	LF-TB-PO	0.34038E+04	0.76000E-02	0.00000E+00	NORMAL	0.28588E+03	0.27154E+04	0.40252E+03	0.00000E+00

Hit any key to continue
>

LDEP-ID	LD-NAME	MEAN	COV	P3	DIST	NE-COEF1	NE-COEF2	NE-COEF3	NE-COEF4
61	HO-TB-PO	0.33262E+04	0.66000E-02	0.00000E+00	NORMAL	-0.14193E+03	0.36610E+04	-0.46887E+03	0.27518E+03
62	HF-TB-PO	0.34781E+04	0.67000E-02	0.00000E+00	NORMAL	-0.26861E+03	0.42106E+04	-0.97850E+03	0.51460E+03

Figure 6.5. LDEP: Dependent Load Database (Continued)

ID parameters are the keys for retrieval and other database operations. The knowledge base also includes engine load model information. The *influence* coefficient set for the engine probabilistic influence model and the 1 sigma gain values are stored in the database INFC. An example of the database is shown in Figure 6.6. The values of the fields INFL-C1, INFL-C2, INFL-C3 and INFL-C4 in the database INFC are the four coefficients c_i's in Equation (4.3). The values of the fields GAIN65, GAIN90, GAIN100, and GAIN104 are the 1 sigma gains of the dependent load at power levels of 65%, 90%, 100% and 104%. These are the gains corresponding to the 1 sigma (standard deviation) change in the respected independent load. The expert system uses these gains to select the most influential independent loads to a dependent load for users and thus shows a seemingly intelligent behavior.

The knowledge base includes also the load dependency and scaling information of the component load models, the duty-cycle-data information, etc. The complete information of the knowledge base will be documented in the load-expert system LDEXPT user's manual.

The Rule Modules

The rule-based module has the expert system driver SESUIM (the user interface module), the load calculation module ANLOAD, the statistical tool box, and the Rule Modules. In LDEXPT version 2.1, the statistical tool box has only a few data-fitting routines: not much effort has gone into developing it. As discussed earlier, the decision tree inference scheme is used to process the rules. Each Rule Module is a decision tree for performing certain tasks and/or solving a particular problem. The advantage of this inference scheme is that it is efficient. System with this inference scheme can be easily coupled with external numerical routines. The disadvantage of the decision tree inferencing is the loss of flexibility of selecting alternative rules to solve problems.

Table 1 (LDEP-ID 1–20)

LDEP-ID	LIDP-ID	INFL-C1	INFL-C2	INFL-C3	INFL-C4	GAIN65	GAIN90	GAIN100	GAIN104
1	2	0.65117E-05	0.00000E+00	0.00000E+00	0.00000E+00	0.16865E-05	0.16865E-05	0.16865E-05	0.16865E-05
2	2	0.23386E-04	0.00000E+00	0.00000E+00	0.00000E+00	0.60570E-05	0.60570E-05	0.60570E-05	0.60570E-05
3	2	-0.10704E-01	0.96549E-02	-0.50301E-02	0.00000E+00	-0.16974E-02	-0.15771E-02	-0.15746E-02	-0.15808E-02
4	2	-0.11581E-01	0.11823E-01	-0.62736E-02	0.00000E+00	-0.16955E-02	-0.15596E-02	-0.15621E-02	-0.15722E-02
5	2	-0.35555E-04	0.86119E-03	-0.67882E-03	0.00000E+00	0.62009E-04	0.49643E-04	0.38543E-04	0.33118E-04
6	2	0.93923E-04	0.59094E-03	-0.56487E-03	0.00000E+00	0.61999E-04	0.43570E-04	0.31078E-04	0.25262E-04
7	2	0.41580E-02	0.87578E-02	0.47107E-02	0.00000E+00	0.11803E-03	0.23735E-04	0.28721E-04	0.37548E-04
8	2	0.33594E-03	-0.51734E-02	0.23001E-02	0.00000E+00	-0.53224E-03	-0.63637E-03	-0.65717E-03	-0.62216E-03
9	2	0.62607E-02	0.00000E+00	0.00000E+00	0.00000E+00	0.16215E-02	0.16215E-02	0.16215E-02	0.16215E-02
10	2	-0.15620E-01	0.14171E-01	-0.50118E-02	0.00000E+00	-0.22082E-02	-0.17937E-02	-0.16733E-02	-0.16324E-02
11	2	0.14136E-01	0.50816E-01	0.34235E-01	0.00000E+00	-0.11472E-02	-0.10016E-02	-0.63305E-03	-0.43596E-03
12	2	0.14781E+00	0.31116E+00	0.21417E+00	0.00000E+00	0.93350E-02	0.10682E-01	0.13162E-01	0.14465E-01
13	2	0.40754E-02	0.31038E-02	0.00000E+00	0.00000E+00	0.53299E-03	0.33202E-03	0.25163E-03	0.21947E-03
14	2	-0.35061E-03	0.00000E+00	0.00000E+00	0.00000E+00	-0.90808E-04	-0.90808E-04	-0.90808E-04	-0.90808E-04
15	2	0.57090E-02	0.00000E+00	0.00000E+00	0.00000E+00	0.14786E-02	0.14786E-02	0.14786E-02	0.14786E-02
16	2	0.14671E-02	-0.12044E-02	0.00000E+00	0.00000E+00	0.17723E-03	0.99250E-04	0.68057E-04	0.55580E-04
17	2	0.42159E-02	-0.89929E-02	0.47903E-02	0.00000E+00	0.11898E-03	0.23928E-04	0.29331E-04	0.38442E-04
18	2	-0.99581E+00	-0.34644E-02	0.15387E-02	0.00000E+00	-0.25833E+00	-0.25840E+00	-0.25841E+00	-0.25842E+00
19	2	0.28671E-02	0.69421E-02	0.38709E-02	0.00000E+00	-0.25269E-05	-0.63530E-04	-0.52841E-04	-0.42951E-04
20	2	-0.12771E+00	0.00000E+00	0.00000E+00	0.00000E+00	-0.33077E-01	-0.33077E-01	-0.33077E-01	-0.33077E-01

Hit any key to continue

Table 2 (LDEP-ID 21–40)

LDEP-ID	LIDP-ID	INFL-C1	INFL-C2	INFL-C3	INFL-C4	GAIN65	GAIN90	GAIN100	GAIN104
21	2	-0.86304E-03	0.00000E+00	0.00000E+00	0.00000E+00	-0.22353E-03	-0.22353E-03	-0.22353E-03	-0.22353E-03
22	2	0.14200E-02	-0.12187E-02	0.00000E+00	0.00000E+00	0.16261E-03	0.83700E-04	0.52137E-04	0.39511E-04
23	2	-0.53323E-01	0.80387E-01	-0.34471E-01	0.00000E+00	-0.40496E-02	-0.23041E-02	-0.19184E-02	-0.18141E-02
24	2	0.66462E-03	-0.34281E-02	0.21403E-02	0.00000E+00	-0.17077E-03	-0.17793E-03	-0.16139E-03	-0.15167E-03
25	2	0.12008E-04	0.00000E+00	0.00000E+00	0.00000E+00	0.31309E-05	0.31309E-05	0.31309E-05	0.31309E-05
26	2	-0.17876E-02	0.16728E-01	-0.64132E-02	0.00000E+00	-0.46290E-03	-0.46290E-03	-0.46290E-03	-0.46290E-03
27	2	-0.15880E-01	-0.22550E-02	0.12033E-02	0.00000E+00	-0.19985E-02	-0.15590E-02	-0.14414E-02	-0.14036E-02
28	2	0.16320E-04	-0.81394E-03	0.49466E-03	0.00000E+00	-0.24372E-03	-0.26896E-03	-0.26815E-03	-0.26608E-03
29	2	0.33371E-03	-0.81394E-03	0.49466E-03	0.00000E+00	0.35339E-05	0.47688E-06	0.37382E-05	0.57602E-05
30	2	-0.14741E-05	0.00000E+00	0.00000E+00	0.00000E+00	-0.38179E-06	-0.38179E-06	-0.38179E-06	-0.38179E-06
31	2	0.97962E-05	0.00000E+00	0.79576E-02	0.00000E+00	0.25372E-05	0.25372E-05	0.25372E-05	0.25372E-05
32	2	0.17144E-01	-0.15664E-01	0.00000E+00	0.00000E+00	0.44403E-02	0.44403E-02	0.44403E-02	0.44403E-02
33	2	0.75700E-02	-0.21763E-01	0.00000E+00	0.00000E+00	0.19440E-03	-0.21184E-04	-0.35284E-04	-0.29382E-04
34	2	0.84480E-02	-0.59834E-01	0.32483E-01	0.00000E+00	-0.14758E-02	-0.28849E-02	-0.34486E-02	-0.36740E-02
35	2	0.32042E-01	0.00000E+00	0.00000E+00	0.00000E+00	0.17703E-02	0.11661E-02	0.12149E-02	0.12815E-02
36	2	-0.21921E-05	0.31221E-02	-0.15427E-02	0.00000E+00	-0.56775E-06	-0.56775E-06	-0.56775E-06	-0.56775E-06
37	2	-0.50150E-02	0.13176E-03	0.00000E+00	0.00000E+00	-0.94208E-03	-0.09475E-03	-0.89001E-03	-0.09007E-03
38	2	-0.50709E-03	0.00000E+00	0.00000E+00	0.00000E+00	-0.10936E-03	-0.10003E-03	-0.97417E-04	-0.96052E-04
39	2	0.00000E+00	0.00000E+00	0.00000E+00	0.00000E+00	0.00000E+00	0.00000E+00	0.00000E+00	0.00000E+00
40	2	0.49467E+00	-0.45957E+00	0.19247E+00	0.00000E+00	0.71812E-01	0.61371E-01	0.58940E-01	0.50246E-01

Hit any key to continue

Figure 6.6. INFC: Influence Coefficient Database for LIDP-ID=2

LDEP-ID	LIDP-ID	INFL-C1	INFL-C2	INFL-C3	INFL-C4	GAIN65	GAIN90	GAIN100	GAIN104
41	2	0.13048E-01	-0.38323E-01	0.21083E-01	0.00000E+00	-0.76502E-03	-0.11305E-02	-0.10855E-02	-0.10370E-02
42	2	-0.48649E-01	0.73611E-01	-0.31178E-01	0.00000E+00	-0.36194E-02	-0.19822E-02	-0.16100E-02	-0.15063E-02
43	2	-0.19901E-02	0.17895E-02	-0.74065E-03	0.00000E+00	-0.29524E-03	-0.25371E-03	-0.24381E-03	-0.24092E-03
44	2	-0.50150E-02	0.31221E-02	-0.15427E-02	0.00000E+00	-0.94200E-03	-0.89475E-03	-0.89901E-03	-0.89007E-03
45	2	-0.82145E-03	0.00000E+00	0.00000E+00	0.00000E+00	-0.21275E-03	-0.21275E-03	-0.21275E-03	-0.21275E-03
46	2	-0.81443E-03	0.00000E+00	0.00000E+00	0.00000E+00	-0.21094E-03	-0.21094E-03	-0.21094E-03	-0.21094E-03
47	2	-0.98544E-02	0.97690E-02	-0.42941E-02	0.00000E+00	-0.13776E-02	-0.11760E-02	-0.11343E-02	-0.11239E-02
48	2	-0.20930E-03	0.00000E+00	0.00000E+00	0.00000E+00	-0.54209E-04	-0.54209E-04	-0.54209E-04	-0.54209E-04
49	2	-0.56668E-01	0.42063E-01	0.60476E-02	0.00000E+00	-0.75956E-03	-0.48720E-02	-0.37826E-02	-0.33468E-02
50	2	0.21955E-02	-0.94917E-02	0.46864E-01	0.00000E+00	-0.36751E-03	-0.37514E-03	-0.32337E-03	-0.29389E-03
51	2	-0.10445E+00	0.11783E+00	0.10900E-01	0.00000E+00	-0.12345E-01	-0.94193E-02	-0.86738E-02	-0.84435E-02
52	2	0.22541E-01	-0.27185E-01	0.21001E+00	0.00000E+00	0.24542E-02	0.17879E-02	0.16202E-02	0.15689E-02
53	2	0.19669E+00	-0.31797E+00	0.26922E+00	0.00000E+00	0.20394E-01	0.20882E-01	0.22981E-01	0.24125E-01
54	2	-0.28269E+00	0.49885E+00	0.00000E+00	0.00000E+00	-0.18696E-01	-0.13415E-01	-0.13743E-01	-0.14264E-01
55	2	-0.27708E-02	0.00000E+00	0.00000E+00	0.00000E+00	-0.71763E-03	-0.71763E-03	-0.71763E-03	-0.71763E-03
56	2	-0.67092E-03	0.00000E+00	0.00000E+00	0.00000E+00	-0.17377E-03	-0.17377E-03	-0.17377E-03	-0.17377E-03
57	2	-0.60108E-01	0.29292E-01	0.73646E-02	0.00000E+00	-0.10637E-01	-0.87399E-02	-0.79813E-02	-0.76778E-02
58	2	-0.13940E-02	0.11215E-01	0.00000E+00	0.00000E+00	0.72110E-03	0.70814E-03	0.63620E-03	0.59674E-03
59	2	-0.86231E+00	0.38681E+00	0.00000E+00	0.00000E+00	-0.21603E+00	-0.21432E+00	-0.21332E+00	-0.21292E+00
60	2	0.23069E-02	-0.97583E-02	0.61974E-02	0.00000E+00	-0.36715E-03	-0.37702E-03	-0.32478E-03	-0.29490E-03

Hit any key to continue

LDEP-ID	LIDP-ID	INFL-C1	INFL-C2	INFL-C3	INFL-C4	GAIN65	GAIN90	GAIN100	GAIN104
61	2	-0.44955E+00	0.45905E+00	-0.19493E+00	0.00000E+00	-0.60482E-01	-0.50323E-01	-0.48026E-01	-0.47390E-01
62	2	-0.10670E-01	0.29692E-01	-0.16087E-01	0.00000E+00	0.47478E-03	0.78276E-03	0.76011E-03	0.72772E-03

Hit any key to continue

Figure 6.6. INFC: Influence Coefficient Database for LIDP-ID=2
(Continued)

Rules are designed to represent the textual information needed for load synthesis. Rules also are written to control the computation process and to retrieve and manage the requested engineering data. The rule modules implemented in LDEXPT version 2.1 are:

Rule-Modules	Function
SLIDPL	Independent load info. retrieval
SLDEPL	Dependent load info. retrieval
SLICGN	Infl. coeff's & gain values retrieval
SLTBCL	Turbine blade pressure load info. retrieval
SLTHCL	Component load info. retrieval
SLSCTH	Component load model info. retrieval
SLICTH	Thermal load influence coeff's retrieval
SLCLFP	Fluctuation pressure load info. retrieval
SLDUCT	Duct geometry info. retrieval
SLDDYN	Duct dynamic load PSD info. retrieval
SLDCD	Duty-cycle-data file info. retrieval
QLM	Quick-Look model calculation
SICM	Deterministic influence model calc.
STBSM	Simple turbine blade scaling model calc.
TBPRLI	Turbine blade linear interpolation calc.
ANLDIN	Prepare ANLOAD input file for load calc.
EXIT	Return to RBMS, rule-based module control

The rule-module ANLDIN, preparing an ANLOAD input file for load calculation, is the module used most often. This module retrieves the user request load information and data from the knowledge base and prompts the user for required parameters such as: length of mission time, time step size, probabilistic

method chosen, etc. Details of each rule module will be discussed in the load-expert system user manual. As an example, the equivalent rules of the rule module SICM are listed below:

a) If   the dependent load ID is N and
         the independent load ID is M
   then the influence coefficient parameter set is c1, c2, c3 and c4.

b) If   the dependent load ID is N and
         the user requests that the expert system selects the M most
         influential independent loads on the dependent load and
         the selection is going to be based on gains for
         power level X
   then the M independent loads are M1, M2, ... (after some
         numerical evaluations)

c) If   the dependent load ID is N and
         the user requests a simple deterministic influence
         model calculation
   then the expert system will either request the user to select
         the independent loads manually or the expert system will
         select them if the user requests that, retrieve influence
         coefficient set and perform the deterministic influence
         model calculation.

It is obvious from the rules above that the SICM rule module will require the services of the following: (1) the rule-module SLDEPL which retrieves the dependent load information, (2) the rule-module SLIDPL which retrieves the independent load information, and (3) the rule-module SLICGN which retrieves the influence coefficient set. The required communication between these rule modules, or any other rule module, is carried out by a simple working memory model.

The Working Memory Model

The working memory model was designed for passing information (short-term memory) between different rule modules. To keep the model simple, the information saved was limited to that needed to pass from one rule module to another module but not to multiple rule modules. The working memory consists of a stack used for storing database indices for record retrieval and a memory array used for storing information (e.g. subgoals, facts). The advantage of implementing a working memory model is that many inference processes can proceed without user intervention. For example, suppose one wants to do a deterministic influence model calculation for the HPFTP turbine speed using rule module SICM. First, one selects the dependent load ID number 3 for the HPFTP speed inside the SLDEPL rule module. This information is then passed to the SLIDPL rule module for selecting the most influential independent loads by the expert system if that is what the user chooses to do. Next, the dependent load ID and the independent load IDs are passed to the SLICGN rule module for retrieving the influence coefficient set. After all information and data are retrieved, an influence model calculation is then performed in the SICM rule module. Without the working memory, one has to manually pass the information between the rule modules in order to complete the process.

Operation

The load-expert system, LDEXPT version 2.1, was installed on the NASA Lewis Research Center's VM/CMS system. To run the expert system, a user needs to have the library for the expert system, the LDEXPT EXEC file, the knowledge base file and duty-cycle-data file, the problem text file and rule file, and a few other data files. The procedure is as follows: (1) Request more virtual memory by executing a CP command:

    CP DEFINE STORAGE 4096K

(2) Returns to CMS:

    CP IPL CMS

(3) Loading the graphic-3d package (LeRC's graphic package):

    GRAPH3D

(4) Loading the load-expert system:

    LDEXPT

The load-expert system LDEXPT is a menu-driven program. To get to the expert system driver, one needs first to go to the rule-based module by entering the command:

    ?RBMS

then, the rule-based module menu is shown on screen. Select the expert system driver by entering the command:

    ?EXDR

A rule modules menu appears on screen and one can select and execute any one of the rule modules.

System operations such as implementing a new knowledge base or adding new database to the existing knowledge base will be discussed in the load-expert system users manual. Implementation of the available generic models, such as the generic static pressure load model, and the generic probabilistic thermal load model, etc. will also be discussed in the users manual.

For those readers who would like to see the load-expert system LDEXPT in action, a commented printout of an actual run of the rule module ANLDIN is attached as Appendix A. The example, an expert-system consultation session shows the dialogue between a user and the expert system for retrieving relevant load information and data to prepare a load calculation input file.

6.5 The Component Load Models

Four space propulsion system components were selected for development of the CLS synthesis: (1) the turbine blade, (2) the transfer ducts, (3) the LOX posts, and (4) HPOTP discharge duct. The loads of interest for these components are exhibited in Table 2.1. The component structures, the mechanics and operation, and the component loads are described in detail in the first CLS annual report (ref. 2.1). In this section, the actual implementation of component loads is summarized. The general approach taken in modeling the component load is to build generic models based on some simple and general principle. For example, one approach that was used in the turbine blade static pressure model is that the differential pressure on the turbine blade surface streamline is proportional to the turbine torque. The techniques employed most often are the scaling technique and the influence coefficient technique. These two techniques were used in developing the static pressure load model and the probabilistic thermal load model. As the CLS technology advances, physical component load models (i.e., based on the physics of component structure and function) will be developed.

The Generic Scaling Model

The component static pressure loads are directly scalable with a system-level dependent load or, in the case of a turbine blade, static pressures with two system-dependent loads. Since there are other component loads which are also scalable with one or two system-level loads, a generic scaling model was implemented on the load-expert system. With this model, the turbine blade centrifugal force, the HPOTP discharge duct static pressure load, the HGM fuel and LOX transfer ducts static pressures, and the LOX posts static pressures were implemented.

A simple scaling model is defined as a load directly scalable by one or two system-level dependent loads with a single scaling coefficient. That means in the case of two dependent loads, the scaling coefficient is the same for the

two loads with possibly a sign difference. Some scaling models are scaled by two or more dependent loads with two or more coefficients. They are not that much different from the simple scaling model except that a data set for the scaling coefficients is required. The simple scalable component load can be evaluated as follows:

$$L_c = a * L_{s1} \qquad\qquad (6.1)$$

or,

$$L_c = a * (L_{s1} - L_{s2}) \qquad\qquad (6.2)$$

where, L_c is the component load,

L_{s1} and L_{s2} are the relevant dependent loads,

a is the scaling coefficient.

Routines have been written to calculate the generic scaling model load using equation (6.1) or (6.2). Rule module has been written to supply the load information and data assuming they were implemented in the knowledge base in the conventional way of the load-expert system. To make the scheme work, the knowledge has to be implemented in a certain way. The following is an implementation procedure of the HPOTP discharge duct static pressure load using the generic scaling model. It will serve as an illustration of what is involved in building load models.

1. Add the load information to the component load database LCTH. This can be accomplished by going into the database system resided in the knowledge-based module KBMS with the following commands:

   (1) After the expert system is loaded,
       enter ?KBMS. A menu of the KBMS module will
       then show up on the screen

(2) Enter ?DBMS to enter the database system,
    a list of available database commands will
    show up on the screen

(3) Enter ?DBRD to open the knowledge base file
    and bring in the database LCTH by following
    the system prompt

(4) Enter ?DBUP to add the new load record to the
    load database LCTH. For example, enter the
    following for the HPOTP discharge duct static
    pressure load:

```
CMPN-ID :  10
C-LD-ID :   2
C-LD-NA : HODD-S-P
MEAN    : 4107.0
COV     : 0.1
P3      : 0.0
DIST    : NORMAL
NE-COEF1:
NE-COEF2:
NE-COEF3:
NE-COEF4:
```

Notes: Component ID CMPN-ID = 10 identifies that the
       component is the HPOTP discharge duct
       Component load ID C-LD-ID = 2 identifies that
       the load is the static pressure load
       Leave blank for NE-COEF1 to NE-COEF4

If the component is a new one which is not in the existing list, select an ID
number for the component.

2. Add the scaling load database to SCTH.

Repeat steps (3) and (4) of the previous procedure for database SCTH. The database for the HPOTP discharge duct is as follows:

```
CMPN-ID : 10
C-LD-ID :  2
C-LD-NA : HODD-S-P
LD-TYPE : ONE
C1-ID   :  0
LDEP1-ID:  3
C2-ID   :  0
LDEP2-ID:  0
C3-ID   :  0
LDEP3-ID:  0
C4-ID   :  0
LDEP4-ID:  0
C5-ID   :  0
LDEP5-ID:  0
SC-COEF :  1.0
```

Notes: LD-TYPE = ONE is for scaling model with one system dependent load
                 = TWO for scaling with two system dependent loads

        Cn-ID is 0 for simple scaling model, it means that the dependent load is one of the system dependent loads on the engine influence model n = 1,2,...,5

        LDEPn-id is the system level dependent load ID, n = 1,2,...,5

        LDEP1-ID = 3 is the system load HO-PM-PO, the HPOTP discharge pressure, which is the static pressure load

        SC-COEF is the scaling coefficient, in this case, which is 1.0

3. Go into the problem text file: "LOADKB PTF", add an entry for the HPOTP discharge duct static pressure load

4. Go into the rule file: "LOADKB RUL", add an entry for the HPOTP discharge duct static pressure load.

Once these four steps are completed, the load-expert system will be capable of evaluating the component static pressure load.

The Probabilistic Thermal Load Model

The generic probabilistic thermal load model is much more complex as compared to the scaling model; nevertheless, the same implementation philosophy is followed. Routines and rule module have been written for generic probabilistic thermal load model, and the load-specific knowledge is required to be implemented in the knowledge base. With such a design, one model serves the needs of all components. The evaluation model stays the same, but the load information and data could change, depending on the engine type and the component design.

The probabilistic thermal load model is really a two-level hierarchical model. It is a coupling of a thermal load influence model and a scaling model. The thermal load influence model is a probabilistic influence model which correlates the system-dependent loads relevant to the component under consideration to a set of boundary condition loads for the component. The scaling model then uses the boundary loads to scale the reference temperature profile of the component to the new temperature profile.

The thermal load influence model implemented on the load-expert system has the following form:

$$\frac{\Delta L_{bc,i}}{L_{bc,io}} = \sum_{j} IC_{ij} \frac{\Delta Y_j}{Y_{jo}}$$

where, $L_{bc,io}$ is the mean of the ith boundary condition load,

$\Delta L_{bc,i}$ is the change of the ith b.c. load,

Y_{jo} is the mean of the jth system dependent load,

ΔY_j is the change in Y_j

IC_{ij} is the influence coefficient

In this model, the influence coefficients are assumed to be constant. This influence model is the same as the engine system influence model except that the influence coefficients of the thermal load model are constant whereas the engine system influence coefficients are a polynomial function of the commanded power level.

With appropriate selection of system level dependent loads and boundary condition loads, the probabilistic thermal load model makes good prediction of the new temperatures. The boundary condition loads information and the load dependency of component thermal load models for four selected components have been implemented on the knowledge base. The component thermal boundary load information is implemented in database SCTH and the thermal load influence coefficients in ICTH.

The probabilistic thermal load evaluation routines have been implemented in the load calculation module ANLOAD. One could use the expert system consultation module ANLDIN to prepare an ANLOAD input file and run an ANLOAD calculation to obtain the thermal load result. With the model and tools available on the expert system, the probabilistic thermal model for any new component can be easily implemented. In the load-expert system LDEXPT version 2.1, the thermal load models for the turbine blade, the HPFTP and the HPOTP transfer ducts, the LOX post and the HPOTP discharge duct have been implemented (ref. 6.1). As an example, the probabilistic thermal load model for the turbine blade is presented in Appendix B.

The Duct Pressure Fluctuation Model

The dynamic pressure load on a duct is the pressure fluctuation exerted to the duct due to the turbulence flow condition inside the duct. The generic pressure fluctuation model was developed (ref. 6.2) to provide a fluctuation pressure load in the form of a pressure PSD and correlation lengths for flows through the ducts at different locations.

The fluctuation pressure PSD of the ducts under investigation (for the Composite Load Spectra project, it is the hot gas manifold transfer ducts, the LOX posts, and the HPOTP discharge duct) has the following general shape as shown in Figure 6.7:

$$(f) \qquad k_o * f^{-s} \qquad \text{for} \quad f_o < f < f_i$$

$$(f) \qquad k_i * f^{-5/3} \qquad \text{for} \quad f_i < f < f_1$$

where s is the shape factor, it can be either 1.0 or 0.4, depending on the component and the geométry location,

f_o is the frequency lower bound cutoff,
f_i is the frequency beyond which inertial subrange is in effect, it is chosen in general at 40% of the entire frequency band f_1,
and f_1 represents the range to which the spectra is of interest.

The PSD is normalized to the root-mean-square fluctuation pressure p' which is proportional to the 1-D flow dynamic head q_{1-D}. The p'/q_{1-D} ratio is an empirical parameter developed based on experimental data. It varies with the flow geometry and flow separation characteristics. The values used in the model will be based on existing experimental data and engineering estimates by our expert if data does not exist. Figures 6.8 and 6.9 show the PSD predictions of the above formulas for the HGM oxidizer upper transfer duct at the entrance top position and the fuel upper transfer duct at the entrance bottom position. In Figure 6.9, the shape factor s of 0.4 gives a better fit to the PSD.
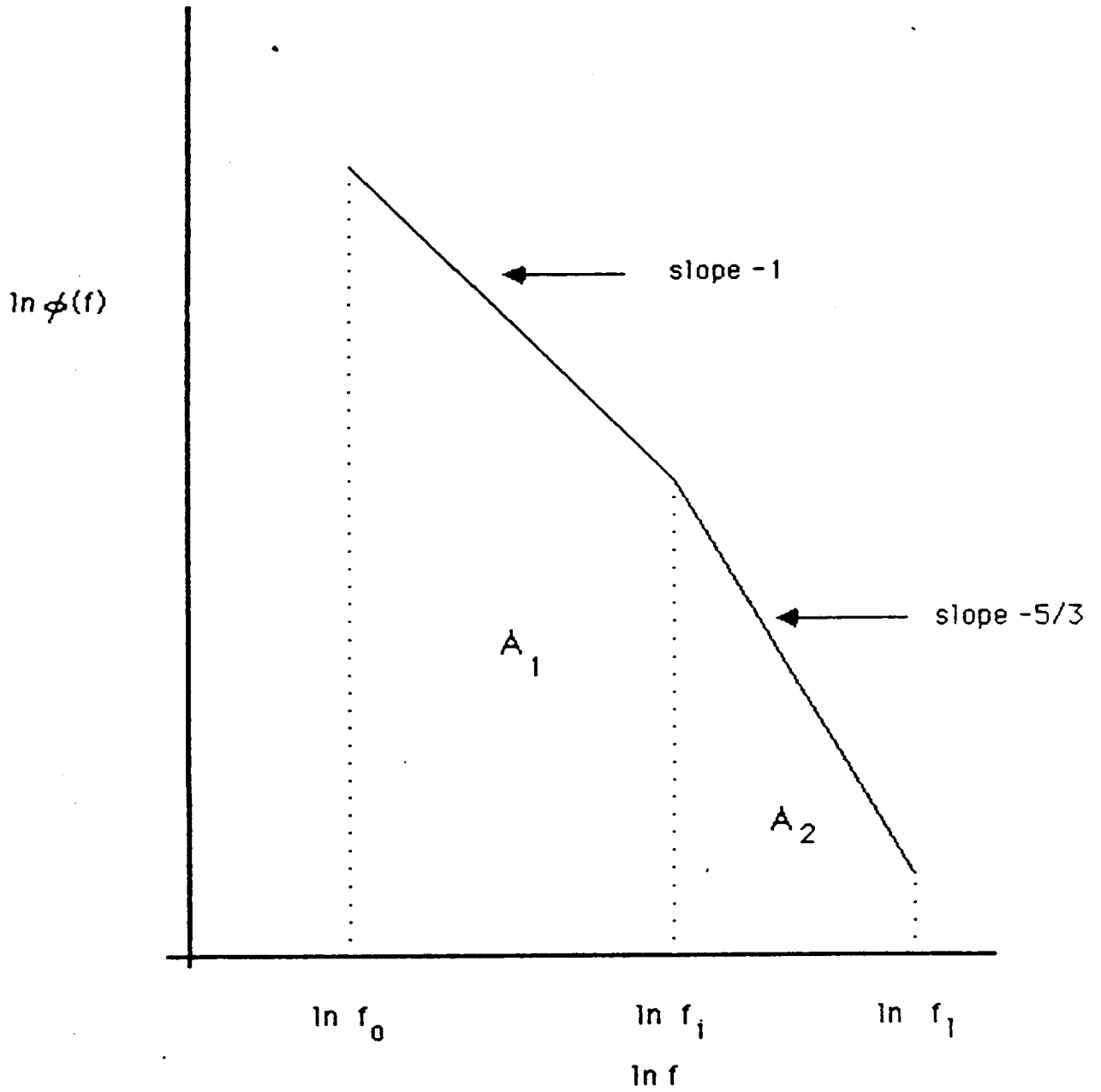
Figure 6.7. Schematic of PSD Curve From Which Various Constants Need to be Determined
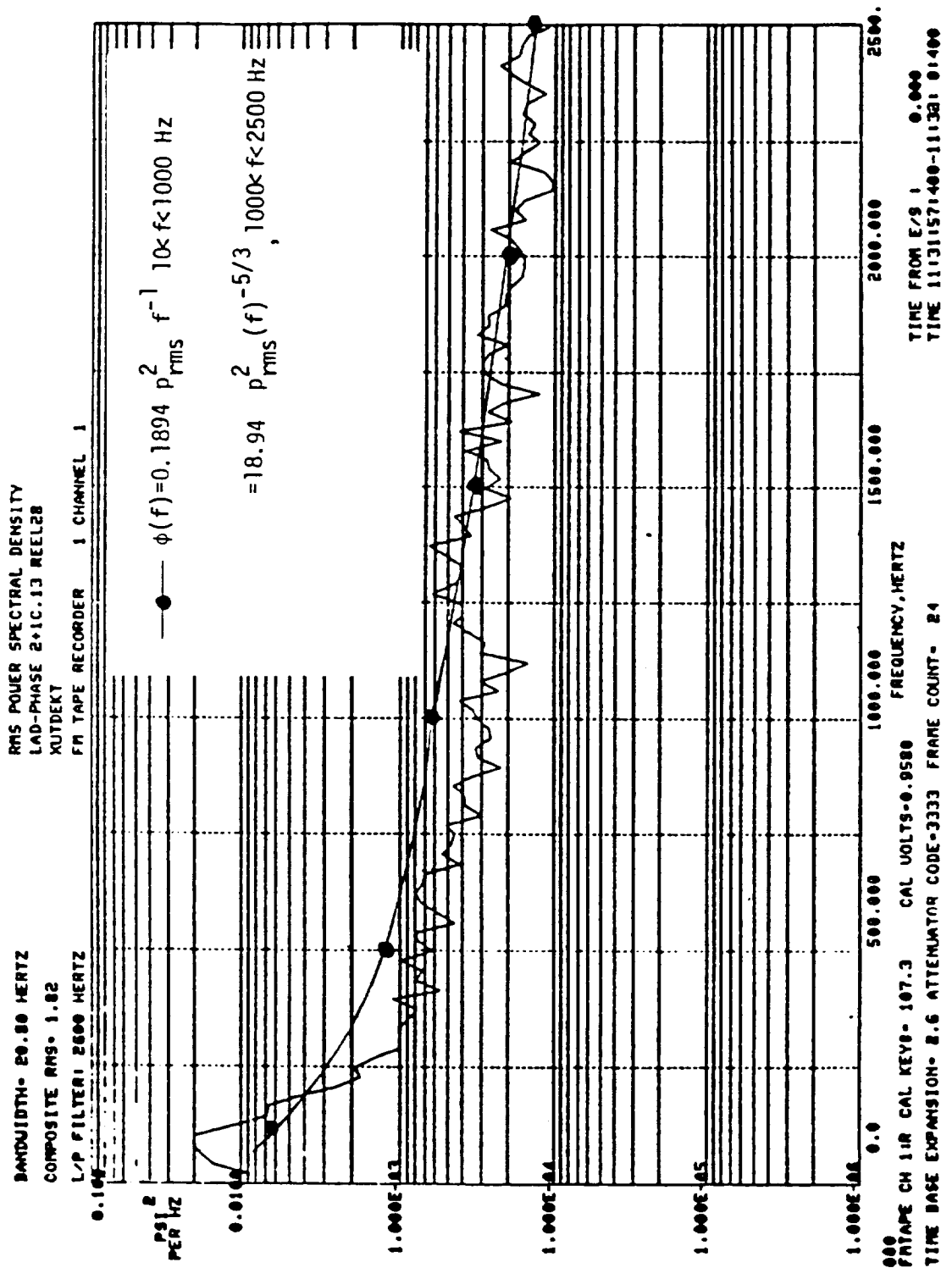
Figure 6.8. Comparison of Prediction and Actual Data at Location XUTDEKT
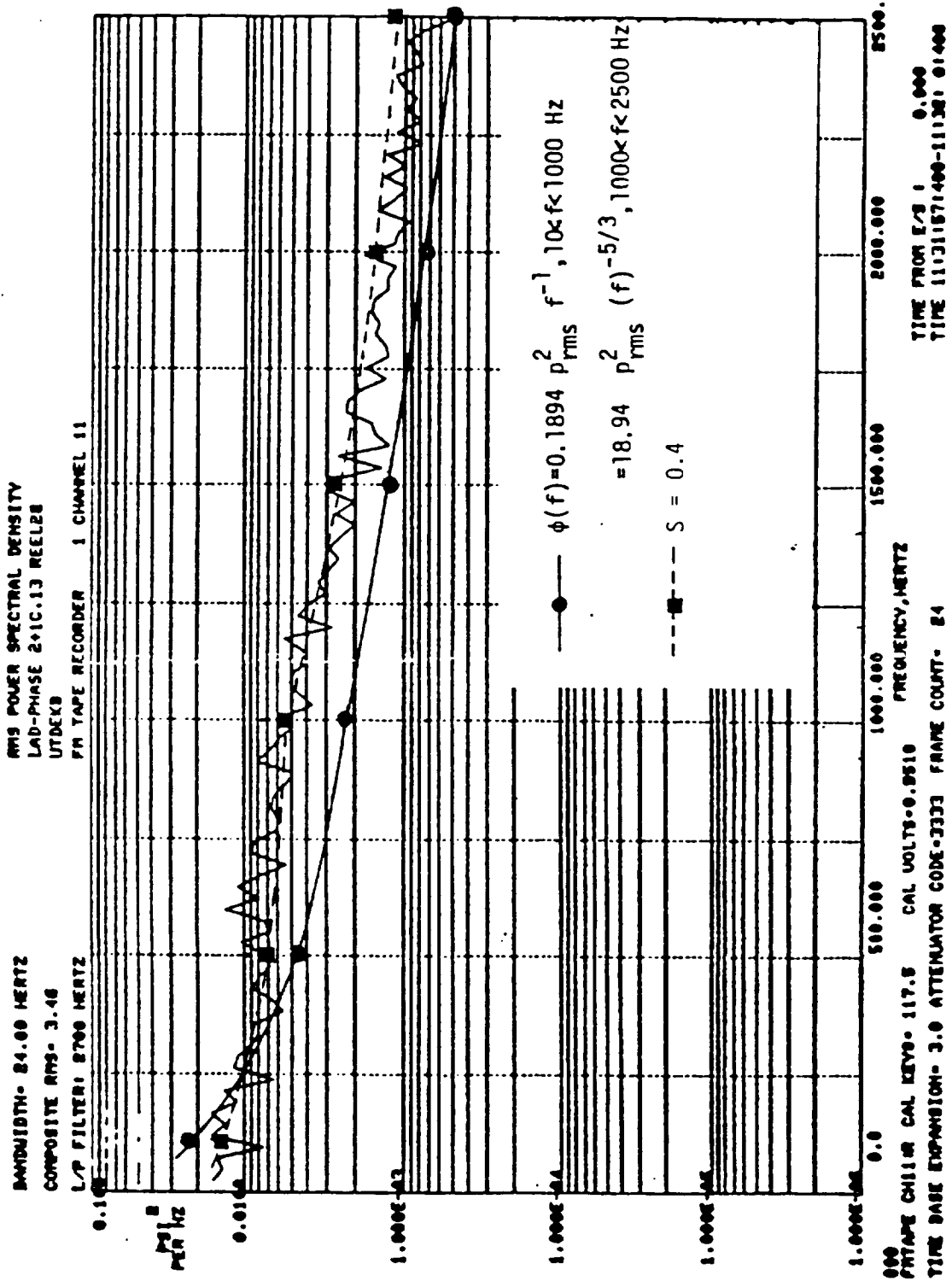
Figure 6.9. Both Initial and Geometric Factor Predictions are Shown

The correlation length L_x, over which the pressure fluctuation acts, can be evaluated as follows:

$$L_x = U_c * T_x$$

$$T_x = \int_0^\infty R(\tau) \, d\tau$$

$$R(\tau) = \int_0^\infty \phi(w) \cos w\tau \, dw$$

where, $U_c = 0.6 * U_{1-D}$ for a boundary layer flow,

U_c is the convection velocity of the large scale eddies,

U_{1-D} is the freestream velocity

The model implemented is generic to the components of interest. Three databases are required. The first database is the dependent load information on flow velocity and dynamic head for each component. The second database is the coarse geometry information related to the ratio of the 1-D (one dimension) root-mean-square pressure to the flow dynamic head. This ratio relates to the turbulent intensity factor of the flow and is geometry dependent. The third database is the pressure fluctuation parameter database. One of the parameters is the geometry-dependent ratio related to the turbulent intensity. Therefore, the parameter database has entries for each coarse geometry region. Examples of the second and third databases are listed below for the HPOTP discharge duct.

DUCT : The geometry database for ducts

```
COMP-ID : 10            /* HPOTP
C-L-ID  : 33            /* Component Fluctuation Pressure Load
N-ZONES :  6            /* Number of coarse zones
LOC-1   : STRAIGHT      /* Straight portion of the duct
LOC-2   : TURN1ALL      /* All area of the wall of the first turn
```

```
LOC-3   : TURN2TOP        /* Top wall of the turn #2
LOC-4   : TURN2BOT        /* Bottom wall of the turn #2
LOC-5   : TURN3TOP        /* Top wall of the turn #3
LOC-6   : TURN3BOT        /* Bottom wall of the turn #3


CLFP:  The component fluctuation pressure load parameter database
COMP-ID : 10
C-L-ID  : 33
C-L-NA  : HODD-F-P        /* HPOTP Discharge Duct Fluctuation Pr.
LOCATION: TURN1ALL        /* Location of the duct
DIA-EQV : 0.333           /* Equivalent diameter in ft
FI-RATIO: 0.15            /* Fluctuation intensity ratio, i.e.
                          /* the ratio of the 1-D root-mean-square
                          /* pressure to the flow dynamic head
CORLEN  : 0.175           /* Nominal fluctuation pressure
                          /* correlation length
SHAPE-F : 0.4             /* Shape factor
FREQ-O  : 10              /* PSD frequency lower bound in Hz
FREQ-I  : 4000            /* PSD intermediate frequency in Hz
FREQ-L  : 10000           /* PSD cut-off frequency in Hz
A-L-FREQ: 0.81            /* Percentage area under the low frequency
                          /* portion of the PSD
```

The fluctuation pressure load model is available in the load-expert system. However, the model requires the evaluation of the 1-D flow velocity and dynamic head which are not available in the present engine influence coefficient set but available in the expanded influence coefficient set which will be implemented in the next version of the load-expert system. A summary paper (ref. 6.3) written by the developer of the pressure fluctuation model is included as Appendix C to provide the theoretical support of this work.

The Vibration Loads

A vibration load model, called periodic load model, was developed (ref. 6.4) which evaluates the variance of the composite vibration load which is a linear combination of a random vibration and synchronous vibration loads. Detail of the model is presented as Appendix D of this report. This model is interesting and is available as a rule module. However, further investigation is needed to develop applications of this model.

In practical applications of a vibration model, the power density spectrum of the vibration load is required. A simple model generating a piecewise linear PSD function is available in the load-expert system. The vibration model will be revisited when an application problem to the HPOTP discharge duct is developed.

REFERENCES

2.1   Newell, J. F., R. E. Kurth and H. Ho, March 1986 "Composite Load Spectra for Select Space Propulsion Structural Components, Annual Report," NASA-CR-179496, NASA/LeRC

2.2   Feigenbaum, E. A. and P. McCorduck, "The Fifth Generation," Addison-Wesley, Reading, MA, 1983

4.1   Ryan, R. S. et al., "Systems Analysis Approach to Deriving Design Criteria (Loads) for Space Shuttle and Its Payload," Vol. I and II, NASA Technical Paper 1949, Dec. 1981

4.2   13M1500"T", "Space Shuttle Interface Control Document (ICD), 1982

5.1   Kurth, R. E., November 1985, "The Development and Application of a New Probabilistic Analysis Technique for Nuclear Risk Calculations," Ph.D. Thesis, Ohio State University

6.1   Romine, W. D., Internal Letter dated 31 July 1987, "HPFTP Second Stage Turbine Blade Thermal Distribution for the Load Shape Simulations Study," ATU 87-5176, Rocketdyne, RI

      Romine, W. D., Internal Letter dated 24 June 1987, "SSME HGM Fuel Center Transfer Tube Thermal Distribution for the Load Shape Simulations Study," ATU 87-5144, Rocketdyne, RI

      Romine, W. D., Internal Letter dated 30 September 1987, "Main Injector LOX Post Thermal Distribution for the Load Shape Simulations Study," ATU 87-5218, Rocketdyne, RI

6.2 Sharma, L. K., December 1987, "Transfer Duct Pressure Fluctuations and Correlation Lengths for the Composite Load Spectra Program," SSME-87-1756, Rocketdyne, RI

Sharma, L. K., December 1987, "HPOP Discharge Duct Pressure Fluctuations and Correlation Lengths for the Composite Load Spectra Program," SSME-87-1757, Rocketdyne, RI

Sharma, L. K., 25 March 1988, "Main Injector LOX Posts Pressure Fluctuations and Correlation Lengths for the Composite Load Spectra Program," SSME-88-000337, Rocketdyne, RI

6.3 Sharma, L. K., 15 April 1988, "Pressure Fluctuations and Correlation Lengths: Summary and Critique," SSME-88-000350, Rocketdyne, RI

6.4 Kurth, R. E., 16 October 1987, "Composite Load Spectra Monthly Technical Report for September, 1987," Battelle Columbus Division

Appendix A

Sample LDEXPT Load-Expert System Consultation Session

Appendix A. Sample LDEXPT Load-Expert System Consultation Session

```
LDEXPT                    /* User input. Running LDEXPT EXEC proc

DUPLICATE IDENTIFIER 'GAMMA'.
EXECUTION BEGINS...
 *  *  *  *  *  *
WELCOME TO THE COMPOSITE LOAD SPECTRA EXPERT SYSTEM

 Available COMMANDS:
         ?RBMS     Rules-Base Management System
         ?KBMS     Knowledge-Base Management System
         ?HELP     List available COMMANDS
         ?QUIT     Exit LDEXPT

LDEXPT ===>
LDEXPT ===> COMPOSITE LOAD SPECTRA EXPERT SYSTEM
LDEXPT ===>
?
.?RBMS                    /* User input. Going to EXPERT SYSTEM


 *  *  *  *  *  *  *  *
WELCOME TO THE RULES-BASE MANAGEMENT SYSTEM
 *  *  *  *  *  *  *  *

 Available COMMANDS:
         ?EXDR : Expert System driver
                 must be executed first before
                 executing ?PEEK and ?PLOT
         ?PEEK : Peek data files
         ?PLOT : Plot the peeked data file
         ?ANLD : Run ANLOAD interactively
         ?RNDW : Perform random walk
         ?PLRW : Plot random walk time series
         ?DFIT : Fit distribution
         ?DMLE : Estimate distribution parameters
         ?HELP : List available COMMANDS
         ?RETN : Return to LDEXPT
```

```
#RBMS ===>        ?QUIT : Exit from the program

#RBMS ===> RULES-BASE MANAGEMENT SYSTEM
#RBMS ===>
#?
#.?EXDR                    /*User input. Calling expert system driver

#     Available rule modules are :
#     SLIDPL : Independent load information
#     SLDEPL : Dependent load information
#     SLICGN : Influence coefficients and Gain values
#     SLIBCL : Turbine blade component load information
#     SLDCD  : Duty-Cycle-Data file information
#     QLM    : Quick Look Model calculation
#     SICM   : Deterministic Influence Coefficient Model
#     STBSM  : Simple Turbine Blade Scaling Model
#     ANLDIN : Preparing ANLOAD INput file
#     EXIT   : Return to RBMS

#.ANLDIN                   /*User input. Calling rule module ANLDIN
                           /*for preparing ANLOAD input file

#     SELECT ONE OF THE ANLOAD CALCULATIONS DESIRED:
#         (1) TURBINE BLADE LOAD CALCULATION  /*This option will be checked
                                              /*soon
#         (2) DEPENDENT LOAD CALCULATION      /*This option is not
#         (3) MONTE CARLO ANLOAD CALCULATION  /*available at this time

#.2                        /*User input. Selecting option 2

#  *  *  *  *  *  *  *   *
#  *  OPEN A DATABASE FILE &/or  *
#  *  READ A DB TABLE DICTIONARY *
#  *  *  *  *  *  *  *   *
#
#  Please Enter DB File NAME           /*This was the first time entering
#  AVAILABLE DB FILE IS LOADKB         /*RBMS module. The system was requesting
#  ?                                   /*a knowledge base file DDNAME
```

A-3

```
? 
.LOADKB                          /*User input. User entered the DDNAME
                                 /*of the load knowledge base
                                 /*only LOADKB is available this time

***** FROM OPNOFL *****
ANAME = LOADKB    LU =    14
           GRP NAME      GRP #    # OF REC.
                                  LAST GRP

DBNREF TABLE    TITL      1        1      /*This is a list of group
DBNREF TABLE    LIDP      1       45      /*data in the knowledge
DBNREF TABLE    LDEP      1       45      /*base. Each group is a
DBNREF TABLE    INFC     16       45      /*DATABASE except that the
DBNREF TABLE    DFAT      1       45      /*group TITL which contains
DBNREF TABLE    LTBC      1       45      /*file header information

                 /*The knowledge base has six (6) DATABASE
                 /*   TITL : file header infor
                 /*   LIDP : independent load database
                 /*   LDEP : dependent load database
                 /*   INFC : influence coefficient DB
                 /*   DFAT : duty-cycle-data database
                 /*   LTBC : turbine blade load database

*    *    *    *    *    *
*    GET INDEX (INDICES)    *
*    *    *

Please Enter KEY Values for the desired Records   /*Expert system requested
Enter BLANK for ALL Values of                     /*user selection of LDEP-ID
character type                                    /*the dependent load ID
Enter -999999 for ALL Values of
integer type
KEY : LDEP-ID    IS
*** EXPERT SYSTEM QUERY NEXT ***
Please select a dependent load ID(LDEP-ID)
Enter ID number
Available LDEP-ID:
 1 HO-TB-SP;2 HF-TB-SP;3 HO-PM-PO;4 HF-PM-PO;5 OPB-CH-P;
 6 FPB-CH-P;7 ENG-O-FL;8 ENG-F-FL;9 ENG-THRU;10 O-PRS-FL;
11 F-PRS-FL;12 OPB-O-VP;13 FPB-O-VP;14 MCC-O-IP;15 MCC-O-IT;
```

```
16 HG-IP  ;17 MCC-IEP ;18 HO-PM-PI;19 HF-PM-PI;20 PB-PM-PO;
21 HO-PM-TI;22 HO-PM-TO;23 HF-PM-TO;24 MFV-TO  ;25 PB-PM-TO;
26 HF-PM-TI;27 LO-TB-SP;28 LF-TB-SP;29 HO-TB-TO;30 HF-TB-TO;
31 OPB-O-VR;32 FPB-O-VR;33 O-PRS-P ;34 F-PRS-P ;35 O-PRS-T ;
36 F-PRS-T ;37 LO-PM-SP;38 LF-PM-SP;39 HO-PM-SP;40 HF-PM-SP;
41 MCC-C-PO;42 MCC-C-TO;43 LO-TB-TQ;44 LF-TB-TQ;45 HO-TB-TQ;
46 HF-TB-TQ;47 LO-TB-FL;48 LF-TO-FL;49 HO-TB-FL;50 HF-TB-FL;
51 LO-TB-PI;52 LF-TB-PI;53 HO-TB-PI;54 HF-TB-TI;55 LO-TB-TI;
56 LF-TB-TI;57 HO-TB-TI;58 HF-TB-TI;59 LO-TB-PO;60 LF-TB-PO;
61 HO-TB-PO;62 HF-TB-PO;    /*The dependent load abbreviations

/* HO: High pressure Oxidizer;     HF: High pressure Fuel;
/* TB: TurBine;                    SP: SPeed;
/* PM: PuMp;                       PO: discharge (Outlet) Pressure;
/* OPB: Oxidizer PreBurner;        CH: CHamber;
/* P: Pressure;                    T: Temperature;
/* FPB: Fuel PreBurner;            ENG: Engine;
/* O: Oxidizer;                    FL: FLow;
/* F: Fuel;                        THRU: THRUst;
/* PRS: PResSurant;                VP: Valve Position;
/* MCC: Main Combustion Chamber;   IP: Injector Pressure;
/* IT: Injector Temperature;       HG: Hot Gas;
/* IEP: Injector End Pressure;     PI: Inlet Pressure;
/* PB: PreBurner;                  TI: Inlet Temperature;
/* TO: discharge (Outlet) Temp;    MFV: Main Fuel Valve;
/* LO: Low pressure Oxidizer;      LF: Low pressure Fuel;
/* VR: Valve Resistance;           C: Coolant;
/* TQ: TorQue;


■.9                      /*User input. Selecting the engine thrust

■TOTAL # OF RECORDS RETRIEVED IS    1
■  *    *    *    *    *    *
■  *    DISPLAY RECORD(S) OR FIELDS    *
■  *    *    *    *    *    *
■
■    Enter display options
■    (1) Display complete record(s)
■    (2) Display field values of the table
```

```
         (3) Display key values
         (4) No display
    ?
    .1                                         /*User input

    Display format
    (1) record by record
    (2) in compact form
    ?
    .1                                         /*User input

RECORD #  1                                    /*The database record for engine thrust
LDEP-ID  :  9
LD-NAME  :  ENG-THRU
MEAN     :  0.47107E+06
COV      :  0.50000E-02
P3       :  0.00000E+00
DIST     :  NORMAL
NE-COEF1 :  0.10474E+04
NE-COEF2 :  0.46729E+06
NE-COEF3 :  0.38848E+04
NE-COEF4 : -0.11461E+04


Do you wish to select another
Dependent Load ? (Y/N)
.N                                             /*User input

    Select Options for INDEPENDENT LOADS
    MANUAL : User selects the independent loads
    ESASIS : Expert System selects the indep. loads
             based on info in BBOARD (working memory)
.ESASIS                                        /*User input. The user requested
                                               /*the expert system to select the
```

```
* * * * * * * *                          /*independent loads based on GAINS
*
* The EXPERT SYSTEM will select the independent
* loads based on the GAIN's in database INFC
*
* How many independent loads need to be selected
* for each dependent load by the expert system ?
*?
*.10                        /*User input. The user asked the expert
                            /*system to select the 10 most influen-
                            /*tial independent loads

* Selection based on which power level
*       (1) 65% POWER LEVEL
*       (2) 90% POWER LEVEL
*       (3) 100% POWER LEVEL
*       (4) 109% POWER LEVEL
*?
*?
*.3                                      /*User input.

* * * * * * * *
* DISPLAY RECORD(S) OR FIELDS *
* * * * * * * *
*
* Enter display options
*       (1) Display complete record(s)
*       (2) Display field values of the table
*       (3) Display key values
*       (4) No display
*       ?
*?
*.2                                      /*User input

* Please Enter the NUMBER of FIELDS or KEYS
* to be displayed
* Enter a LARGE number for Displaying
```

```
all FIELDS and KEYS
Enter 0(zero) to quit displaying
?
.15                                           /*User input. 15 is larger than the
                                              /*number of fields which is 10 in
                                              /*this case


LIDP-ID   LD-NAME     MEAN         COV          P3          DIST
NE-COEF1  NE-COEF2    NE-COEF3     NE-COEF4
12        MOV-R       0.10700E-01  0.64000E-01  0.00000E+00 NORMAL
0.10700E-01 0.00000E+00 0.10700E-01 0.10000E-01 0.00000E+00 NORMAL
7         HF-TB-FM    0.10125E+01  0.10000E-01  0.00000E+00 NORMAL
0.10125E+01 0.00000E+00 0.10125E+01 0.16000E-01 0.00000E+00 LOGNORM
4         F-TI        0.37000E+02  0.16000E-01  0.00000E+00 LOGNORM
0.37000E+02 0.00000E+00 0.37000E+02 0.55695E-01 0.15000E-01 0.00000E+00 NORMAL
18        O-PRS-FL    0.90168E+02 -0.27112E+02
0.36669E+02 -0.99669E+02 0.30000E+02 0.25900E+00 0.00000E+00 EV-I
2         F-PI        0.30000E+02  0.25900E+00  0.00000E+00 EV-I
0.30000E+02 0.00000E+00 0.13800E-01 0.64000E-01 0.00000E+00 NORMAL
11        MFV-R       0.13800E-01  0.64000E-01  0.00000E+00 NORMAL
0.13800E-01 0.00000E+00 0.60000E+01 0.50000E-02 0.00000E+00 NORMAL
1         MR          0.60000E+01  0.50000E-02  0.00000E+00 NORMAL
0.60000E+01 0.00000E+00 0.10000E+01 0.88000E-01 0.00000E+00 NORMAL
13        CCV-R       0.10000E+01  0.88000E-01  0.00000E+00 NORMAL
-0.19429E-15 0.10000E+01 0.16206E+01 0.65000E-02 0.00000E+00 NORMAL
19        F-PRS-FL    0.16206E+01  0.65000E-02  0.00000E+00 NORMAL
0.16767E+00 0.17642E+01 -0.31119E+00 0.10090E+01 0.10000E-01 0.00000E+00 NORMAL
6         HF-TB-EM    0.10090E+01  0.10000E-01  0.00000E+00 NORMAL
0.10090E+01 0.00000E+00
```

/*The above listing is the independent
/*load infor for the loads that were
/*selected by the expert system.
/*This is a very interesting list in
/*order of descending influence on the
/*variation of the engine thrust

* * * * * * * *
DISPLAY RECORD(S) OR FIELDS

A-8

```
*  *  *  *  *  *  *  *  *  *

Enter display options
(1) Display complete record(s)
(2) Display field values of the table
(3) Display key values
(4) No display
?
.2                    /*User input

Please Enter the NUMBER of FIELDS or KEYS
to be displayed
Enter a LARGE number for Displaying
all FIELDS and KEYS
Enter 0(zero) to quit displaying
?
.15                   /*User input


LDEP-ID  LIDP-ID  INFL-C1     INFL-C2     INFL-C3     INFL-C4
GAIN65   GAIN90   GAIN100     GAIN104
9        12      -0.56499E+00-0.27012E+00 0.00000E+00 0.00000E+00
-0.47397E-01-0.51719E-01-0.53448E-01-0.54139E-01
9        7                  -0.89562E-01-0.91527E+00 0.24514E+00 0.00000E+00
-0.58092E-02-0.71474E-02-0.75970E-02-0.77630E-02
9        4        0.20780E+00 0.00000E+00 0.00000E+00 0.00000E+00
0.33248E-02 0.33248E-02 0.33248E-02 0.33248E-02
9        18       0.18224E-01-0.12652E+00 0.00000E+00 0.00000E+00
-0.96026E-03-0.14347E-02-0.16245E-02-0.17004E-02
9        2        0.62607E-02 0.00000E+00 0.00000E+00 0.00000E+00
0.16215E-02 0.16215E-02 0.16215E-02 0.16215E-02
9        11       0.18987E-02 0.20240E-01-0.86587E-02 0.00000E+00
0.72939E-03 0.83850E-03 0.86275E-03 0.86935E-03
9        1        0.20166E+00-0.48616E-01 0.16720E-01 0.00000E+00
0.88562E-03 0.85725E-03 0.84882E-03 0.84592E-03
9        13       0.94935E-03 0.27960E-02 0.00000E+00 0.00000E+00
```

```
0.24347E-03 0.30498E-03 0.32959E-03 0.33943E-03
9          19         -0.74478E-02-0.31953E-01 0.00000E+00 0.00000E+00
-0.18341E-03-0.23534E-03-0.25611E-03-0.26441E-03
9           6         -0.32588E-01 0.10112E+00-0.57827E-01 0.00000E+00
0.87097E-04 0.11582E-03 0.10708E-03 0.10034E-03
                           /*The above is the influence coefficient
                           /*set

       Available Duty-Cycle-Data files
       CONS    : Constant input by user
       STS61-A : SSME flight profile data with ID=STS61-A
       902-384 : SSME A2 TEST DATA with ID=902-384
       902-387 : SSME A2 TEST DATA with ID=902-387
       750-262 : SSME A3 TEST DATA with ID=750-262
       901-495 : SSME A1 TEST DATA with ID=901-495
       901-491 : SSME A1 TEST DATA with ID=901-491
.902-387                   /*User input. Selecting the test data
                           /*Each group except CONS includes
                           /*duty-cycle-data profile curves for
                           /* the power level, the mixture ratio
                           /* fuel inlet pressure and temperature
                           /* LOX inlet pressure and temperature

Default values for load MOVR
IGO = 2                    /*IGO is the distribution type,
                           /* 2 is NORMAL distribution
   P1 = 0.10700E-01        /*P1,P2,P3 listed here are
   P2 = 0.64000E-01        /* Mean, COV, and rare event probability
   P3 = 0.00000E+00
Do you wish to change the defaults ?(Y/N)
.N                         /*User input

Default values for load HFTBFM
IGO = 2
   P1 = 0.10125E+01
   P2 = 0.10000E-01
   P3 = 0.00000E+00
Do you wish to change the defaults ?(Y/N)
.N                         /*User input
```

```
■ Default values for load OPRSFL
■ IGO =  2
■   P1 =  0.55695E-01
■   P2 =  0.15000E-01
■   P3 =  0.00000E+00
■ Do you wish to change the defaults ?(Y/N)
■.N                        /*User input


■ Default values for load MFVR
■ IGO =  2
■   P1 =  0.13800E-01
■   P2 =  0.64000E-01
■   P3 =  0.00000E+00
■ Do you wish to change the defaults ?(Y/N)
■.N                        /*User input


■ Default values for load CCVR
■ IGO =  2
■   P1 =  0.10000E+01
■   P2 =  0.88000E-01
■   P3 =  0.00000E+00
■ Do you wish to change the defaults ?(Y/N)
■.N                        /*User input


■ Default values for load FPRSFL
■ IGO =  2
■   P1 =  0.16206E+01
■   P2 =  0.65000E-02
■   P3 =  0.00000E+00
■ Do you wish to change the defaults ?(Y/N)
■.N                        /*User input


■ Default values for load HFTBEM
■ IGO =  2
■   P1 =  0.10090E+01
■   P2 =  0.10000E-01
■   P3 =  0.00000E+00
```

A-11

```
# Do you wish to change the defaults ?(Y/N)
#.N                              /*User input

# *    *    *    *    *    *    *    *
# *     DISPLAY RECORD(S) OR FIELDS  *
# *    *    *    *    *    *    *    *
#
# Enter display options
# (1) Display complete record(s)
# (2) Display field values of the table
# (3) Display key values
# (4) No display
#    ?
#?
#.2                              /*User input

# Please Enter the NUMBER of FIELDS or KEYS
# to be displayed
# Enter a LARGE number for Displaying
# all FIELDS and KEYS
# Enter 0(zero) to quit displaying
#?
#.15                             /*User input

#
#
#DCD-ID    LIDP-ID   ENGINE   MISSION   DCD-GRPN
#902-387      0      SSME     TEST      PWR4
#902-387      4      SSME     TEST      TIF4
#902-387      2      SSME     TEST      PIF4
#902-387      1      SSME     TEST      MXR4
                              /*The above list is the database
                              /*for test 902-387

# ***** FROM OPNOFL *****
# ANAME = BLOADAT     LU = 11
#          GRP NAME      GRP #    # OF REC.
#                                 LAST GRP
#DBNREF TABLE    TITL    1        1       /*This is a list of
```

```
#DBNREF TABLE    PWR1    1    6    /*group names for the
#DBNREF TABLE    FLF1    1    6    /*duty-cycle-data file
#DBNREF TABLE    FLO1    1    6    /*The duty-cycle-data
#DBNREF TABLE    TIF1    1    6    /*filename is
#DBNREF TABLE    TIO1    1    6    /*    BLOAD DAT
#DBNREF TABLE    PIF1    1    6    /*The file DDNAME is
#DBNREF TABLE    PIO1    1    6    /*    BLOADAT
#DBNREF TABLE    PWR2    1    6
#DBNREF TABLE    PWR3    1    6
#DBNREF TABLE    PIF3    1    6
#DBNREF TABLE    PIO3    1    6
#DBNREF TABLE    TIF3    1    6
#DBNREF TABLE    TIO3    1    6
#DBNREF TABLE    MXR3    1    6
#DBNREF TABLE    PWR4    1    6
#DBNREF TABLE    PIF4    1    6
#DBNREF TABLE    PIO4    1    6
#DBNREF TABLE    TIF4    1    6
#DBNREF TABLE    TIO4    1    6
#DBNREF TABLE    MXR4    1    6
#DBNREF TABLE    PWR5    1    6
#DBNREF TABLE    PIF5    1    6
#DBNREF TABLE    PIO5    1    6
#DBNREF TABLE    TIF5    1    6
#DBNREF TABLE    TIO5    1    6
#DBNREF TABLE    MXR5    1    6
#DBNREF TABLE    MXR1    1    6
#DBNREF TABLE    PWR6    1    6
#DBNREF TABLE    PIF6    1    6
#DBNREF TABLE    PIO6    1    6
#DBNREF TABLE    TIF6    1    6
#DBNREF TABLE    TIO6    1    6
#DBNREF TABLE    MXR6    1    6
#DBNREF TABLE    PWR7    1    6
#DBNREF TABLE    PIF7    1    6
#DBNREF TABLE    PIO7    1    6
#DBNREF TABLE    TIF7    1    6
#DBNREF TABLE    TIO7    1    6
```

DBNREF TABLE   MXR7   1   6

An ANLOAD input file will be prepared
Please supply the information requested
by the program
Enter DATA separated by commas

MODEL
  (1) Barrier crossing
  (2) DPD
  (3) Monte Carlo
?
?
.2   /*User input

NBIN,NEND
?
?
.25,20   /*User input

TLAST,DELTM,NPRT,FAIL
?
?
.200.0,2.0,5,99999   /*User input

Please enter LOADAN,LOADDA,LOADET,LOADST,LOADNS
for INPUT LOAD # 1 MAIN OXID VALVE R
?
?
.1,0,0,0,0   /*User input

Please enter LOADAN,LOADDA,LOADET,LOADST,LOADNS
for INPUT LOAD # 2 HPFTP T-B FLOW MULT
?
?
.1,0,0,0,0   /*User input

Please enter LOADAN,LOADDA,LOADET,LOADST,LOADNS
for INPUT LOAD # 3 FUEL INLET TEMP(R)

A-14

#?
#?
#.1,0,0,0,1   /*User input

#Please enter LOADAN,LOADDA,LOADET,LOADST,LOADNS
#for INPUT LOAD # 4 OXID PRES FLOW(LB/S)
#?
#.1,0,0,0,0   /*User input

#Please enter LOADAN,LOADDA,LOADET,LOADST,LOADNS
#for INPUT LOAD # 5 FUEL TOTAL PI(PSIA)
#?
#?
#.1,0,0,0,1   /*User input

#Please enter LOADAN,LOADDA,LOADET,LOADST,LOADNS
#for INPUT LOAD # 6 MAIN FUEL VALVE R
#?
#?
#.1,0,0,0,0   /*User input

#Please enter LOADAN,LOADDA,LOADET,LOADST,LOADNS
#for INPUT LOAD # 7 MIXTURE RATIO
#?
#?
#.1,0,0,0,1   /*User input

#Please enter LOADAN,LOADDA,LOADET,LOADST,LOADNS
#for INPUT LOAD # 8 COOL CONTL VALVE R
#?
#?
#.1,0,0,0,0   /*User input

#Please enter LOADAN,LOADDA,LOADET,LOADST,LOADNS
#for INPUT LOAD # 9 FUEL PRES FLOW(LB/S)
#?
#?

```
■.1,0,0,0,0                                      /*User input

■Please enter LOADAN,LOADDA,LOADET,LOADST,LOADNS
■for INPUT LOAD # 10  HPFTP T-B EFF MULT
■?
■?
■.1,0,0,0,0                                      /*User input

■NTRAN
■?
■?
■.0                                              /*User input

■ *****
■ ***** Input data file  HAS BEEN PREPARED
■ *****
                                          /*ANLDIN has generated a input file
                                          /*for ANLOAD. The input filename is
                                          /*   INFILE DAT
                                          /*The file DDNAME is INFILE
                                          /*One can exit the expert system driver
                                          /*and enter ?ANLD to execute ANLOAD
                                          /*interactively

         Available rule modules are :
■          SLIDPL : Independent load information
■          SLDEPL : Dependent load information
■          SLICGN : Influence coefficients and Gain values
■          SLTBCL : Turbine blade component load information
■          SLOCD  : Duty-Cycle-Data file information
■          QLM    : Quick Look Model calculation
■          SICM   : Deterministic Influence Coefficient Model
■          STBSM  : Simple Turbine Blade Scaling Model
■          ANLDIN : Preparing ANLOAD INput file
■          EXIT   : Return to RBMS
■.EXIT                                            /*User input

■    DO YOU WANT TO SAVE THE LOGFILE (Y/N) ?
```

A-16

Appendix B

Turbine Blade Thermal Load Model

TURBINE BLADE THERMAL LOAD MODEL

An algorithm has been developed for determining the steady-state temperature distribution in the HPFTP second stage turbine blade over the engine operating range from MPL to FPL. Geometric influences (tolerance stackup and seal wear) are included in the algorithm.

Thermal Model

A three-dimensional steady-state ANSYS thermal analysis of the SSME HPFTP second stage turbine blade has previously been made on the SSME contract effort. The thermal model is shown in Figure 1. The model includes the blade, platform, and shank. The damper is not included and firtree region is accounted for with an added coarse model. A small portion of the aft region of the shank including the aft face of the shank has a nicraly/zirconium oxide thermal barrier coating to reduce the thermal gradients in this region. This coating is accounted for by adjusting the coolant side heat transfer coefficient. The airfoil itself is also coated. The model does not include this coating since, at steady-state, the airfoil operates at the turbine gas temperature with or without a coating. For a transient analysis, the coating should be considered so that the transient thermal gradients within the airfoil would be properly taken into account. The model was run for FPL conditions.

Method of Determining Thermal Distribution

The same basic procedure used for the HGM transfer tube is also used for the turbine blade. One change for the blade analysis is that, in addition to using the maximum and minimum temperatures of the part (max. T_{wg} and min. T_{wc}) to scale the reference internal temperatures to other conditions, two intermediate temperatures are also used T_{m1} and T_{m2}). These two intermediate temperatures correspond to the intermediate gas temperatures that are used in the thermal model. This has the effect of dividing the blade into three regions (the region between max. T_{wg} and the T_{m1} isotherm, the
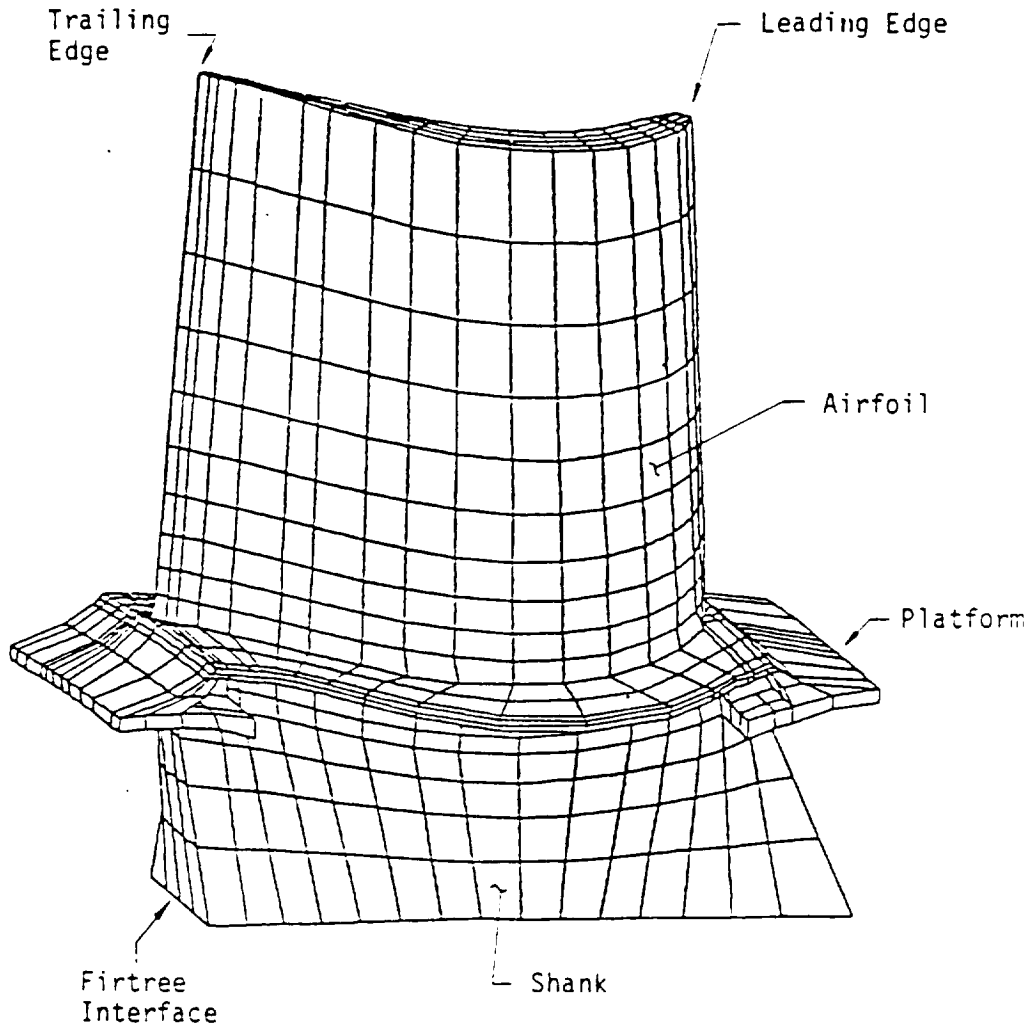
Figure B.1 Thermal Model for the SSME HPFTP
Second Stage Turbine Blade

region between the T_{m1} and T_{m2} isotherms, and the region between the T_{m2} isotherm and min. T_{wc}). These three regions correspond approximately to the airfoil and platform, the major portion of the shank, and the aft portion of the shank, respectively. These three regions will be discussed further in the section on the blade temperature distribution.

Independent Parameters. Because the flowrates are so high and the disk rotates so rapidly, the heat transfer coefficients are high enough that change in the heat transfer coefficients have a negligible influence on the blade thermal distribution. The thermal distribution is controlled by the fluid temperatures surrounding the blade. The following independent parameters control the fluid temperatures which surround the blade.

- Turbine inlet temperature (T_{in})
- Turbine discharge temperature (T_{out})
- Pump discharge temperature (T_p)
- Geometric influence on the coolant flowrate (G_c). This parameter is primarily determined by the tolerance stackup and seal wear. It determines the amount of coolant going to the aft face of the second stage disk. Increases in G_c correspond to increases in coolant flow (greater seal leakage).
- Geometric influence on the hot gas leakage into the coolant circuit (G_h). This parameter is also primarily determined by the tolerance stackup and seal wear. Increases in G_h correspond to increases in hot gas leakage. There is not, as yet, enough data to determine whether the tolerance stackup or the seal wear is the predominant factor. Also, the rate at which seal wear occurs is not known (whether it occurs primarily early in testing or continues gradually from test to test).

Blade Boundary Conditions. The four temperatures (max. T_{wg}, T_{m1}, T_{m2}, and min. T_{wc}) used to define the thermal distribution in the blade are functions of the above five independent parameters described in the previous section. Equations for the four temperatures in terms of the five independent parameters are derived below.

The turbine hot gas (T_g) at the location of the second stage blade is a function of the turbine inlet and discharge temperatures (T_{in} and T_{out}).

Based on hydrodynamic calculations (Fig. 2) it can be reasonably approximated by the following equation

$$T_g = 0.84^*T_{out} + 0.16^*T_{in} \tag{1}$$

The maximum temperature of the blade (max. T_{wg}) is the same as the temperature of the turbine hot gas. Therefore, Equation (1) also represents the maximum temperature of the blade.

$$\text{Max. } T_{wg} = 0.84\ T_{out} + 0.16\ T_{in} \tag{2}$$

The coolant temperature for the aft part of the disk (T_c) is determined by the pump discharge temperature (T_p) and the geometric influence (G_c) on the coolant flow. For baseline geometry conditions the coolant temperature is assumed to be 250°R greater than the pump temperature and to vary directly with the pump temperature.

$$T_c = 250 + T_p \tag{3}$$

Experience has shown that the coolant temperature has an approximate range from 250°R to 450°R, depending primarily on the magnitude of the coolant flowrate. For a geometry influence parameter (G_c) value of 1.0 at the reference conditions and a reference coolant temperature of 350°R the maximum range for the coolant geometry influence parameter is from 0.71 to 1.29. The 0.71 value will give a coolant temperature change of +100°R (450-350) and the 1.29 value will give a coolant temperature change of -100°R (250-350). In equation form the change in the coolant temperature due to geometric influence is

$$\Delta T_c = 344.8\ (1-G_c) = 344.8 - 344.8 G_c \tag{4}$$

Equations (3) and (4) can be added to give the equation for the coolant temperature.

$$T_c = 594.8 + T_p - 344.8 G_c \tag{5}$$
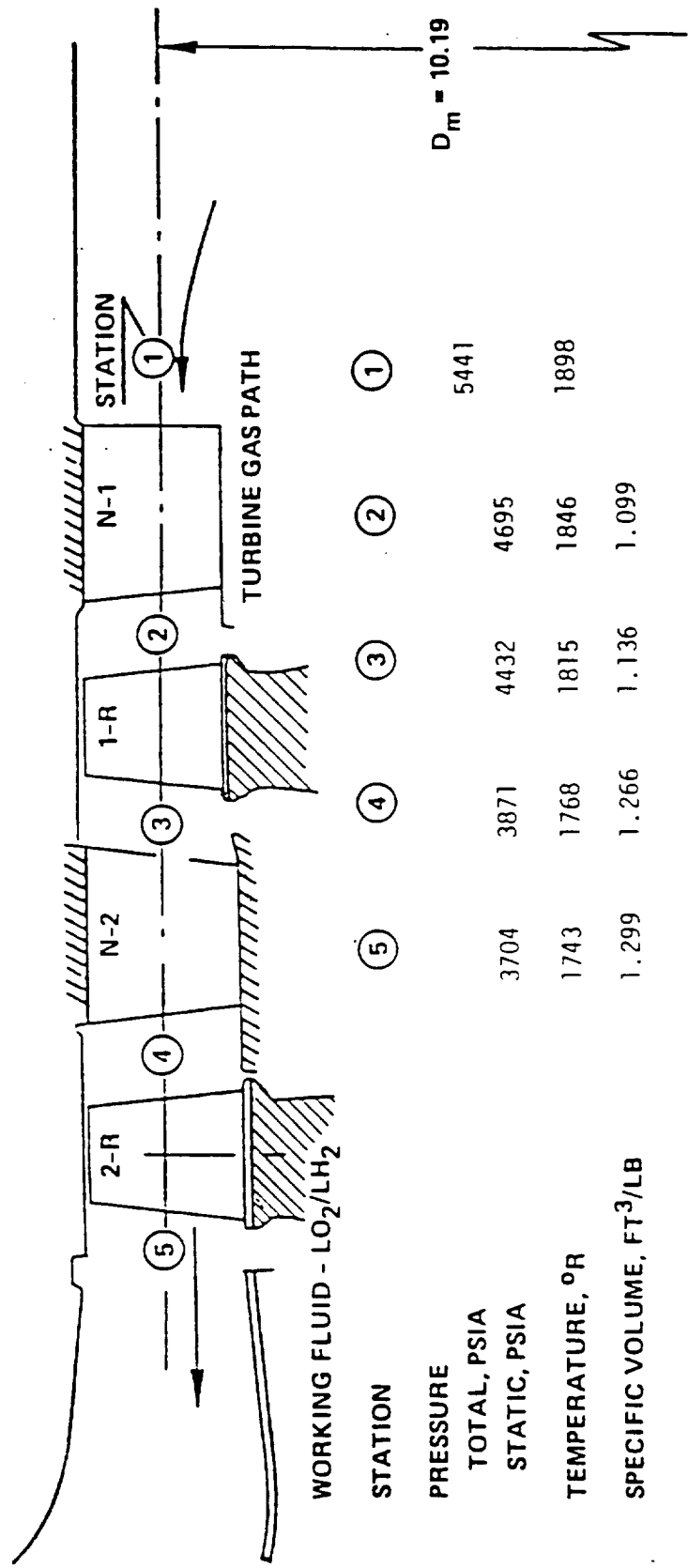
STATION	5	4	3	2	1
PRESSURE					
TOTAL, PSIA	3704	3871	4432	4695	5441
STATIC, PSIA	1743	1768	1815	1846	1898
TEMPERATURE, °R	1.299	1.266	1.136	1.099	
SPECIFIC VOLUME, FT³/LB					

WORKING FLUID – LO_2/LH_2

$D_m = 10.19$

Figure B.2 SSME HPFTP Phase II Turbine Gas Data

The minimum temperature of the blade (min. T_{wc}) is assumed to vary identically with the change in the coolant temperature (T_c) and to be 88°R higher than it. Using equation (5) the equation for the minimum temperature of the blade becomes

$$\text{Min. } T_{wc} = 682.8 + T_p - 344.8G_c \tag{6}$$

The first mixed gas temperature (T_{ml}) is determined from the turbine gas temperature (T_g), the coolant temperature (T_c), and the geometric influence (G_h) on the hot gas leakage into the coolant circuit. From the reference case data (nominal geometric conditions), the equation for T_{ml} can be given as

$$T_{ml} = 0.1325T_c + 0.8675T_g \tag{7}$$

There is also a geometry influence on this mixed temperature. This parameter (G_h) is set to a value of 1.0 for the reference case. Experience has shown that the mixed temperature can vary from 1350°R to 1860°R. For a reference mixed gas temperature of 1660°R, the maximum range for the hot gas geometry influence parameter becomes 0.813 to 1.12. The 0.813 value will give a change in the mixed gas temperature of -310°R (1350-1660) and the 1.12 factor will give a change in the mixed gas temperature of +120°R (1860-1660). The equation for the change in the first mixed gas temperature as a function of the geometric influence parameter can be given as

$$\Delta T_{ml} = 1660 (G_h - 1) = 1660G_h - 1660 \tag{8}$$

Adding equations (7) and (8) and substituting equations (1) and (5) for T_g and T_c, respectively gives the equation for the first mixed gas temperature.

$$T_{ml} = -1581.2 + 0.1325T_p - 45.69G_c + 0.7287T_{out} + 0.1388T_{in} + 1660G_h \tag{9}$$

The second mixed gas temperature (T_{m2}) is just the average of the first mixed gas temperature (T_{m1}) and the coolant temperature (T_c). By taking the average of the sum of Equations (5) and (9), the influence coefficient equation for T_{m2} is obtained.

$$T_{m2} = -493.2 + 0.566 T_p - 195.2 G_c + 0.3644 T_{out} + 0.0694 T_{in} + 830 G_h \qquad (10)$$

Equations (2), (6), (9), and (10) define, in terms of the five independent parameters, the four temperatures used in determining the temperature distribution.

Influence Coefficients. Equations (2), (6), (9), and (10) can be rewritten in influence coefficient form. The values of the coefficients are determined by multiplying the coefficient for each independent parameter in equations (2), (6), (9), and (10) by the ratio for the reference value of the independent parameter to reference value of the dependent parameter. For equation (2), this procedure is shown below.

$$\frac{\Delta \text{ max. } T_{wg}}{\text{Ref. max. } T_{wg}} = 0.84 \frac{\text{Ref. } T_{out}}{\text{Ref. max. } T_{wg}} \frac{\Delta T_{out}}{\text{Ref. } T_{out}} + 0.16 \frac{\text{Ref. } T_{in}}{\text{Ref. max. } T_{wg}} \frac{\Delta T_{in}}{\text{Ref. } T_{in}} \qquad (11)$$

The four influence coefficient equations are

$$\frac{\Delta \text{max. } T_{wg}}{\text{Ref. max. } T_{wg}} = 0.8269 \frac{\Delta T_{out}}{\text{Ref. } T_{out}} + 0.1731 \frac{\Delta T_{in}}{\text{Ref. } T_{in}} \qquad (12)$$

$$\frac{\Delta \text{min. } T_{wc}}{\text{Ref. min. } T_{wc}} = 0.2283 \frac{\Delta T_g}{\text{Ref. } T_g} - 0.7872 \frac{\Delta G_c}{\text{Ref. } G_c} \qquad (13)$$

$$\frac{\Delta T_{m1}}{Ref.\ T_{m1}} = 0.00798\ \frac{\Delta T_g}{Ref.\ T_g} - 0.0275\ \frac{\Delta G_c}{Ref.\ G_c} + 0.8038\ \frac{\Delta T_{out}}{Ref.\ T_{out}}$$

$$+ 0.1682\ \frac{\Delta T_{in}}{Ref.\ T_{in}} + 1.0\ \frac{\Delta T_h}{Ref.\ G_h} \qquad (14)$$

$$\frac{\Delta T_{m2}}{Ref.\ T_{m2}} = 0.0563\ \frac{\Delta T_p}{Ref.\ T_p} - 0.1942\ \frac{\Delta G_c}{Ref.\ G_c} + 0.6639\ \frac{\Delta T_{out}}{Ref.\ T_{out}}$$

$$+ 0.1389\ \frac{\Delta T_{in}}{Ref.\ T_{in}} + 0.8259\ \frac{\Delta T_h}{Ref.\ G_h} \qquad (15)$$

<u>Blade Temperature Distribution</u>. As mentioned previously, the blade is effectively divided into three sections. The reference isotherms for T_{m1} and T_{m2} form the internal boundaries. The physical locations of these internal boundaries (isotherms) do not change for different operating conditions. Only the temperatures associated with these two isotherms will change, being the adjusted values for T_{m1} and T_{m2}. The temperature distribution equation for each of the three sections is given below, based on the four temperatures determined from equations (2), (6), (9), and (10) and the reference conditions. Ref. T refers to the reference temperature at a specific location within the thermal model of the blade.

For Ref. T > Ref. T_{m1}:

$$T = T_{m1} + (Ref.\ T - Ref.\ T_{m1})\ \frac{max.\ T_{wg} - T_{m1}}{Ref.\ max.\ T_{wg} - Ref.\ T_{m1}} \qquad (16)$$

For Ref. $T_{m2} \leq$ Ref. T < Ref. T_{m1}:

$$T = T_{m2} + (Ref.\ T - Ref.\ T_{m2})\ \frac{T_{m1} - T_{m2}}{Ref.\ T_{m1} - Ref.\ T_{m2}} \qquad (17)$$

For Ref. T < Ref. T_{m2}:

$$T = mix. \ T_{wc} + (Ref. \ T - Ref. \ min. \ T_{wc}) \ \frac{T_{m2} - min. \ T_{wc}}{Ref. \ T_{m2} - Ref. \ min. \ T_{wc}} \qquad (18)$$

Reference Parameters. The temperature distribution from the previously constructed thermal model (ref. 2) of the HPFTP second stage turbine blade is used as the reference case. This reference case is at the FPL operating point. The values for the reference parameters are

$$
\begin{aligned}
Ref. \ T_{in} &= 2011°R \\
Ref. \ T_{out} &= 1831°R \\
Ref. \ T_{p} &= 100°R \\
Ref. \ G_{c} &= 1.0 \\
Ref. \ G_{h} &= 1.0 \\
Ref. \ Max. \ T_{wg} &= 1860°R \\
Ref. \ T_{m1} &= 1660°R \\
Ref. \ Min. \ T_{Wc} &= 438°R
\end{aligned}
$$

In addition, the reference temperature distribution will need to be used. This temperature distribution is saved on a file. The coordinate locations for the temperatures are also on this file.

A three-dimensional model of the second stage blade, including the firtree and the disk, has recently been run. A case has been run with this model using the same reference conditions as for the model. The thermal distribution for the blade, platform, and shank from this case could be substituted for the reference temperature distribution described in the previous paragraph.

Conclusions. For purposes of this study the procedure developed for determining the thermal distribution is adequate. As this study progresses the following further work should be addressed.

- A more sophisticated approach to the influence of geometric variations should be considered.

- The geometric influence parameters (G_h and G_c) need to be correlated with actual engine dimensions and dimensional changes due to wear.

- A more refined second stage turbine blade model which includes the firtree and disk is now available. Eventually it should be used.

- Parameters which have a secondary influence on the temperature distribution have been ignored. Ultimately, these should be included in determining the thermal load.

Appendix C

Pressure Fluctuations and Correlation Lengths
Summary and Critique

Pressure Fluctuations and Correlation Lengths: Summary and Critique

Three previous I.L.s (refs. C1-C3) have documented the work that was carried out to predict the pressure fluctuations PSD and the correlation lengths for the transfer duct, high pressure oxidizer pump discharge duct (HPOPDD) and the main injector regions of the SSME for the CLS program. Figures C1-C3 summarize, in a flowchart format, the techniques established. Extensive use was made of the cold-flow experimental data and hot-fire engine data, where available, to yield these results. For example, a survey of the scaled-up transfer duct data showed that 81% percent of the energy was contained in the 10-1000 Hz range. A similar survey yielded the same energy in the 10-4000 Hz range for the HPOPDD data. These observations were used to determine the frequency domain in which the various scaling laws were valid.

Since the CLS program is generic in nature, it would be worthwhile to understand the rationale for these frequency values as a function of the flow geometry. A list of issues that need discussion are:

i)   Upper frequency bound which contains a major percentage of the energy,

ii) Extent of correlated pressure zones,

iii) Decay of wall pressure fluctuations, and

iv) Separated region prediction.

i) UPPER FREQUENCY DETERMINATION

Past research on nondimensionalizing wall pressure fluctuation data on flat plates and cylinders has shown that the displacement thickness, δ^*, and the free stream velocity, U_∞, are parameters that cause the data at differ- ent Reynolds numbers to collapse. Since this detailed information is not available for the complex flow geometries studied in this program, the best one can do is to survey the data that is available to determine the cross-over frequency at which the PSD data changes slope. In ref. C1, an estimate   of

this frequency was made, based on the convection velocity and the duct radius, and a value within +20% of 1000 Hz was determined for the fuel and LOX side transfer ducts. However, the same technique yielded too low a value for the HPOPDD, since the flow geometry involves bends which lead to the wallbounded shear layers to be of different thicknesses on opposite walls. In any case, the geometries are far too complex for any simple technique to work adequately for all cases. From a review of the techniques developed in refs. C1-C3, it is observed that for "skimming" type flows, i.e., flows parallel to surfaces, the frequency at which the data shifts from a -1 or -0.4 slope (on a log-log scale) to a -5/3 slope occurs at 40% of the wideband frequency. For instance, the transfer duct data PSD frequency limits were 0-2500 Hz, and 1000 Hz was determined as the frequency below which 81% of the energy exists.

Similarly for the HPOPDD, 4000 Hz was determined as the point below which the same energy content exists, and the wideband frequency was 10,000 Hz. Similarly, a skimming-type flow exists for the main injector in the region of posts 70-71 and again, 40% of the wideband frequency limit was determined as the cross-over frequency point. In ref. C3, 75% of the energy was determined to exist in this frequency limit. For this summary report, this percentage was raised to 81% and no significant difference was observed in the PSD values. Hence, a 40% of the wideband frequency which contains 81% of the energy appears to hold true for the data studied.

As a check, a data set for measurements taken on the LOX-side transfer duct, which was analyzed in the frequency ranges of 0-2500 Hz and 0-10,000 Hz was used to check this hypothesis. Figures C4 and C5 show the result of this exercise. The results show that the fit to the data is rather good. This means that either there is proportionately the same amount of energy in the 10-1000 Hz range or that the addition to the energy from 1000-4000 Hz is not significant. Since the composite rms values (3.51 psi and 3.56 psi) are almost the same, the latter observation is true.

Consequently, one has to make sure that the data has been analyzed using an adequate frequency range so that a large fraction of the energy has not been omitted for this technique to work. Of course, by the same token, one cannot increase the upper frequency limit at random and expect the technique to work. A realistic bandwidth should be chosen based on either observing the highest frequencies seen in the data or basing it on past experience.

For the main injector, at posts 01-02, a stagnation-type flow is envisioned. This is especially true for the top, i.e. towards the LOX dome, location. Revisiting the data in ref. C3, it is observed that a 40% split does hold true (ref. Fig. C6) provided one uses a geometric shape factor, $S = 0.99$ for the computer program or $S = 1.0$, if one determines the coefficients K_o and K_i explicitly, as was done for the initial analysis in ref. C1.

Hence, as a rule of thumb, a 40% value of the wideband frequency can be used as a guideline for the frequency at which the PSD changes slope. Also, in general, a shape factor value of $S = 0.4$ is advisable for flows which are separated or with adverse pressure gradient, since these conditions lead to more energy at the lower frequencies. Otherwise, $S = 1$ will generally prove to be adequate to predict the PSD decay.

With regards to predicting P_{rms} values, significant differences are observed, depending upon the region under consideration. For geometries that do not have separated regions, it is observed that P_{rms} values of 0.15 q_{1-D} or 0.30 q_{1-D} can be used, depending upon accelerating or decelerating regions, respectively. This is observed to be true for both the two-duct transfer duct and the HPOPDD data, where $0.15 q_{1-D}$ was used. Large departures from these values are observed when one uses estimates of q_{1-D} which do not hold true over a major portion of the flow. This is observed in the three-duct hot gas manifold where it is known that a large area of the center transfer contains separated flow. Consequently, the effective flow area is reduced, leading to a higher γ value. Yet, since this study is generic in nature, detailed information regarding the flowfield is not known. Consequently, large estimates of the P_{rms}/q_{1-D} ratio result based on

C-4

one-dimensional estimates. Furthermore, because of the complex nature of the flow in the main injector region, the local value of q could be almost an order of magnitude different from q_{1-D} depending upon the location. Again, from a generic viewpoint, the values shown in Figure C3 essentially bracket the P_{rms} based on one-dimensional estimates of q in the transfer duct, and should be used. It should be mentioned that a similar analysis should be done for the two-duct hot gas manifold to determine the P_{rms}/q_{1-D} variation.

ii) CORRELATION ZONE DETERMINATION

An estimate of the correlation length is obtained by determining the integral time scale and multiplying it by the convection velocity. The procedure is outlined in ref. C1. The upper limit for the integration is typically set equal to a characteristic dimension divided by the convection velocity (equal to 0.6 times the U_{1-D}). Since this study limits itself to wall pressure fluctuations, the extent of the correlated zone is of importance. Two sur-faces that describe any surface are: flat and curved. For flat surfaces, Willmarth and Wooldridge (ref. C4) have shown that both the transverse and longitudinal scale are on the order of the boundary-layer displacement thick-ness. The transverse and longitudinal scales of both large and small-scale wall pressure fluctuations were also found to be approximately the same. For this study, curved surface geometries are more applicable. Past research on determining the ratio of longitudinal to transverse length scales (ref. C5 and C6) have shown that the transverse scale is typically smaller than the longitudinal scale. For flowthrough straight pipes, ref. C5 quantifies this ratio to be approximately 0.5. Qualitatively, this can be explained visualiz-ing a large eddy adjacent to a curved wall. For a convex surface, it is apparent that in the transverse direction, at either side of the periphery of the large eddy, the mean velocity would be higher than it would be at the sides of the same eddy in a plane boundary layer. Thus, there is a streamwise shearing motion along the sides of large eddies in a boundary layer with transverse curvature that is not present in a plane boundary layer. This shearing motion also acts to reduce the transverse scale of the large eddies. A similar scenario can be envisioned for a concave surface, e.g. flow inside a

pipe. In this case, the edges of the large eddy are experiencing a lower mean velocity than the center. Again a streamwise shearing action ensues, thereby reducing the extent of the transverse scale. It should be noted that if δ^*, the displacement thickness, is taken as a measure of the scale of turbulence, and if indeed the data does scale in the -5/3 slope regime, then one can use this technique to determine another estimate of the length scale, as follows.

If, for instance, for the LOX side transfer duct one determines, at $f = 1000$ Hz,:

$$\omega\delta^*/U_c = \frac{(2^*\pi^*1000)^*(2.50/12)}{(0.6^*386)}$$

$$= 5.65.$$

Then equating this value of $\omega\delta^*/U_c$ to the HPOPDD case yields:

$$\delta^*_{HPOPDD} = 0.24 \text{ inches,}$$

which is almost an order of magnitude smaller than that predicted in ref. C2. This difference signifies the complexity of the flow and danger of putting too much faith in a single point measurement. From a worst-case point of view, obviously, the larger value for the correlation length scale should be used. Similarly, for the main injector, one obtains:

$$\delta^*_{MI} = 1.84 \text{ inches,}$$

which compares well with values obtained in ref. C3.

iii) DECAY OF WALL PRESSURE FLUCTUATIONS

In order to obtain a more realistic estimate of the extent of the correlation zone, it is best to determine the decay of the wall pressure fluctuations. It

should be noted that the correlation length discussed earlier is the average size of the large scale, energy-containing eddy over which the eddy retains its characteristics. Thus, by using this to be the length over which the pressure-producing eddy is fully correlated is, in a sense, assuming worst-case conditions. In reality, due to viscous interaction and dissipation, both large- and small-scale pressure producing eddies decay after travelling a distance proportional to their scale (ref. C4). More precisely, a pressure-producing eddy of large or small wavelength λ decays and vanishes after travelling a distance of approximately 6λ.

In order to relate the PSD at one point to another point requires an in-depth knowledge of the flowfield. This has been done in ref. C4 for measurements over a flat plate turbulent boundary layer and analyzed in ref. C7 to yield the expression shown below:

$$PDS\ (\xi,\eta,\omega) = PSD\ (o,o,\omega)A(\omega\xi/U_c)B(\omega\eta/U_c)exp(-i\omega\xi/U_c) \tag{1}$$

with the corresponding space-time correlation given by:

$$R(\xi,o,\tau) = \int^\infty PSD(o,o,\omega)A(\omega\xi/U_c)exp[i(\omega\tau-\omega\xi/U_c)]d\omega \tag{2}$$

and

$$R(o,\eta,\tau) = \int^\infty PSD(o,o,\omega)B(\omega\eta/U_c)exp[i\omega\tau]d\omega \tag{3}$$

In eq.(1), functions A and B are determined experimentally, see Figs. C7 and C8, and can also be fit by the following two expressions:

$$A(\lambda) = exp(-0.1145|\lambda|) + 0.1145|\lambda|\ exp(-2.5|\lambda|) \tag{4}$$

$$B(\beta) = 0.155\ exp(-0.92|\beta|) +0.70\ exp(-0.789|\beta|)$$
$$+0.145\ exp(-2.916|\beta|) +0.99\ exp(-4.0|\beta|) \tag{5}$$

where $\lambda = \omega\xi/U_c$ and $\beta = \omega\eta/U_c$. The variation of U_c with the frequency is shown in Figure C9. Thus, using these relationships it is feasible to predict the PSD as a function of distance from a reference location where the PSD is known. A similar database, developed by Willmarth and Yang, flows over cylinders aligned with the flow.

In order to develop this capability for the CLS program, an experimental program needs to be carried out to develop this database for geometries relevant to the program. Since data for such geometries is scant, the best one can do is to use the PSD prediction technique in conjunction with the correlation lengths described earlier.

iv) SEPARATION REGION PREDICTION

Separated regions are of interest because they lead to irrecoverable total pressure loss which can lead to degraded engine performance. In addition, large values of the PSD at low frequencies are observed, which, if they are coincident with the resonance frequency of the local structure, could lead to structural problems or failures.

Furthermore, the streamwise extent of the separated region is usually larger than the normally computed correlation length. This, therefore, leads to larger, correlated pressure zones which also aid to amplify the problem.

Typically, the prediction of separated regions requires a detailed knowledge of the flowfield. As a minimum, for instance, a wall static pressure distribution is needed to determine if adverse pressure gradients exist which could lead to flow separation. Ideally, this information should be coupled with velocity measurements that are capable of resolving flow reversals.

However, this is unrealistic for the time being since no program currently exists to measure, in a nonintrusive manner, the flowfield in a hot-fire engine test. Thus, for the current wall, static pressure distribution coupled with high frequency pressure fluctuation measurements are more realistic. It

is anticipated that the current database will be substantially increased with the advent of the technology test bed program.

For the present, however, one is left to make intuitive judgments with regard to separated regions based purely on geometric considerations and past experience. For instance, the axisymmetric turnaround duct program (ref. C8) showed that a separated region exists starting at the 154 deg location on the inner wall of the duct. Similarly, the solid wall hot gas manifold test program (ref. C9) showed that the center transfer duct of the three-duct configuration contained flow which was essentially all separated.

Past work on flow through pipes with bends could also be researched in the literature to determine the relationship between Reynolds number, bend geometry and incoming turbulence intensity.

The bottom line is that quantitative separation zone prediction for the complex geometries being studied is difficult at best. One has to revert to past experience or intuitive judgment. Of course, with the continued development of computational fluid dynamics models, these predictions could also be used to aid in this process. However, current CFD capability is not at the point where it can be used routinely and cost-effectively for complex three-dimensional geometries that are of interest in the rocket engine environment.

CONCLUSIONS

A technique has been determined which can be used to predict the PSDs and the correlation lengths for the transfer duct, HPOPDD, and the main injector region of the SSME. The technique has been based on existing cold-flow or hot-fire engine data. It is observed that generally good agreement is achieved with other existing PSD data. However, the level of the PSD or the P_{rms} level is a strong factor for the turbulence intensity assumed. Based on one-dimensional estimates, large variations in the p_{rms}/q_{1-D} ratio are observed when different regions are compared. This issue can be only resolved

by acquiring more experimental data, thus widening the database. Similarly, due to the lack of a detailed database, no assumptions can be made regarding the decay of the wall pressure fluctuations. This knowledge would ultimately resolve the question of how the entire structure is loaded. This currently is a weak point since it is not known whether the locations at which past measurements have been made are those at which the turbulence is greatest. Such detailed information would give clues to the existence of separated regions since velocity profile measurements are not forthcoming in the near term.

Summarizing, the technique developed in the current study is a step in the right direction since it is anchored to actual data rather than intuitive guesses regarding the turbulence levels. Also, the PSD prediction is compared with actual data rather than data obtained from geometries which have little or no resemblance to those in a rocket engine. Future verification of the technique developed herein will be based by comparing it with more data as it becomes available.

5753a/bes

REFERENCES

C1) Sharma, L. K., "Transfer Duct Pressure Fluctuations and Correlation Lengths for the Composite Load Spectra Program," SSME-87-1756, December 1987.

C2) Sharma, L. K., "HPOP Discharge Duct Pressure Fluctuations and Correlation Lengths for the Composite Load Spectra Program," SSME-87-1757, December 1987.

C3) Sharma, L. K., "Main Injector Lox Posts Pressure Fluctuations and Correlation Lengths for the Composite Load Spectra Program," SSME-88 000337.

C4) Willmarth, W. W. and C. E. Wooldrige, "Measurements of the Fluctuating Pressure at the Wall Beneath a Thick Turbulent Boundary Layer," J. Fluid Mechanics, Vol. 14, Part 2, pp. 187-210, 1962.

C5) Bakewell, H. P. et al, "Wall Pressure Correlations in Turbulent Pipe Flow," U.S. Navy Underwater Sound Laboratory Report No. 559, August 1962.

C6) Willmarth, W. W. and C. S. Yang, "Wall-pressure Fluctuations Beneath Turbulent Boundary Layers on a Flat Plate and a Cylinder," J. Fluid Mechanics, Vol. 41, Part 1, pp.47-80, 1970.

C7) Willmarth, W. W. and R. W. Roos, "Resolution and Structure of the Wall Pressure Field Beneath a Turbulent Boundary Layer," J. Fluid Mechanics, Vol. 22, Part 1, pp. 81-94, 1965.

C8) Sharma, L. K. and B. J. Ostermier, "Test Report: Turnaround Duct Turbulence Test," RSS-8741, ATU-86-5162, 15 May 1987.

C9) "Solid Wall Hot Gas Manifold Testing Series IV Test Results," ATU-83-006, 13 January 1983.

TRANSFER DUCT

TOP WALL

(TOWARDS LOX DOME)

BOTTOM WALL

(TOWARDS NOZZLE)

$$p' = 0\ 15\ q_{1-D}$$

$$p' = 0\ 30\ q_{1-D}$$

$$\phi = K_0\ f^{-1}\quad,10<f<1000\ Hz,$$

$$\phi = K_1\ f^{-5/3}\quad,1000<f<2500\ Hz$$

$$\phi = K_0\ f^{-0\ 4}\quad,10<f<1000\ Hz$$

$$\phi = K_1\ f^{-5/3}\quad,1000<f<2500\ Hz$$
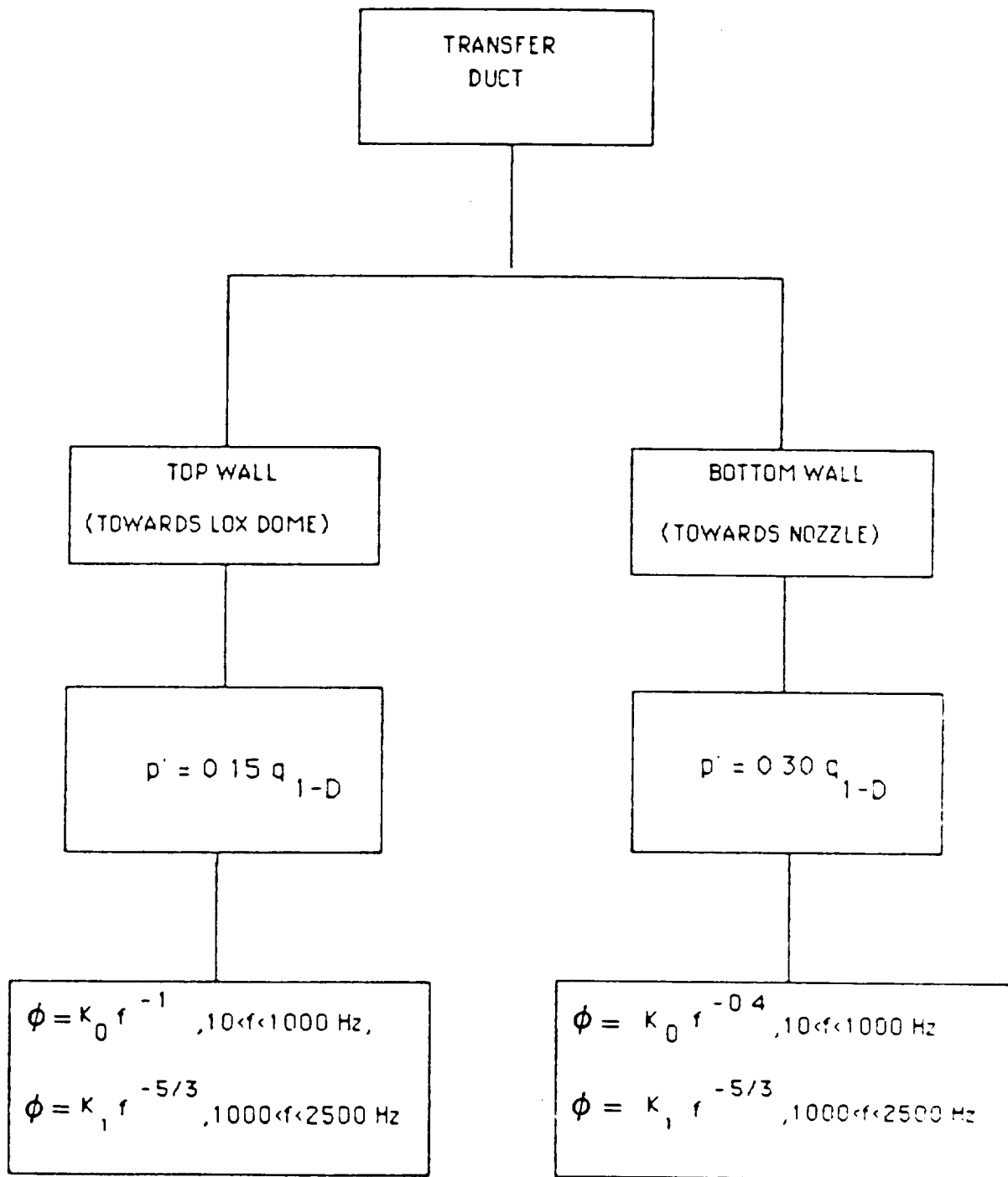
To evaluate K_0 and K_1 need to assume $0\ 81\ p^2_{rms}$ in the frequency range $10 < f < 1000$ Hz

Figure C1.   Flow Chart to Determine Transfer Duct PSDs

$$\boxed{\begin{array}{c}\text{HIGH PRESSURE}\\\text{OXIDIZER PUMP}\\\text{DISCHARGE DUCT}\end{array}}$$

$$p' = 0.15\, q_{1-D}$$

$$\phi = K_0\, f^{-0.4}, \quad 10 < f < 4000\ \text{Hz},$$

$$\phi = K_1\, f^{-5/3}, \quad 4000 < f < 10000\ \text{Hz}$$
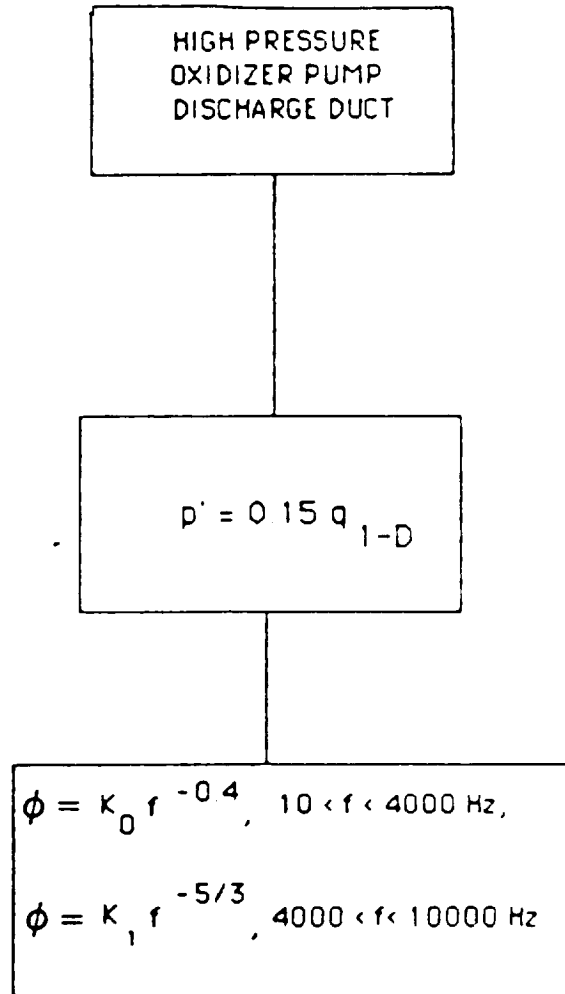
To evaluate K_0 and K_1 need to assume $0.81\, p^2_{rms}$ in the frequency range $10 < f < 4\,000$ Hz

Figure C2. Flow Chart to Determine HPOP Discharge Duct PSDs

```
                    ┌─────────────┐
                    │    MAIN     │
                    │  INJECTOR   │
                    └─────────────┘
```

┌──────────────────────────┐   ┌──────────────────────────┐
│   STAGNATION TYPE   │   │   SKIMMING FLOW   │
│   FLOW   │   │   │
│ (e g. POSTS 01-02 TOP)   │   │   (e g. POSTS 70-71)   │
└──────────────────────────┘   └──────────────────────────┘

┌──────────────────────────┐   ┌──────────────────────────┐
│   │   │   │
│ $p' = 1.10 \, q_{1-D}$ │   │ $p' = 0.70 \, q_{1-D}$ │
│   │   │   │
└──────────────────────────┘   └──────────────────────────┘

┌────────────────────────────────┐ ┌────────────────────────────────┐
│ $\phi = K_0 \, f^{-1}$, 10 < f < 2000 Hz,│ │ $\phi = K_0 \, f^{-0.4}$, 10 < f < 2000 Hz │
│   │ │   │
│ $\dot\phi = K_1 \, f^{-5/3}$, 2000 < f < 5000 Hz│ │ $\phi = K_1 \, f^{-5/3}$, 2000 < f < 5000 Hz │
└────────────────────────────────┘ └────────────────────────────────┘
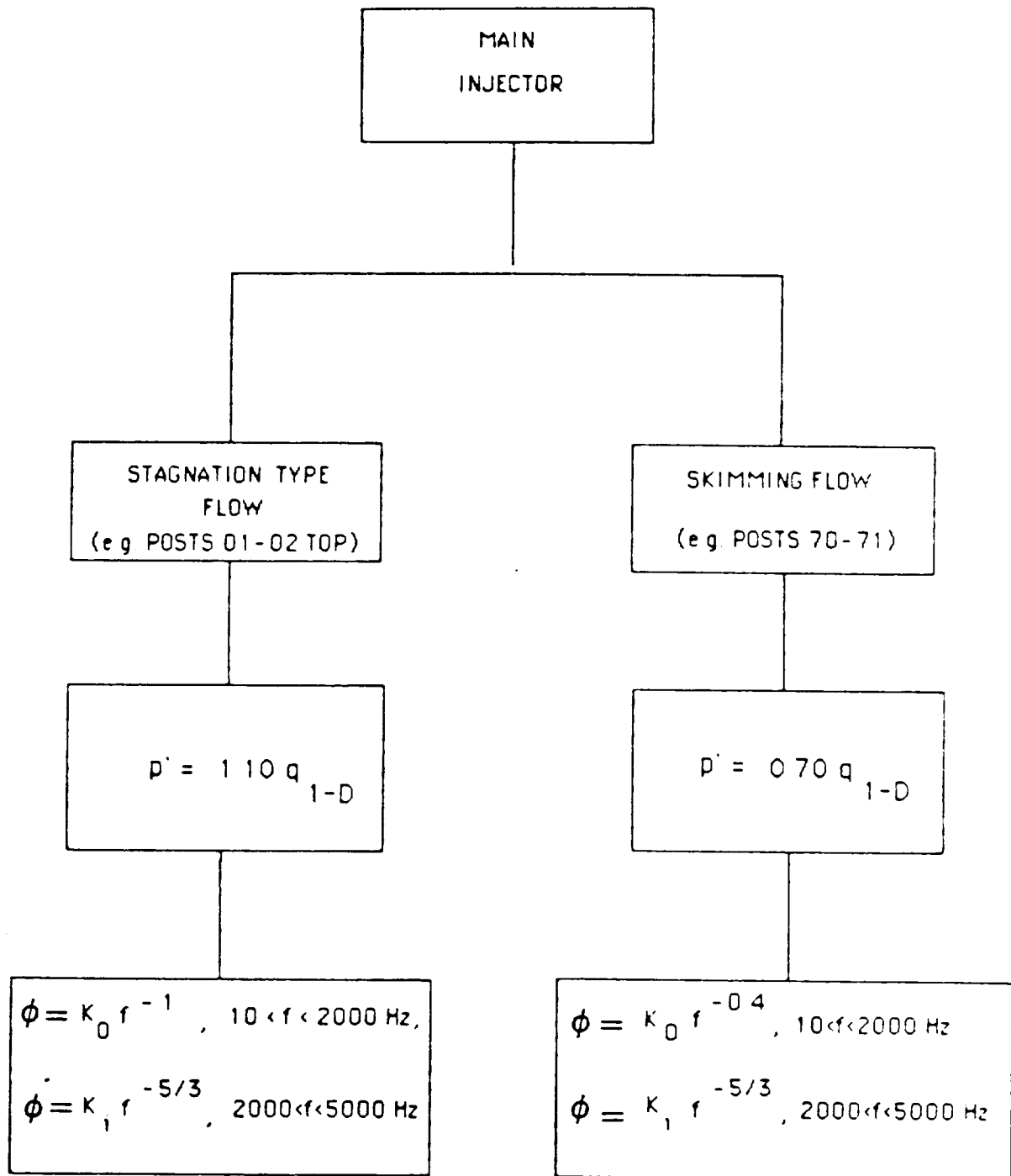
To evaluate K_0 and K_1 need to assume $0.81 \, p^2_{rms}$ in the frequency range 10 < f < 2000 Hz

Figure C3.   Flow Chart to Determine Main Injector PSDs

C-14
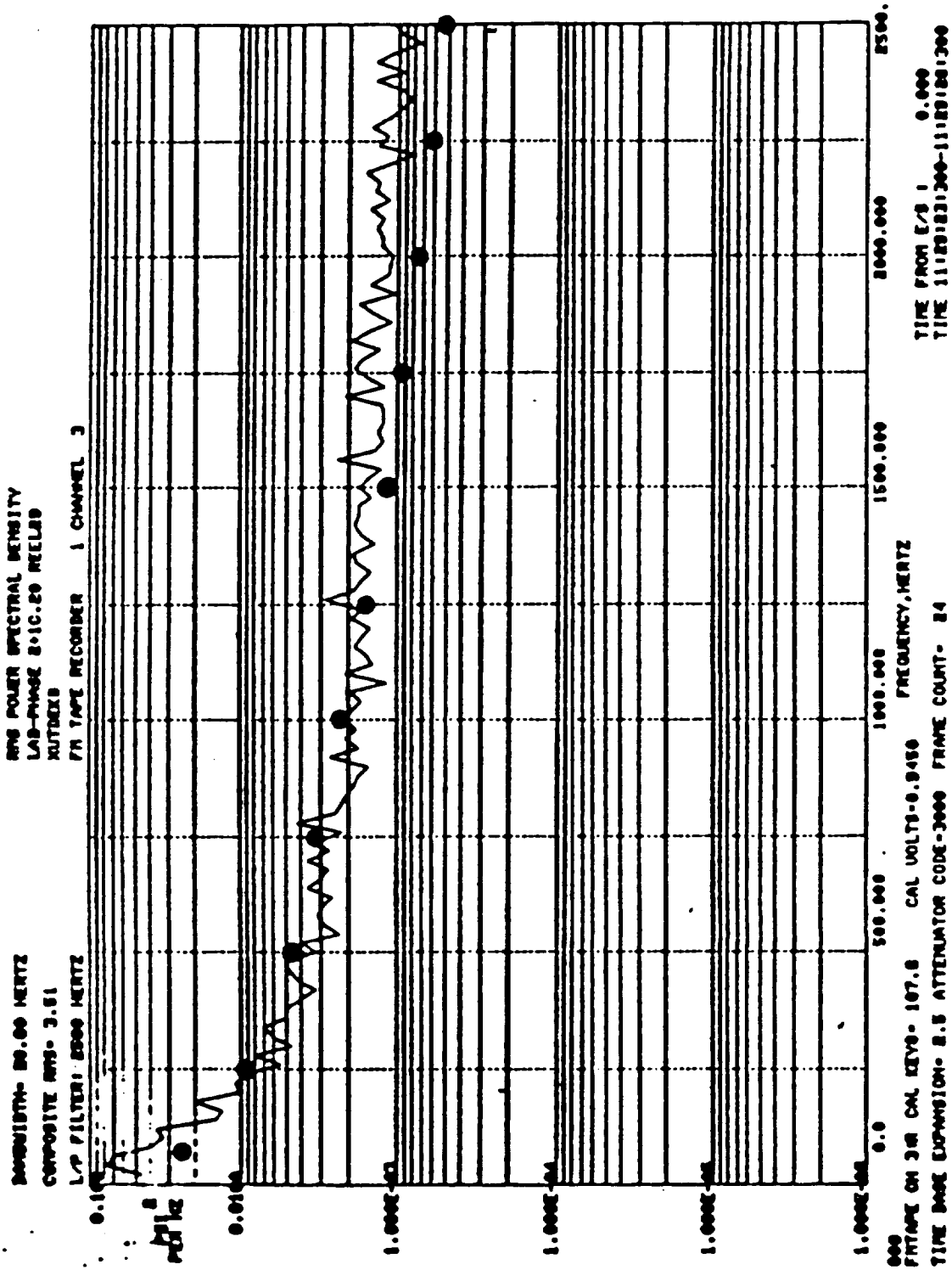
Figure C4. Measured PSD at Location XUTDEKB; •, Prediction S = 0.99
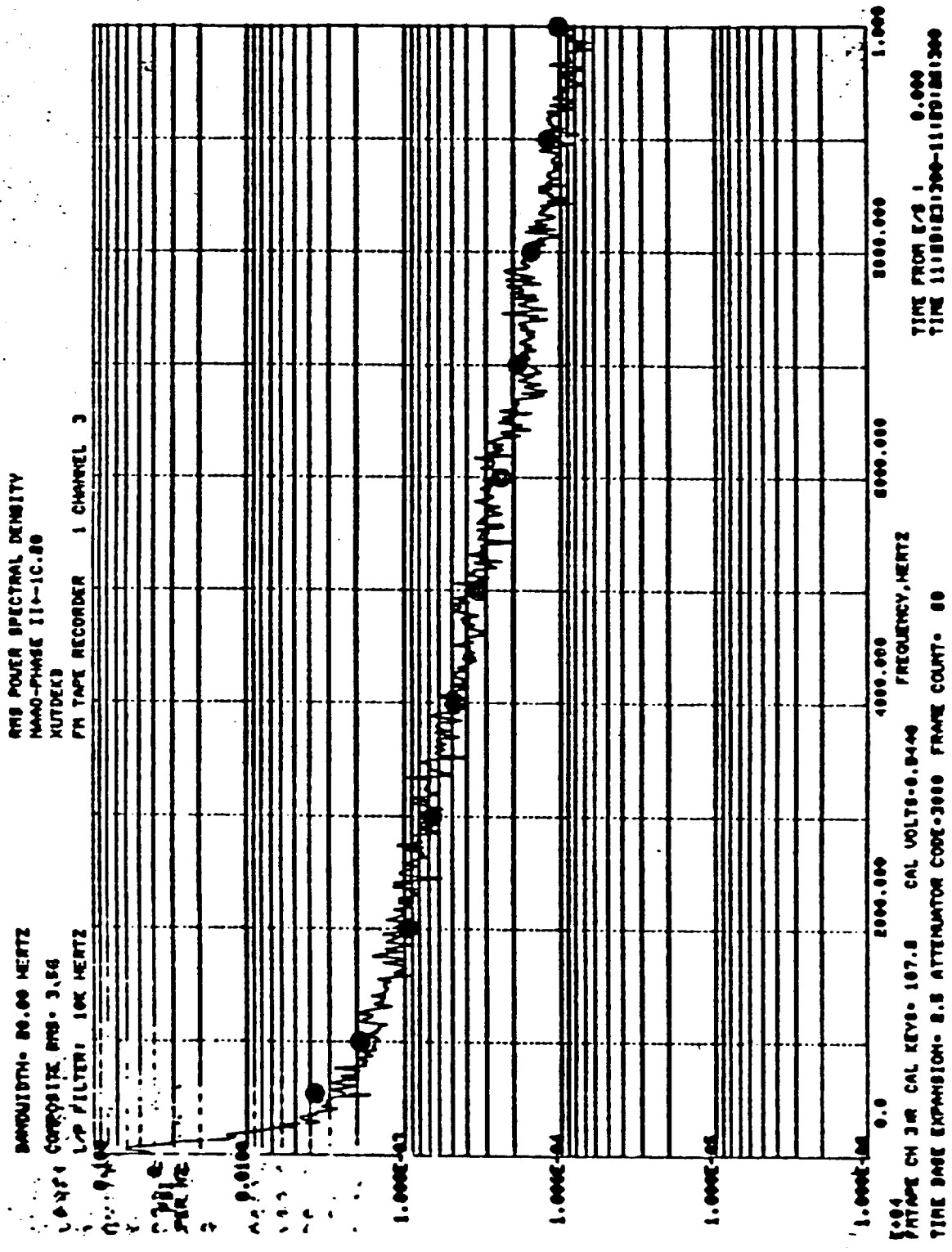
Figure C5.   Measured PSD at Location XUTDEKB: •, Prediction S = 0.99

FIGURE C6. PSD MEASURED AT TOP LOCATION OF POST 01-02;
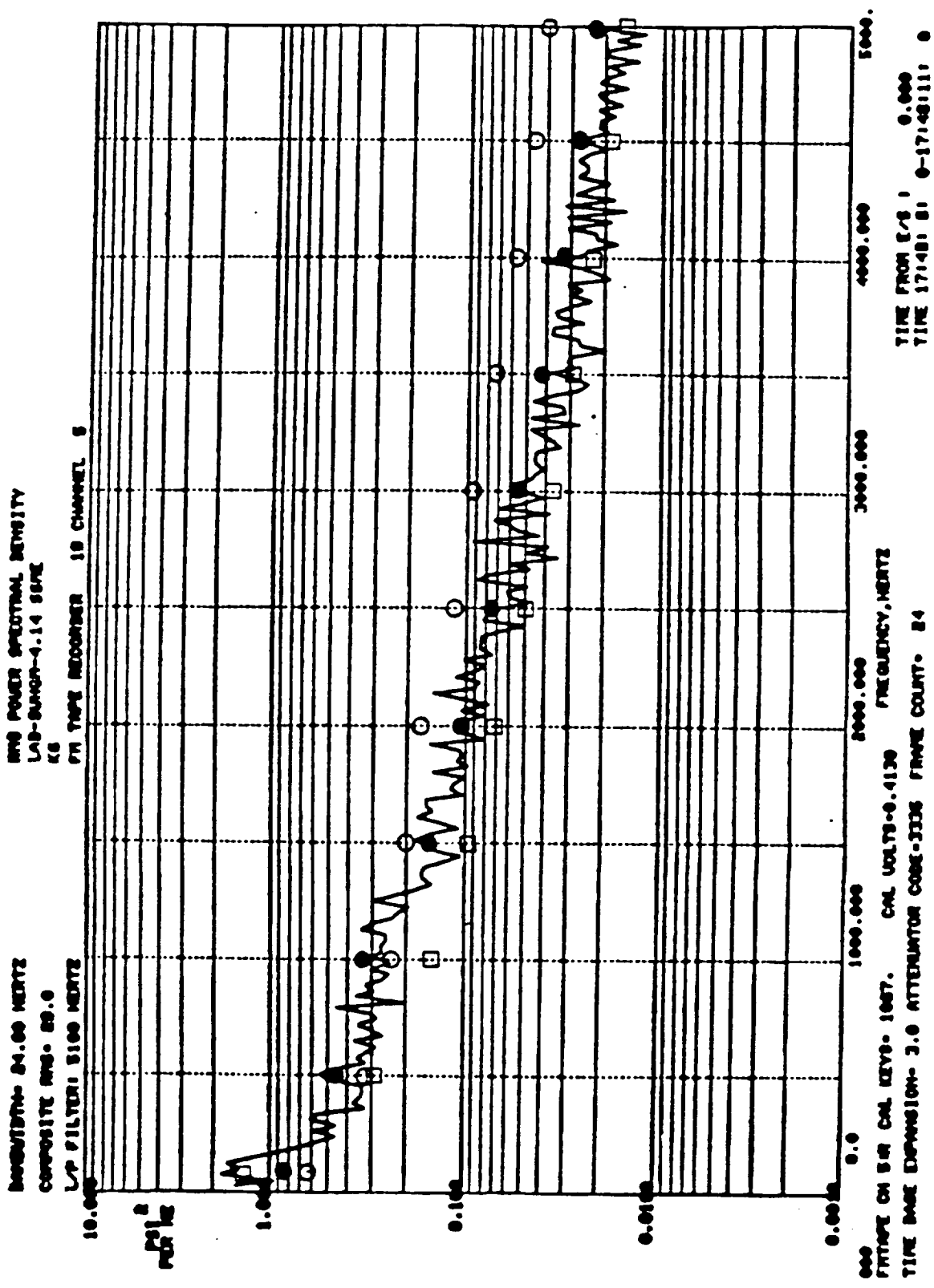
●, S = 0.4, 81% energy in 10 <f < 1000 Hz

○, s = 0.4, 81% energy in 10 <f < 2000 Hz

□, s = 0.99, 81% energy in 10 <f< 2000 Hz
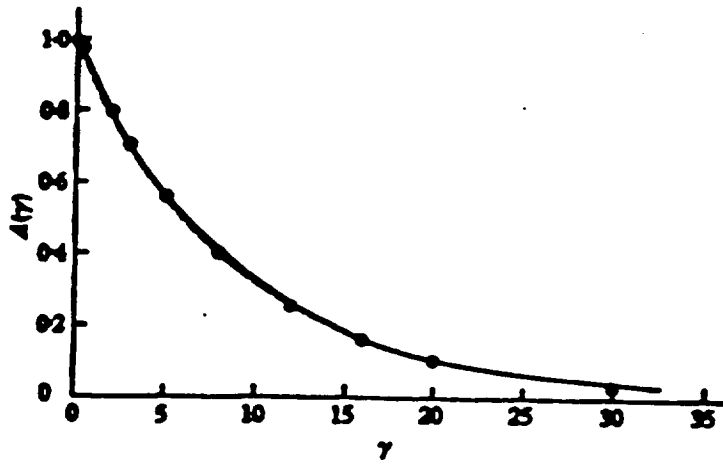
Figure C7. The Function A(γ), $\gamma = \omega E/U_{c*}$
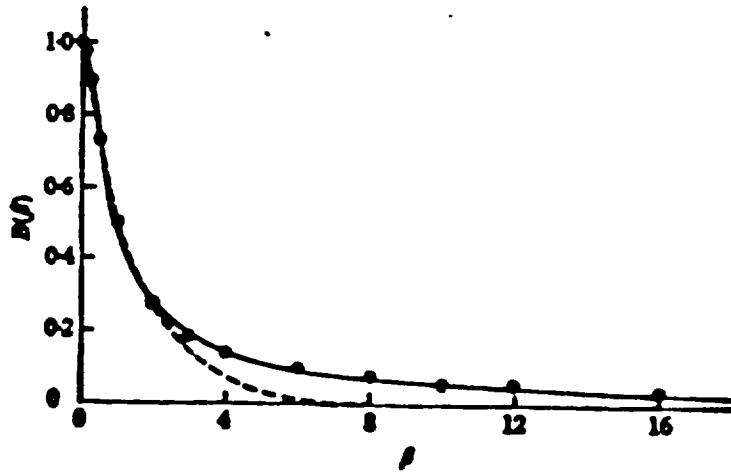
Figure C8. The Function B(β), $\beta = \omega q/U_{c*}$
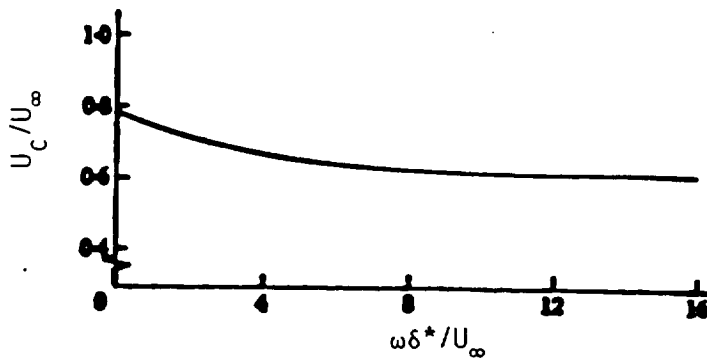
Figure C9. The Dependence of Convection Velocity on Frequency

Appendix D

Periodic Load Model

PERIODIC LOAD MODEL

Introduction

The modeling of vibration or, more generally, periodic loads, requires that a more rigorous treatment of dependent load models be developed. This is because the forced vibration loads, especially at multiples of pump speed (in the frequency domain) show a strong dependency. The variability in the predicted load will also be incorrect if the dependence effect is not accounted for in the model. In fact, when the correlation is in position, the variability will always be underpredicted. Therefore, a more thorough treatment of these types of loads has been developed.

Model Development

The basic model requires some estimates of the correlation between various types of vibration loads. These correlations are then used to predict the spread in the variable of interest. As an example, assume that one is interested in the composite vibration load, where the composite load is composed of all of the synchronous and random levels for all frequencies. The composite load, denoted C, is given as a function of a constant term and the synchronous vibration magnitudes:

$$C = a_0 + a_1 L_1 + \ldots + a_m L_m \qquad (2)$$

where L_i is the magnitude of the ith synchronous level and the coefficients, a_i are to be determined. It is worth noting that this can just as easily be written as the first synchronous load, L_1, as a function of the composite level, C, but this is the example chosen for discussion.

For the model shown in Equation (1), how does one predict the composite levels? To do this we will need to compute the covariance matrix of the individual inputs, L_i, of the model. But first it is wise to adopt some additional notation and normalize some terms.

First we denote the normalized load levels as N_i and

calculate N_i as:

$$N_i = (L_i - m_i)/s_i \qquad (2)$$

where m_i is the mean of L_i and s_i is the standard deviation. The actual equation which will fit is then given by:

$$C = c_o + b_1 N_1 + \ldots + b_m N_m \qquad (3)$$

If we denote the variance of C by Var(C), then

$$Var(C) = b^T R b \qquad (4)$$

where b is the vector composed of the coefficients in Equation (3) and R is the matrix of the correlation coefficients, r_{ij}, between variable L_i and L_j.

At this point we take advantage of some useful properties of the covariance matrix, R. We know that the matrix Q, whose columns consist of the eigenvectors of R can be used to reduce Equation (4) to the form:

$$Var(C) = \Sigma q_i p_i^2 \qquad (5)$$

where q_i are the eigenvalues and p_i are the components of the vector obtained by multiplying b times Q^T.

To perform calculations using these equations, it becomes necessary to examine the available data to obtain estimates for m_i and s_i, i.e. the mean and standard deviations for the ith synchronous load level.

Most of the available data deals with maximum PSD values over the test or mission. These values are used to monitor the wear and health of various engine components, but they do leave out some of the statistical information that is needed. Therefore, the probabilistic information is obtained from the database, assuming that the peak values represent a three-standard deviation spread from the mean value. A visual examination of tracking filter data indicates that a COV value is approximately 20%. This implies that the mean and standard deviation values can be found from the following set of equations:

$$\text{Mean} = 0.625 \times \text{Peak amplitude} \tag{6a}$$
$$\text{Standard deviation} = 0.125 \times \text{Peak amplitude} \tag{6b}$$

Of course, it is assumed that the PSD values are distributed normally about their mean values. The peak amplitudes are obtained from data analyses. Figure D1 shows the distribution of peak values for both pump and turbine data for 104% and 109% power levels. This data represents the HPFTP peak PSD data where an 11-point moving average has been used. It is interesting to note that the 109% power level curve is to the left of the 104% power level curve.

The other factor to examine is the variability in the vibration type load with location. Figures D2 through D5 show this variation for composite and synchronous pump data at both 104% and 109% power level. The turbine data has also been examined but the plots do not provide any new information; therefore, they are not included.

This information is useful for obtaining peak amplitudes for vibration loads either for pumps or turbines and adjusting for location. However, the peak amplitudes cannot be obtained as independent random variables, as has been done previously, since there is a high degree of correlation between some of the synchronous modes. The correlation of the peak composite data with the peak synchronous data is shown in Figures D6, D7, and D8. The correlation of the composite and synchronous data has a correlation coefficient of 0.818 when all of the power level data is included: 0.797 for the 104% power level data, and 0.987 for the 109% data for the pump radial position (O). The other

correlation coefficients for the remaining locations is shown in Table 1. The plots of these remaining data sets do not show any new information, they just more or less scatter about the trend lines and therefore are not included.

New information is obtained when higher multiples of the pump or turbine speeds are examined. For the 2N, 3N, and 4N multiples, there is little correlation among the peak amplitudes. This is shown in Figures D9 and D10. In Figure D9 we see the same plot as in Figure D7 but now the 2N data is superimposed on top of that plot. As this figure indicates, there is a clear relationship between the composite and synchronous data, but a very weak one between the composite and the 2N data. The relationships between higher multiples is even weaker, as indicated in Figure D9.

At this point it is noted that after this analysis was performed, it was discovered that the data for the PSDs found in Table 1 were taken only through 850 Hz. This implies that a significant portion of the energy imparted to the engine, due to the 2N, 3N, and 4N forced vibration levels, is not represented in the PSD values. While this is a problem for calculating the coefficients that will ultimately be contained in the expert system, it is not a problem for the purposes of this sample calculation. What will be changed when the complete frequency range is changed is the coefficients in the matrix R. However, a change in the numerical values will not affect the methodology.

To provide additional clarification of the steps taken so far, a sample calculation is performed. The data for this calculation is shown in Table 1 where the composite, synchronous, and pump multiple forced vibration loads, through four times the pump speed (4N), are shown. These data were analyzed to produce the correlation coefficients shown in Table 2. The data in Table 1 depicts the peak amplitudes measured during 63 separate tests. There are additional tests available for the composite and synchronous levels, but the data were missing for higher multiples. Since we are concerned with developing correlations, only these 63 tests were used. Ultimately, the actual PSD levels used in the vibration model will be transformed by Equation (6) where it is assumed that these peaks are at the 3-sigma level.

TABLE 1. VIBRATION LOAD DATA USED FOR SAMPLE CALCULATION

///

Composite	Synchronous	2N	3N	4N
2.3	0.5	1.4	1.1	0.9
2.4	0.8	0.8	1.2	1.9
2.5	1.7	0.7	1.3	0.7
2.6	1.8	0.7	0.8	1.0
2.9	2.2	1.6	0.9	0.9
3.0	2.0	1.8	0.9	0.9
3.1	2.3	0.9	1.2	1.2
3.1	2.0	1.0	1.5	1.0
3.2	2.2	1.6	0.9	1.1
3.2	2.4	0.6	1.7	0.9
3.2	2.0	0.8	0.8	2.3
3.3	2.2	0.8	1.0	0.9
3.4	2.5	0.5	1.1	1.0
3.4	2.6	0.5	1.4	1.3
3.5	2.7	0.5	0.6	1.0
3.5	3.0	1.8	0.9	1.4
3.5	2.2	0.9	1.3	1.9
3.6	2.8	1.0	0.7	0.8
3.6	2.9	0.9	0.9	0.6
3.6	2.9	0.6	1.0	0.8
3.6	2.5	1.0	1.1	1.9
3.7	2.9	0.7	1.4	0.8
3.7	2.7	0.9	1.4	0.8
3.8	2.6	2.4	1.3	1.0
3.8	2.0	0.9	1.0	0.7
3.9	2.9	0.6	1.2	1.6
3.9	3.2	0.8	0.5	0.7
3.9	3.0	0.9	1.8	1.1
4.0	3.1	2.4	2.0	1.4
4.1	2.0	2.2	1.4	1.7
4.1	3.4	0.5	1.4	1.2
4.2	3.3	2.2	1.6	0.9

TABLE 1. (Concluded)

Composite	Synchronous	2N	3N	4N
4.2	3.2	0.9	1.0	1.2
4.2	3.4	0.6	1.2	1.5
4.2	3.3	0.8	1.0	1.4
4.2	3.4	0.9	1.8	0.8
4.2	3.5	0.6	1.0	1.0
4.5	2.7	1.1	1.0	1.0
4.7	4.1	1.4	1.0	3.3
4.9	3.2	1.2	1.2	1.4
4.9	4.5	1.8	1.3	2.1
4.9	4.2	0.6	1.0	1.0
4.9	4.1	1.0	1.3	1.9
5.0	4.2	2.1	1.2	1.4
5.4	4.7	1.1	1.1	0.9
5.4	4.6	1.5	0.8	0.9
5.5	4.8	1.0	1.0	1.2
5.8	5.1	1.1	1.1	1.0
5.9	5.0	1.0	0.9	0.8
5.9	5.2	1.3	0.9	1.0
5.9	5.4	0.9	1.9	1.0
6.1	5.4	1.6	1.5	1.0
6.1	5.4	0.9	1.1	1.1
6.2	5.4	0.8	1.9	1.4
6.5	5.2	1.1	1.1	0.9
6.8	6.2	1.0	1.0	0.6
6.9	6.4	1.9	1.4	1.0
7.5	6.7	1.6	1.6	0.9
7.8	6.2	1.2	1.8	0.9
9.3	9.0	2.0	1.3	1.0
9.4	9.0	1.7	0.9	1.2
9.7	8.8	2.2	2.3	1.6
10.8	4.2	2.0	1.7	1.7

///

During the first phase of this program, there are no physical model requirements for the vibration model. Therefore, the probabilistic synthesis of the individual components into an overall composite, random vibration load is being accomplished by a simple linear fit:

$$\text{Composite} = a_0 + a_1{}^*L_1 + a_2{}^*L_2 + \ldots + a_n{}^*L_n \tag{7}$$

where L_i is the individual synchronous loads and a_i are the coefficients obtained from regression analysis. The variability in the composite load can then be obtained, using the variance as a measure of the variability from the covariance matrix:

$$\text{Var}(C) = b^T R b \tag{8}$$

where b is the vector of normalized coefficients $(b_1, \ldots, b_n)$, and R is the covariance matrix. The covariance matrix is made up of elements given by:

$$R_{ij} = r_{ij} \cdot s_i \cdot s_j \tag{9}$$

where r_{ij} is the correlation coefficients between variables i and j, s_i is the standard deviation of variable i, and s_j is the standard deviation for variable j. This provides a first approximation model for the composite, periodic load spectrum.

Before proceeding with additional calculations, it is necessary to first describe the numerical procedure used and how the eigenvalues and eigenvectors are determined.

C-3

TABLE 2. CORRELATION OF VIBRATION LOADS

///

Correlation of:

With:	C	L_1	L_2	L_3	L_4
C	1	0.903062	0.405069	0.343665	0.030434
L_1	0.903062	1	0.329034	0.273249	0.038454
L_2	0.405069	0.329034	1	0.274478	0.147398
L_3	0.343665	0.273249	0.274478	1	0.087954
L_4	0.030434	0.038454	0.147398	0.087954	1

///

The Calculation Of Eigenvalues And Eigenvectors

The eigenvalue and eigenvector calculation is performed numerically using the Leverrier method as modified by Faddeeva (ref. D1). This method was selected because it simultaneously calculates the eigenvalues, eigenvectors and inverse matrix. It is somewhat of a brute force technique but is robust; just the type of method that is needed for generic applications.

For the R matrix (shown in Table 2 in rows 2 through 5 and columns 2 through 5), the eigenvalues and eigenvectors which were calculated are shown in Table 3. Because the covariance matrix is real and symmetric, a simple check of the accuracy of the calculation can be made. This check is performed by multiplying the eigenvector matrix, Q (ref. Table 3) by its transpose. This should produce the identity matrix. The calculation demonstrated four significant figures after the decimal point which was judged to provide the needed accuracy for these calculations.

At this point we can begin the calculation for the variance of the composite load, Var(C). If we use the correlation coefficients of C with the forced vibration levels, then these correlation coefficients represent the b_i in Equation (3). If we compare Equations (1) and (3), it is clear that in the calculation of the variance vector b in Equation (4) must be changed to

TABLE 3.   EIGENVALUES AND EIGENVECTORS FOR SAMPLE CALCULATION
///

Eigenvalues:

1.62570E+00   9.78083E-01   7.43709E-01 6.52502E-01

Eigenvectors:

Q_1	Q_2	Q_3	Q_4
5.56692E-01	-3.12676E-01	3.92960E-01	-6.61853E-01
5.85605E-01	2.03978E-02	3.86287E-01	7.12258E-01
5.34772E-01	-1.31845E-01	-8.34468E-01	1.68408E-02
2.47343E-01	9.40444E-01	5.24853E-03	-2.33145E-01

///

$$b' = (b_1 \cdot s_1, \ldots, b_m \cdot s_m)$$

Therefore:

$$Var(C) = \Sigma b_i^2 \cdot s_i^2 \cdot \dot{q}_i \qquad (10)$$

The mean values and the standard deviations calculated from the data are shown in Table 4. Using these values for the standard deviation s_i, the correlation coefficients from Table 2 for the composite with four synchronous levels for b_i, and eigenvalues from Table 3 for q_i, the variance of the composite level is found to be:

$$Var(C) = 3.08682$$

Taking the square root yields an estimate of the standard deviation for the composite load of 1.745 which compares very well with the value of 1.826 found from the data analysis. Generally, we do not expect agreement that is this close because the entire frequency range has not been included. To check, the entire analysis was repeated for the pump radial position (90). For this analysis, the calculated standard deviation for the composite vibration PSD is 1.435 while the data analysis gave a result of 1.852. While these are of the

same order, we would expect the agreement to improve as more of the frequency range is included. This expectation arises because the covariance matrix did not include all of the cross-correlations and, thus, the estimated variance should be low (for positive correlation). However, standard deviations should not match exactly because there is still one other source of variability that

TABLE 4. MEAN AND STANDARD DEVIATIONS FOR VIBRATION DATA
//

	Composite	Synchronous	2N	3N	4N
Mean:	4.719047	3.711111	1.171428	1.215873	1.180952
Standard Deviation:	1.825903	1.795772	0.528678	0.356440	0.463546

//

has not been accounted for in analysis. This source of variability is the random component of the periodic load.

To account for the random portion of the composite PSD, we modify Equation (3) to include this component:

$$C = c_o + b_1 N_1 + \ldots + b_m N_m + b_{m+1} Z \qquad (11)$$

where Z is the random component. Because the random component must, by definition, be uncorrelated with all of the other modes, the covariance matrix will have another row and column added that contains all zeroes except the $(m+1, m+1)$ component which will be equal to 1. That is, the new covariance matrix, denoted R', is given by:

$$R' = \begin{matrix}
r_{1,1} & r_{1,2} & \cdots & r_{1,m} & 0 \\
r_{2,1} & r_{2,2} & \cdots & r_{2,m} & 0 \\
 & & \vdots & & \\
r_{i,1} & r_{i,2} & \cdots & r_{i,m} & 0 \\
 & & \vdots & & \\
r_{m,1} & r_{m,2} & \cdots & r_{m,m} & 0 \\
0 & 0 & & 0 & 1
\end{matrix}$$

It is a well known fact from linear algebra that this modification to the covariance matrix will leave the original eigenvalues and eigenvectors unchanged. It will introduce a new eigenvalue equal to 1 and an eigenvector equal to the identity matrix column. Therefore b_{m+1} will be equal to 1 and the variance of the random component can now be calculated from:

$$Var(Z) = Var(C) - \Sigma b_i^2 s_i^2 q_i \qquad (12)$$

TABLE 5: CORRELATION COEFFICIENTS BETWEEN COMPOSITE AND SYNCHRONOUS DATA

Location	Correlation Coefficient		
	All Data	104% Power	109% Power
Pump Radial (0)	0.818	0.797	0.987
Pump Radial (90)	0.740	0.761	0.657
Pump Radial (174)	0.719	0.693	0.845
Pump Radial (186)	0.729	0.735	0.819
Turbine Radial (90)	0.554	0.594	0.491
Turbine Axial	0.874	0.873	1.000*
Turbine Radial (180)	0.642	0.702	0.661

*Only two data points were in this data set, the remaining sets had as few as 21 and as many as 89.

Table 5 presents the results of these calculations for a variety of pump and turbine positions. In some cases, the variance of the composite PSD is less than the predicted value from the correlated data analysis. This is believed to be due to the restricted range of frequencies that are used for the data collection and is not indicative of the results which would be obtained from a more complete frequency spectrum. There is one interesting trend in the data that shows that the 90-deg positions for both pump and turbine loads has a larger correlation contribution to the variance than the (approximately) 180-deg position. This may warrant further investigation when the frequency range is increased.

Changing The Peak Values to Nominal Values

All of the calculations performed to this point have been for the peak value data. As was previously discussed, the mean and standard deviation for the nominal PSD levels are calculated using the previous set of equations. Now, we can simply estimate the variance of the composite load for the nominal conditions using this equation. Therefore, the standard deviation is changed by dividing by 8 and the new variance of 0.38585 is obtained.

This model has been used to compare its prediction with the available data. A typical plot is shown in Figure D11. In this figure, the actual data is compared to the prediction obtained from RASCAL. The mean predictions remain accurate but the standard deviation, or spread in the data, is underpredicted. This is primarily due to the limited number of samples available from these runs. The cases are being reanalyzed to determine if the smaller predicted variability is due to the method or to the need to increase the sample space selected for the analyses.

CDF For HPFTP Data
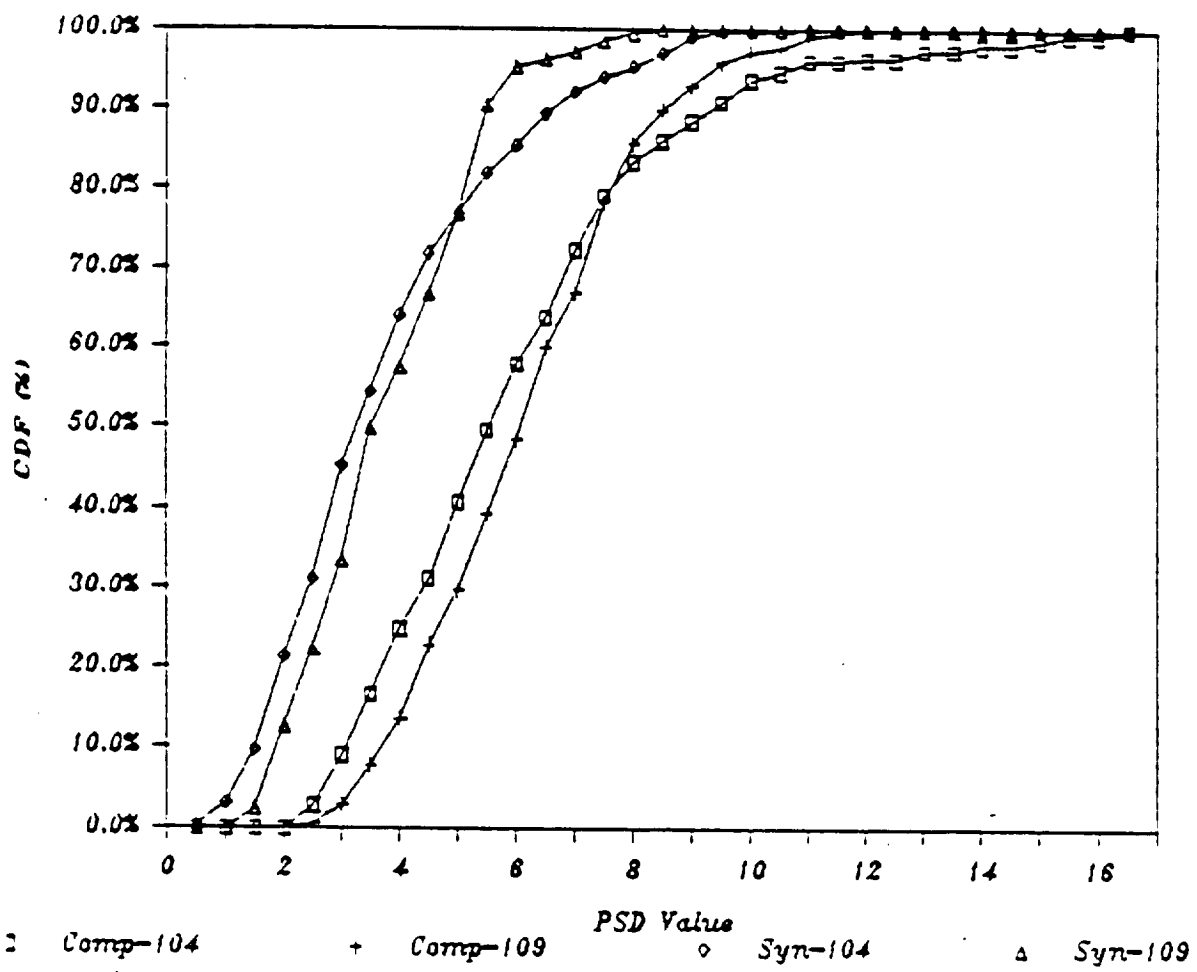
Figure D1. Cumulative Distribution Functions for Peak PSD Values

CDF For Pump Radial Positions

Figure D2. Cumulative Distribution Functions For Differing Pump Locations

CDF For Pump Radial Positions

Composite: 109% Power
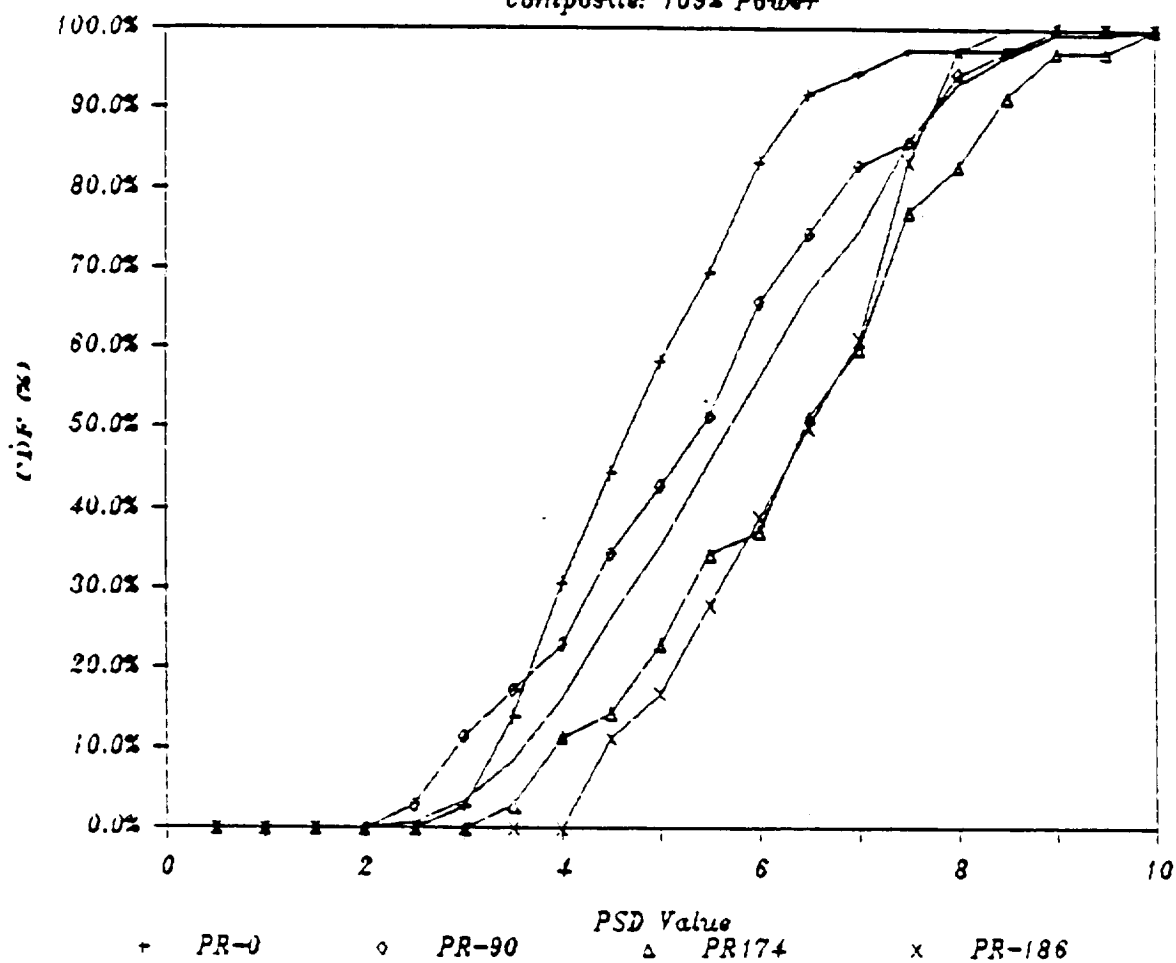
Figure D3. Cumulative Distribution Functions For Differing Pump Locations

Figure D4. Cumulative Distribution Functions For Differing Pump Locations

CDF For Pump Radial Positions

Synchronous: 109% Power
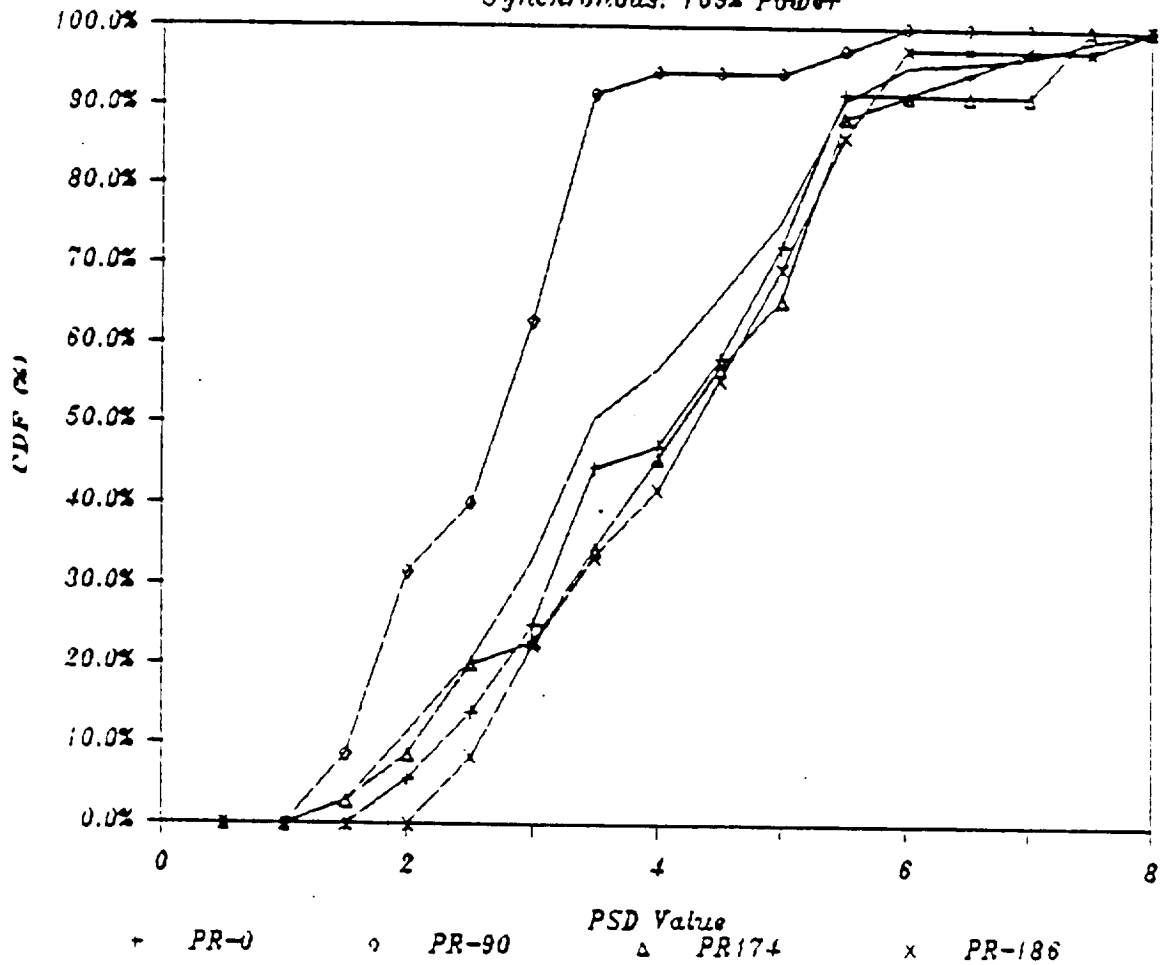
Figure D5. Cumulative Distribution Functions For Differing Pump Locations
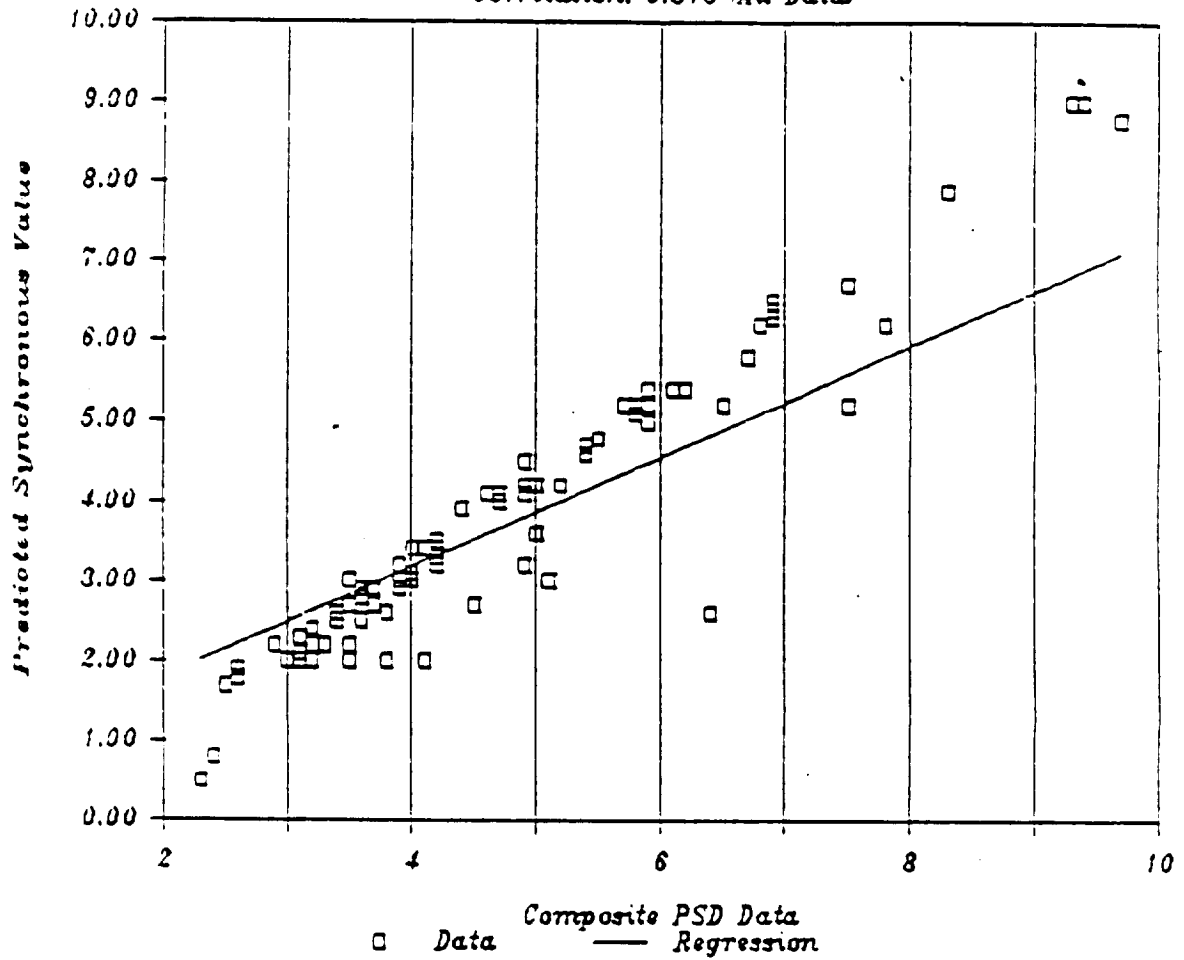
Figure D6.   Composite And Synchronous Correlation For All Power Levels
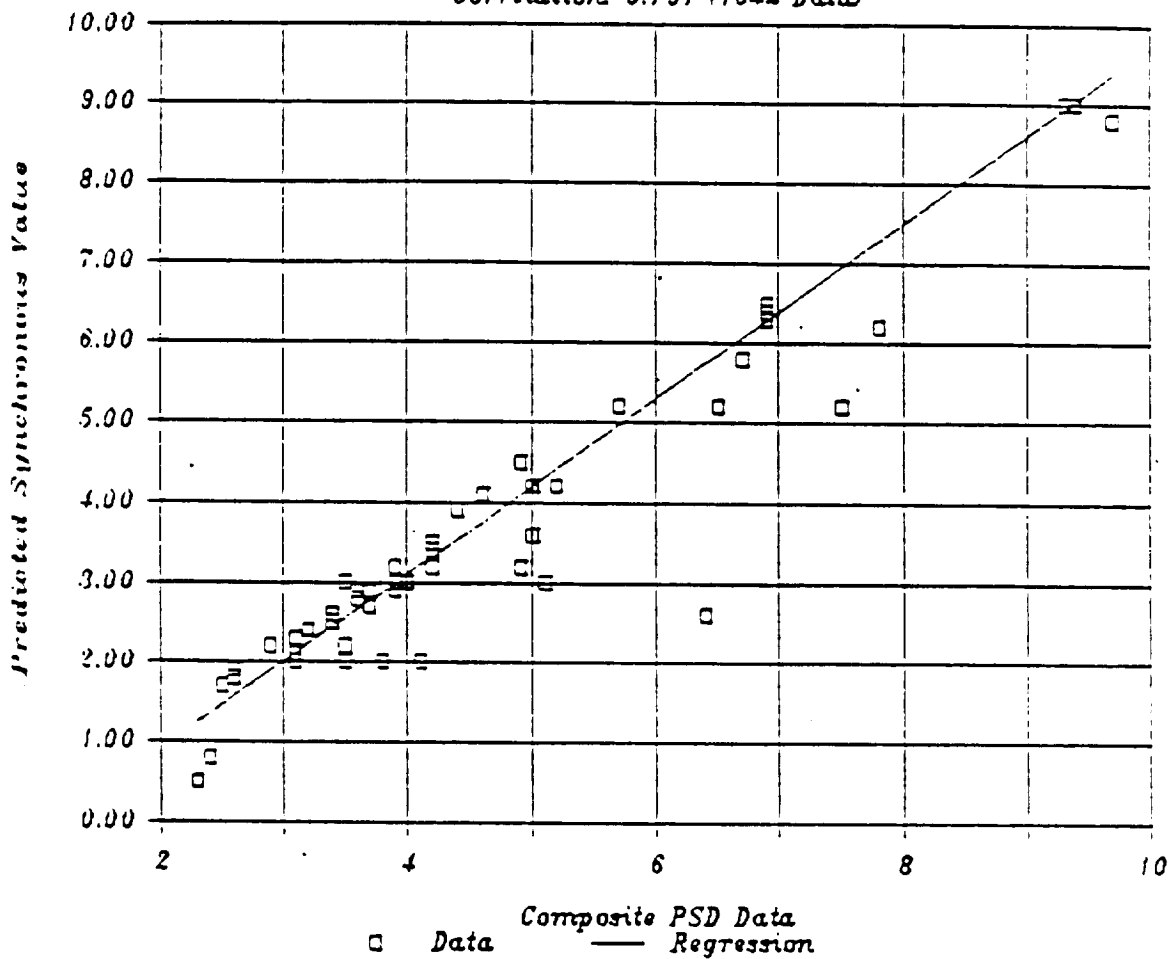
Figure D7. Composite And Synchronous Correlation For 104% Power Levels
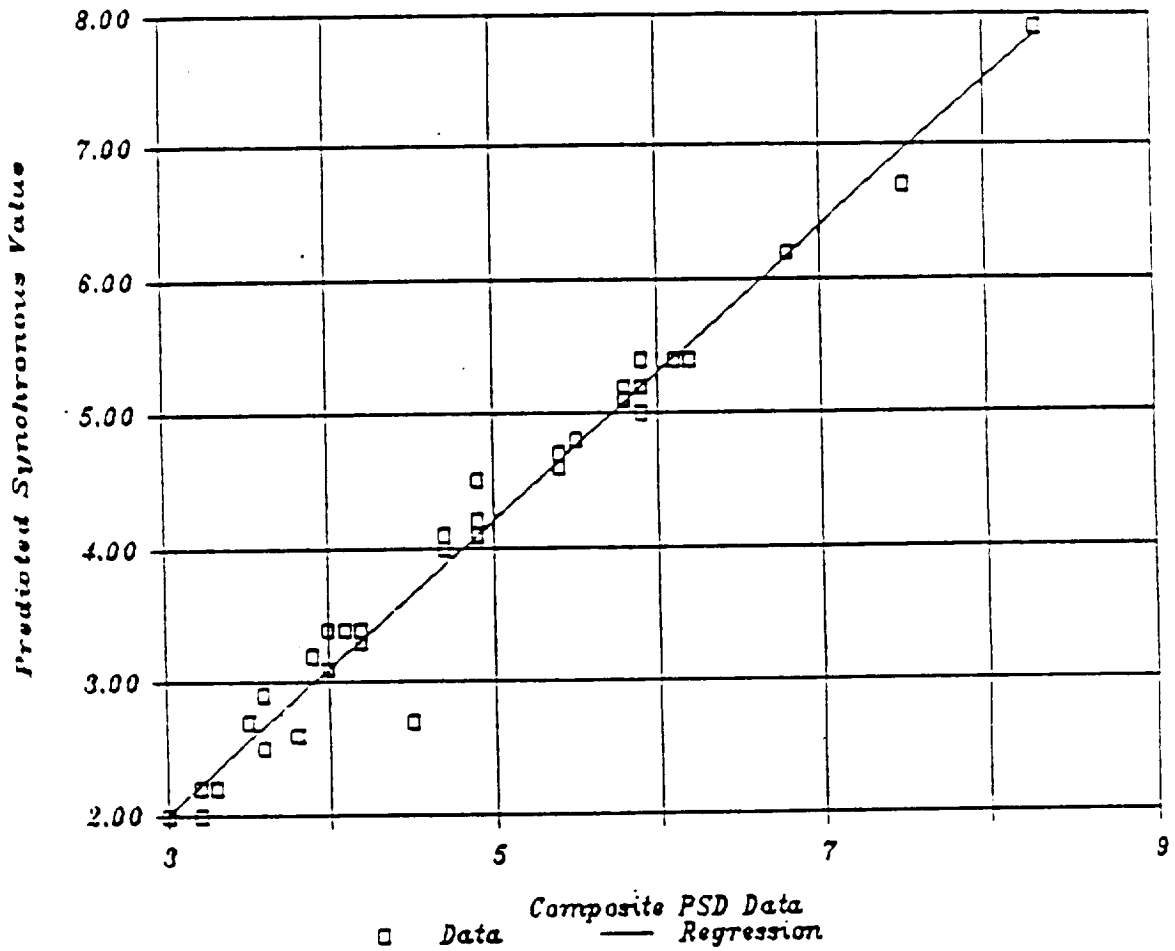
Figure D8. Composite And Synchronous Correlation For 109% Power Levels

Figure D9. Correlation Of Higher Multiple Synchronous Data

Correlation For Synchronous PSD's
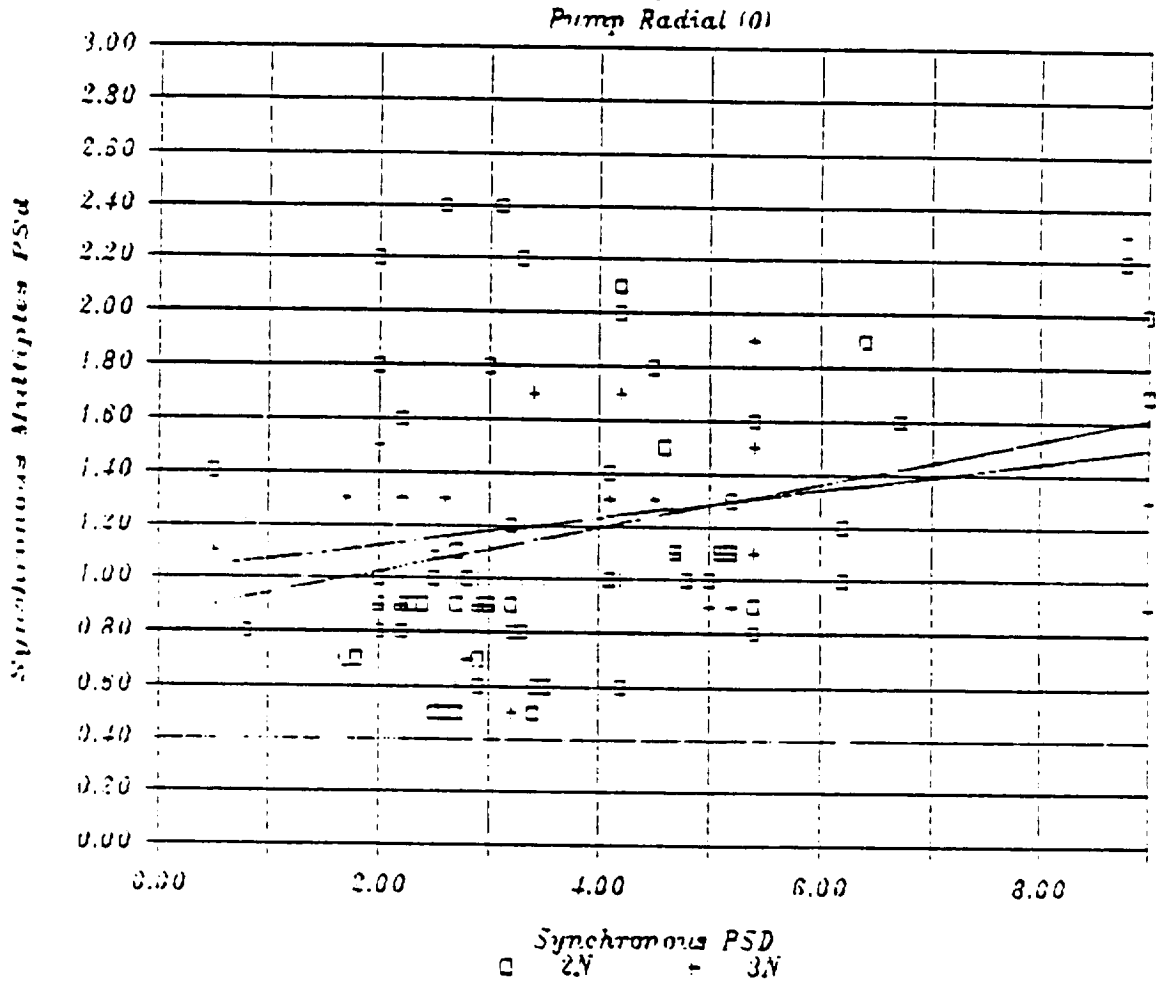
Figure D10.   Correlation Of Higher Multiple Synchronous Data

Comparison Of Periodic Model And Data

Mean: 3.345
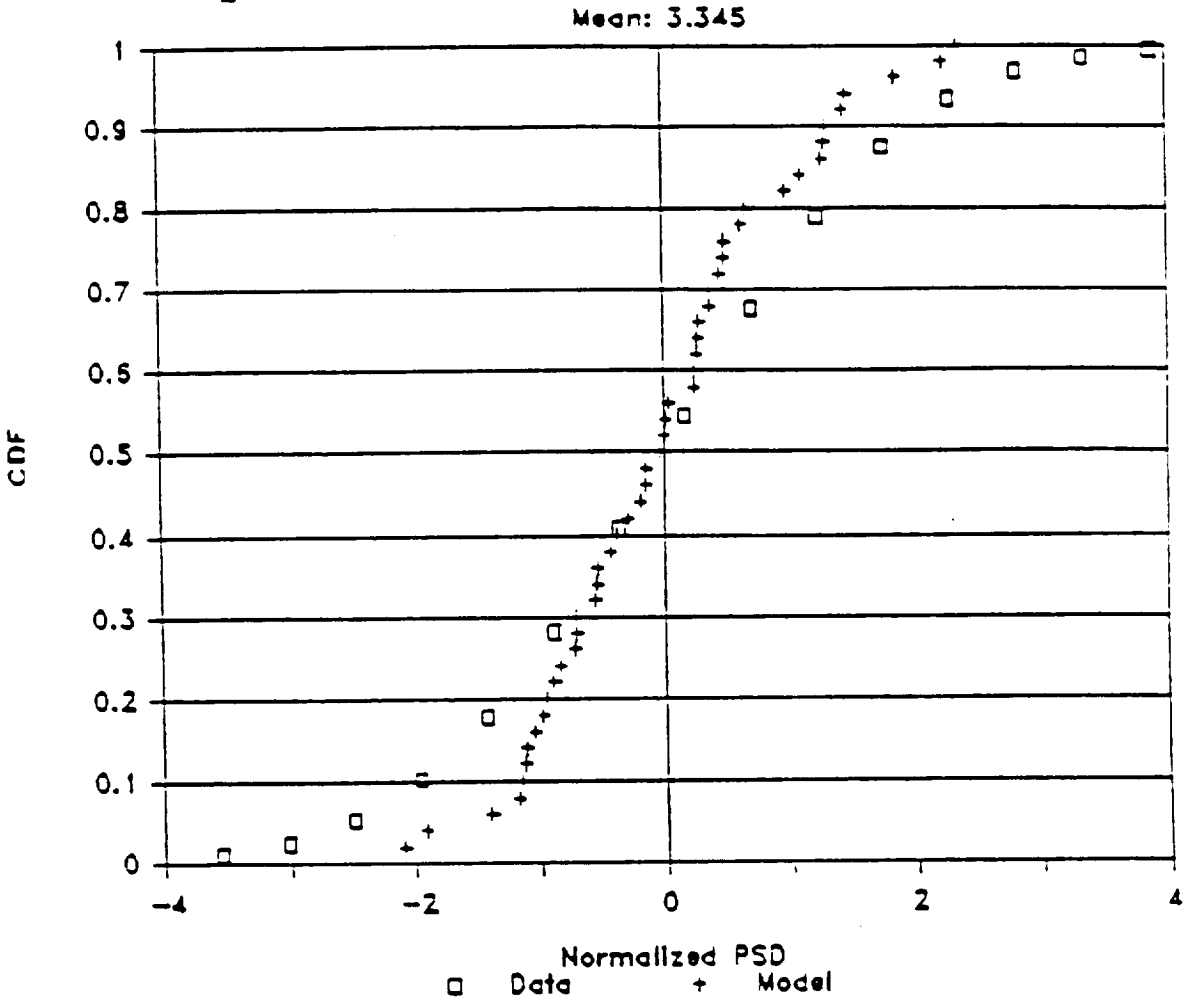
Figure D11. Comparison of MSFC Pump Rad (O) Data and Model Prediction

REFERENCES

D.1 Faddeeva, V. N., "Computational Methods of Linear Algebra," Dover Publications, 1959.

REPORT DOCUMENTATION PAGE

1. AGENCY USE ONLY *(Leave blank)*	2. REPORT DATE November 1991	3. REPORT TYPE AND DATES COVERED Final Contractor Report

4. TITLE AND SUBTITLE

Composite Load Spectra for Select Space Propulsion Structural Components
Final Report

6. AUTHOR(S)

J.F. Newell, H.W. Ho, and R.E. Kurth

5. FUNDING NUMBERS

WU- 553 - 13 - 00

C - NAS3 - 24382

7. PERFORMING ORGANIZATION NAME(S) AND ADDRESS(ES)

Rockwell International
6633 Canoga Avenue
Canoga Park, California 91303

8. PERFORMING ORGANIZATION REPORT NUMBER

None

9. SPONSORING/MONITORING AGENCY NAMES(S) AND ADDRESS(ES)

National Aeronautics and Space Administration
Lewis Research Center
Cleveland, Ohio 44135 - 3191

10. SPONSORING/MONITORING AGENCY REPORT NUMBER

NASA CR - 189072
RI/RD90 - 128

11. SUPPLEMENTARY NOTES

Project Manager, C.C. Chamis, Structures Division, NASA Lewis Research Center, (216) 433 - 3252.

12a. DISTRIBUTION/AVAILABILITY STATEMENT

Unclassified - Unlimited
Subject Category 39

12b. DISTRIBUTION CODE

13. ABSTRACT *(Maximum 200 words)*

The final report describes the work performed to develop Composite Load Spectra (CLS) for the Space Shuttle's Main Engine (SSME) using probabilistic methods. The three methods were implemented to be the engine system influence model. RASCAL was chosen to be the principal method as most component load models were implemented with the method. Validation of RASCAL has been performed. High accuracy comparable to the Monte Carlo method can be obtained if a large enough bin size is used. Generic probabilistic models were developed and implemented for load calculations using the probabilistic methods discussed above. Each engine mission, either a real flight or a test, has three mission phases: The engine start transient phase, the steady state phase, and the engine cut off transient phase. Power level and engine operating inlet conditions change during a mission. The load calculation module provides the steady-state and quasi-steady state calculation procedures with duty-cycle-data option. The quasi steady state procedure is for engine transient phase calculations. In addition, a few generic probabilistic load models were also developed for specific conditions. These include the fixed transient spike model, the poison arrival transient spike model, and the rare event model. These generic probabilistic load models provide sufficient latitude for simulating loads with specific conditions. Four SSME components, turbine blades, transfer ducts, LOX post, and the high pressure oxidizer turbopump (HPOTP) discharge duct were selected for application of the CLS program. They include static pressure loads and dynamic pressure loads for all four components, centrifugal force for the turbine blade, temperatures of thermal loads for all four components, and structural vibration loads for the ducts and LOX posts.

14. SUBJECT TERMS

Load models; Probabilistic methods; Monte Carlo; Engine mission; Duty-cycle; Spikes; Rare-events; Turbine blades; Transfer ducts; Thermal loads; Dynamic loads expert system; Computer code

15. NUMBER OF PAGES
214

16. PRICE CODE
A10

17. SECURITY CLASSIFICATION OF REPORT Unclassified	18. SECURITY CLASSIFICATION OF THIS PAGE Unclassified	19. SECURITY CLASSIFICATION OF ABSTRACT Unclassified	20. LIMITATION OF ABSTRACT